Conference-Workshop

Bio-inspired Robotics

Frascati
14-15 May 2014

Edited by Claudio Moriconi and Ramiro dell'Erba

I A R P
International Advanced
Robotics Programme

ENEA
Italian National Agency for New Technologies,
Energy and Sustainable Economic Develpment

Proceedings of the Conference-Workshop

Bio-inspired Robotics

Frascati

14-15 May 2014

Edited by Claudio Moriconi and Ramiro dell'Erba

Proceedings of the Conference-Workshop

Bio-inspired Robotics

Frascati

14-15 May 2014

Edited by Claudio Moriconi and Ramiro dell'Erba

PRESENTATION

The Conference has been opened by a Welcome of Dr. G. M. Monti, director of the Frascati ENEA Research Center.

In two days many works on Bio-Inspired robotics have been presented and many questions was raised to the authors.

Together with the classical presentations, the Conference have presented the innovative element to organize a session completely reserved to young PhD, to offer them the opportunity to present their work to an high level international audience (there were present some delegates of IARP and several high level researchers in robotics).

It is our intention to introduce a new topic of conferences, that will be supported by ENEA, dedicated to the most young researchers. It will call YRRC (Young Researchers Conference Robotics). YRRC will continue to have the sponsorship IARP with significant international participation and will remain open to young people of all countries, but it will have as a reference site Italy. Therefore the policy of this new kind of Conference will be the attention to the younger people. To this aim the economical policies of the Conference has been oriented to very cheap fee, for the students and, anyway, low for other people regularly affiliated to Research Organizations and industries. To keep the fee low ENEA will cover the remaining costs of the organization.

In addition, we have organized a round table, with the participation of delegates of some of the major international research organization. Moderator of the discussion was the chairman, Dr. Claudio Moriconi, head of the Robotics laboratory of ENEA. The discussion was dialing on the different research developments into the laboratories, to offer to the young people attending the Conference an indication on how to continue their works.

To the discussion have contributed high level international experts as Prof. Paolo Arena of Catania University, Prof. Silvello Betti of University of Tor Vergata, Prof. Philippe Bidaud of the University Pierre et Marie Curie, Prof. Geoff Pegman, Prof. V. Gradetsky of Russian Academy of Sciences, Prof. M.M Knyazkov, Prof. Cecilia Laschi of Scuola S.Anna, Prof. A. Molina of Edimburgh University, Prof. Agostino Bruzzone and Prof. Francesco Martinelli.

The attendance was about 50 people for both the days.

The Conference has been closed by a voting process carried out by only the young researchers involved in a contest to select the most effective paper under the didactical point of view and the best paper under the capability hit the attendees attention. Also a special ranking of the two combined issues has been awarded. Just small prize of minor value was assigned, within an official ceremony, as follow:

Best paper for the capability to hit the attendees attention:

Structural Dynamic and Propulsion Modelling of a Pulsed-Jet Underwater Soft Robot *(Presented by Dr. F. Renda– Bio Robotics Institute Scuola Superiore S. Anna Pisa)*

Best paper for the capability to inform the attendee:

Large underwater swarm communication: high priority reaching of target areas via a shortest path approach *(Presented by Dr. C. Snels - ENEA)*

Best paper for the combination of the two issues:

A bioinspired intentional architecture for situated agents to explore human cognitive abilities *(Presented by Dr.A.M. Franchi – Politecnico di Milano)*

International Program Committee

Chair: Prof. Geoff Pegman

Vice Chair: Prof. William Hamel

IARP Members (IPC)

IPC Member: Etienne Dombre

IPC Member: Mun-Sang Kim

IPC Member: Manuel Armada

IPC Member: Andrzej Maslowski

IPC Member: Dirk Lefeber

Local Committee

Chair: Dr. Claudio Moriconi

Vice Chair: Dr. Ramiro dell'Erba

Local member: Ing. Vincenzo Nanni

Local member: Dr. Andrea Zanela

Local member: Dr. Sergio Taraglio

Index of contents

AGENDA

09:00   **Registration**

09:30   **Introduction to the IARP Conference on bioinspired robotics**
- Welcome from Frascati Center (Director Center Dr. G. M. Monti)
- *The role of IARP in encouraging national and international communities: a stable national Conference for the new incoming researchers (Dr. Claudio Moriconi-* ENEA)

Morning session
(After each talk there will be 5' time for questions and discussions)

Robotics in the human society

10:00   **An innovative program to teach robotics at the primary school**
(*Dr.D. Scaradozzi – Univ. Politecnica delle Marche).*

10:25   **The social role of Robotics from the learning scholar activities to the Job opportunities**
(*Dr. A. Molina – Fondazione Mondo Digitale)*

10:50   **Cooperation opportunities within the National Robotics Initiative**
(*Prof. P. Bidaud– ICT Scientific Deputy ONERA French AerospaceLab Professor Université Pierre et Marie Curie- Paris)*

11:15   **Coffee break**

11:35   **Research and Experimentation on Autonomous Systems within the Extended Maritime Framework** *(Prof. A. Bruzzone– CMRE Centre for Maritime Research and Experimentation La Spezia)*

Social inspired Robot Behaviours -1

12:00   **Levy flight search of moving objects**
(Ing. V. Fioriti - ENEA)

12:25   **Cognitive Underwater Communications for Swarm Unmanned Vehicle Network**
(Dr M. Tabacchiera – Univ, of Rome "Tor Vergata".)

13:15   **Lunch**

May 14, 2014 - Afternoon session
(After each talk there will be 5' time for questions and discussions)

Social inspired Robot Behaviours -2

14:15   **Large underwater swarm communication: high priority reaching of target areas via a shortest path approach**
(Dr. C. Snels - ENEA)

14:40   **A bioinspired intentional architecture for situated agents to explore human cognitive abilities**
(Dr.A.M. Franchi – Politecnico di Milano)

Biological Body inspired functions - 1

15:05	**Human-Adaptive Control of Compliant Actuators** *(Dr. A. Calanca Univ. of Verona)*	

15:30	**Bio-Inspired Object Detection and Pose Estimation Algorithms for Underwater Environments** *(Dr F. Kallasi – Univ. of Parma.)*	

15:55	Coffee break

Round Table session

16:10	**Round table topics:**
	• **The IARP Status Report of the international community**
	• **Robotics for education**
	• **The engagement of ENEA within the national robotics community: the White Book of Robotics and RoboticaItalia initiatives**

17:10	**End of first day**
17:30	**Visit to the archeological park "barco borghese" by bus in ENEA** **http://www.barcoborghese.com/**

19:00	**Aperitif in Villa Vecchia garden**
19:30	**Classic trio concert in Villa Vecchia**

20:15	**Social dinner in Villa Vecchia** **http://www.villavecchia.it/index.php?lang=it**

Thursday May 15, 2014

__Morning session__
(After each talk there will be 5' time for questions and discussions)

Biological Body inspired functions – 2

09:00	**PSO-Based Automatic Object Registration for Interactive Augmented Reality** *(Dr.G. Micconi - Univ of Parma)*

09:25	**BIOMIMETIC PROPULSION FOR SWIMMING ROBOT** *(Prof.M. Armada – Centro de Automatica y Robotica Madrid)*

09:50	**Entrainment to natural oscillation modes using adaptive frequency oscillators for limbless locomotion** *(Dr. A. Alessi – Univ. Campus Biomedico Rome)*

10:15	**Supporting Presbyacusic Drivers in Detection and Localization of Emergency Vehicles: Alarm Sound Signal Processing Algorithms** *(Dr.M. Paoloni - ENEA.)*

10:40	**Motion Principles for Designing Biologically Inspired Robots** *(Prof. V. Gradetsky Institute for Problems in Mechanics of the Russian Academy of Sciences)*

11:05	**Coffee break**

11:20	**Whole body humanoid motion control: as human do !** *(Dr. C. Granata– ICT Scientific Deputy ONERA French AerospaceLab Professor Université Pierre et Marie Curie- Paris)*

11:45	**Structural Dynamic and Propulsion Modelling of a Pulsed-Jet Underwater Soft Robot** *(Prof. C. Laschi Dr. F. Renda– Bio Robotics Institute Scuola Superioe S. Anna Pisa)*

Social inspired Controls -1

12:10	**Safe Physical Human-Robot Interaction Based on Dynamic Analysis and Use of Residuals** *(Dr. C. Roberto Gaz - Univ. of Rome "La Sapienza")*

12:35	**KALMAN underwater acoustic 3D localisation in group of Robots** *(Dr. S. Taraglio - ENEA)*

13:00	**Environmentally induced task partitioning in competing bio-robots** *(Prof. P. Arena – Univ. of Catania)*

13:25	**Lunch**

May 15, 2014 - Afternoon session
(After each talk there will be 5' time for questions and discussions)

Social inspired Controls -2

14:30	**Localisation task for underwater swarms with minimum data** *(Dr. R. dell'Erba ENEA)*

When robots operate in place of men

14:55	**The challenge of architectonic survey and restoration of historical sites for service robotics** *(Prof. G. Carbone – LARM Univ. di Cassino e Lazio Meridionale.)*

15:20	**Using of small unmanned aerial vehicle and machine vision algorithms for environmental protection** *(Dr. S. Pagnottelli University of Perugia.)*

15:45	**Coffee break**

16:00	**Voting for the best presentation and Award**
16:10	**Open discussion for the Next National IARP Conference**
16:35	**Conference ending**

An innovative program to teach robotics at the primary school

Laura Sorbi*, David Scaradozzi*, Anna Pedale*+
*Dipartimento di Ingegneria dell'Informazione
Università Politecnica delle Marche
Via Brecce Bianche – Ancona – Italy
d.scaradozzi@univpm.it,
{laura.sorbi, pedaleanna}@gmail.com
+National Instruments Italy
Centro Direzionale Milanofiori Nord - Palazzo U4
Via del Bosco Rinnovato, 8
20090 Assago (MI)

Mariantonietta Valzano, Cinzia Vergine
Istituto Comprensivo Largo Cocconi
Laro Girolamo Cocconi, 10 – Roma – Italy
{mari.valzano, cinzia.vergine}@gmail.com

Abstract— **Many researchers and teachers agree that the inclusion of Science, Technology, Engineering, and Math in early education provides a strong motivation and a great improvement in learning speed. Most curricula in primary schools include a number of concepts that cover science and math, but less effort is applied in teaching problem solving, computer science, technology and robotics. The use of robotic systems and the introduction of Robotics as a curricula subject can bring the possibility of transmit to children the basics of technology and to teach them other kind of human and organizational values. This work presents a new program introduced in an Italian primary school thanks to the collaboration with National Instrument and Università Politecnica delle Marche. The subject of Robotics becomes part of the Primary school curricula for all the five years of education. The program has allowed the teachers training and a complete way through which children have demonstrated great learning abilities, not only in mere technology but also in collaboration and teamwork.**

Keywords— **Robotics, primary schools, innovative program.**

I. INTRODUCTION

Many researchers have been investigating the use of robots to support education. Studies have shown that robots can help students develop problem-solving abilities and learn computer programming, mathematics, and science. The educational approach based mainly on developing logic and creativity in new generations since the first stage of education is very promising. To these aims, the use of robotic systems is becoming fundamental if applied since the earlier stage of education. In primary schools, robot programming can be fun and therefore represents an excellent tool for both introducing to ICT and helping the development of children's logical and linguistic abilities. Robotic teaching experiences have been carried out in Italian schools since 2000-2001, when the first project was proposed. It was called "Building a robot" and its description can be found in [1]. Moreover, learning robots programming also becomes an opportunity for primary school pupils in order to develop their linguistic and logical skills, always focusing on pedagogical rather than technological

issues. This paper presents an innovative program developed in order to teach robotic basis at the primary school as a curricula subject. The same instruments are used as a multidisciplinary validation and motivation for other subjects (Italian, Mathematics, Science, etc…). Education in Italy is compulsory from 6 to 16 years of age and is divided into five stages: kindergarten (scuola dell'infanzia), primary school (scuola primaria), lower secondary school (scuola secondaria di primo grado or scuola media), upper secondary school (scuola secondaria di secondo grado or scuola superiore) and university (università). The Scuola primaria (primary school), also known as "scuola elementare", is commonly preceded by three years of non-compulsory nursery school (or kindergarten, "asilo"). Scuola elementare lasts five years. Until middle school, the educational curriculum is the same for all pupils: although one can attend a private or state-funded school, the studied subjects are the same. The principal are Italian, English, Mathematics, Natural Sciences, History, Geography, Social Studies, Physical Education and Visual and Musical arts.

Until 2004, pupils had to pass an exam to access the Scuola secondaria di primo grado (Middle school), during which they had to demonstrate their abilities in composing a short Italian essay, passing a Math and an oral test regarding all the other subjects. The exam was abolished, only private primary schools legally recognized have maintained it. In order to introduce Robotics as a curriculum subject during the five years of Primary school, a special program has been introduced. The global five-years schedule is divided into two main blocks: during the first two years pupils are introduced to logics and mechanical feel with remotely controlled independent machine (using Lego WeDo system); in the last three years children are asked to design, build and program their own independent robots, using Lego NXT system.

The LEGO Education WeDo is an easy-to-use robotics platform that introduces young students to hands-on learning through LEGO bricks and the easiest form of graphical programming software that National Instruments has to offer. It is a fun and simple way to get younger students exposed to

basic engineering concepts at an early age. The use of LEGO Education WeDo provides a hands-on learning experience that actively engages children's creative thinking, teamwork, and problem-solving skills. LEGO Education WeDo is a hands-on platform that primary school students can use to build simple robotics applications driven by a personal computer with a simplified version of LabVIEW. By combining the intuitive and interactive interface of LEGO Education WeDo software with the physical experience of building models out of LEGO bricks, students can bridge the physical and virtual worlds to provide the ultimate hands-on, minds-on learning experience (see [2]). The system has being applied in other countries, proposing their use in primary schools and studying the possible benefits for children education. In [3], for example, the author analyzes the first-contact situation in which 3rd grade pupils in primary school encounter LEGO WeDo for the first time. In [4], a pilot study of robotics in primary schools is described, together with motivation of choosing the LEGO WeDo for children activities: the low learning curve of the programming language (visual programming rather than code writing), and the educational content provided with it. Another project called Edurob (European project on educational robotics and cognitive disabilities) began in late February 2014, and it will involve the School of Robotics, a non-profit organization founded in 2000 on the initiative of a group of robotic and humanities researchers and several European countries: UK, Lithuania, Bulgaria, Poland and Turkey. The partners are heterogeneous, belonging to worlds that seem distant from each other: psychology, pedagogy, and engineering. The purpose of the project is to understand how to use the educational robotics to improve learning for students with different learning difficulties [5].

Recent years have seen the development of cooperation between National Instruments, Università Politecnica delle Marche and primary schools to improve the use of new technologies since the first grade of the school. National Instruments has donated LEGO WeDO kits for teaching Engineering principles to kids. In a recently well-structured project, National Instruments donated 10 LEGO WeDo kits to a non-governmental agency (NGO) in Cambodia, which will use the kits in their creative learning classes. In particular, an NI delegation traveled to the village of Chanleas Dai, Siem Reap, in Cambodia to deliver the kits to a school run by PEPY (Protect the Earth Protect Yourself, [6]), an NGO that aids rural communities in improving their own standards of living, with a focus on increasing access to quality education. Teachers were learned on how to use LEGO WeDo in the classroom and brainstorming on how to teach kids engineering concepts and how to develop solutions to engineering problems; at the same time, the WeDo kits was introduced to Cambodian students. Although they had never seen LEGO or other rapid prototyping systems before, they quickly discovered how to build models, think critically about systems, and persevere through problems. The students even learned how to integrate their different WeDo models to play a soccer game, with each member of the soccer team represented and controlled by a different program. The club could meet throughout the year to perform various engineering activities and learn about different fields of engineering beyond just robotics. After this period, student interest in the club was so great that PEPY teachers had to create an application process to manage the large number of responses. PEPY hopes that through these engineering initiatives, students and villagers can develop skills to solve problems locally and retain a sense of ownership over the solutions [7].

Both the scientific and educational communities recognize the role of ICT company investment in improving science and engineering education, engaging students with technology, and equipping educators with resources to help them teach fundamental engineering concepts in a fun, hands-on way. Specifically, the National Instruments and Lego provide interactive, real world learning experiences; low-cost and free training opportunities; a strong global mentorship program; technology and funding.

Initiatives such as K12Lab.com for primary and secondary school teachers and the NI courseware portal for university professors feature effective content that educators can use directly or adapt to their learning environments [8]. The K12Lab is a website where teachers can browse and share lesson plans, find inspiration from what others are accomplishing with technology, and get tools and support to help their students connect theory to reality faster. K12Lab users gained access and contributed to a growing library of 86 lesson plans for subject areas such as physics, robotics, and computer science. In 2011, NI expanded its mentoring efforts by deploying robotics workshops in underdeveloped areas within India, Costa Rica, and Mexico. In Bangalore, India, NI employees launched a program by conducting a workshop to mentor more than 30 students at Anatha Shishu Nivasa children's home. They used the WeDo robotics platform to teach students the basics of designing, building, and programming robots. In Mexico, NI supports a Tecnologico de Monterrey initiative called "Learning Math with Robots at Primary Schools" [9]. The long-term goal of the project is to incorporate robotics into every math program within every primary school in Mexico. This program helps all students, to experience the same level of technology access. In Costa Rica, a lab was opened at Centro de Educación Salesiana Don Bosco, which is supported by Colegio Técnico Don Bosco, a local technical high school. The project educates and trains individuals from low-income areas on the outskirts of San José. The lab is equipped with National Instruments Educational Laboratory Virtual Instrumentation Suite (NI ELVIS) hardware and LabVIEW software to give students access to the latest technology for hands-on, project-based learning. The Austin Children's Museum (ACM) creates innovative learning experiences for children that equip and inspire them to be the next generation of creative problem solvers. The ACM program, TechReach, provides students from low-income families with opportunities to gain hands-on science, technology, engineering, and math skills. Working with LEGO MINDSTORMS NXT kits, participants learn the basics of designing, building, and programming robots. The TechReach program addresses a three-fold problem for economically disadvantaged children in Austin: shortage of access to technology, the need to build 21st century skills, and the lack of interest and awareness in a science-related future [10, 11]. Another interesting experience could be found in the Lana Stone, a technology instructor, with the Govalle Primary school team partecipation on the FIRST LEGO League [8]. National Instruments recently chose to collaborate with "The Boys & Girls Club", a non-profit organization dedicated to enabling all young people to reach their full potential as productive, caring, and responsible citizens. At the clubs, youth are provided a safe place to learn and grow ongoing relationships with caring adult professionals, life-enhancing programs and character development experiences, as well as hope and opportunity. In the project, the LEGO Education WeDo has been used. The kids who attended the workshop ranged in age from 6 to 15 years old. It was clear that they had not been exposed to this type of technology before which

made the volunteer's experience particularly rewarding. Many of them had interacted with LEGOs but were extremely excited to make a LEGO robot that moved. One child was surprise at a LEGO alligator that bit his finger through the use of a motion sensor is: "It is always motivating to see the eyes of a child light up when they learn something new." It was also rewarding to watch the proud, glowing faces of the parents who were dragged into the computer lab by their kids who wanted to show off the robots that they had built and programmed [12]. In Italy, Pinocchio 2.0, an Italian project of Educational Robotics was born and has been developed. Pinocchio is in Italian children's imagination the character that recalls the idea of the robot, which is an artificial entity mechanically animated. This project promotes the exchange of information and collaboration between students of different grades and levels, allowing them to be part of an experience with a larger group [13].

Following what already done in the past by a lot of institutions and the experiences in pedagogical, technological and teaching aspects the here presented project arises from the collaboration among three principal groups of researchers from Università Politecnica delle Marche (UNIVPM), of teachers from Istituto Comprensivo Largo Cocconi and the National Instruments Company for the hardware involved in this work.

The paper will present the different aspects of the project and the preliminary results. The presentation is organized as follows: Section II describes the objectives and the expected results of the project; Section III explains the instruments and times used to realize this project, while Section IV illustrates the preliminary results, while the conclusions and future developments are illustrated in Section V.

II. OBJECTIVES AND EXPECTED RESULTS

The first and main aim of this project concerns the introduction of Robotics at the Primary school as a normal subject in the curricula besides being proposed as a lateral extra curricula activity to be performed out of official school hours. Studying and applying robotics is not only important for learning how to build or use robots, but also to develop a method of reasoning and experimentation in the world [14]. The projects wants the children to increase their capabilities, teaching them to program a machine and to consider robotics as a normal method of work rather than an exceptional way of operating. With robotics, the students can have a different opportunity for developing their logical ability and their creativity, features at the base of reasoning and critical thought. The first experimental work done in the last five years has been covering a complete Primary school cycle; it has been performed with the priority of introducing the subject ROBOTICS as a curriculum component, improving the usual Gantt of the regular Ministry plans with a new teaching theme. The subject has been involved in its Didactic years, weekly programming and the regular learning evaluation methods.

The presented scholastic program has been divided within the five years of Primary school and the new study program for each Class is proposed in the following.

The main objectives of the project are distributed as follows:

1) Class I

- Learning the roboethics concepts with the introduction of the Asimov's literature and the three robotics laws;

- Gaining knowledge of the single mechanical elements through simplified programs of ordering and planning: learning the differences among shapes, materials, colors and functionalities of the elements presented on the market;

- Planning a model using LEGO system through a simplified program;

- Understanding the model verification and validation concepts in the work environment.

2) Class II-III

- Acquiring the ability to attribute coherent purposes to a constructed robot;

- Introducing to the concept of ROBOT as a machine that must complete a specific task;

- Studying sensors and actuators through the comparison with human apparatuses;

- Introducing the software programming for the LEGO WeDo system.

- Realizing a simple robot able to interact with the environment.

3) Class IV-V

- Acquiring the ability of attributing coherent purposes to a complex constructed robot.

- Acquiring the ability of building a robot in accordance with specific and relative complex purposes.

- Planning a robot for a specific scope of research, able to live in a defined environment.

- Introducing software for robot analysis.

- Realizing a technical manual for the final operator in order to explain how to design and realize a robot.

During the quinquennial of the educational training, the main objectives are accomplished by mean of different activities.

The activities are scheduled in didactic units, different for each school year and class. Each didactic unit consist of specifics aims and skills developed in activities, increasing and pursuing children competences.

The first activity is aimed firstly at involving the children to collect the changes in the surrounding environment about the technologies development. Secondly, the same activity is focused on the relevance of practical activities, to increase curiosity, fantasy, and logic in the children. The evaluation of the accomplished knowledge is checked asking children to realize a document filled with images about different robot duties and aims useful for human being.

The second activity concerns the approach to the Robotics laws, in particular guiding them to analyze the necessity of the three laws and their connection to society laws. The purposes are educating children to social values and to have respect for others; moreover, it becomes important to underline the necessity of establishing rules that save and increase the well-being of all people. Another aim is to learn technological progress as a positive aspect in life, and to increase collaboration with other subjects giving own contribution to

the group. Practically, teachers help children to learn and to apply the three robotics laws working with pictures.

The third activity is aimed at planning and building a robot made of structured and not structured materials, using WeDo for the first two years, NXT for the third and the fourth classes and custom hardware with COTS and LabVIEW for the last year). The objective is to increase logic in the activity of materials discrimination and classification, coherently increase creativity in order to handle different materials, and try to make objects with the use of acquired skills. The children are asked to pass two final tests. The first, where the children have to correctly classify different robot pieces and a second where the children have to put in order the different parts to make a robot. Other evaluation activities are carried out in groups; each group have to assemble pieces and to build a robot.

The fourth activity concerns the training on how to program with visual development tools (mainly the WeDo and the NXT with an introduction to LabVIEW). The final aim is to give some basics about programming, using a visual framework, which is, therefore, quite simple and intuitive; at the same time, they start discovering the new functionalities made available by a computer. They learn how programming a robot and its specific functions that change according to the abilities the robot itself has to show. Then it is important to stimulate children to think about personalizing the robot program. The skills developed with this work are the comprehension and the execution of deliveries and instructions for understanding and communicating own experiences in clear way, being able to use computer and graphic programs and lastly to attribute purpose to an object. This work is aimed at understanding the single blocks during the elaboration of the program realized. The teacher supports the children when they have difficulties during the software production, or they can be tutored by classmates.

The fifth activity aims at building and programming a robot, according to specific aims: examination of the robot skills, classification of building pieces, robot software production and check of robot work. This project is aimed at getting pupils confident with materials manipulation, stimulating their curiosity, dealing with new challenges. Moreover, it is important to transmit the feeling of group spirit and working together towards a common goal. This activity helps children to understand how to solve a problem or mistakes in their work by finding alternatives, and at the end to understand the necessity of respecting the three laws of robotics in building and programming robots. The final test of this activity wants to verify how the children create the Robot according to the assignment. They are required to produce a text where the process is explained. The above composition can be done individually or collectively.

The last activity involves the elaboration of fantasy texts in which the protagonists are the constructed robots. The aims are: collaborating with classmates, bringing positive contributions to the group, learning to accept other people ideas, to respect differences, understanding the necessity of rules that safeguard the well-being of everybody and finally increasing creativity and fantasy through the production of a coherent text. The enhanced skills are instead to understand and to execute deliveries and instructions, communicating own experiences in clear way, interacting in a conversation through questions and narrating direct experiences, observing and confronting.

These scholastic activities will emphasize the importance of the prefixed objectives for children and it is very important

stimulating logic and ability of analysis. The continuous exercise encourages them to stimulate the curiosity in specific cognitive instruments, to reinforce the abilities to attention and concentration and to observe experiments with the use of the scientific method.

III. INSTRUMENTS AND TIMES

The time established for these activities is placed within the "hours for the optional disciplines" established by Ministry in the regular timetable weekly magazine of the curriculum activities. The plan include didactic trips, beginning from second-third class of the primary school, inherent to the programmed activities, in science museums or research institutes, where the pupils will be involved in more specific workshops about mechatronics and robotics.

The hardware and software involved in this project for the children training include five kits of LEGO WeDo® (Fig. 1) for the first and second classes, five Kits LEGO MINDSTORMS® NXT (Fig. 2) in the other classes.

Figure 1. Lego WeDo® kit and the relative software

Figure 2. LEGO MINDSTORMS® NXT kit and the relative software

Università Politecnica delle Marche, LEGO Education and National Instruments together provide the framework for learning how to systematically and creatively solve problems. This means understanding key science, technology, engineering and math concepts. The UNIVPM, LEGO Education and NI platform helps teachers with the power of robotics, useful to create learning opportunities for students for developing the skills like creation, problem solving and contribution to a global society.

National Instruments and LEGO, sharing a vision of inspiring creativity and innovation in children, have already collaborated to develop the next generation of LEGO MINDSTORMS® - programmable robots that are smarter, stronger, and more intuitive. Starting from LabVIEW, graphical system design software used by scientists and engineers, a more user-friendly desktop software has been developed which turns any LEGO MINDSTORMS® Education set into a full-feature science and engineering learning station, preparing students for high grade school, university courses and engineering careers where LabVIEW is already used. LabVIEW for LEGO MINDSTORMS® is the most advanced software environment for programming the NXT. LEGO MINDSTORMS products take maximum advantage of NI's world-class software for their latest hardware innovations, delivering LabVIEW software to applications spanning from kindergarten to rocket science. The WeDo Robotics Construction Set is a set of pieces and mechanical parts that can be used to build robots. The WeDo is designed to teach simpler concepts to slightly younger kids, and it uses many recognizable Lego pieces. The WeDo Software allows programming the robots, controlling its actions, sounds and responses. All the programming is drag-and-drop; just line up programming blocks to tell the robot what to do. The educational training is focused to a specific knowledge of the robotic subject and the base language for programming its functions. The teachers also will gain these specific competences, so they will be modernized on the topic of computer science, industrial and theoretical robotics. Educational developing meetings with the teachers about the construction of activities for the pupils in the class will be scheduled.

IV. PRELIMINARY RESULTS

Preliminary results are based on activities described in the second Section, carried out in a given period of time. The proposed criteria have been able to teach new concepts to children, to attribute coherent purpose to a constructed robot, and to teach the roboethics with the introduction of the Asimov's three robotics laws. Selected groups of professional operators will have also invited to attend and to take part to intermediate tests and experiments.

The first experimental Robotics subject has been taught in the Istituto Comprensivo Largo Cocconi in Rome – Italy. Primary school teacher Mariantonietta Valzano and university professor David Scaradozzi developed the experimental project after their observation about primary pupils. They focused the project on increasing and pursuing logical and creativity, just because these are educational skills in modern school. Then the pilot project started four years ago in the mentioned school.

During the project, a responsible role has been assigned to one teacher of the Primary school (Mariantonietta Valzano). Her main role has been the definition of educational objective, the localization of the learning strategies, and the organization of formative activities with the pupils involved. The second person involved in the project is Cinzia Vergine as adviser of didactic activities, with the role of controlling the participation to these learning strategies. She has been responsible of formative activities with the pupils. The third person involved has been David Scaradozzi, as the technical designer supervisor. He has studied and developed the technical instruments and he head the technical training for teachers and pupils.

Actually, at the middle of the fifth year, the preliminary results concerns:

- Definition of educational objectives;

- Creation of strategies to learn;

- Planning of formative activities with the pupils in classes;

- Planning of the times to release software, hardware and technical training for the teachers.

- Verification and validation of the didactic program

- Technical and computer science training to learn the bases of robotics.

Figure 3. Children programming with Lego Mindstorm

Figure 4. Children constructing a simple robot with Lego components

Figure 5. Children during their trip at University

Improvements registered by teachers are very relevent and have demonstrated the grate value of using robotic system in eahc aspect of teaching. Pupils have been always courious, receiping the single aspects of the training, from the pure robotic construction and programming to the importance of working together, in group, of achieving new skills, and facing new problems. Fig. 3 and 4 show some students directly involved during the practical activities, in particoular the visual programming and the mechanical construction of the robots. The last figure shows students during the planned trip to Università Politecnica delle Marche during the last year, where they were intriduced to the world of administration and learning at University, and they participated to a workshop about the LabVIEW framework. Teachers have stated positive differences in educational results if compared with other classes not involved in the project.

V. CONCLUSION

In September, the fourth year of the pilot project "ROBOTICS IN SCHOOL" has been started in the Institute Comprensivo Largo Cocconi in coperation with the engineers of the Università Politecnica delle Marche and National Instruments, who believed in the validity of the training project providing the tools used in these years.

The project allows children to get awareness of the robotic science and to develop a good knowledge of the technology they are using. Lessons are aligned with the students' curriculum. This project showed a great upgrade in the children education, in particular to develop general skills necessary in their life. The curriculum involves the entire engineer design process from ideation, to construction and implementation. This innovative way of transmitting skills revealed to be useful for all types of academic pursuits. This program helped students to develop the skills that will be necessary to be successful in the 21th century.

REFERENCES

[1] S. Merlo, "Costruiamo un robot – Il progetto e la sfida", *Rassegna Istruzione*, Volume 4, 2010-2011.

[2] LabVIEW Graphical System Design – From Kindergarten to Rocket Science, http://www.ni.com/newsletter/50596/en/

[3] K. Mayerová, "Pilot Activities: LEGO WeDo at Primary School", *Proceedings of 3rd International Workshop Teaching Robotics*, Teaching with Robotics. 2012. p. 32-39.

[4] E. Romero, A. Lopez, O. Hernandez, "A pilot study of robotics in elementary education", *10th Latin American and Caribbean Conference for Engineering and Technology*, Panama City, Panama. 2012.

[5] http://www.scuoladirobotica.it/it/Item/550/Parte%20EDUROB%2C%20progetto%20europeo%20sulla%20robotica%20educativa%20e%20le%20disabilit%C3%A0%20cognitive.html

[6] http://pepycambodia.org/

[7] NI Donates LEGO WeDo Kits to Help Teach Cambodian Kids about Engineering,
https://decibel.ni.com/content/groups/ni-news-in-real-time/blog/2010/12/20/ni-donates-lego-wedo-kits-to-help-teach-cambodian-kids-about-engineering
http://pepycambodia.org/

[8] http://k12lab.com/

[9] Mentoring Young Minds -
https://www.ni.com/company/programs/inspire/classrooms.htm

[10] http://impactnews.com/austin-metro/southwest-austin/system-design-trade-show-kicks-off,-govalle-student-to-present/

[11] http://labviewrobotics.wordpress.com/tag/austin-childrens-museum/

[12] http://austintexas.gov/sites/default/files/files/Redevelopment/CH_380_Agreements/NI/National%20Instruments%20STEM%20Investments.pdf

[13] Pinocchio 2.0: A recording methodology for vertical educational robotics experiences -
http://www.gjc.it/2012/sites/default/files/pinocchio2.0-l2-didamatica.pdf

[14] Dalla realtà all'astrazione e ancora alla realtà: la robotica a scuola come strumento conoscitivo -
http://www.descrittiva.it/calip/RoboticaScuola_Siel2010B.pdf

Levy flight search of moving objects

IARP Conference, Frascati 14-16 May 2014

Vincenzo Fioriti, Fabio Fratichini, Stefano Chiesa

ENEA, Italy

vincenzo.fioriti@enea.it

Abstract—**A Levy flight is a particular case of the random walk. Its displacements on a 2-D surface are drawn from the Pareto-Levy probability distribution, characterized by power law tails. The Levy flight search has many applications in optical material, ladars, optics, large database search, earthquake data analysis, location of DNA sites, human mobility, stock return analysis, online auctions, astronomy, ecology and biology. Although still in debate, it was suggested that predators follow this search pattern when foraging, because it avoids being trapped in a local search if the food is beyond the sensory range. Almost all studies and simulations concerning the Levy flight foraging examine static or slowly moving (with respect to the forager) uniformly distributed resources. Moreover, in recent papers a small swarm of underwater autonomous vehicles has been used to test the Levy search in the underwater environment, with good results. In this work we extend the classical Levy foraging framework taking into consideration a moving target allocated on a 2-D surface according to a radial probability distribution and comparing its performance with the random walk search. The performance metric used in the numerical simulations is the detection rate. Simulations include the sensor resolution, intended as the maximum detection distance of the forager from the target. Furthermore, contrarily to the usual Levy foraging framework, we use only one target. Results show that Levy flight outperforms the random walk if the sensor detection radius is not too small or too large. We also find the Levy flight in the velocity of the center of mass model of a fish school. Finally, a short discussion about the controversy concerning the innate or evolutionary origin of the Levy foraging is given.**

Keywords— Levy foraging; Levy flight; random walk; blind search.

I. INTRODUCTION

In this paper, we extend the well-known Levy search for fixed objectives located on a surface with uniform probability distribution. A random walk with steps (spatial displacements) from a Pareto-Levy distribution is called a Levy flight. Visually it is a set of many small displacements and just a few very large "jumps". In the Levy flight the steps are considered instantaneous, i.e. the velocity is high with respect to other motions, otherwise we have a Levy walk (finite velocity steps). It has been speculated that a Levy flight (LF) is used by predators to locate the prey, if the food is rare in the predator's

environment [1]. As a matter of fact, this claim has been criticized several times, advancing that on the field records do not confirm the Levy flight statistics, rather approximate an innate composite correlated random walks [2], [12].

Nevertheless, LF is an appealing working hypothesis for naturalists, while it is an interesting hint for technicians. Here we focus on the marine environment with explicit reference to the underwater autonomous vehicles (AUV), robots used to patrol marine areas possibly in groups called swarms.

The blind search for targets resembles closely the animal foraging and therefore one tries to apply this biological inspired methodology to optimize the search, when no *a priori* information is available.

Usually the Levy search scenario consists of a number of non-mobile targets uniformly distributed on a surface. We extend these scenarios to a single mobile target distributed according to a radial probability distribution, testing the performance of the Levy flight search and of the random walk.

II. THE LEVY DISTRIBUTION

Let us consider the Levy distribution expression [11]:

$$P_r(x) \sim x^{-\alpha} \qquad \text{with } 1 \leq \alpha \leq 3 \qquad (1)$$

Where the random variable x is the displacement (see in Fig. 1 the Levy histogram). Note in Fig. 2 some large displacements and clusters on a plane representing the foraging area. The large jumps allow a more complete exploration of the plane with respect to the random walk, (see Fig. 3).
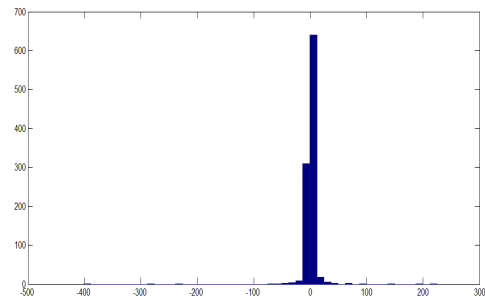
Fig. 1. The Levy flight histogram (with α =1.9 and 1000 samples).
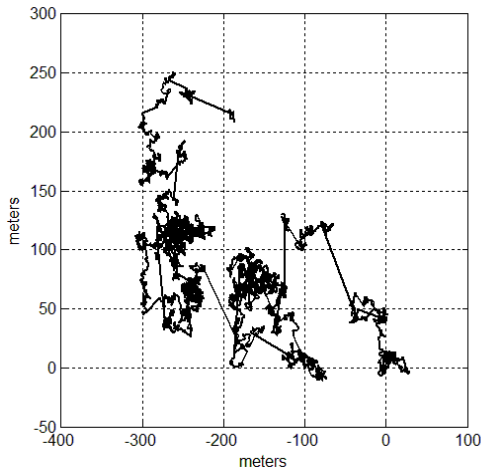
Fig. 2. Example of a Levy flight on a plane. "Jumps" are the longer straight lines connecting the cluster formed by shorter lines.

The random walk (RW) concentrates its search in a more reduced area, as the step size is constant and the direction is random.

The number of RW steps is larger than the LF case to keep a fair comparison, as the LF step is not restricted to a fixed euclidean distance.
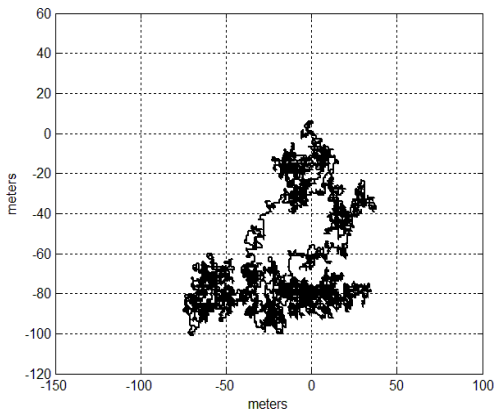
Fig. 3. Example of a random walk on a plane.

III. RADIAL PROBABILITY AND MOVING TARGET

Usually it is assumed that targets are uniformly distributed in the plane (Fig. 4), are static or moving with a speed very low with respect to the forager and no *a priori* information is available.

Although this is a common circumstance in animal foraging, it is not a unique possibility: for example, in [3] an information biased Levy flight is investigated, but in a static environment with a Gaussian probability distribution and a large number of targets. Recently, mini-AUV have been tested in patrolling activities with success [4]. The robot foraging may require a different point of view, i.e. moving targets and radial probability distributions. Moreover, targets often are reduced to just one.

These needs often arise during surveillance tasks or rescue activities in the marine environment. Sometimes it is necessary to find a target whose position is previously known to be close to a certain point, while departures can be considered less probable proportionally to the distance from the point (Fig. 5).

In other cases, targets could move inside a circular ring centered on a point (Fig. 6). More complex radial distribution are also possible, see Fig. 7.

(1)
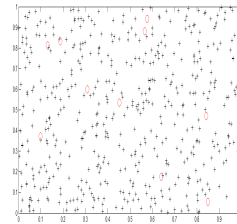
Fig. 4. Example of the classic Levy foraging; the probability distribution is uniform. The red circles are the actual multiple targets.
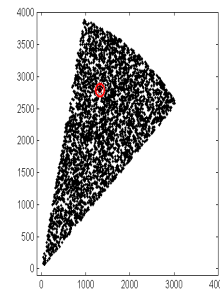
Fig. 5. The probability decreases form the Origin. The red circle is the single target.
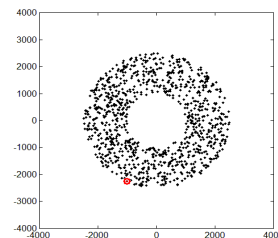
Fig. 6. Here the probability is uniform inside the ring centered on the Origin. The red circle is the single target.
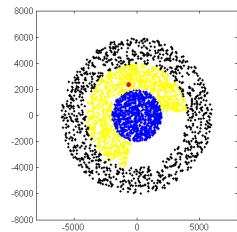
Fig. 7. A composite probability distributions; the colours indicate various uniform distributions. The red circle is the single target.

The Levy and the random walk search start from a randomly chosen point inside the allowed area. The operating autonomy is limited by the available number of steps. The velocities of the patrol and the target are not taken into consideration. Targets move linearly (Fig. 8) or along an open curve as Fig. 9, in a surface area of 400x400 meters.
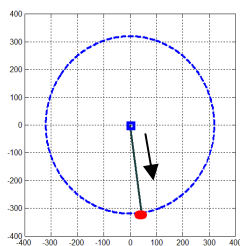
Fig. 8. From the blue square the target is directed towards a point (in red) on the dotted blue circumference, following the straight line. The search starts form a random point inside the circumference. The arrow indicates the motion direction of the single target.
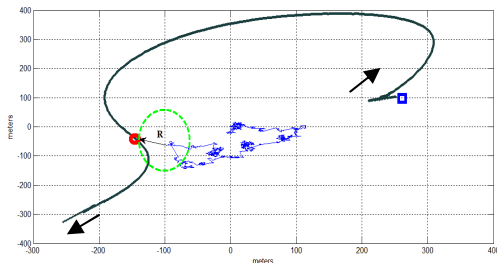
Fig. 9. From the blue square the target (the red point) follows the curve, while the search starts from a random point, in this case close to the Origin. The green dotted circle represents the detection sensor range. The arrows indicate the motion direction of the single target.

The sensor resolution, meaning the maximum detection distance of the forager/patrol from the target, is usually neglected in the simulations.

However, the same concept of locality search depends from it: when the range of detection is very large or very small, the advantages of the Levy search tend to disappear and the random search may even result a better strategy. Therefore we are interested in investigating this rule of thumb in the case of

extended Levy flights as specified before. The search is considered successful if the patrol meets the target within a radius R, see Fig. 9.

IV. SIMULATION RESULTS

For each scenario of Table I a minimum of 10000 numerical simulation have been completed to determine the successful target detection operated by the LF or RW patrol. The patroller has an autonomy of $N = 6400$ steps (but the euclidean path is the same for LF and RW). The starting point of the patrol's search has been selected randomly.

From Table I and Fig. 10, 11, 12, 13 it is clear that the Levy Flight finds the target more easily than the Random Walk search if $5 < R < 100$ m, because out of this range we have a local search and the RW is favoured. The radial probability distribution has no particular effect on the LF/RW search. This means that the detection of moving targets follows the pattern of the static case and it is even more emphasized, as shown in Fig. 13.

Therefore, the Levy Flight search of a moving target following a generic trajectory outperforms the Random Walk.

V. INNATE OR EVOLUTIONARY

The debate on the evolutionary nature of the Levy foraging has been discussed by several Authors [1], [2], [11], [12]. Note that here we refer to the term "evolutionary" in the sense of "learned behaviour".

It is not only a theoretical issue: practical implications concern how to implement the LF in the AUV driving logic. In fact, due to the complexity of the AUV motion model, the LF implementation is not straightforward [4]. In [5] this driving logic is inspired by the Central Pattern Generator (CPG) paradigm that controls the animal locomotion, but the procedure in [5] introduces errors, even in the experimental environment.

Determining that the LF in nature has been learned could direct the research of the driving logic towards cognitive models such as neural networks. On the other hand, an innate LF would imply a build-in structure, maybe a hardware device. Following the actual bio-inspired model would save time and work, but unfortunately it is unclear what the model is like.

In this paper we suggest an innate model for the LF search. Firstly, the evolutionary-cognitive alternative would require a bio-neural network to learn, at least to some extent, (1). It is a very hard task even theoretically and anyway it would be too energetically expensive for mammalians, therefore we reject it. Instead, we conjecture that the brain can be modelled as a set of non linear oscillators able to produce a LF pattern spontaneously. In [6], [7] the CPG has been modelled by the Kuramoto equation and we follow this choice, rather than [5]. Other non linear oscillator models should provide the same results, although we do not provide any formal demonstration for this assumption.

TABLE I.   SIMULATION RESULTS

Patrol search scenario	Successful search percentage / Detection Radius (meters)										
	R	1	5	10	20	30	50	100	150	200	300
Levy Flight, one static target, ring probability distribution	%	1.6		6.6	9.9			36.3		74	99
Random Walk, one static target, ring probability distribution	%	2.1		4.94	6.1			30.3		67	99
	R	1	5	10	20	30	50	100	150	200	300
Levy Flight, multiple static targets, radial decreasing probability istribution	%	7		26.5				89.5		99.9	
Random Walk, multiple static targets, radial decreasing probability distribution	%	6.21		12.7				76		100	
	R	1	5	10	20	30	50	100	150	200	300
Levy Flight, one static target, circle probability distribution	%	2.32		9				42			100
Random Walk, one static target, circle probability distribution	%	3.2		4				28			100
	R	1	5	10	20	30	50	100	150	200	300
Levy Flight, one moving target on a curve	%	1.3		6.7				41		74	100
Random Walk, one moving target on a curve	%	0.5		2.4				30		80	100
	R	1	5	10	20	30	50	100	150	200	300
Levy Flight, one moving target on a line	%	1.74		7.45				34.86		60	
Levy Flight, one moving target on a LF trajectory	%	1.64		8.17				32.86		54.4	
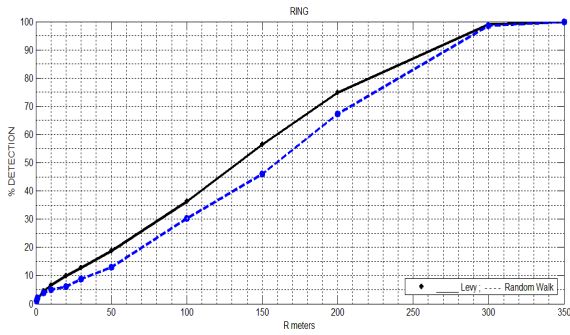
Fig. 10. Ring probability distribution with one static target.
Plot of success rates vs. detection ranges. On the right the same plot but with a logarithmic scale (LF, black continuous, RW, blue dotted).
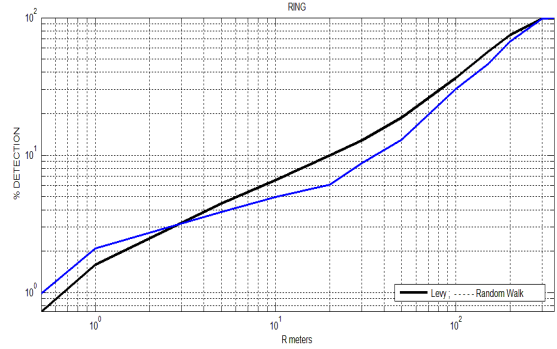
Fig. 11. Same as left, but with a log-log plot.
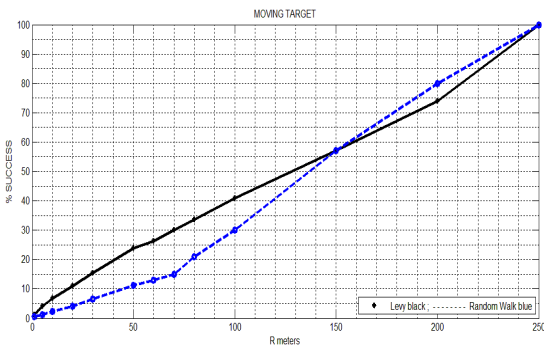
Fig. 12. Moving target, symbols as above. (LF, black continuous, RW, blue dotted).
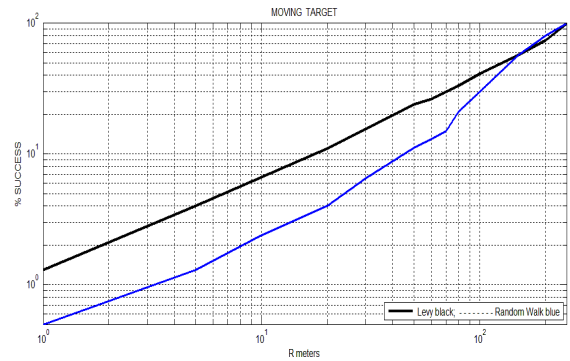
Fig. 13. Same as left, log-log plot. Levy search has a higher performance.

It has been reported that the human brain uses LF to accomplish some high level activities [11], so let us consider the brain divided in several regions as in Fig. 14. Each region is modelled as an oscillator, connected one another to form a network. While this simplification may look excessive, it may be reasonable to group the 10^{11} nodes of the net in 66 weakly coupled regions [6].

Now we show briefly how to obtain a LF statistics from this network. Each region i is modelled as a Kuramoto non linear oscillator [8]:

$$d\theta_i/dt = W_i + k/N \sum_j \sin(\theta_j - \theta_i) \qquad (2)$$

where θ_i is the i-th phase of the oscillating quantity (an electrical signal in our case), W_i the natural frequency of the i-th oscillator, k the coupling constant, N the overall number of coupled oscillators in the networks. Kuramoto showed that for $N \rightarrow \infty$ the network synchronizes the oscillations (here we have $N = 24$ oscillators).

(2) indicates the non linear reaction of each oscillator related to the rest of the network with a certain topology (see Fig. 14). (2) is widely used to describe the non linear synchronization phenomena because can be solved exactly using a complex-valued parameter (in the next expression i is the imaginary unit), called order parameter:

$$\Phi(t) = \left| 1/N \sum_j e^{i\theta_j} \right| \qquad (3)$$

When $\Phi = 1$ the synchronization is complete, otherwise it degrades to random oscillations ($\Phi = 0$). Large values of the coupling parameter k push the network toward synchronization, small k values produce a weak synchronization.

In our simulation of (2) k has a low value, in order to implement the weak coupling required in [6]. In fact, Fig. 15 shows the order parameter close to the unity, but not exactly 1.

Fig. 15, 16, 17, and 18 show the value of the order parameter and one of the N solutions of the differential system (2) in the time domain, as well as their histograms. Fig. 16 and Fig. 18 resemble clearly the Levy histogram (Fig. 18 is the histogram of the *differentiated* time series $\theta_{10}(n) - \theta_{10}(n-1)$).
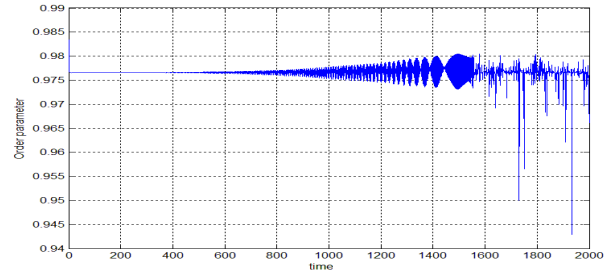
Fig.15. The order parameter $\Phi(t)$ time series oscillates around 0.96. The small k produces the loss of synchronization visible after t=1600 time units.
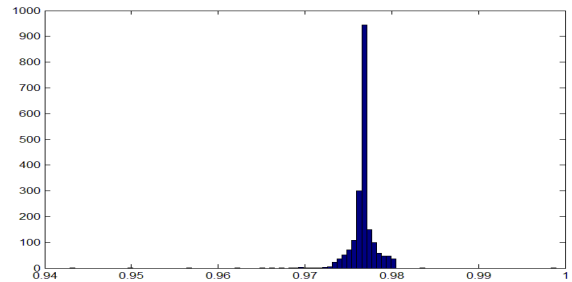
Fig. 16. Histogram of the order parameter $\Phi(t)$ time series.

Fig. 14. The brain as a collection of regions modelled by non linear coupled oscillators. The resulting network is a Kuramoto differential system, able to phase synchronize itself.
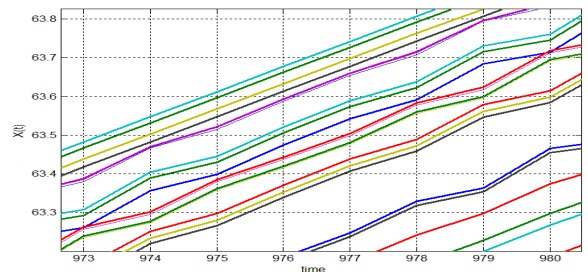
Fig. 17. All the time series solutions $\theta(t)$ of the Kuramoto equation.
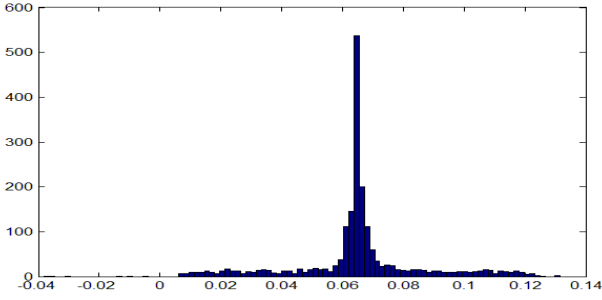
Fig. 18. Histogram of the $\theta_{10}(n) - \theta_{10}(n-1)$ time series.

Fig. 19. Simulation of the fish school 2D circular motion around a fixed center in the x-y plane. Black points are the initial positions, the green points are the final positions. Note the small irregularities of the trajectories.

Although these are only qualitative evidences, it seems that (2) is a LF generator. As a consequence, no learning is needed, thus evolution is not mandatory.

On the other hand, the innate alternative is simpler with respect to the slow and difficult learning process dependent on the local environment. Interestingly, it is also a convenient solution to the problem of generating a low-cost Levy search control in AUV robots based on simple electronic oscillating circuits.

Recently an interesting contribution to the debate was provided. In [2] Reynolds suggests that the mussels movement pattern approximate very well a composite correlated random walk (CCRW). According to Reynolds, the CCRW is a better approximation than LF to the real data.

A CCRW occurs when frequently movements with relatively short steps are interspersed with less frequent longer steps, switching between two or more patterns. These movements allow mussels to minimize the time required to form patterned beds. The same movement patterns are present in Mesozoic deep sea strata that are therefore a record of ancient organisms, persisting nowadays [2].

Although these organisms are very different from the mammalians, the innate nature of the movement pattern generation is nevertheless supported, whether it is a Levy flight, a Levy walk, a truncated Levy walk or a composite correlated random walks.

Of course it could be argued that, in a more extensive meaning, also the brain oscillating structure may result from an evolutionary process. However, the biological oscillating structure needed to produce a Levy flight bio-generator in simple organisms (such as the lamprey [9] and invertebrates [10]), is not particularly complex. Therefore evolution does not seem to play the major role, since no sophisticated mechanism was developed.

Finally, we point out that the very same Kuramoto equation (2) can model also the center of mass velocity of a
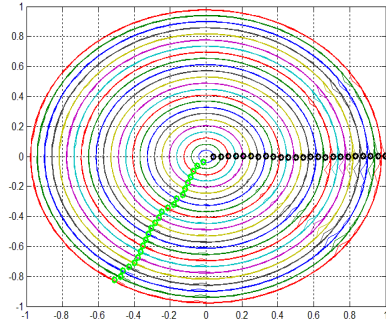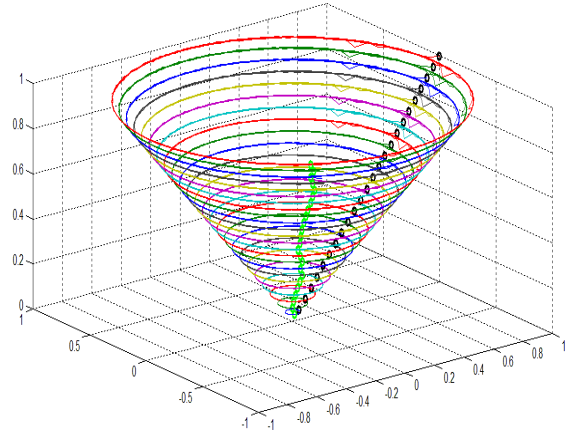
Fig. 20. Simulation of the fish school circular motion. The z-axis represents the velocity. Black points are the initial positions, the green points are the final positions. The irregularities produce the poor alignment here and in Fig. 19, depending on the limited number N of elements in the school.

fish school, as investigated in [13]. In fact, in the complex notation, the expressions of position (4) and velocity (5) of the i-th element are:

$$r_i = x_i + iy_i \qquad (4)$$

$$e^{i\theta_i} = \cos\theta_i + i\,\sin\theta_i \qquad (5)$$

It turns out [13] that:

$$\dot{r}_i = e^{i\theta_i} \qquad (6)$$

and from the expression of the center of mass:

$$P(t) = 1/N \sum_j r_j(t) \qquad (7)$$

differentiating $P(t)$ and replacing (6)

$$dP/dt = 1/N \sum_j dr_j/dt = 1/N \sum_j e^{i\theta_j} \qquad (8)$$

that is, the Kuramoto order parameter $\Phi(t)$:

$$dP / dt = \Phi(t)$$

This is the velocity of the fish school center of mass. The result seems confirmed by real fish data [13].

We have used this model to simulate the circular movement of the school with a small number ($N = 24$) of elements. Results in Fig. 19 and Fig. 20 demonstrate how actually the Kuramoto model is able to represent the basic patterns of the swarm motion as a whole as well as a single element.

Moreover, the velocity pattern follows the Levy flight statistics (Fig. 16). This means that a group of animals is able to reproduce the same Levy foraging strategy used by the single organism. The swarm or school synchronizes its movements and so doing generates something that looks like a Levy flight, at least qualitatively.

VI. CONCLUSIONS

The Levy flight search has been suggested as the animal foraging strategy, because large areas are covered with a minimum energy expenditure. Since in many technological fields similar problems are encountered, the same methodology could be used, for example in marine robot patrolling tasks.

In this paper, we have extended the Levy paradigm to one moving target with a radial pdf, considering also the detection range, i.e. the resolution of an onboard sensor. Numerical simulations confirm the Levy flight superiority compared to the random walk, if the search is in the intermediate range of the sensor resolution.

We have also shown that the center of mass of a swarm modelled by the Kuramoto equation shows a Levy flight pattern.

Finally, the controversial question of the innate or evolutionary origin of the animal foraging strategies has been addressed; regardless to the particular search behaviour (LF or RW), the innate hypothesis seems more grounded.

REFERENCES

[1] A. Edwards et al, "*Revisiting Levy flight patters*", Nature, Vol. 449, pp. 1044-1048, October 2007.

[2] A.Reynolds, "*Mussels realize Weierstrassian Levy walks as composite correlated random walks*", Nature Sci. Rep., Vol. 4, March 2014.

[3] D. Marthaler, A. Bertozzi, and I. Schwartz, "*Levy searches based on a priori information: the Biased Levy Walk*", UCLA CAM Report, 04-05, 2004.

[4] D. Sutantyo and P. Levi, C. Moslinger, M. Read,"*Collective-Adaptive Levy Flight for Underwater Multi-Robot Exploration*", ICMA IEEE Int. Conf., August 2013.

[5] J. Ijspeert, "*Central pattern generation for locomotion*", Neural Networs, Vol. 21, pp. 642-653, 2008.

[6] D. Manson, "*Characterizing Brain Activity at the Mesoscopic Scale*", 2012, http://www.ucl.ac.uk/~ucbpdma/sp.pdf.

[7] R. O. Ekeberg and S. Grillner, "*Simulations of neuromuscular control in lamprey swimming*" , Philos Trans. R. Soc. Lond. B. Biol. Sci., Vol. 354, 1385, pp. 895–902, May 29, 1999.

[8] Y. Kuramoto, Chemical Oscillations, Waves, and Turbulence, Springer-Verlag, New York, 1984, p. 164.

[9] A. Cohen, P. Holmes, R. Rand, "*The nature of the coupling between segmental oscillators of the lamprey spinal generator for locomotion: a mathematical model*", J. Math. Biol. Vol. 13, 3, pp. 345-69, 1982.

[10] D. Lamb and R. Calabrese, "*Small is beautiful: models of small neuronal networks*", Curr. Opin. Neurobiol., Vol 4, pp. 22, August 2012.

[11] A. Baronchelli and F. Radicchi, "*Levy flights in human behavior and cognition*", Chaos, Solitons & Fractals, Vol. 56, 101, 2013.

[12] A. James, M. Plank and A. Edwards, *Assessing Lévy walks as models of animal foraging,* J. R. Soc. Interface, Vol. 8, pp. 1233-1247, 2011.

[13] D. Paley, N. Leonard, R. Sepulchre, D. Grünbaum, And J. Parrish, "*Oscillator models and collective motion*", IEEE Control Systems Magazine, pp. 89-105, August 2007.

Cognitive Underwater Communications for Swarm Unmanned Vehicle Network

Marco Tabacchiera, Silvello Betti

Department of Electronics Engineering
University of Rome "Tor Vergata"
Rome, Italy
{tabacchiera, betti}@ing.uniroma2.it

Samuela Persia

Fondazione Ugo Bordoni
FUB
Rome, Italy
spersia@fub.it

Abstract— **Within underwater wireless networks, particular attention has been recently devoted to swarm networks (where mobile nodes are anyway very close one to each other) in which decisions are taken in collaborative manner. Actually, the main drawbacks of underwater acoustic networks are limited bandwidth and high signal latency. Performance improvement could be achieved by optical communications among the nodes when water conditions permit. With respect to traditional acoustic communications, that solution can lead to an increase in data rate, to the absence of signal latency and to significant energy saving. Optical communications can be viewed as complementary to underwater acoustic communications, so to design flexible integrated systems, which can exploit cognitive communication elements. In this work we want analyze the main aspects relative to performance evaluation in a swarm network with nodes that are suitable to switch the communication in optical or acoustical mode in function of many parameter and the decisions are taken in collaborative manner.**

Keywords— *Acoustic Underwater Communications; Optical Underwater Communications; Swarm Configuration.*

I. INTRODUCTION

Recently, a growing attention has been devoted to Underwater Wireless Networks (UWNs) [1,2,3]. Applications of UWN includes pollution monitoring, tactical surveillance, study of marine life, etc.. Within this context, Multiple Autonomous Underwater Vehicles (MAUVs), able to monitor wide underwater areas, are assuming even deeper interest, due to the possibility of considering them not simply as autonomous devices acting independently, but as an innovative concept of underwater swarm network, in which the robot-nodes move and take decision in collaborative manner and behave like a single robot. This novel mobile network paradigm can exploit cognitive capabilities of the swarm and inspire new applications in which collaborative intelligence of the swarm is required. More deeply, it suggests applications in which the robot-nodes decide to move together towards or within areas where an alert is activated by one of them, and an increased amount of data (i.e., pictures, video) has to be sent to a collector node (i.e., surface node). Typical UWNs use acoustical communications with considerable constraints due to limited channel bandwidth. Moreover, the temporal and spatial variability of the underwater acoustic channel leads to communication performance dramatically dependent on range and frequency [4]. The main challenge of these systems is related to the possible configurations in which the nodes are deployed, which influence communication among themselves [5]. Actually, the short distances between underwater robots in swarm configurations suggest to consider optical communication with consequent improved performance with respect to the acoustic one [6,7]. On the other hand, underwater optical communications strictly depend on water physic characteristics (i.e., torpidity, salinity, etc.). Hence a trade-off between different requirements must be achieved to select the more suitable communication system for different operative contexts. A typical benchmark for performance evaluation is the bandwidth-distance product achievable by the two different technologies. It suggests to consider acoustic communication when low data rates are required and the nodes are in monitoring configuration. When the swarm is instead in alert configuration, the nodes move very close one to each other and a lot of data have to be exchanged to take decision in collaborative manner, and thus optical communication is more recommended. The choice of using a type of transmission on the other is not only given by the type of information to be transmitted (photo, video, control), but is strongly influenced by the distance between the nodes, from the conditions of the water and from the global configuration of the whole network. This combination of factors leads to a complex decision mechanism known as cognitive communication. This paper presents a performance comparison between acoustic and optical communication systems. This study is the basis for the definition of a new pioneer MAUV robot, equipped of both acoustic and optical communication systems and able to decide, in cognitive manner, switch from one to another according to the environmental changes and applications. The paper is organized as follows: a brief introduction to underwater swarm networks in Section II, performance evaluation for acoustic and optical channels in Section III and IV, comparison between the two systems and definition of cognitive network in Section V and finally, conclusions are drawn in Section VI.

II. UNDERWATER SWARM NETWORK

The mobile network is a swarm of underwater robot-nodes, which take decision in collaborative manner for different purposes, such as:

- underwater surveillance and security;

- oceanography;
- inspective services for different application (archeology, etc).

The swarm is composed of MAUVs as shown in Fig. 1. In a case the communication is obtained through a system of two LEDs which realizes a bi-cone, while in b case acoustic communication is considered omnidirectional [7]. Aim of this study is to define a possible communication system among robot-nodes that have on board both acoustic and optical communication systems so to switch from one to another according to the different scenarios. More specifically, the main challenge is the minimum distance between MAUVs according to different operative scenarios: from 3 m (*alert situation*) to 10 m (*monitoring situation*) and consequently, the maximum information amount that can be transmitted, which depends on channel capacity and signal propagation conditions.

III. ACOUSTICAL COMMUNICATION

Acoustic communications are affected by high latency, since the speed of sound in water is five orders of magnitude lower than the speed of light. In addition, the sound propagation is affected by absorption and multipath is highly variable because the nodes are constantly moving and operate in depths of shallow water where reflections are more. This has led to adopt the M-FSK modulation format because is more robust to the effects of this channel. Moreover, since the swarm network is considered in shallow water scenarios with strong multipath effects, the acoustic channel has been assumed as affected by Rayleigh fading (RFC, Rayleigh Fading Channel). Thus, the Error Probability per symbol, P_M, can be expressed as [1,2]:

$$P_M = \sum_{n=1}^{M-1} (-1)^{n+1} \binom{M-1}{n} \frac{1}{1+n+nk \cdot SNR} \qquad (1)$$

where M is the levels number, k the bits per symbol, SNR is the signal-to-noise ratio, related to the ratio E_b/N_0 by:
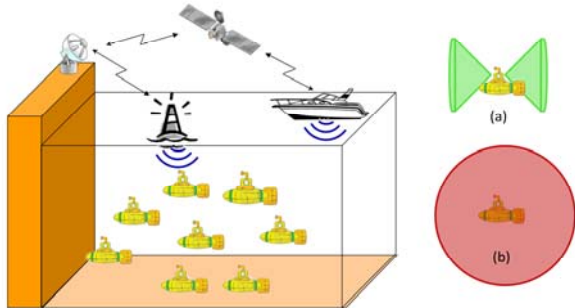
Fig. 1. Swarm system model with optical (a case) and acoustic (b case) communications.
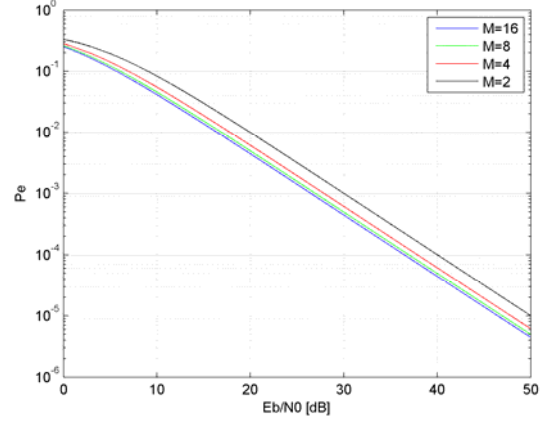
Fig. 2. Bit error probablility versus E_b/N_0 in RFC channel for M-FSK modulation.

$$\frac{E_b}{N_0} = SNR \cdot \frac{BW}{BR} \qquad (2)$$

where BW is the bandwidth and BR is the bit-rate. In Fig. 2, the error probability per bit P_e versus E_b/N_0 is shown assuming a RFC channel. For the acoustic communication system, a Reson TC4034 transducer is considered with operation frequency of 300 kHz, whose working parameters are reported in [6]. The SNR is given by [5]:

$$SNR = SL + 2 \cdot DI - (NL + BW + TL); \; [dB] \qquad (3)$$

where *SL* is the Source Level, *DI* the Directivity Index, *NL* the Noise Level, *BW* the bandwidth and *TL* the Transmission Loss. By assuming a SL of 152 dB (re 1 μPa @ 1m), the SNR for different values of M is reported in Fig. 3. From Figs. 2 and 3, an error probability of 10^{-5} requires E_b/N_0=50 dB, so that it is guaranteed for distances of *110 m* for M=16, *120 m* for M=8 and *130 m* for M=4. In addition, it was also considered the bandwidth-distance product in function of the transmitted power for different modulation format (see Fig. 4). This element is important to compare the performance of the acoustical communication system and the optical communication system described in Section IV.
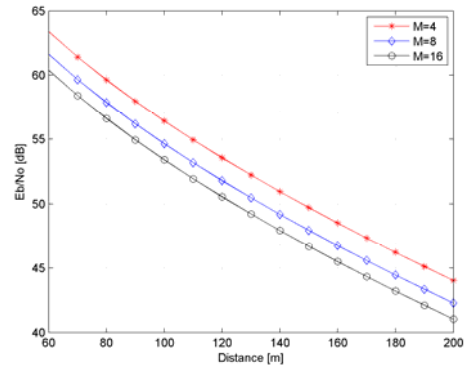
Fig. 3. E_b/N_0 versus distance for different M-FSK modulation formats.
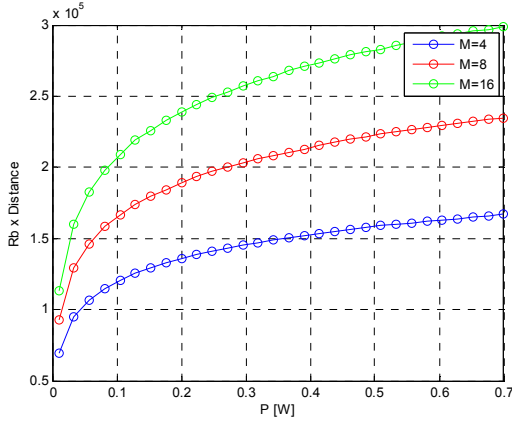
Fig. 4. Bit Rate distance product in function of transmitter power for different M-FSK modulation formats.

Fig. 6. Bit Rate distance product in function of transmitter power different types of water.

IV. OPTICAL COMMUNICATIONS

For the optical communication system, a transmitter based on LED technology is considered. Thus, each node can operate as transmitter covering a biconical volume with coupled rear-to-rear LEDs sources at the vertex and angular aperture depending on the emission diagram of the device itself, as shown in Fig.1. Performance evaluation has been carried out starting from the SNR relative to the typical underwater optical link [6]:

$$SNR = \left[\frac{P_t \cdot e^{-cr} \cdot D^2 \cdot \cos\Phi}{(\tan^2\theta) \cdot 4r^2 \cdot NEP} \right]^2 \qquad (4)$$

where P_t is the transmitted power, θ the half angle transmitter beam width, K=c/3 the diffuse attenuation coefficient, which typically ranges from 0.02 m^{-1} for the cleanest water, to 0.8 m^{-1} for the more turbid coastal water, c being the beam attenuation coefficient, r is the optical link length, D the receiver aperture diameter, Φ the angle between the receiver optical axis and the line-of-sight between

Fig. 5. E_b/N_0 versus distance in optical underwater channel for different types of water.

transmitter and receiver, NEP is the noise equivalent power [6,7]. For a typical optical communication system based on OOK modulation format, the bit error probability P_b versus E_b/N_0 is a typical Marcum function and a bit error probability $P_b =10^{-6}$ requires a value E_b/N_0=16 dB. Signal-to-noise values for different types of water, for a transmitted power of 500 mW, are shown in Fig. 5: Pure Sea Water, (K=0,0025), Clear Ocean, (K=0.0037), Coastal Ocean (K=0.22), and Turbid Harbour (K=0.8) are considered. The maximum distances achievable between swarm nodes are: 66 m for Pure Sea Water, 51 m for Clear Ocean, 13 m for Coastal Ocean and 4.5 m for Turbid Harbour. Fig. 6 show a bandwidth-distance product in function of the transmitted power referred to difference water conditions. Fig. 7 show a comparison between acoustic and optical systems, referred to difference water conditions. As far as water conditions permit acceptable operation of the optical system, its bandwidth-distance product turns out to be higher, up to one order of magnitude. Anyway, in case of turbid water, the optical system performance rapidly decreases [7], and the acoustic signaling remains the unique reliable transmission technique, although at low bit-rate.

V. COGNITIVE NETWORK

The limitations of acoustic and optic propagation are then subject to many conflicting requirements that have prevented so far the development of an ultimate solution capable of providing a suitable answer to the needs of the underwater application domains. Acoustic communication permits to work regardless water conditions with very low performance on the hand; optic communication permits to reach high performance in terms of data rate and power consumption even if the dependence with water condition is strictly closed on the other. To overcome these limitations and enable the development of suitable solution, we propose the joint application of the two complementary technologies. The complementary features of the two technologies provide more degrees of freedom and enable the swarm to adapt to the specific requirements of the applications. More deeply, we consider nodes equipped of both acoustic and optic module.

They use acoustic channel to share information among the network, and after by measuring proper
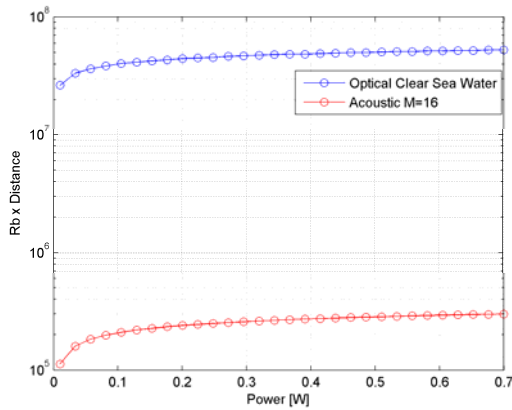
Fig. 7. Bandwidth-distance product versus transmitted power (optical communication in Clear Sea water and acoustic 16-FSK modulation format).

water parameter (i.e. turbidity) they can decide to switch in optic one to deliver data into the network. This attitude requires a new concept of swarm: the cognitive network for which all nodes share information about environment condition and decide to change channel communication. Generally, a cognitive network is a network able to make a cognitive process to perceive current network conditions, and then plan, decide and act on those conditions. The network can learn from these adaptations and use them to make future decisions. This novel approach requires the definition of new algorithms to manage complex cross-layer optimizations: high data delivered to obtain high network performance of the swarm, low power consumption to preserve lifetime of the swarm. Hence, the main issue to define a suitable underwater swarm cognitive network is to evaluate how much information regarding network state is necessary to take local decisions. In the next future we analyse the amount of the control data needed to introduce in the network without impact on swarm performance (i.e. power consumption, activities of nodes in control state, etc.).

VI. CONCLUSION

A comparison between acoustic and optical communication systems for underwater swarm networks is presented. With limited power levels of swarm robot-nodes, acoustic systems permit to operate at distances up to 300 m, with data rates up to several tens of kbit/s. Optical communication systems can work at much higher bit-rates, up to tens of Mbit/s and higher, but covering considerably lower distances which, anyway, do not represent a severe constraint for underwater swarm configurations. The results suggest a "novel" swarm concept, based on MAUVs equipped of both optical and acoustic communication systems and able to switch from one to the other according to water physic parameters, which are anyway measured and processed by robot-node on board sensors. To reach this new concept of nodes investigations about the amount of control data is needed to share among nodes is required. In the next future we analysed the tradeoffs between operating "in ignorance" and in the case of disseminating information throughout the network in terms of swarm performance such as power consumption of the swarm.

References

[1] E.M. Sozer, M. Stojanovic, J.G. Proakis, "Underwater acoustic networks," Oceanic Engineering, IEEE Journal of, 2000, vol. 25, pp. 72-83.

[2] I.F. Akyildiz at all, "A survey on sensor networks," Communications Magazine, IEEE 2002, Vol. 40, Issue 8, pp. 102 - 114.

[3] I. F. Akyildiz, D. Pompili, T. Melodia, "Challenges for Efficient Communication in Underwater Acoustic Sensor Networks," ACM Sigbed Review, vol. 1, no. 2, July 2004

[4] Andrew C. Singer, Jill K. Nelson, Suleyman S. Kozat "Signal Processing for Underwater Acoustic Communications," Underwater Wireless Communications, IEEE Communications Magazine, January 2009.

[5] M. Tabacchiera, S. Persia, E. Marchetti, and S. Betti, "Configurations effects over swarm underwater acoustic network performance," SENSORCOMM, The Sixth International Conference on Sensor Technologies and Applications, 2012.

[6] J.W. Giles and I.N. Bankman, "Underwater optical communications systems – part 2: Basic design considerations", IEEE Military Communications Conference, 2005.

[7] M. Tabacchiera, S. Persia, P. Cidronelli, and S. Betti, "Routing Optimization for Underwater Optical Networks in Swarm configuration," Microwave And Optical Techonology Letters, Vol.56, No.1, January 2014.

Large underwater swarm communication: high priority reaching of target areas via a shortest path approach

Stefano Chiesa, Claudio Moriconi, Claudia Snels
UTTEI-ROB ENEA C.R. Casaccia
Rome, Italy
name.surname@enea.it

Abstract— **In large and dense underwater swarms of AUVs, the broadcasting of even very short messages should be limited because of the features of the acoustic transmission channel often slow and unreliable. In this context we developed a collision free communication protocol tailored on the case where a single AUV needs to send a message to a specific subset of swarm members about perceived danger. The protocol includes a handshaking procedure that creates a silence region before the transmission of the message obtained through specific acoustic tones out of the normal transmission frequencies or through optical signals,. This region will include all the members of the swarm involved in the alarm message and their neighbors, thus preventing collisions from them. When an AUV sends a message to a target area, it computes a delay function on appropriate arcs and, on the resulting subnetwork, it runs a Dijkstra-like algorithm obtaining a multicast tree. Building the shortest path tree it iteratively checks if the tree itself introduces collisions between nodes and, if the case, it schedules the transmission on conflicting nodes and consequently updates the delay function on the arcs. The whole building of this collision free multicast tree is explained in details and preliminary simulations results are shown.**

Keywords—swarm robotics, underwater networks, dense networks

I. INTRODUCTION

Underwater swarms are usually formed by few vehicles and the relative communications are usually simple and relatively rare. The research that we considered is based on a different case that represents the final target of our research: the realization of a dense mobile network characterized by short range (typ. 5-10 m. of internodal distance), multihop and high speed communication capabilities. During our work we have proven that this kind of network can be physically realized maintaining the cost of the whole system compatible with practical applications. The use of a large number of very low cost vessels can have significant advantages on the few, much more sophisticated and expensive, vehicles that are the current market reference in all of the cases where the monitoring/surveillance of a wide area in short times is the main target of the mission and when a significant interaction between surface and submerged agents is important. In fact, apart the advantages and disadvantages relevant to specific functionalities, one of the most important issues is that the availability of a high speed communication network, distributed on a large volume can allow a real time communication with the multibody system and therefore a direct control "during" the mission.

Nevertheless, such a kind of mobile network can exhibit significant problems when absolute priority messages must be sent to far areas of the network. The reasons are mostly relevant to the limitations of the physical channel that implies very long times for each hop because of the high competition caused by the "swarm" operation. This study, carried out with the purpose to cope with this specific problem, is part of a larger research activity that has the objective to define how far and in which times an information can arrive in a large, multihop network to still allow a real time response. We called this locus the "knowledge horizon".

In the paper anyway we will not discuss the Knowledge horizon problem (see a preliminary discussion in [1]) but we will focus on the alarm transmission. It represents often a trade-off between the mission success and the failure of the system so that an efficient solution has been proven to be mandatory.

II. MODELING THE PROBLEM

Suppose that an AUV perceives a threat for a target subset of the swarm which is far from it (i.e. it cannot directly send a message to all members of the subset avoiding forwarding). Clearly this AUV, that we will further call source (denoted with s) has to send an alarm message to the subset in such a way that:

1. The message arrives to all the members of the target set.

2. The message arrives as fast as possible to all the members of the target set.

We also assume that the message is sent by an acoustical channel.

Requirement 1 in our experience usually imply the need for a deterministic communication protocol (and in particular a

deterministic MAC). We underline that in most practical cases deterministic MAC protocols in the framework of large underwater swarms of AUVs are not a good solution if associated to every kind of messages, mostly for the high delay introduced by approaches like TDMA or the technical challenges introduced by CDMA approaches with narrow bandwidth and Doppler effect [2].

In the following we are going to propose a model to tackle requirement 2. First of all we need to specify the assumptions under which we develop our model. We will assume that we can treat our set of embodied agents and the communication network between them as a static network. However mobility of the AUVs (and their specific dynamics) is considered when a node perceiving a threat has to determine a subset of nodes that will be affected by the threat.

Every agent is identified with a node of the network and two nodes u and v are connected by a directed edge uv, or more simply an arc uv, if u can communicate with v. In order to maintain maximal flexibility we maintain directions, because it may be possible that u can communicate with v but v cannot communicate with u.

The assumption of a static network is justified by the fact that in dense networks of AUVs the mobility of the agents is not very relevant with respect to the transmission speed (time of flight, duration of the data transmission) in the selected channel.

Finally we assume that each node of the network knows the positions of all the other members of the swarm, the approximate amount of delays (introduced by noisy transmission of data, by the MAC protocol and by the chosen modulation scheme), the average number of retransmissions required for a packet of length L, and the capacity (i.e. the bit rate) available on each connection of the network.

Given all the assumptions, we reasonably suppose that the source (and every other node) can associate to each arc e of the network a delay function $\tau(e)$. Moreover to each arc of the network is associated a capacity (or bitrate), that we denote with $c(e)$. Let us indicate with P a directed path as defined in [3]: we associate with P its delay and its capacity $\tau(P) = \sum_{e \in P} \tau(e)$, $C(P) = \min_{e \in P} c(e)$. We observe that given a path P from a source to a member of the target set v the time necessary for a packet of length L to reach the destination can be expressed as $\tau(P) + L/C(P)$, where the second term $C(P)$ accounts for direct transmission. Hence in order to satisfy requirement 2 we may simply find a path P from s to v that minimizes $\tau(P) + L/C(P)$. This problem is known as finding the quickest path from s to v and was introduced by Chen and Chin in 1990. The problem is polinomially solvable in time $O(|A|^2 + |A||N| \log |A||N|)$ (where A is the set of arcs of the network we are considering in the algorithm and N is the set of nodes) [4, 5] when we fix the packet length L, and the algorithm requires the transformation of the original network in an auxiliary network without capacities where Dijkstra's algorithm [6] is run. The quickest path problem has also being analyzed by Chen and Hung in 1993, where they solve the problem for every pair of vertices in the graph in time $O(|A||N|^2)$ [7, 8], without requiring any graph transformation. We observe that even if one would like to solve the problem from a single source to multiple sinks, in the worst case he needs the same computations performed by the algorithm of Chen and Hung for the all pairs problem.

As Chen and Chin interestingly observe, the term $L/C(P)$ prevents us from using a Dijkstra like algorithm, because it does not hold true that "parts of a quickest path are quickest paths". In particular this means that when we find a set of paths from a source to multiple destinations, in general this set cannot be reduced to a tree, as it happens for shortest paths.

In a first approach, for the sake of simplicity we assume that every arc e has the same bit rate or capacity that we denote with C. This assumption can be realistic when the packet length L is small compared to the bit rate of every arc and also in every practical framework where the only reliable bitrate information is the peak bitrate (which is uniform in a network where every AUV has the same modem). In this case we want to minimize $\tau(P) + L/C$ where L/C is a constant, that is we can find a shortest path (in terms of delays) from s to v. As all the transit times are non-negative we can use for shortest path computation the algorithm of Dijkstra. Doing this for every source-destination pair we end up with finding a shortest path tree via the Dijkstra's algorithm, where s is the root, and the set of nodes considered could be the entire network or a subset of it, selected by the source through its sensing of the threat.

We finally recall some basics about the Dijkstra's algorithm. First of all in this case we can use it because our weight function is non-negative. Dijkstra's algorithm visits the vertices of a network according to a potential function built during its execution. This potential function is associated to every node and at the beginning of the algorithm is 0 for the source and a very high value (ideally infinity) for every other node. At run time the potential function associated to a node represents the currently shortest time to reach that node. At the end of Dijkstra execution, when every node has been visited, the potential function of a node v, that we will further indicate with $p(v)$, will represent the shortest time to reach v with the alarm message

III. Building a collision-free multicast tree

In section II we have described a simple model for the quickest delivery problem. In order to give appropriate weights to the edges and in order to treat the problem deterministically we have to tailor a specific MAC and routing protocol in the same framework. We remind here that we want to build a collision-free protocol, because in a slow channel collision and retransmission modes are time consuming and unpractical.

A. Signaling procedure

When an underwater swarm of vessels is in a normal cruising mode, all the members exchange each other various kind of messages, mostly about positions, velocities and data

coming from internal and external sensors, but also commands and long sensing datasets. When an external threat is perceived by the source, the first thing the source should do is to silence its first and second neighborhood in order to avoid collisions on its neighbors.

In the following we describe a simple signaling procedure that aims at creating a silence area around the transmitter(s). The main feature of this procedure is that it has to be performed on a different channel then the one used to transmit messages, it does not interfere with messages transmission and reception, and two signaling messages do not collide each other (i.e. who receives can still distinguish that it has received a signaling message of a certain type). As an example we can think of optical signals, i.e. "colored" light flashes generated by suitable leds. Two different signaling signals will have two different colors. Note that color is just a practical scheme to think about: we could use two different flash sequences or more suitable markers. Also note that light signals can only be adopted in "dense" swarms; in less strict distance requirements only low frequency pure acoustical tones could be adopted.

We start describing the procedure for the source:

1. s sends a first RTS signal and waits an appropriate time before starting the transmission of the alarm message.

2. All the neighbors of s receiving the RTS will not start transmission of new messages (they just finish their ongoing transmissions if the case).

3. All the neighbors of s receiving the RTS send a CTS signal after finishing the ongoing transmission if any.

4. Upon reception of the CTS signal, the second neighborhood of s acts like the neighbors of s in step 2.

In step 1 the source indicates that it has the need to start the transmission of the alarm message and warns its neighbors. In step 2 the neighbors of s silence themselves in order to properly receive the alarm message and in step 3 they warn their neighbors in order to avoid collision upon multiple reception. In step 4 the second neighborhood of s silences upon reception of the CTS signal in order to avoid collision for multiple reception at the first neighborhood of s.

A final note about how much s has to wait: suppose the maximum packet length admitted on the network is P_1, then s has to wait

$$2\tau + 2\,d^1_{max}/c + 2\,d^2_{max}/c + 2\,P_1/10\ Kbit/s$$

where tau is the transmission time of the RTS and CTS signal, d^1_{max} and d^2_{max} are the distance between s and the most far first neighbor and s and the most far second neighbor respectively, c is the speed of sound in water and R is the bitrate.

For what concern the first neighborhood of s, every node has to wait until it receives the alarm message, whilst the second neighborhood has to way until it receives a new RTS signal or a timeout.

Once s has completed this signaling procedure it sends the alarm message, which will not collide with any other message due to the signaling procedure. The neighbors of s that are in the shortest path tree (which is sent together with the alarm message) have to forward the message. Before doing this each one of them starts the signaling procedure, with the only difference that they have to wait before transmitting the alarm message a shorter time, because their neighbors are already silent due to step 4. In particular they have to wait a time

$$2\tau + d^1_{max}/c + 2\,d^2_{max}/c + P_1/10\ Kbit/s$$

B. Communication Protocol

Suppose s has to send an alarm message to a target area. The steps it has to perform are:

- Select an appropriate region where the message has to go in order to arrive to the target area (mainly using simple geometrical criteria).

- Using the last available data and the number of AUV in the selected region compute the length of the alarm message and the delay function on the edges of the network; the delay function will include the time spent by each node running the signaling procedure.

- Run a Dijkstra-like algorithm on the network.

- Append the computed shortest path tree and the potentials of each node to the alarm message, this step is crucial for "smart forwarding".

- Start the signaling procedure.

- Send the message.

Next we have to specify the protocol rules for every other node different from s in the region selected by s. In the following we will indicate with *leaf* a node of the tree that has indegree 1 and outdegree 0. In other words a leaf should be a node in the target set that does not have to further forward the alarm message. When we will say that two nodes are at the same level of the tree, it means that they have the same distance in the tree from the source s in terms of number of hops.

The base protocol rule describes what should be the behavior of a node v receiving an alarm message:

1. If v does not have any neighbor at the same level then it must forward the alarm message.

2. If v has a neighbor at the same level, say u, and $p(v) > p(u)$, then v has to wait one round time before transmitting. If the cardinality of the set U of the neighbors at the same level is σ then v has to wait σ round times.

3. If v has a neighbor at the same level, say u, and $p(v) < p(u)$, and this holds for all the other neighbors at the same level if any other, then v must forward immediately the alarm message.

4. If v has a neighbor at the same level, say u, and $p(v) = p(u)$, then the node with smaller third position coordinate will transmit first, the other will wait one round time.

5. Every node forwarding an alarm message must start the signaling procedure and indicate itself as the source of the message it is sending.

From the signaling procedure we obtain for each node collision avoidance with respect to its predecessor and its successors (both at the transmitter and at the receiver). Nevertheless, just with this rule, collision could still be possible for nodes at the same level of the tree. In order to avoid this, we have designed rules 2, 3 and 4 that describe what we call a *turnation rule*. In next subsection we explain in details how this rule has to be correctly integrated inside the Dijkstra like algorithm. Finally, rule 5 is simply a parity-breaking rule, any other parity-breaking rule could be implemented.

C. Turnation Rule

We recall that the algorithm of Dijkstra selects the next node to visit as the one with the smallest potential. This means that, if we fix a level of the network section determined by the source s, the first node that will receive the alarm message is exactly the first node of that level selected by Dijkstra's algorithm.

We can exploit this property in the following way. First we append our network from s, and we run a BFS; in this way for each node we know the distance from s, i.e. its level. When a node v is visited during Dijkstra's algorithm, then we check if there are neighbors of v at its same level that have not been visited yet; if this is the case we modify the weight of all the edges going out from these nodes to the next level of the network. The rationale behind this is that all those nodes have to wait the transmission of v, and we include this waiting time in the weight function on the edges. The quantity that we add to each edge is

$$d_{max}/c + A/10\frac{Kbit}{s} + \delta$$

where d_{max} is the distance between v and its most far neighbor at its level, A is the length in terms of bits of the alarm message, while δ is a small quantity of choice.

The standard Dijkstra's algorithm visits each node once, but in the approach we are proposing we change the edge weights during execution, so that we need to do a little preprocessing after the BFS. In particular we remove all the edges going back to the source s, that is we remove for every $2 \leq k \leq K$, all the edges going from level k to level $k-1$. We underline that this procedure could delete some paths, but reasonably these paths are not interesting as they do not promote the forward propagation of the alarm.

Finally we observe that this weight augmenting procedure is coherent with rules 2, 3 and 4 (and the parity has to be broken in the same way), and what we have called there *round time* is exactly the quantity we are adding to the weight of each appropriate edge.

D. Pruning

After the running of the Dijkstra like algorithm, we obtain a tree, which includes all the nodes selected at the beginning by s. If some of the leaves of this tree are not included in the target area, we may delete them from the tree and iterate this procedure until all the leaves of the tree are in the target area. This pruning could be effective if for example s makes a very rough selection of the area interested by the transmission of the alarm. As a consequence of deleting all these nodes, we can save bytes in the length of the alarm packet A, because it contains all the names and potentials of the nodes in the tree. On the other hand all the components of the delay function are computed considering the original number of nodes, so we are really not going faster than in the case the pruning is omitted, but we know that the waiting times are more safe and maybe we can benefit for this also in terms of mobility (i.e. if two nodes are more far than we thought we may still be safe because the nodes are waiting a little bit more than necessary).

IV. PRELIMINARY SIMULATIONS

In order to assess the efficacy of our algorithm, we performed several simulations. We assume the source AUV *s* knows the positions of each element of the swarm. We restrict our attention to the case the target is a subset of the entire swarm and the source node is outside that target. The target set consists of all the AUVs that belong to an ellipsoidal volume defined by *s* in the world reference frame. We now present and discuss the results collected during the execution of the following three interesting settings.

In the first one a formation composed by 100 AUVs is arranged on a spherical flattened volume. The source node is located on the opposite side of the swarm with respect to the target set, which includes 12 nodes. The paths computed by the algorithm running on the source node are show in Figure 1. The nodes involved in signaling procedure are highlighted in Figure 2 and they are approximately the half of the entire swarm (57/100) whilst the multicast tree has 25 nodes (i.e. the silence area approximately involves two times the number of nodes in the multicast tree). We can therefore observe that in this case the protocol seems effective, in the sense that This alarm transmission does not affect communications over the remaining part of the swarm.

In the second simulation a formation composed by 50 AUVs is located on an ellipsoidal volume. The source node is located approximately in the middle of the swarm. The paths computed by the algorithm running on the source node are show in Figure 3.
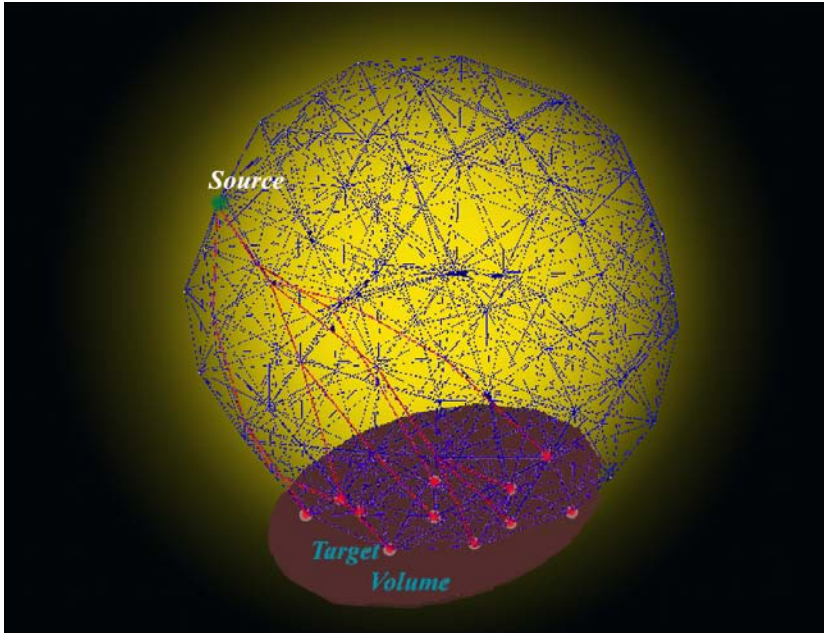
Figure 1. Source node s wants to communicate an alarm message to a target set located on the opposite side of a swarm consisting of N=100 AUVs arranged in a spherical flattened formation.

Figure 2. Nodes involved in signaling procedure are highlighted.
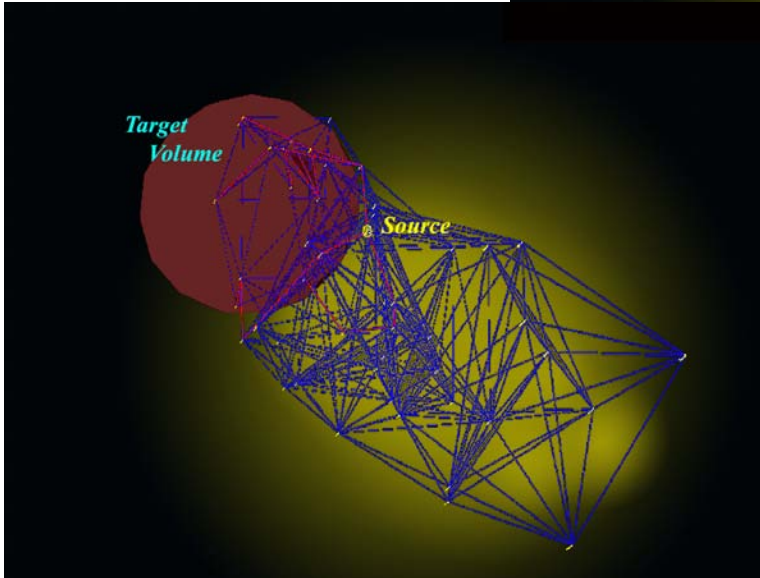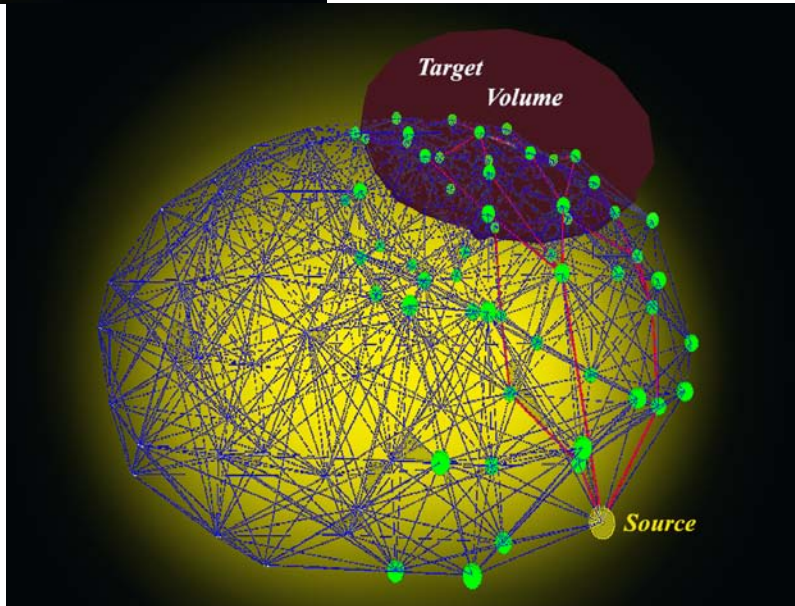
Figure 3. Source node s wants to communicate an alarm message to a target set located on the rear of a swarm consisting of N=50 AUVs arranged in a ellipsoidal formation.

In the third setup we decreased the amount of AUVs placed on a spherical volume, in order to graphically understand how much every single step of the algorithm is effective.

In Figure 4 the graph representing the swarm communication links is depicted. In Figure 5 we show the multicast tree computed by the algorithm.
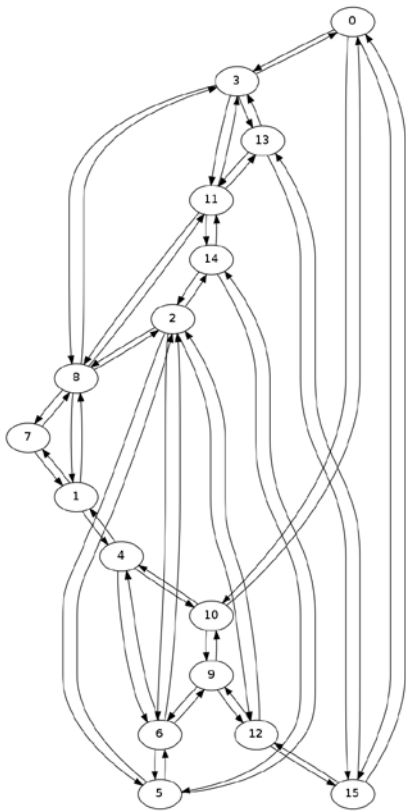
Figure 4. The graph representing the swarm communication links between nodes.

Figure 5. The multicast tree computed by the algorithm in a 16 AUVs scenario. The source node with id=12 wants to trasmit an alarm message to a target set composed by nodes 1, 7 and 10. On the edges involved in alarm retrasmission, propagation delays are diplayed (in seconds).
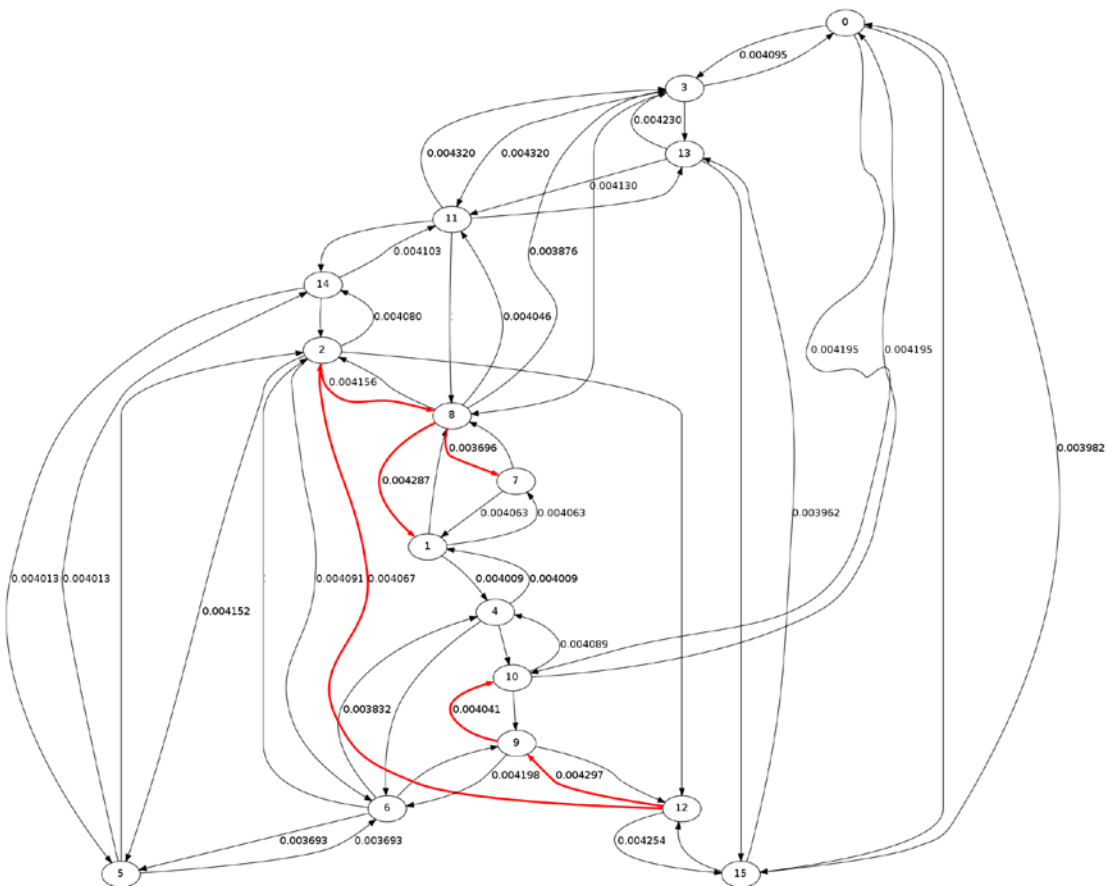
V. CONCLUSIONS AND NEXT STEPS

The work shown in the paper was quite promising in terms of possibility to transmit high priority messages along a mobile wireless network characterized by a variable configuration. We expect that the modems that have been already developed by our research group will be able to implement and test (in a very small scale) the operation of the algorithm and to tune its parameters.

More in general, as anticipated in introduction, the whole research is a job that is expected to span on a several other months: we need to verify the efficiency of the physical protocol in real conditions also adjusting many variables like guard times, power versus distance and others; in addition we need to investigate the efficiency of the simulated system when the motion of the nodes becomes a non negligible variable of the configuration. This can happen when the number of the hops and of the relevant weight (total delay) in Dijkstra algorithm can be compared with the time requested to one or more of the boundary vessels getting out or coming in to the alarm target zone.

In addition the project is now studying and developing an integrated optical-acoustical communication network. Depending on the performances and the characteristics of the optical communication transceivers under realization, the acoustical alarm transmission time could be strongly improved up to achieve a complete optical alarm transmission in the most favourable cases (all the hops within the few meters range of an optical transmission) or to implement a partial acoustical optical transmission where the details of the protocol are still to be studied.

More advanced steps will be addressed to the study of protocols suitable to the Knowledge propagation, as mentioned in [1], to the management of multizone simultaneous traffic in large networks and to the extension of the currently described protocol to different cases when the silence zone must be kept for long times. This could be the case of intense, high speed communication from a massive source (lie a camera) to a final target (like a gateway to a control console outside of the sea).

References

[1] C. Moriconi and C. Snels, "Knowledge horizon and routing in embodied agents network," Proceedings of IFAC on Telematics Applications, Seoul, November 2013.

[2] M. Stojanovic and L. Freitag, "Multichannel detection for wideband underwater acoustic CDMA communications," IEEE Journal of oceanic Engineering, Vol. 31, No. 3, pp. 685-695, 2006

[3] A. Schrijver, Combinatorial Optimization: Polyhedra and Efficiency. Springer-Verlag, Berlin, 2003.

[4] Y.L. Chen and Y.H Chin, "The quickest path problem," Computers Operations Research, Vol. 17, No. 2, pp. 153-16, 1990.

[5] J.B. Rosen, S.Z. Sun, and G.L. Xue, "Algorithms for the quickest path problem and the enumeration of quickest paths," Computer Operations Research, Vol. 18 No. 6, pp. 579-584, 1991.

[6] E.W. Dijkstra, "A note on two problems in connexion with graphs," Numerische Mathematik, Vol. 1, pp. 269–271, 1959.

[7] G.H. Chen and Y.C. Hung, "On the quickest path problem," Information Processing Letters, Vol. 46, pp. 125-128, 1993.

[8] T.D. Lee and E. Papadopoulou, "The all-pairs quickest path problem," Information Processing Letters, Vol. 45, pp. 261-267, 1993.

A bioinspired intentional architecture for situated agents to explore human cognitive abilities

Alessio Mauro Franchi* and Flavio Mutti† and Giuseppina Gini‡
Dipartimento di Elettronica, Informazione e Bioingegneria
Politecnico Di Milano - Milan, Italy
*alessiomauro.franchi@polimi.it
, †flavio.mutti@polimi.it
‡giuseppina.gini@polimi.it

Abstract—The area of this research is cognitive bioinspired robotics; the focus is in the cognitive development shown by humans in terms of conceptual resources, information processing and language learning; these are among the most important aspects for humans to be aware of the surrounding environment.

The IDRA architecture (Intentional Distributed Robotic Architecture) here presented wants to reproduce in situated agents the ability of humans to develop these mental capabilities. There are two main properties the IDRA architecture is interested in: the first is the autonomous development of new goals starting from some simple hard-coded ones; the second is neural plasticity, an important property of cerebral cortex supporting learning. The IDRA architecture addresses an intermediate level of cognition, the key for humans to be aware of surrounding environment.

Three main brain areas are involved, cerebral cortex, thalamus and amygdala. These have been transposed in the architecture by four modules: the Intentional Module (IM), the Category Module (CM, the cortex), the Ontogenetic Module (OM, the thalamus) and the Global Phylogenetic Module (GPM, the amygdala). A various number of IMs forms a network and they all communicate with each other by a couple of links, while the GPM contains all the innate instincts.

The IDRA architecture has been designed to be as general as possible and independent from the type of robot; it is written in Microsoft C# but can be easily transposed in other programming languages to exploit their computational power.

Two simple experiments with the Aldebaran NAO humanoid robot supporting our claim will be described here; collected results are promising and have demonstrated that our architecture is able to autonomously develop new behaviours.

I. INTRODUCTION

Human beings are able to develop several mental abilities during their life. This process is called cognitive development and refers to those mechanisms of perception, thinking and understanding of the world; it is a mixture of both genetic and learned factors [1]. How humans are able to develop these capabilities during their existence is not completely understood, but it is known that the autonomous generation of new goals and behaviours upon simple innate criteria is a crucial factor in this evolution; it allows the individuals to adapt to the various situations he faces every day and to behave correctly even in unknown situations.

In order to build artificial agents capable of interacting in an effective way with humans and to be really integrated in our life, robotics should now take inspiration from the processes that allow our brain to show this cognitive development, as well from the modalities underlying the generation of new goals and objectives. The here presented work tries to give a contribution to the achievement of this objective: its purpose is to create a bioinspired robotic agent based on the overseen human brain processes that should make the robot able to autonomously develop new goals and behaviours that could be consistent with these goals.

This problem of robot's adaptation has been addressed in several ways in literature; a first example is behaviour-based robotics, which states that the agent should adapt its behaviour to changes in the environment in order to accomplish its goals, but these lasts are only the hard-coded ones and no others may be developed during the agent's life. On the contrary, developmental robotics tries to imitate the emergence of cognition in natural and artificial systems [2]. Developmental robotics leads to the cognitive development of the agent, making it able to adapt to the environment and autonomously develop new motivations that were not present at design time. With this research we are specifically addressing an intermediate level of cognition; it is this that allows mammals and humans to be aware of the surrounding environment and then to interact with it, even without very complex reasoning.

In our mind this capability of goal generation is an essential precondition to enable robots to fit into humans everyday life; what is missing nowadays in robots is this skill of acting in a consistent manner with respect to changes in both the surrounding environment and their own structure; agents able to develop new goals emerging from manipulating the environment would be able to interact effectively with people and would also lead to the development of a sort of unique personality, depending on the agent's experiences.

This work wants to meet its goals imitating nature, in particular focusing on the human brain, its structure and communication network; it is know that three areas of the brain and their interconnections are involved in this cognitive development: cortex, thalamus and amygdala. Our Intentional Distributed Robotic Architecture (IDRA) is a network of elementary units, called Intentional Modules (IM), which enable the development of new goals; this network is composed by several layers, connected both in feedforward and feedback mode. Beside these modules it is also present a single Global Phylogenetic Module (GPM) containing the hard-coded ob-

jectives, i.e. the "innate instincts", exactly as in the amygdala. The GPM spreads all over the network a signal which reflects the emotional state of the agent: the more the current state of the robot meets its own goals, the higher is the signal coming out. Each IM is in turn composed of two internal modules: Categorization (CM) and Ontogenetic (OM). CM is like the cerebral cortex and returns a vector that represents the neural activation of the cortex in response to the input; the OM is the basis of the development of new goals; it receives the vector of neural activations from the CM, and through an Hebbian learning function it lets new objectives emerge; it returns a scalar signal indicating whether the current state meets these new goals.

The output of the Intentional Architecture (IA) is a couple of vector and scalar signals; they are sent to the Motor System (MS) which generates movements consistent with the goals of the agent. Each movement is a composition of a series of elementary signals, called Motor Primitives, which represent the muscles activations over time; this muscular synergy leads to the execution of complex movements [3], [4].

Two experiments have been conducted with this architecture; we wanted to verify the goal generation skills of IDRA as well as its ability in adapting its behaviour with respect to new objectives. In a first experiment the agent (a NAO robot, a humanoid produced by Aldebaran Robotics) learns how to distinguish a particular shape starting from an innate instinct related to highly saturated figures; in a second experiment we focused on the motor capabilities, making NAO robot learning new and more complex movements of its arm to fulfil its goal.

The main contributions of this work are:

- the design and full implementation of a cognitive architecture based on an amygdala-thalamo-cortical model, as proposed in [5];
- the integration of an Intentional Architecture and a Motor System;
- the validation of the architecture, by testing the goals' generation and movement skills.

II. THE AMYGDALA, THALAMO, CORTICAL MODEL

The core of the IDRA architecture is the amygdala-thalamo-cortical model, an artificial representation of these three brain areas and their interconnections; several studies in literature have shown the importance of these brain parts in cognitive development [6]. In the following we sketch out their most significant functionalities and abilities (Fig. 1).

The cortex is the external part of the brain; it is divided into two hemispheres and receives signals from the sensory organs. There is a specific section connected to each sensory input, e.g. the visual cortex or the auditory cortex, but several studies have proven that different areas can properly react to different stimuli sources [7], [8]; the statistic of the incoming signal is the key for the cortex to adapt to new inputs [9]. The whole cortex is composed of the same kind of cells and therefore each cortical area has the ability to virtually implement any computational skill [10], [11]. Stating this, we need a general approach for stimuli representation; the
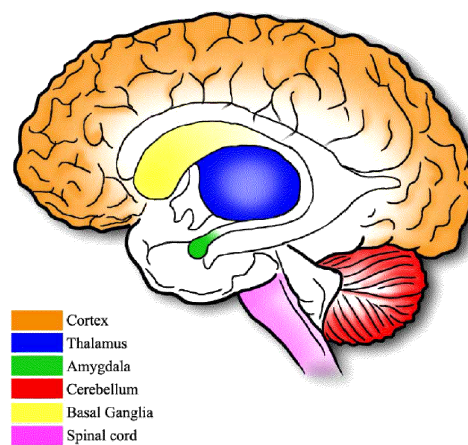
Fig. 1. A simplified structure of the human brain

Independent Component Analysis (ICA) is a valid candidate for this high level representation [12].

The thalamus is located deep in the brain; it plays a central role for mammals in the development of new motivations, as well in the choice of what goal to pursue. The thalamus is a "central, convergent, compact miniature map of the cortex" [13]; its structure is partitioned into segments, each one in synchronized projection to a specific sub-area of the cortex. Since the latter carries on most of the data processing, storing and distribution, the thalamus must provide to the corresponding cortical area which goals have to be pursued [14]. Consciousness and goal generation appear thus to be closely correlated.

The amygdala is a group of nuclei located within the medial temporal lobes; it is heavily connected to the cortical areas and is involved in the generation of somatosensory response on the basis of innate goals [15]. Experimental evidences show that the brain bootstraps the generation of new goals taking advantage of these innate criteria located in the amygdala [16].

Asides from these three areas, this work focuses also on the generation of motion; in the brain the cerebellum deals with motor learning and motor coordination [17]. The spinal cord, in particular, receives and processes sensory information from the various parts of the body and controls the movement of the muscles. It acts as a bridge between the body and the mind [18]. It is widely accepted the motor primitives model, that refers to the generation of complex behaviour by combining a limited set of waveform modules.

III. THE IDRA ARCHITECTURE

The model presented in the previous section has been transposed in a "goal-generating" architecture, that is the IDRA architecture [5]. It is essentially a network of Intentional Modules (IMs) (Fig. 2) plus a single Global Phylogenetic Module (GPM), simulating connections and interactions between the cerebral cortex, the thalamus and the amygdala.

Each IM is in turn composed by one Category Module (CM) and one Ontogenetic Module (OM), modelling the interaction between the thalamus and a single sub-area of the cortex. All
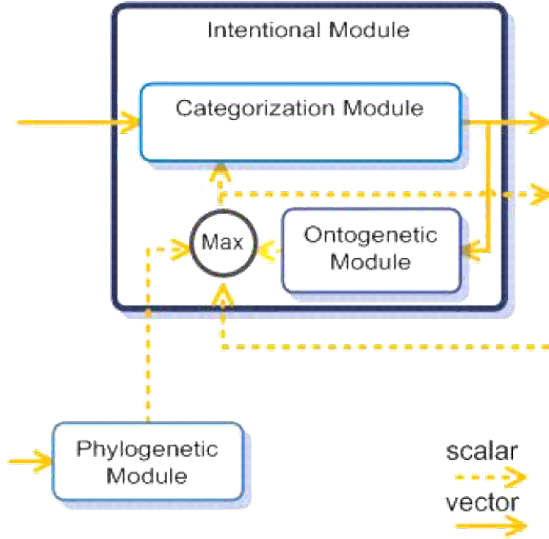
Fig. 2. The structure of the Intentional Module

Fig. 3. Motor primitives composition creating a complex movement

the IMs are linked in any ways, while the GPM broadcasts its signal to all the IMs, without receiving data back. This network has one input coming from sensors, eventually filtered to extract meaningful features, and two outputs, one vector representing the neural activation generated by sensory input, and a scalar signal, stating how much the actual input satisfies internal goals.

The architecture here depicted, thanks to the OM (the thalamus), is able to autonomously develop new goals upon some simple innate criteria; these are implemented as hard-coded functions in the GPM (the amygdala of the system) and the signal this module sends to IMs tells the agent its emotional state with respect to instincts.

The CM represents the cerebral cortex; it receives input from sensors or from other IMs and performs categorization. The input is elaborated twice: first with Independent Component Analysis (ICA) [19] then with a clustering algorithm. ICA allows this module to generalize the input representation regardless the type of incoming stimuli; after a training stage, the input is projected in the space of the independent components to build a general representation (Eq. 1):

$$\overline{W} = IC \times \overline{I} \qquad (1)$$

where $\overline{W}$ is the resulting vector of weights, IC is the matrix of independent components and $\overline{I}$ is the input vector. Clustering is then performed on this set of weights $\overline{W}$ to get a neural code of the input, a sort of translation of a stimulus into a neural activation. With these two mechanisms each IM is able to adapt to changes in sensory input. A new category is created by the CM depending on the value of the internal relevant signal; only relevant inputs are categorized, so that the module saves only meaningful information.

Finally, the OM is closely connected to the Categorization Module and uses the activations of categories computed by the
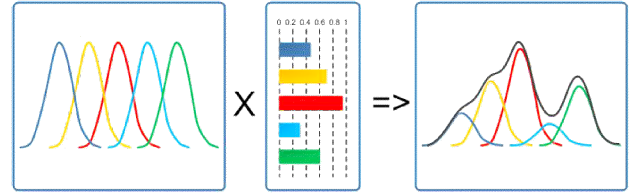
CM and an Hebbian learning function to develop new goals; it also returns a signal stating how much new goals are satisfied.

The output of the network is sent as is to the Motor System (MS); here we propose a solution based on Dynamic Behaviours for movement evaluation and on the concept of Motor Primitives for their composition; several evidences have led to the idea that movements are composed of elementary building blocks, called motor primitives; voluntary actions are composed by movement primitives that are bonded to each other either simultaneously or serially in time (Fig. 3) [3], [4].

Following this idea we use motor primitives to create complex muscular activations: the higher the value of the primitives, the faster the execution of the movements.

The first step for movement generation is a clustering of the input by a K-means algorithm, with a priori defined clusters; we need also a module for selecting the best movement with respect to the current state of the environment, that is the Dynamic Behaviours; each of these is a list of actuators to move for reaching a specific goal and, coupled with a State-Action table (Fig. 4), the architecture is able to selects the set of movements to be executed.

This simple table associates a state and a movement (in term of weights of motor primitives) to a relevant signal. When the system is in a certain state and performs a movement, the relevant signal generated by this state-performed movement combination is stored in the table. There are three different possibilities:

1) if there is a movement associated with a relevant signal above a defined threshold, that movement is selected;
2) if there is a movement not yet performed, that movement is selected;
3) if all movements have already been performed at least once and no one is associated with an high relevant signal a new random movement is added to the list

This last chance which selects a random movements is necessary for the agents to explore and learn new possible, and maybe even better, behaviours or movements.

IV. IMPLEMENTATION

The biological model and the architecture here presented is implemented in the IDRA software; the main idea behind the realization of this system is to create a very simple, readable and modular code, so that users may "Plug&Play" its own robot in a few steps, regardless its type, its structure or the available sensors. The entire project is written in Microsoft
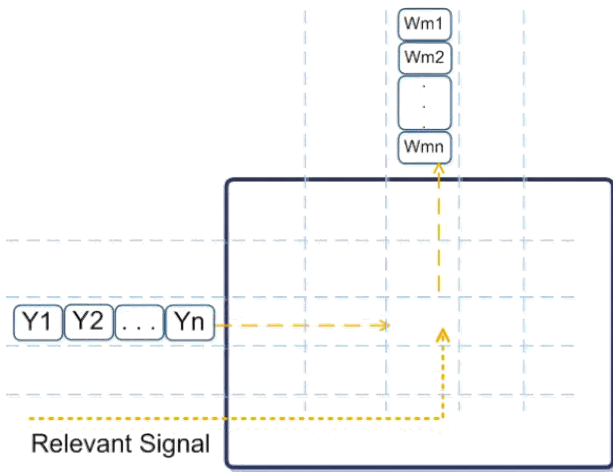
Fig. 4. An example of State-Action Table; $Y_1, .., Y_n$ represents the actual state, $W_{m1}, .., W_{mn}$ are the weights for movements generation

Fig. 5. Visual Studio 2010 project

.NET C#, with the use of the IDE Visual Studio 2012 (VS 2012).

We pay also special attention in respecting all the basic software engineering rules in order to deploy a code with high scalability, easy to upgrade and maintain. As you will see later on one fundamental property is its independence from the robot used and its modularity, so that new instincts or new sensor's types may be easily added.

We started from the definition of all the classes and the VS projects needed (Fig. 5), collecting them in an UML class diagram.

The flow of information in the architecture is fairly simple: everything starts with the "Body Class" retrieving data from all the enabled sensors installed on the robot; these signals are passed to the "Filter Class", which elaborates raw data to extract meaningful information (e.g. colors, lines, edges); then the "Intentional Architecture" class receives this filtered information; in here is defined the network of IMs and the GPM, and when a new input is ready the system starts the computation, making the information flows from one layer of the network to the following. The two final outputs are sent back to the "Body Class", where a set of available "Behaviours" (e.g. head's movements, right arm movements) is defined and a proper movement is generated.

Going down into further details, the definitions of all the implemented robots are in the "AgentsLib" folder; all the .cs files describing a new robot must respect the "RobotInterface", which imposes all the necessary functions for this architecture to communicate with the agents (e.g. macros for connecting to robot, for sensors' reading). All the data manipulation functions are defined in the "InputLib" project; it contains an "inputProcessing" class which instantiates all the filters necessary to deal with raw data; these filters are clustered into different classes, one for each type of sensor (e.g. audio, video) and they contain specific filtering algorithm and methods for encapsulating data into predefined formats; this re-formatting of raw sensory data into an high level structure is the key
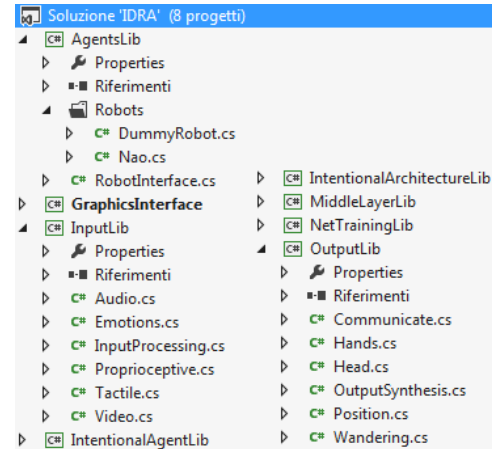
that makes the Intentional Architecture independent form the number and the type of sensors implemented on the robot. On the opposite side there is an "OutputLib" project, which is necessary for the "BodyLib" to know which actuators and behaviours are available on the robot in use. Right after the Intentional Architecture has finished a cycle, the two outputs are sent to the "outputSynthesis" class, which contains all the "Behaviours' for the generation of robot's movements, each one with its list of actuators to be used and a State-Action table for the choice of the best movement. The "outputSynthesis" class forwards its input to each Behaviors, which return the movements to apply to a specific actuator; a total list of movements is created and sent back to the Body class and then again to the Robot class for movement actuation.

The brain of the architecture is the "IntentionalArchitectureLib", the actual implementation of the amydala-thalamo-cortical model previously presented; it contains the definition of all the necessary modules: "CategorizationModule", "IntentionalModule", "OntogeneticModule" and "PhylogeneticModule", which is in turned a collection of subclasses (the hard-coded instincts) each one dealing with a specific sensor type. The IntentionalArchitectureLib is responsible for creating and managing network of IMs, taking care of synchronization, data forwarding, inter-IMs communications and input/output retrieving.

All the software here detailed makes use of several XML files for saving and restoring all the configuration's settings of the system; they are stored in a fixed directory structure and are editable both by hand and via the GUI for the most complex ones (Fig. 6).

The "Robot Folder" contains one XML file for each yet defined robot, which describes for example its IP address for communication, its name, all the on board sensors and actuators; in the "Net Folder" are listed the description of the available IMs networks, in terms of sensor-filters couples, layers composing the network and all the IMs; finally the two directories "SavedData" and "TrainingData" contains respectively data stored for off-line analysis and saved working
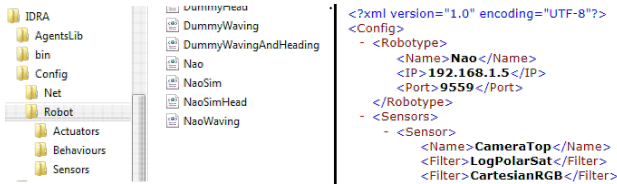
Fig. 6. The directory structure of the XML configuration files

Fig. 8. The two tables of shapes used in experiment one

Fig. 7. Screenshot of the viewer form, with the FormFocus on the top

sessions in binary format (to allow users to stop and resume the execution of the program later) and saved training data generated by the IDRA architecture during training phases (e.g. the independent components for CMs and the clusters of environmental states necessary for the Motor System).

In Fig. 7 is shown a screenshot of the main form of the IDRA software; from this it is possible to start, stop or resume the application, to look at all the internal parameter of each module via the "FormFocus" and to save all the data and graphs of signals for off-line analysis.

V. EXPERIMENTAL RESULTS

This section describes the experimental phase; the purpose of this step is to check whether the IDRA architecture here described is able to control the agent and to generate new goals also with consistent behaviours (movements), starting from simple hard-coded criteria. The IDRA architecture may potentially be used for controlling any kind of robot, regardless its type, its available sensors and actuators; as case of study we select the NAO, a humanoid robot by Aldebaran Robotics, with 25 degrees of freedom (DOF), two cameras on the head, four microphones, two sonars and many other sensors.

Two experimental setups are selected: the first deals with shapes and colors, as reported in [5], the second explores the creation of new and more complex arm's movements.

A. Dealing with shapes

For the first experiment the network of IMs is very simple; it has a single IM and two filters dealing video input, the first computing the log-polar transform [1] of the input, the second extracting the overall saturation of the image; the only innate instinct hard-coded in the amygdala is the attraction for colors. As behaviour we select the head movements, namely HeadPitch and HeadYaw; to simulate attention mechanisms these two values are randomly generated by a uniform distribution for the angle and a bell-shaped Gaussian function for the amplitude of the movement in a way that the lower the relevant signal computed by the network the greater the movement.

The IM receives data from the log-polar filter in an array form, while signal from saturation filter is sent to the GPM; visual input is made of two boards put in front of the top Nao's camera (Fig. 8). The first board presents a series of black shapes, among which there is a black star; the second board presents only stars filled with three different highly saturated colours. This test consists in three different phases; first the board shown to NAO contains only black figures and we see that the interest of the agent is spread equally all over the board, not showing any interest for a specific shape; then the second board is shown; now the NAO robot, following its instinctive attraction for colors, strongly focuses on the three star-shaped figures; in conclusion, the board is switched again to the first one. Unlike before, the interest of the robot is now focused on the star-shaped figure, even if is totally black, a new behaviour showing us that the OM has developed a novel interest in the shape of the figure, a behaviour that goes in addition with the previous interest for its colour.

B. Movement generation

The aim of this second experiment is to test the Motor System, in particular the Behaviour and OutputSynthesis sections of the architecture. We use again as case of study the NAO robot, but this time the head's yaw and pitch is fixed while we select as behaviour the movement of the right arm, controlling four joints: RShoulderPitch, RShoulderRoll, RElbowRoll, RElbowYaw. As innate instinct in the GPM we left unchanged the attraction for coloured objects. We highlight here that nothing is specified in the system about arm's movements, except the implementation of five motor primitives defined as Gaussian function (Eq. 2)

$$p = e^{\frac{-(x-c)^2}{2\rho^2}} \tag{2}$$

[1]The log-polar images allow faster sampling rates on artificial vision systems without reducing the size of the field of view and the resolution on the central part of the retina.

where c is the center of the muscular activation of p and ρ is the standard deviation; for this experiment we set each Gaussian with $\rho = 6.7$ (empirically evaluated) and a mean value calculated in order to equally distribute these functions on a scale from 0 to 100.

The network of IMs is slightly more complex than in experiment one; beside the two previously used filters (log-polar and saturation), we add a third one for proprioceptive data, called "rightArm Position", to get information about joint's value for the right arm; moreover there are now two layers in the network: the first contains two IMs, one for processing Log-Polar images and record the shapes, the other for receiving proprioceptive data about the right arm. Both send their output vector and relevant signal to a third IM situated in the second layer; the output of the network is set equal to the output of this last IM. Finally, the GPM receives input data from the saturation filter and broadcasts its signal to all the IMs.

Starting from these simple assumptions, we expect the robot to start composing random arm's movements, to finally learn how to choose more complex and adequate movements in order to reach the goal of looking at the red heart the robot has in its right hand (looking at the red heart corresponds to an high internal relevant signal); these new behaviours are not coded, but are autonomously generated by the architecture for improving its emotional state with respect to innate instincts.

In order to have all the CMs projecting their input on the correct basis space, independent components are extracted a priori through ICA for each IM separately; the first IM computes ICA on video images, the second on the joints' values of the right arm and the last on the combination of the outputs of the previous modules. Once the net is trained, clusters for the Motor System are computed.

The experiment starts with the robot in a random position; at the beginning, the State-Action table is empty and movements are chosen and executed randomly, following the three rules of the State-Action's table seen in Section II; for each trial the system records in the table the associated relevant signal coming from the Intentional Architecture and after several, even useless, movements the table starts filling; the system may now choose movements coherently with the maximization of the relevant signal received from the architecture. Going on with repeating these schema, the table is completely filled and so best movements start to be frequently repeated.

Looking at the robot's movements we can observe that the same positions are reached cyclically: several positions of the arms know the reference to a movement that brings the hand to a position with an high relevant signal; several positions with a high relevant signal know many movements, but none of them brings the hand to a position with an high relevant signal. Therefore we observe the robot starting from a random position, going towards a good one, and then moving to a second random position, and so on.

Fig. 9 shows the positions reached by right hand during a thousand iterations in a three-dimensional space; the frame of reference is centered in the body of the robot; we can see that
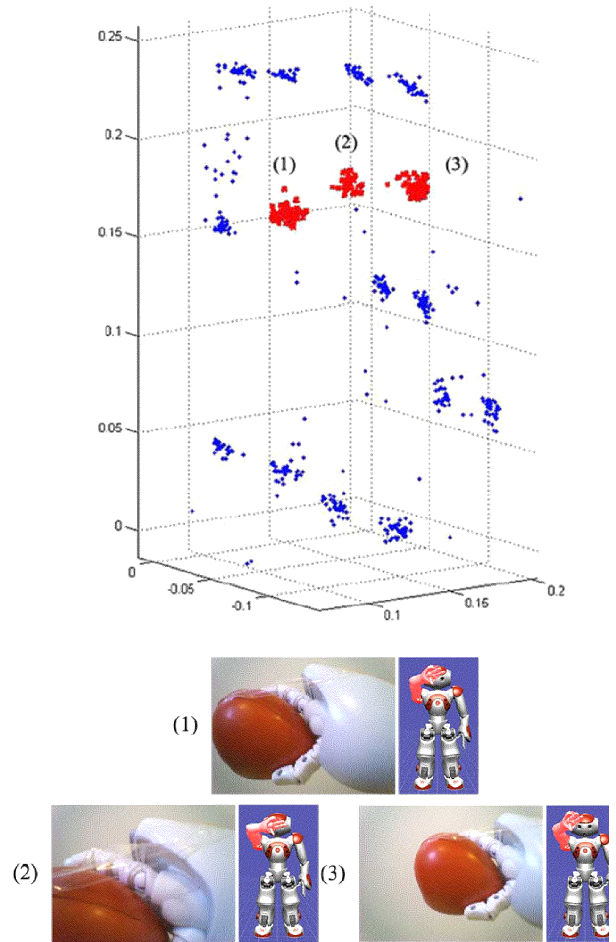
Fig. 9. Results of experiment two: the 3D representation of positions' clusters reached by the hand and the respective robot's configurations

emerged the creation of several clusters, which represent the various positions cyclically reached by the robot. The red ones are those associated with the highest relevant signal and for these a 3D representation of the NAO is reported, showing its configuration and what it sees through its top camera. We can notice how in the three pictures the ball is roughly at the center of its visual field, meaning it reached its goal.

The implemented Motor System is simple, with obvious limitations; the movements that maximize the relevant signal are performed only if the state is known, and if the State-Action table has the corresponding entry; furthermore, the motor training has run for a relatively short period of time. As a consequence, the State-Action table presents a limited extension in comparison with the high dimension of the input representing all the possible states. Even more, although the brain has been proven to have an associative memory of sequences of patterns [8], the system here presented actually does not show this kind of ability. Despite these limitations results are coherent with the objective of the experiment: the robot moves according to the linear combination of primitives, and is able to learn what movement has to be performed to go from a known state to a second one with a high reward. In

addition, the experiment led to the creation of a sensorimotor map through the cognitive architecture.

VI. CONCLUSION

This paper wants to introduce a new way to approach developmental robotics; it presents an intentional "goal-generating" architecture, namely IDRA, which simulates structure and interaction among three specific cerebral areas, amygdala, thalamus and cortex; these are known to play a key role in the so called cognitive development, that focuses on children's development in terms of information processing, conceptual resources, perceptual skill, language learning and other aspects of brain development. We also integrated this architecture with a Motor System, which gives the opportunity for the robot to explore the environment; we propose here a solution based on Dynamic Behaviours for movement evaluation and on the concept of Motor Primitives for their composition.

The three mentioned cerebral areas are translated in our system with three corresponding modules, the Category Module (CM, the cortex), the Global Phylogenetic Module (GPM, the amygdala) and the Ontogenetic Module (OM, the thalamus); CM and OM are grouped in a fourth module, the Intentional Module (IM), representing the strict interaction between the thalamus and a single sub-area of the cortex. Several IMs are grouped in a layered network, each one connected to the others; this network has its input coming from sensors and two outputs representing a neural code of the sensory input. These two are sent to the Motor System, which is in charge of selecting and composing the best movement to fulfil the actual goal.

Two main properties of this system hold. First it is structured to be as general as possible with respect to the robot used, regardless its type, the actuators it uses or the sensor's network on board; secondly it is able to adapt to virtually any kind of sensory input, mimicking the so called neural plasticity; this term refers to the ability of the brain to modify its structure in response to changes in the environment, in the behaviour and in neural processes, and it is known to be also strictly correlated to the learning processes.

The experimental phase allows us to check the IDRA architecture abilities, both in terms of controlling the agent, autonomously generating new goals and composing new behaviour consistent with these goals by the motor primitive mechanism. We perform two simple tests; in the first the NAO robot has to autonomously learn how to distinguish shapes of figures starting from the attraction for colors; the second focuses on the ability of selecting and composing new movements via the motor primitives paradigm in order to maximize its internal relevant signal.

Even if these tests are quite simple, results clearly show that the agent is able to keep memory of the past situations, and act accordingly to the achievement of its goals, whether innate or acquired. Besides this, the intrinsic dynamicity of the architecture allows the agent to acknowledge the changes in the environment that are independent from its own actions, and then to recalibrate its behaviour for this new particular situation.

In the future we plan some improvements; we want for example to explore the generation of new IMs and the connections plasticity among them into the network; we would like also to work on the Motor System, introducing a less rigid structure than the State-Action table. Finally, more extensive tests are needed to investigate the capability of this cognitive architecture.

REFERENCES

[1] D. F. Bjorklund, *Childrens Thinking: Cognitive Development and Individual Differences*. Wadsworth Publishing, 2011.

[2] M. Lungarella, G. Metta, R. Pfeifer, and G. Sandin, "Developmental robotics: a survey," *Connection Science*, vol. 15, no. 4, pp. 151–190, 2003.

[3] C. B. Hart and S. F. Giszter, "Modular premotor drives and unit bursts as primitives for frog motor behaviors," *The Journal of Neuroscience*, vol. 24, no. 2, pp. 5269–5282, 2004.

[4] F. S. Mussa-Ivaldi and E. Bizzi, "Motor learning through the combination of primitives," *Philosophical Transactions of the Royal Society*, vol. 1404, no. 355, pp. 1755–1769, 2000.

[5] R. Manzotti, F. Mutti, G. Gini, and S.-Y. Lee, "Cognitive integration through goal-generation in a robotic setup," *Advances in Intelligent Systems and Computing*, vol. 1, no. 196, pp. 225–231, 2013.

[6] O. Sporns, *Networks of the Brain*. The MIT Press, 2010.

[7] G. Dileep, "How the brain might work: A hierarchical and temporal model for learning and recognition," Ph.D. dissertation, Stanford University, 2008.

[8] J. Hawkins, *On intelligence*. St. Martin's Griffin, 2004.

[9] B. A. Olshausen and D. J. Field, "Emergence of simple-cell receptive field properties by learning a sparse code for natural images," *Nature*, no. 381, pp. 607–609, 1996.

[10] J. Sharma, A. Angelucci, and M. Sur, "Induction of visual orientation modules in auditory cortex," *Nature*, no. 404, pp. 841–847, 2004.

[11] M. Sur, A. Angelucci, and A. Sharma, "Rewiring cortex: the role of patterned activity in development and plasticity of neocortical circuits," *Journal of Neurobiology*, vol. 1, no. 41, pp. 33–43, 1999.

[12] A. Hyvrinen and J. O. Hoyer, "A two-layer sparse coding model learns simple and complex cell receptive fields and topography from natural images," *Vision research*, vol. 41, no. 18, pp. 2413–2423, 2001.

[13] S. M. Sherman and R. W. Guillery, *Exploring the Thalamus*. Elsevier, 2000.

[14] D. S. Modhaa and R. Singhb, "Network architecture of the long-distance pathways in the macaque brain," *Proceedings of the National Academy of Sciences*, vol. 107, no. 30, p. 1348513490, 2010.

[15] R. Adolphs and M. Spezio, "Role of the amygdala in processing visual social stimuli," *Progress in Brain Research*, vol. 156, pp. 363–378, 2006.

[16] S. Duncan and L. F. Barrett, "The role of the amygdala in visual awareness," *Trends in Cognitive Science*, vol. 11, no. 5, pp. 190–192, 2007.

[17] J. S. Albus, "A theory of cerebellar function," *Mathematical Biosciences*, vol. 10, no. 1-2, pp. 25–61, 1971.

[18] J. Doyon, P. Bellec, R. Amsel, V. Penhune, O. Monchi, J. Carrier, S. Lehricy, and H. Benali, "Contributions of the basal ganglia and functionally related brain structures to motor learning," *Behavioural Brain Research*, vol. 1, no. 199, pp. 61–75, 2009.

[19] A. Hyvrinen and E. Oja, "Independent component analysis: algorithms and applications," *Neural Network*, vol. 13, no. 4-5, pp. 411–430, 2000.

Human-Adaptive Control of Compliant Actuators

Andrea Calanca, Riccardo Muradore, Paolo Fiorini

Abstract—**Compliant actuators mimics the elastic behavior of biological muscles to obtain a soft interaction with the environment. This paper analyzes the particular case when the environment is identified with a human and proposes a bio-inspired force control algorithm. As a result we are able to provide predictable and well-defined force control dynamics in spite of environment uncertainties. The experimental validation shows that the proposed algorithm outperforms the best state of the art solutions.**

I. INTRODUCTION

If we look at the animal kingdom we can see that mechanical compliance is the main enabling factor of animal soft interaction and efficient locomotion. Muscles and tendons include a significant level of elasticity which allows fine force control and also reduced energy consumption. A couple of decades ago elasticity started to be widely used also in robotics with the concept of series elastic actuator (SEA). The original motivation of (series) elasticity came from difficult force control of stiff actuators. The series spring aims to decouple the motor from the environment thus dramatically reducing the motor inertia coupling and the disturbance due to environment displacement. Such SEAs have become popular in of novel physical human-robot interaction (pHRI) applications such as assistive and rehabilitation robotics. In particular force controlled SEA are used in rehabilitation robotics to accomplish the paradigm "assist as needed". In this approach the patient is compliantly guided to a target trajectory by progressively reducing the interaction forces as the patient learns to better follow the desired path. This is because it has been shown that the patient should be active to enable the motor learning process, implying the rehabilitative device to be non coercive. Several control algorithms have been proposed following this approach like for example "path control" or "virtual model control" algorithms [14], [7]. All these algorithms are build upon an ideally fast force/torque controller. However when putting things in practice the force variable cannot be commanded instantaneously and its transient depends both on robot and patient dynamics. In fact when the patient displays a low mechanical impedance (e.g. robot impedance matching, swing phase) we can have slow force/torque responses while when the patient is stiff (e.g. muscle co-contraction, stance phase) we can have force/torque overshoot. Of course these effects are undesirable because they can generate disturbances and delays that can invalidate our rehabilitation strategy and even partially obstruct movements. These observations have been reported in the literature (see for instance [9]) and can also be found in our previous experience [6], [5].

To solve this issue we propose a patient-adaptation mechanism that dynamically tunes force control gains to match a desired force/torque transient. In our approach we use a

simplified model for the human because its whole modeling is really complex. However it is known that a detailed model of the system is actually not necessary for control purpose, if we assume adequate robustness margins. Combining such a simple human model with adaptivity we obtain two advantages: first, we can account for a generic human joint, no matter its actual parametrization, second, the considered model can adapt to changing situations such as when a grasped mass is added or when co-contraction is modified.

The advantage of our approach with respect to state of the art passivity based (PB) control is well-defined force/torque dynamics despite environment uncertainties. In fact in PB control it is not possible to force any servo specifications because the controller has to be stable against any kind of external passive environment. Any passive controller has stability warranty against any passive environmental coupling: being a mass, a wall, a spring or a combination. It follows that this approach is conservative and by neglecting almost *at all* environmental dynamics it is not possible to speculate on control performance. As a matter of facts authors that propose passive controllers for rehabilitation or pHRI usually do not comment about control tuning, that involves specifications. The implicit idea is that of tuning the system (by trial and error process) trying to match a desired transient and then verify the passivity condition. However some issues can arise:

1) In our experience it is quite difficult to carry on a tuning process with the human in the loop, both from the point of view of safety and of practical feasibility. Of course it is possible to overcome it by using artificial limbs or manikins but in this case the solution could be rather inadequate.
2) The human dynamics changes in response to the external environment and the specific task. When we walk on rough terrain we usually increment leg stiffness by co-contraction and the same happens if we want to do precise positioning. In latter case also our inertia changes depending on the object mass and the same happens when we carry something on the back. In this scenario controller tuning should adapt to changing situations;
3) Pathologies can specifically affect limbs. In existing approaches the control tuning procedure should be carried out separately for each patient and for each patient joint. It follows that an automatic tuning process is of paramount importance.

These are the basic reasons why a human-adaptive approach is advantageous in real-life applications such as rehabilitation robotics. By using adaptive control we can have an automatic tuning process which online adapts to diverse conditions. Other kinds of solutions to overcome the above issues cannot be find in the literature with few exceptions. An example is
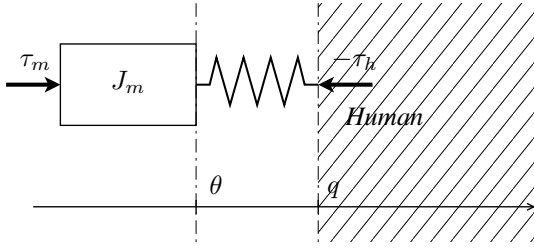
Figure 1. A wide used model for series elastic actuator interacting with an unstructured environment i.e. a human.

Figure 2. SEA force control schema relative to equation (10) with $k_b < 1$ to prevent feedback inversion. The dotted arrow represents motor backdrivability.

[12] where authors introduce the human acceleration feedback in the control law and prove the passivity of the resulting controlled actuator impedance. This acceleration feedback actually predicts for the human dynamics and allows for deterministic force performance in spite of environment uncertainties. However the authors do not highlight this feature in their work. Consequently this acceleration term has been neglected in later works related to passive force control e.g. [22], [18]. Another example of algorithm that tries to deal with changing human dynamics is [1] where a continuous approximation of sliding-mode control changes control gains depending on different gait phases, i.e. different human dynamics.

In this paper we propose an approach inspired by model reference adaptive control (MRAC) where control specifications can be determined by the reference model, letting the tuning process to be automatic and to adapt online accordingly to the actual conditions.

The paper is organized as follows. Section II presents the currently available solutions for SEA control in pHRI. Section III describes the system to be controlled and section IV analyzes the property of the acceleration-based controller proposed in [12]. Section V introduces the proposed adaptive controller and gives a theoretical stability analysis. Experimental results are presented in section VI. Finally, conclusions are drawn in section VII together with the future work plan.

II. STATE OF THE ART

A. Series Elastic Actuators

SEAs have been proposed to overcome force control difficulties that arise using stiff actuators [12]. In SEAs a spring is arranged between the motor and the environment, which in our case the human. This is shown in figure 1 where τ_m is the motor force/torque, k is the series spring stiffness, θ is the motor position, τ_h is the human interaction force/torque and q is the human joint position. The relations among these variables can be expressed as

$$\tau_h = k(\theta - q) \qquad (1)$$
$$J_m \ddot{\theta} = \tau_m - \tau_h \qquad (2)$$

where the first equation describes the force exerted by the spring to the human and the second one accounts for the motor inertia J_m.

The main advantages of SEAs are the increased force control robustness, augmented shock tolerance and improved safety due to lower reflected inertia. Moreover force can be measured through spring deformation that is cheaper than using a load cell (in the case of force) or a rotative torsiometer (in the case of torque).
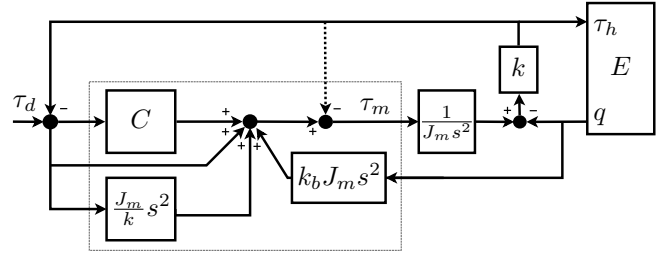
To the best of authors knowledge all the proposed SEA implementations make use of high transmission ratios. For example: in [13] a screw ball with a pitch of $2mm$ per revolution (linear actuator) is used, whereas in [9] the transmission ratio is $n = 130$ (rotative actuator). The reason why SEAs usually employ reducers or gearboxes is to obtain high force and high power density. However a geared motor results very stiff and difficult to control in force. By adding a series spring, SEAs transform the force control problem into a position control problem (spring displacement) where high ratio transmissions are known to be helpful: the motor results stiffer and the effects of external disturbances are reduced.

B. Passive Control of Series Elastic Actuators

Currently the main technique used to stabilize pHRI is based on passivity theory. PB controllers are quite easy to implement and impressively robust as they are stable with *any* passive coupling. However nothing can assure us that a PB controller is a "good controller". For example, the passivity-based force controller proposed in [12] consists of a standard PID controller with an integral roll-off

$$F(s) = P + \frac{Ds}{1 + T_d s} + \frac{I}{1/T_i + s} \qquad (3)$$

where P, D and I are positive gains and the integral roll off must satisfy $T_i \leq \sqrt{D/I}$. The performance of this passive PID controller depends both on gain values and the coupled environment whose dynamics is usually unknown and so produces unknown control performance. For passivity analysis of different control architectures, including inner velocity loops and pure integrators, the reader can refer to [21], [19] where it is shown that, depending on the architecture, the passivity constraint imposes upper or lower bounds on certain control gains. It has also been reported that "discrete control, time delays, actuator and sensor limitations, and unmodeled dynamics can also compromise passivity, making the implementation of passive control on real systems extraordinarily challenging" [2].

C. Force Control of Series Elastic Actuators Based on Acceleration Feedback

The basic idea of this solution is that, given a desired interaction torque τ_d, it can be translated into a desired motor

position $\theta_d = \frac{\tau_d}{k} + q$. This means that we can transform an interaction control problem into a position control problem where we need to track the environment position q plus the offset $\frac{\tau_d}{k}$ which depends on the force/torque reference. As usual, this tracking problem requires environment velocity and acceleration. No further measurement from the environment are required because the (decoupled) motor is a second order system.

The force control system proposed in [12] and reported in figure 2 is de-facto an example of such kind of approach even if the position tracking is masked by a force tracking problem. We highlight that this acceleration-based algorithm is currently the only existing passive algorithm that can ensure a deterministic force dynamics. However it was not originally proposed with the aim of assuring well defined performance or at least this was not explicitly stated by the authors. In section IV we derive an analysis of stability, passivity and performance of this controller, considering a proportional-derivative structure for the block C in figure 2.

III. SYSTEM ANALYSIS

In this work we follow the approach of using second order linear models to approximate the human joint impedance[1]. Such simple models have two main advantages. First fewer parameters have to be adapted. Second a single adaptive controller structure can work for every human joint and also for human endpoints, broadening the applicability of the approach.

In a first step we model the human joint as a pure inertia J_h. In this case we have the following human model

$$J_h \ddot{q} = k(\theta - q) = \tau_h \qquad (4)$$

to be considered together with SEA model (1) and (2). To describe the torque control application, the overall model should be arranged with an input torque τ and an output torque τ_h. To this aim it is possible to arrange (1), (2) and (4) as

$$\frac{J_m}{k} \ddot{\tau}_h + (1 + \frac{J_m}{J_h}) \tau_h = \tau_m. \qquad (5)$$

Note that this torque to torque relation results in a second order system in spite of being originally a fourth order system. The reason is because, if we do not account for friction and/or human joint stiffness, there are pole-zero cancellations. Thus the second order approximation is reasonable only in the case of a pure inertial load, otherwise a higher order system has to be considered. In particular, the model becomes a third order system in the presence of human joint damping and a forth order if we account also for stiffness, leading to the following equations

$$\frac{J_m}{k} \ddot{\tau}_h + (1 + r) \tau_h - rh(q - q_0) - rd\dot{q} = \tau_m \qquad (6)$$

$$J_h \ddot{q} = \tau_h - h(q - q_0) - d\dot{q} \qquad (7)$$

where $r = \frac{J_m}{J_h}$. The structure of human joint model (7) can be used to represent both a passive and an active human condition. In the passive case the stiffness term $h(q - q_0)$

[1]This oversimplification is widely used (and tested) in literature, see for example [16], [8], [17], [23], [20], [11].

can be considered a linear approximation of the gravitational torque and the damping term $d\dot{q}$ describes the mechanical joint friction due to muscle, tendons and articulations. In the active case the human is supposed to actively control the joint to reach a position q_0 and the damping and stiffness terms are mainly due to muscle co-contraction.

In both models (5) and (6) the dynamical equation of τ_h has two parameters:

$$a = \frac{J_m}{k}, \; c = (1 + \frac{J_m}{J_h}) = 1 + r. \qquad (8)$$

Interestingly the inertia uncertainty (i.e. J_h) is lumped in c while a can be known a-priori, as it characterizes the actuator. In a control application, the worst case is when c, or equivalently r, is high, showing high sensitivity to human joint model. This can be see in (6) where r multiplies human forces/torques. Unfortunately this is often the case of SEAs where geared motors are usually adopted. In fact the (reflected) motor inertia J_m, which is proportional to r, acts as a sensitivity gain. If the reflected motor inertia is augmented by a factor n^2, where n is the transmission ratio, it follows that in most applications the system can be very sensitive to uncertainties

IV. ACCELERATION-BASED CONTROL

Let us refer to the system represented in figure 1 and rewrite the system model (6) in a more convenient form

$$\frac{J_m}{k} \ddot{\tau}_h + \tau_h = \tau_m - J_m \ddot{q} \qquad (9)$$

where $hq + d\dot{q}$ in (6) is replaced with $\tau_h - J_h \ddot{q}$, according to equation (7). Now if we consider the following control law

$$\tau_m = \frac{J_m}{k} \ddot{\tau}_d + \tau_d + J_m \ddot{q} - k_p e - k_d \dot{e} \qquad (10)$$

where $e = \tau_h - \tau_d$ is the force/torque error, we have that the resulting dynamics of the error is

$$\ddot{e} + \frac{k k_d}{J_m} \dot{e} + \frac{k(k_p + 1)}{J_m} e = 0. \qquad (11)$$

If $k_d > 0$ and $k_p > -1$ the autonomous system (11) is asymptotically stable and provides well-defined closed loop force dynamics.

The main drawbacks of this approach are related to the presence of human accelerations in the control law (10). In fact the acceleration is usually a noisy measurement or an approximate estimation. Moreover the above control law brings the system close to instability. For this reason in [12] the authors proposed to decrease the acceleration feedback $J_m \ddot{q}$, by a gain $k_b < 1$, "to prevent feedback inversion and instability". With such a modification the error dynamics becomes

$$\ddot{e} + \frac{k k_d}{J_m} \dot{e} + \frac{k(k_p + 1)}{J_m} e = (k_b - 1) J_m \ddot{q}. \qquad (12)$$

Given $k_p > 0$, stability can be proved by means of passivity, including the acceleration feedback gain k_b, as reported in [12]. However well defined dynamics is retained only when the human is not moving or when he/she is moving at a constant

velocity. As mentioned before algorithm (10) is currently the only existing passive algorithm that can ensure a certain level of predictability.

Passivity can be proved as follows. Let us discard the feedforward terms which do not affect stability and consider the following law consisting of a proportional-derivative action and the acceleration feedback

$$\tau_m = J_m \ddot{\theta}_h - k_p e - k_d \dot{e}.$$

The actuator transfer function seen by the environment can be computed through the following passages

$$\tau_h = k(\theta - q) = k[\frac{1}{J_m s^2}(\tau_m - \tau_h) - \frac{\dot{q}}{s}]$$
$$\tau_h = k[\frac{1}{J_m s^2}(-(k_p + 1 + k_d s)\tau_h + k_b J_m s\dot{q}) - \frac{\dot{q}}{s}]$$
$$(k_p + 1 + k_d s + J_m s^2)\tau_h = k(k_b - 1)J_m s\dot{q}$$
$$\tau_h = \frac{-\mu s}{s^2 + 2\psi\omega s + \omega^2}\dot{q}$$

where $\mu = k(k_b - 1) < 0$, $\omega^2 = (k_p + 1)/J_m$ and $\psi = 0.5 k_d/\omega$. The resulting transfer function at the environment port $(-\tau_h, \dot{q})$ has two stable poles, a derivator and a positive gain. The relative Nyquist diagram lies in the right half complex plane thus ensuring passivity of the controller (i.e. the transfer function is positive real [15]).

V. HUMAN-ADAPTIVE CONTROL

Within the MRAC framework, control specifications are given using a model reference. This is particularly convenient when it is easy to specify the desired bandwidth and damping/overshoot, as in a linear second order reference model. However in MRAC the reference model should have the same order of the plant to assure adaptation convergence (perfect tracking assumption). In this work we propose a slight modified approach to use a second order reference model even if the system (6-7) is a fourth order one. Let us consider the following model reference

$$\ddot{\tau}_r(t) + \lambda_1 \dot{\tau}_r(t) + \lambda_2 \tau_r(t) = \lambda_2 r(t) \qquad (13)$$

where the parameters λ_1 and λ_2 are chosen according to desired bandwidth and damping of the controlled system and $\tau_r(t)$ is the desired torque dynamics for τ_h in response to the bounded reference input $r(t)$.

We consider the following control law:

$$\tau_m = \frac{J_m}{k}(\ddot{\tau}_r - 2\lambda\dot{e} - \lambda^2 e) + \hat{b}\dot{\tau}_h + \hat{c}\tau_h \qquad (14)$$

with adaptation dynamics given by

$$\dot{\hat{b}} = -\rho(p\dot{\tau}_h + \sigma\hat{b}), \quad \dot{\hat{c}} = -\rho(p\tau_h + \sigma\hat{c}) \qquad (15)$$

where $e = \tau_h - \tau_r$ is the error with respect to the reference model (13) and $p = \dot{e} + \lambda e$ is a measure of tracking performance. The parameter ρ determines the adaptation speed and σ is a forgetting factor which can be set arbitrarily small [10]. This controller can be translated in a more traditional form, having a proportional-derivative structure and some feed-forward terms:

$$\tau_m = a\ddot{\tau}_r + \hat{b}\dot{\tau}_r + \hat{c}\tau_r - k_p e - k_d \dot{e} \qquad (16)$$
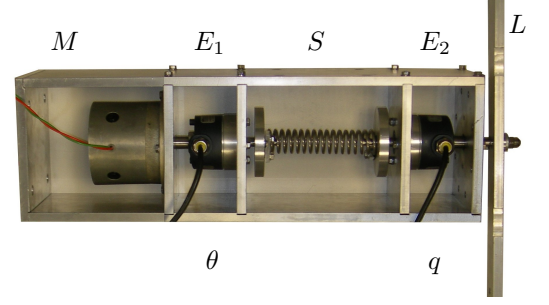
Figure 3. The SEA prototype used as testbed. The motor M is connected to the torsional spring S and the angular quantities θ_m and θ_e are measured by encoders E_1 and E_2 respectively.

where $k_p = a\lambda^2 - \hat{c}$ and $k_d = 2\lambda - \hat{b}$. In brief such a controller uses high force gains when in contact with a soft and dissipative environment and low force gains when the environment is rigid. Note that this is quite similar to animal behavior. If we are in an unstructured rigid environment we will move carefully, with high compliance and at low velocities, to prevent the risk of injury. On the other hand if we move in a soft environment we usually move faster and less compliantly. For example when we walk on a very soft terrain we keep balance by involving higher muscle co-contraction.

Two kinds of results can be derived for this controller. First the controller is passive with respect to the environmental port. In fact adaptivity and passivity are not incompatible concepts. Existing passive controllers cannot ensure well-defined force performance not because of passivity itself but because they miss an environment model, which in current literature is merely considered passive [21]. Second it can be proved that the system (6-7) with τ_m determined by the adaptive control law (14-15) converges to the reference model (13) in the sense of boundedness i.e. tracking errors e, $\dot{e}$ and adaptation errors $\tilde{b} = \hat{b} - b$, $\tilde{c} = \hat{c} - c$ converge to a neighborhood of zero. Moreover the area of such neighborhood decreases monotonically with λ, meaning that by a proper choice of λ the attracting region can be sufficiently small and we can have the desired convergence to the reference model (13), see [4] for details.

VI. EXPERIMENTAL VALIDATION

In this section we present an experimental validation of the approaches described in the previous section. Experiments are conducted in a pHRI scenario where a human can exert his/her force on a controlled elastic joint. The considered joint is the SEA prototype shown in figure 3, composed of a DC motor connected in series with a torsional spring and then to a lightweight wood frame[2]. Two high precision encoders ($20000 ppr$) are used to measure motor position and spring displacement while velocities and accelerations are obtained numerically. System parameters have been estimated as in [3] obtaining $k = 1.040\,Nm/rad$, $J_m = 0.00041\,Kg/m^2$ and $J_{frame} = 0.00025\,Kg/m^2$. These parameters gives $r = 1.62$

[2]The metal support L in figure 3 have been replaced by a wood frame to achieve a worst case condition $r \gg 0$.

meaning that the test bed itself is sensitive to the coupled dynamics.

The objective of experiments is to test robust performance of controllers (10) and (14) that we call "acceleration based" (AB) and "adaptive" (AD). We want to track a $4Hz$ harmonic torque profile within a changing environment. Both controllers are tuned to reach a critically dumped closed loop response with $15Hz$ bandwidth. To this aim we set $\lambda_1 = 40\pi$, $\lambda_2 = 400\pi^2$ for the AD controller and $k_p = \frac{J_m}{k}\lambda_2 - 1$, $k_d = \frac{J_m}{k}\lambda_1$ for the AB controller. As acceleration is computed by double differentiation we need to set the gain $k_b = 0.5$ to reduce noise.

Results are shown in figure 4 where, we create first a high impedance condition by holding the wood frame by hand (trying to be as stiff as possible) and after about $1.5s$ we release the frame to create a low impedance condition. Thus the environment is identified first with the human and then without the human (considering solely the wood frame). Errors are computed with respect to the expected performance, which are plotted in dashed line. One can see that the AB algorithm shows a different behavior among the high and low impedance conditions, meaning that it is affected by the environment. On the other hand the adaptive algorithm seem to show indistinguishable behavior between the high and low impedance conditions. Also the adaptive algorithms is more close to expected performance, showing some errors only during the short adaptation transient.

In table I we report the root mean square (RMS) and maximum (MAX) errors for the same kind of experiments. Each controller is tested in high and low impedance conditions separately and indexes are computed for each reference period[3] and considered as random processes. Considering both 3σ or 2σ confidence intervals, the AD algorithm do not shows statistical differences between performance in high and low impedance conditions. The same does not hold for AB algorithm because, as explained equation (12), the error convergence is influenced by human acceleration, which is different between the high and low impedance conditions.

The data of table I is graphically represented in figure 5 where we also show a comparison w.r.t. standard passive controllers which are not based on acceleration feedback. In particular we consider the passive PID controller (3), tuned for the high impedance condition and a PD controller tuned for the low impedance condition. The PID controller is tuned with $P = 10$ and $D = 0.1$ and $I = 4$ with a $1Hz$ roll-off frequency, accordingly to passivity constraints (higher gain values introduce noise in the system). To reach a high performance in the low impedance condition we avoid the integral term and use a passive PD controller designed using the pole placement method where the environment is considered in the low impedance condition.

An interesting observation can be derived from figure 6 where we plot the outcome of an intermittent contact test with an hard surface of AD and AB controllers. This situation usually represents a difficult control condition for robots and

[3]We collected a total of 240 periods for each controller, 120 in the high impedance condition and 120 in the low. As the reference is a $4Hz$ sinusoid the each period is $0.25s$.

	High Impedance		Low Impedance	
	AB	AD	AB	AD
RMS	16.3	**5.8**	29.6	**6.2**
σ_{RMS}	0.3	0.30	1.4	0.54
Max	26.0	**12.1**	44.6	**13.9**
σ_{Max}	0.7	1.1	1.7	1.3

Table I
COMPARISON OF RMS AND MAXIMUM ERROR $[mNm]$
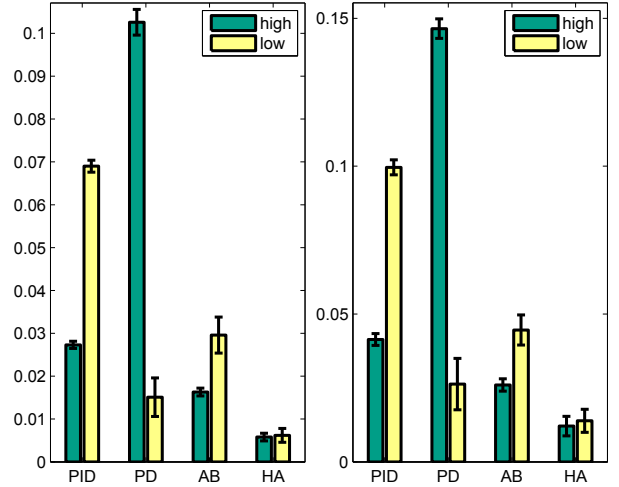
Figure 5. RMS and maximum torque tracking error for passive PID, passive PD (tuned for the low impedance), AB and AD controllers in high (green) and low (yellow) impedance conditions. Three-σ confidence intervals are shown.

to maintain safety (low contact forces) is usually challenging. In this test the adaptive controller reacts by lowering its gains because it estimates an environment which is in the middle between the contact and free conditions. As a consequence it reduces the impact forces and augments control robustness, even if at the cost of loosing a bit of accuracy. On the other hand the AB controller shows high impact forces.

VII. CONCLUSIONS

We proposed a simple and effective force control algorithm for SEAs that enables stable and predictable interaction with a human both in passive and active configuration. With respect to existing PB controllers, the proposed solution has several advantages. First it can meet desired force control specifications even when the coupled dynamics changes, second it implements patient-specific and joint-specific self-tuning, third it proved to be very accurate and robust. We think that these advantages are of paramount importance for control engineers to build effective rehabilitation or assistive devices.

In this paper we also highlight the acceleration feedback whose importance seem to be not fully recognized in the literature. We showed (1) that the acceleration based controller has a better behavior than other existing solutions and (2) that the proposed human-adaptive approach outperforms this algorithm.

(A) Force Control Based on Acceleration Feedback

(B) Adaptive Control
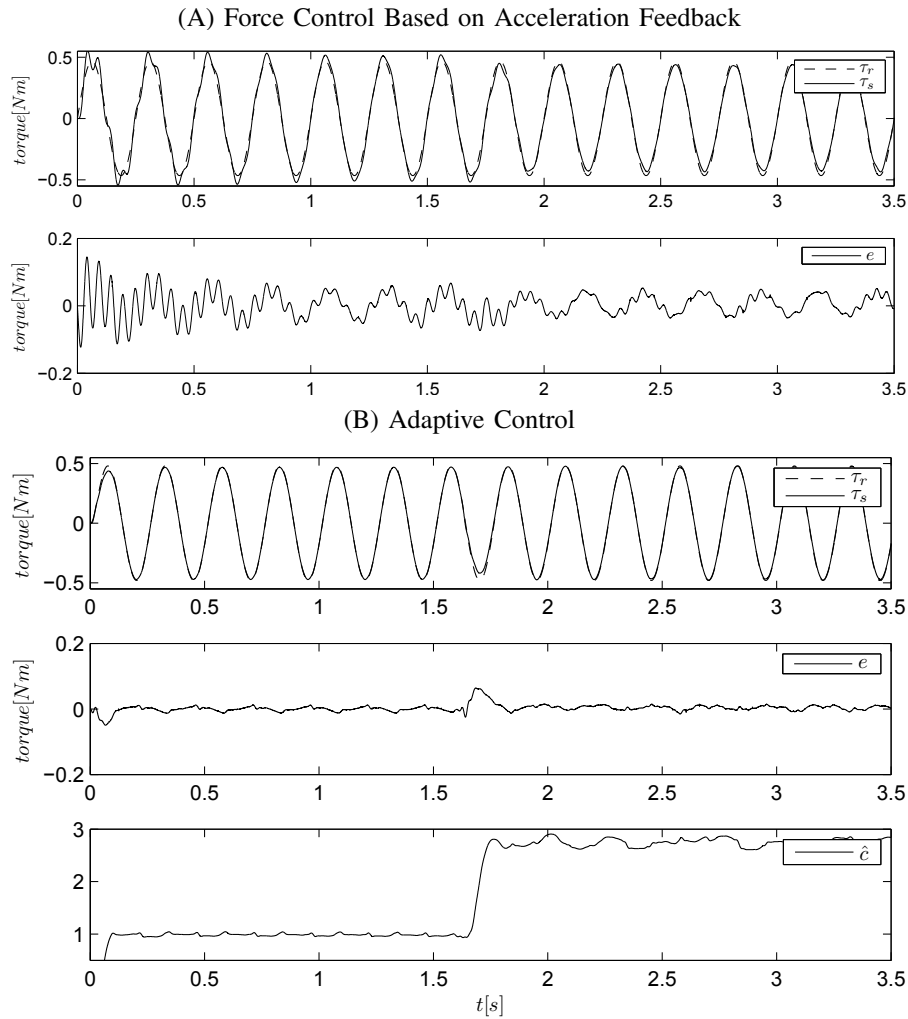
Figure 4. A comparison between the AB and AD controllers in a torque tracking experiment where at about $1.5s$ the environment impedance changes from high to low. The lower plot shows adaptation of the parameter $\hat{c}$ that in theory should be about 1.0 in the high impedance condition and 2.62 in the low impedance condition. When the environment changes some error occurs which drives $\hat{c}$ to an higher value.
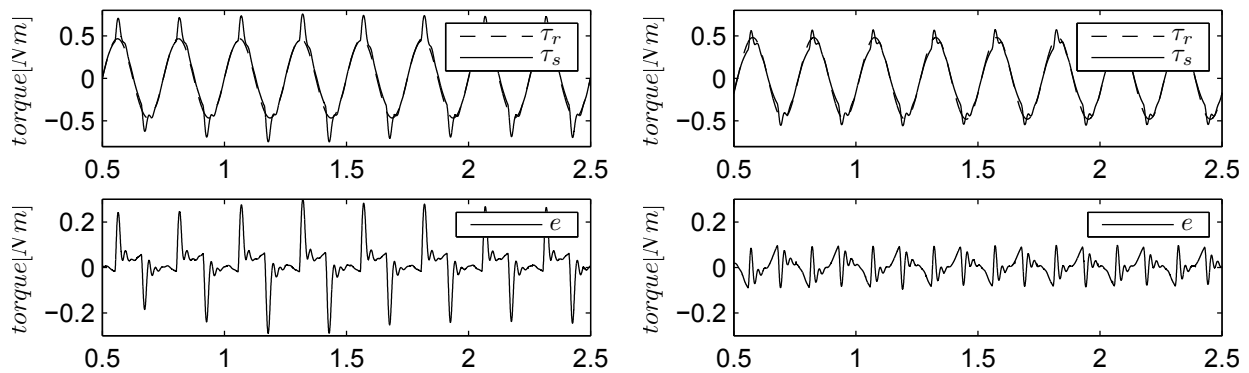
Figure 6. A comparison between the AB (left) and AD (right) controllers in an intermittent contact test.

Passivity proof is not reported in this paper and will be accounted in future works. We highlight that passivity and adaptivity are not incompatible concepts. The passivity of human-adaptive approach can lead to significant advantages both from theoretical and practical viewpoints, as summarized in the followings.

1) Stability can be proven by means of passivity meaning that we can extend the coupled stability region provided in [4].

2) The estimation can be improved by integrating more advanced estimation methods also based on prediction errors. When advanced estimation procedures are introduced the stability proof can be very challenging. However, if we provide to stay inside the passivity constraint, stability is guaranteed.

3) The proposed model reference approach necessarily introduces some latency in the control response due to the model itself and its simulation. This latency can be critical in application such as impedance control where the inner force loop needs to be as fast as possible. By using prediction error methods which does not use a reference model this issues can be solved.

4) Finally PB control allows to go beyond pHRI because a passive environment is typical of several robotic applications.

References

[1] Joonbum Bae, Kyoungchul Kong, and Masayoshi Tomizuka. Gait Phase-Based Smoothed Sliding Mode Control for a Rotary Series Elastic Actuator Installed on the Knee Joint. In *American Control Conference*, pages 6030–6035, Marriott Waterfront, Baltimore, MD, USA, 2010.

[2] SP Buerger and Neville Hogan. Complementary stability and loop shaping for improved human-robot interaction. *Robotics, IEEE Transactions on*, 23(2):232–244, 2007.

[3] Andrea Calanca, L.M. Capisani, Antonella Ferrara, and Lorenza Magnani. MIMO closed loop identification of an industrial robot. *IEEE Transactions on Control Systems Technology*, 19(5):1214–1224, 2011.

[4] Andrea Calanca and Paolo Fiorini. Human-Adaptive Control of Series Elastic Actuators. *Accepted for pubblication, Robotica, Special Issue on Rehabilitation Robotics,*, June, 2014.

[5] Andrea Calanca, S Piazza, and Paolo Fiorini. Force Control System for Pneumatic Actuators of an Active Gait Orthosis. In *Biomedical Robotics and Biomechatronics (BioRob), 2010 3rd IEEE RAS and EMBS International Conference on. 26-29 Sep, 849-854, 2010*, pages 64–69, Tokyo, 2010.

[6] Andrea Calanca, S Piazza, and Paolo Fiorini. A motor learning oriented, compliant and mobile Gait Orthosis. *Applied Bionics and Biomechanics*, 9(1):15–27, 2012.

[7] Alexander Duschau-Wicke, Joachim von Zitzewitz, Andrea Caprez, Lars Lunenburger, and Robert Riener. Path control: a method for patient-cooperative robot-aided gait rehabilitation. *IEEE transactions on neural systems and rehabilitation engineering : a publication of the IEEE Engineering in Medicine and Biology Society*, 18(1):38–48, February 2010.

[8] R E Kearney, R B Stein, and L Parameswaran. Identification of intrinsic and reflex contributions to human ankle stiffness dynamics. *IEEE transactions on bio-medical engineering*, 44(6):493–504, June 1997.

[9] Kyoungchul Kong, Student Member, and Joonbum Bae. Control of Rotary Series Elastic Actuator for Ideal Force-Mode Actuation in Human-Robot Interaction Applications. *IEEE/ASME International Conference on Mechatronics*, 14(1):105–118, 2009.

[10] Kumpati S Narendra and Anuradha M Annaswamy. Robust Adaptive Control. *1984 American Control Conference*, (TFRT-1035):848, 1985.

[11] Jerome J Palazzolo. *Robotic Technology to Aid and Assess recovery and learning in stroke patients*. PhD thesis, Massachusetts Institute of Technology., 2005.

[12] Gill A Pratt and M.M. Williamson. Series Elastic Actuators. In *International Conference on Intelligent Robots and Systems*, volume 1, pages 399–406. IEEE, 1995.

[13] Gill A Pratt, Pace Willisson, and Clive Bolton. Late motor processing in low-impedance robots: Impedance control of series-elastic actuators. In *American Control Conference*, pages 3245–3251, 2004.

[14] Jerry Pratt, Chee-meng Chew, Ann Torres, Peter Dilworth, and Gill Pratt. Virtual model control: An intuitive approach for bipedal locomotion. *International Journal of Robotics Research*, 20(2):129–143, 2001.

[15] Jean-Jacques E Slotine and Weiping Li. *Applied Nonlinear Control*, volume 62. Prentice Hall, 1991.

[16] R B Stein, E P Zehr, M K Lebiedowska, D B Popović, a Scheiner, and H J Chizeck. Estimating mechanical parameters of leg segments in individuals with and without physical disabilities. *IEEE transactions on rehabilitation engineering : a publication of the IEEE Engineering in Medicine and Biology Society*, 4(3):201–11, September 1996.

[17] S Stroeve. Impedance characteristics of a neuromusculoskeletal model of the human arm I. Posture control. *Biological cybernetics*, 81(5-6):475–94, November 1999.

[18] Nevio Luigi Tagliamonte and Dino Accoto. Passivity Constraints for the Impedance Control of Series Elastic Actuators. *Journal of Systems and Control Engineering*, 228(3):138–153, 2013.

[19] Nevio Luigi Tagliamonte, Fabrizio Sergi, Dino Accoto, Giorgio Carpino, and Eugenio Guglielmelli. Double actuation architectures for rendering variable impedance in compliant robots: A review. *Mechatronics*, 22(8):1187–1203, December 2012.

[20] K P Tee, E Burdet, C M Chew, and T E Milner. A model of force and impedance in human arm movements. *Biological cybernetics*, 90(5):368–75, May 2004.

[21] Heike Vallery, Ralf Ekkelenkamp, Herman van der Kooij, and Martin Buss. Passive and accurate torque control of series elastic actuators. *2007 IEEE/RSJ International Conference on Intelligent Robots and Systems*, pages 3534–3538, October 2007.

[22] Heike Vallery, Jan Veneman, Edwin H F van Asseldonk, Ralf Ekkelenkamp, Martin Buss, and Herman van Der Kooij. Compliant actuation of rehabilitation robots. *IEEE Robotics & Automation Magazine*, 15(3):60–69, September 2008.

[23] Y Xu and J M Hollerbach. A robust ensemble data method for identification of human joint mechanical properties during movement. *IEEE transactions on bio-medical engineering*, 46(4):409–19, April 1999.

Object Detection and Bio-Inspired Pose Estimation Algorithms for Underwater Environments

Fabjan Kallasi[1] and Fabio Oleari[1] and Marco Bottioni[1] and Dario Lodi Rizzini[1]

Abstract— In this paper we describe a novel object detection algorithm designed for underwater environments. In water, light propagation introduces distortions in acquired images that reduce their quality. The proposed object detection method operates as a pipeline in which each phase works at a different level of abstraction. First, the method starts with a preprocessing of the input image and a feature-based segmentation without specific assumptions. Then, each segmented cluster is classified according to several hypotheses on the object properties and a corresponding 3D point cloud is generated by stereo processing. Finally, a geometric alignment between a model of the target object and the obtained point cloud is performed with bio-inspired algorithms to estimate the pose. An embedded prototype stereo vision system consisting of commodity sensors has been used for the acquisition of a dataset of underwater stereo images representing several objects with different sizes and colors. In spite of the poor quality of the stereo reconstruction, the dataset has allowed the evaluation of the single-image object detection algorithms in underwater environment and of the pose estimation techniques. The algorithms described provides insights for the development of more advanced vision systems suitable for Autonomous Underwater Vehicles.

Index Terms— Underwater imaging, Image segmentation, Stereo vision, Object detection.

I. INTRODUCTION

In recent years, the interest of the scientific community for underwater computer vision has increased thanks to the evolution of sensor technology and image processing algorithms. The main challenges of underwater perception are due to the device costs, the complex setup and the distortion in signals and light propagation introduced by in the water medium. In particular, light propagation in underwater environments suffers from phenomena such as absorption and scattering. This paper describes algorithms for object detection and pose estimation in underwater environments with stereo-vision perception.

The algorithms have been developed in the context of the *Marine Autonomous Robotics for InterventionS* project (MARIS, Italian National Project). The MARIS project aims at developing a coordinated multi-AUV (Autonomous Underwater Vehicle) system able to execute generic intervention, search-and-rescue and scientific tasks in underwater environments.

[1]Authors are with RIMLab - Robotics and Intelligent Machines Laboratory, Dipartimento di Ingegneria dell'Informazione, University of Parma, Italy, {kallasi, oleari, bottioni, dlr}@ce.unipr.it

The proposed algorithms are designed to operate in four steps. The first two steps aim to detect the target object in single images through image enhancement and feature-based segmentation. The image segmentation produces a *Region of Interest* (ROI) that may represent or at least contain an object. Several approaches for ROI generation have been exploited using different assumptions on the target object. The third step uses the stereo images, combined with the generated ROI, to obtain a point-cloud representing the target in the scene w.r.t. the stereo vision frame. The final phase performs a geometric alignment of a model of the target object and the obtained point-cloud to estimate the object pose. Different bio-inspired algorithms have been exploited for the pose estimation.

Evaluation of the algorithms has been based on a dataset generated with a low-cost embedded stereo vision system developed as a prototype of the MARIS vision system [12].

The paper is organized as follows. Section II review the state of the art in object detection for underwater environments. Section III describes the image processing pipeline and section IV reports results of the evaluation of the object detection method. Section V concludes the paper with some consideration of the method developed.

II. RELATED WORK

Computer vision is a major perception modality in robotics. In underwater environments, vision is not widely used due to the light transmission problems in water fields. Instead, sonar sensing is largely used as robust perception modality for localization and reconstruction in underwater environment. In [16] Yu et al. describe a 3D sonar imaging system used for object recognition based on sonar array cameras and multi-frequency acoustic signals emissions. An extensive survey on ultrasonic underwater technologies and artificial vision is presented in Jonsson et al. [8]. Underwater laser scanner guarantee accurate acquisition [7]. However, underwater laser scanners are very expensive and suffer of the same noise of vision systems.

Computer vision provides information at lower cost and with higher acquisition rate compared to acoustic perception. Artificial vision applications in underwater environments include detection and tracking of submerged artifacts [10], seabed mapping with image mosaicing [11] and underwater SLAM [5]. Kim et al. [9] present a vision-based object detection method based on template matching and tracking

for underwater robots using artificial objects. Gracia et al. [6] compare popular feature descriptors extracted from underwater images with high turbidity. Stereo vision systems have been only recently introduced due to the difficulty of calibration and the computational performance required by stereo processing. For increasing homologous point matching performance Queiroz-Neto et al. [14] introduced a stereo matching system specific for underwater environments. Disparity of stereo images can be exploited to generate 3D models ([2];[3]).

III. ALGORITHMS

Object detection may be addressed by different techniques according to the input data: through image processing of an image acquired by a single camera or through more complex shape matching algorithms based on stereo processing.

The proposed algorithm consists of several phases (fig. 1) each operating at decreasing level of abstraction and under different assumptions. The initial step aims at detecting salient regions w.r.t. the background representing candidate objects, while the final pose estimation requires a detailed geometric description of the target object. Furthermore, the first two phases operate on a single image to detect the object whereas the two final phases use stereo images to obtain the object pose. In our evaluation we assumed that the target to be detected has cylindrical shape and can be represented by a geometric parametric model. This assumption is exploited only in the later phases of the pipeline.
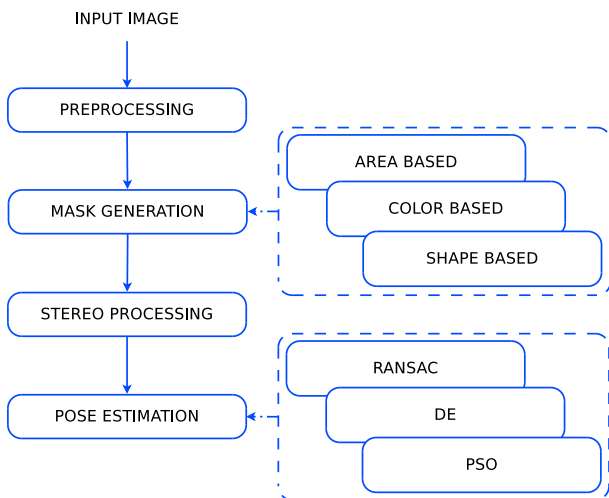
Fig. 1. Algorithmic pipeline for object detection and pose estimation.

A. Image Pre-Processing

Underwater object detection requires a vision system designed to cope with the difficult underwater light conditions. In particular, light attenuation produces blurred images with limited contrast, and light back-scattering results into artifacts in acquired images. Object detection becomes even more difficult in presence of suspended particles or with an irregular and variable background.
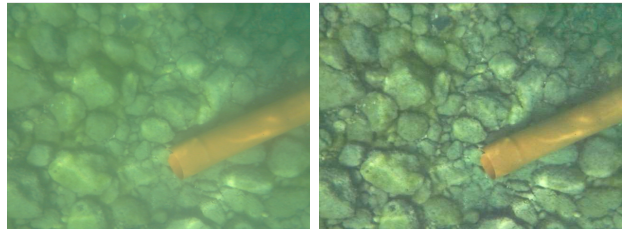
Fig. 2. An underwater image before (left) and after (right) the application of contrast mask and CLAHE.

Hence, with underwater images special attention must be paid to algorithmic solutions improving their quality.

The first phase of the algorithmic pipeline in fig. 1 is designed to compensate the color distortion due to the light propagation in water through image enhancement. No information about the object is used in this phase since the processing is applied to the whole image. Popular techniques for image enhancement are based on color restoration [1]. The approach adopted in this paper focuses on strengthening contrast to recover the blurry underwater images. A *contrast mask* method is first applied to the component L of CIELAB color space of the input image. In particular, the component $L_{in,i}$ of each pixel i is extracted, a median filter is applied to the L-channel of the image to obtain a new blurred value $L_{blur,i}$, and the new value is computed as $L_{out,i} = 1.5\ L_{in,i} - 0.5\ L_{blur,i}$. The effect of the contrast mask is a sharpened image with increased contrast.

Next, in order to re-distribute luminance, a contrast-limited adaptive histogram equalization (CLAHE) [13] is performed. The combined application of contrast mask and CLAHE compensates the light attenuation and removes artifacts in the image. Figure 2 shows an example of the pre-processing application in underwater images. It was observed that the image enhanced by CLAHE alone is not discernible from the one achieved after applying both filters. Hence, the contrast mask may not be required.

B. Mono-Camera Processing

Processing of individual images is performed on the image stream produced by one of the cameras and aims at detecting the region of the image that contains the target object. The identification of a ROI restricts the search region of the target object in later processing stages and, therefore, prevents possible detection errors. Since object recognition on a 3D point cloud is computationally expensive, mono-camera processing helps in decreasing the requested overall computation time. Furthermore, the object can be accurately detected in a single image, although the estimation of its pose remains rather difficult.

The second phase operates to detect a ROI that may represent or at least contain an object. The ROI may be searched according to different criteria based on a specific

feature of the object to be found. We developed three different approaches that exploit different assumptions on the properties of the target. The HSV (Hue Saturation Color) color space is used to improve the color segmentation results [15] since it better represents the human color perception. In particular, to quantize the total color level a color reduction is performed on the H channel of the input image. The method described in this paper uses 16 level of quantized color.

The first segmentation method is based on the assumption that the unknown object never occupies more than a given portion of image pixels and has a uniform color. The input image is partitioned into subsets of (possibly not connected) pixels with the same hue level according to the value of reduced channel H. The rough level quantization is not affected by the patterns generated by light back-scattering. The region corresponding to a given hue level is estimated as the convex hull of the pixels. Only regions whose area is less than 50% of the image are selected as part of the ROI_{area}. This heuristic rule rests on the hypothesis that the object is observed from a distance such that only the background occupies a large portion of the image. ROI estimation only exploits the relative color uniformity of a texture-less object, but it does not identify a specific object. This approach tends to overestimate the area that potentially contains the object.

The second approach exploits the information on the target color. When the object color is known, a more specific *color mask* (ROI_{color}) can be applied to detect the object with an accurate estimation of object contour. Hence, the ROI_{color} is obtained composing the regions where color is close (up to a threshold) to the target color.

The third method is based on target shapes. The detection of object shapes required an accurate image segmentation that cannot be achieved through color. Indeed, a feature vector can be associated to each pixel in order to better partition the image. Each pixel is labeled according to the Euclidean metric in the feature space. The application requires two labels corresponding to the background and to the object. A vector of two features, the value of channel H and the gradient response to *Sobel* is used to cluster with a K-means algorithm [4] and to label the corresponding pixels. The feature vector can be expanded to include other features in future applications.

The ROI_{shape} is obtained by matching each cluster-region to a projected cylinder. In particular, since the cluster-region representing the target shape is unknown, external contours for each cluster are obtained. Each closed contour represents a cluster-region and shape matching between the contours and the target shape allows the identification of the target region. Since this work is focused on the detection of cylindrical object, parallel lines effectively approximate the contour of a projected cylindrical shape. Under this assumption, the target region is recognized by detecting the two longest parallel segments in the shape. These segments are obtained using the *Hough Transform* of each contour. The longest parallel lines are computed with a cumulative histogram of the line angle w.r.t. the image origin. One of the two cluster-regions is classified as the target object if the pixel number is close to the area of the rotated rectangle generated with the parallel line angle. In contrast to the other two approaches (ROI_{area} and ROI_{color}), this method is able to detect whether there is the target object before performing pose estimation. An example of ROI generated by the second phase is shown in figure 3.

Fig. 3.   Mask generation example.

In general, object pose estimation cannot be performed on a single image, and requires 3D perception. However, if the object shape is known, as in our case, pose estimation is possible also with a monocular camera. In particular, a cylinder is defined once the cylinder radius c_r and its axis, a line with equation $c(t) = c_p + c_d\, t$, are given. The contour of a cylinder in the image plane is delimited by two lines with equations $l_i^T\, u = 0$ with $i = 1, 2$, where $u = [u_x, u_y, 1]^T$ is the pixel coordinate vector and l_1, l_2 are the coefficients. Let l_0 be the parameters of the line representing the projection of the cylinder axis in the image. The two lines with parameters l_1 and l_2 are the projections on the image plane of the two planes, which are tangent to the cylinder and contain the camera origin. The line with parameter l_0 is the projection of the plane passing through the cylinder axis and the camera origin. The equations of these three planes in the 3D space are given by

$$l_i^T\,(Kp) = (K^T\, l_i)^T\, p = n_i^T\, p = 0 \qquad (1)$$

where K is the camera matrix obtained from the intrinsic calibration, $n_i = K^T\, l_i$ the normal vectors of the planes corresponding to the lines l_i with $i = 0, 1, 2$ (in the following, the normalized normals $\hat{n}_i = n_i/\|n_i\|$ are used), and p a generic point in camera reference frame coordinates. The direction of the cylinder axis is given by direction vector $c_d = \hat{n}_1 \times \hat{n}_2$. If the cylinder radius c_r is known, then the distance of the cylinder axis from the camera center is equal to

$$d = \frac{c_r}{\sin\left(\frac{1}{2}\text{acos}\left(|\hat{n}_1 \cdot \hat{n}_2|\right)\right)} \qquad (2)$$

The projection of the camera origin on the cylinder axis is equal to $c_p = d(c_d \times \hat{n}_0)$ (if $c_{p,z} < 0$, then substitute $c_p \leftarrow -c_p$). These geometric constraints allow estimation

of the object pose in space using only a single image. The accuracy of such estimation depends on the image resolution and on the extraction of the two lines. It can be used as an initial estimation that can be refined by processing the 3D point cloud computed using stereo vision, or to validate the results.

C. Stereo-Camera Processing

The generated ROI is used as a filtering mask in the third phase to generate a lighter point-cloud that represents the 3D scene limited to the object. This filtering permits an estimation the pose of the object, with no need for further detection, in the final phase. The benefit of restricting the region size where stereo processing is performed is limited when the disparity image is computed using incremental *block-matching SAD* (sum of absolute differences) algorithm. Since the SAD of a block is computed using the SAD values of adjacent blocks, the advantage of computing the disparity image only on the ROI is reduced. Indeed, estimation of noisy point cloud limited to the ROI saves about 15% of the time for each frame.

D. Pose estimation

The final phase of the pipeline uses the geometric information of the target object to estimate the pose w.r.t. the stereo vision frame. The importance of a ROI is more apparent in object recognition, since this step requires computationally expensive operations on point clouds. In particular, the ROI can be used to select the point cloud $\mathcal{C}$ where to search objects. The objects to be recognized have a cylindrical shape and can be represented by a parametric model. In particular, we represent cylinders using 7 parameters: the three coordinates of a cylinder axis point $c_p = [c_{p,x}, c_{p,y}, c_{p,z}]^T$, the axis direction vector $c_d = [c_{d,x}, c_{d,y}, c_{d,z}]^T$, and the radius c_r. The model matching algorithm simultaneously searches for a subset of the point cloud that better fits a cylindrical shape and computes the value of the cylinder parameters $c = [c_p^T, c_d^T, c_r]^T$. For pose estimation three algorithms have been applied:

- PSO: *Particle Swarm Optimization*. Bio-inspired global optimization algorithm based on the movement of individuals swarms.
- DE: *Differential Evolution*. Bio-inspired global optimization algorithm based on the evolution of a set of individuals.
- RANSAC: *RANdom SAmple Consensus*. Model fitting algorithm.

The pose estimation is obtained through geometric alignment between the model of the searched object and the point-cloud obtained from the stereo processing.

These algorithms require a fitness function that measures the consensus of a subset of the point cloud $\mathcal{C}$ over a candidate model c. A natural fitness function is the percentage of points $p_i \in \mathcal{C}$ such that their distance to the cylinder c is less than a given threshold d_{thr}. The more obvious measure of the
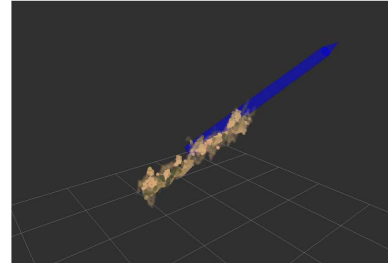
Fig. 4. An example of pose estimation by matching the raw point cloud and a cylinder model (blue).

displacement between a point p_i and a cylinder c is the Euclidean distance

$$\mathrm{d}_E(p_i, c) = \left| \frac{\|c_p \times (c_p - p_i)\|}{\|l_d\|} - r \right| \qquad (3)$$

However, the Euclidean distance may not take into account some orientation inconsistencies. If the normal vector n_i on point p_i can be estimated, the angular displacement between the normal and the projection vector of the point p_i on the cylinder c (called $\mathrm{proj}(p_i, c)$ hence after) provides

$$\mathrm{d}_N(p_i, n_i, c) = \min(\alpha_i, \pi - \alpha_i) \qquad (4)$$
$$\alpha_i = \arccos\left(\frac{n_i \cdot \mathrm{proj}(p_i, c)}{\|n_i\| \, \|\mathrm{proj}(p_i, c)\|} \right)$$
$$\mathrm{proj}(p_i, c) = p_i - c_p - \left(\frac{p_i \cdot c_d - c_p \cdot c_d}{\|c_d\|^2} \right) c_d$$

The chosen distance function is a weighted sum of two distances

$$\mathrm{d}(p_i, n_i, c) = w \cdot \mathrm{d}_E(p_i, c) + (1 - w) \cdot \mathrm{d}_N(p_i, n_i, c) \qquad (5)$$

Figure 4 shows an example where the cylinder pose is approximately recovered from the point cloud. It should be observed that the cylinder model parameters and the point-to-model distance are the only parts of the algorithm depending on the specific object shape.

IV. EXPERIMENTAL EVALUATION

The dataset required for the experimental evaluation has been acquired using the low cost stereo vision system described in [12]. This system consist of three cameras to test multiple baselines. Unfortunately, the lack of synchronism between the cameras and the quality of sensors limited the quality of the disparity images obtained from stereo processing.Two experimental sessions were conducted at the Lake of Garda (Italy) to acquire an underwater image dataset with multiple ambient situations and different objects (Fig. 5). The dataset present also several submerged cylindrical objects (depth range goes from $1.8m$ to $3m$). In both sessions the average depth of the camera was about $40cm$ below water level.

The image pre-processing algorithms discussed in section III-A significantly influence underwater object detection performance. In order to assess the effectiveness of the pre-processing algorithms, the ROI_{color} and the ROI_{area} have been computed on a set of 304 sample images. Results have been computed on both the raw and the pre-processed

Fig. 5. Images of the experimental sessions.

	Gray target	Orange target	Total
Frame number	304	443	965
TP	522	248	665
TN	417	153	216
FP	63	29	66
FN	37	13	18
Precision	91.9%	89.5%	91.0%
Recall	98.8%	95.0%	97.4%
Accuracy	92.0%	90.5%	91.3%
1-FPRate	64.0%	84.1%	76.6%
F-Measure	95.2%	92.2%	94.1%

TABLE II

SHAPE BASED SEGMENTATION PERFORMANCE.

images. The average percentage of ROI_{color} and ROI_{area} pixels over the whole image and the ratio between the two quantities are reported in Table I. The region found by the ROI_{color} only slightly depends upon the quality of the input image (since it exploits the information about the color of the object), whereas the computed ROI_{area} is more affected by the image quality. The ROI_{area} in the pre-processed image is on average only one third of the ROI_{area} computed in the raw image. Thus, assuming that the ROI_{color} reasonably approximates the ground truth, the ROI_{area} provides an adequate estimate of the object for underwater detection, as long as appropriate pre-processing is performed. Figure 6 shows an example of ROI_{area} and ROI_{color} computed on the same input frame. The complete mono-camera processing is performed on average in $74.82\ ms$, with a standard deviation of $3.20\ ms$.

Pre-processing	Frames	ROI_{color}	ROI_{area}	$\frac{ROI_{area}}{ROI_{color}}$
no	304	9.32%	33.18%	3.72
yes	304	9.07%	11.98%	1.31

TABLE I

ROI_{area} AND ROI_{color} COMPUTATION W.R.T. IMAGE PRE-PROCESSING.
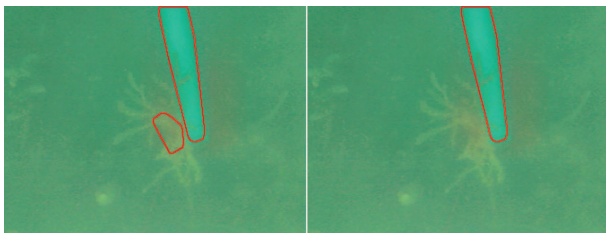
Fig. 6. Example of ROI_{area} (left) and ROI_{color} (right) computed on the same input frame.

The third mono-processing method presented in section III-A is somewhat different than the area/color based segmentation. This algorithm, besides the subset pixel representing the target object, also detects whether the image contains the target. An evaluation of the effectiveness of the shape based ROI generation is performed. The algorithm has been performed on a set of 965 frames, two kinds of color for the

cylindrical object (orange and gray) and images both with and without the target object framed. Table II illustrates the performance of shape based segmentation.

Mono-camera images have been used to estimate the pose of a cylindrical pipe, as discussed in section III-B. The algorithm computes all the parameters of the cylinder axis that allow localization of the target object. However, during experiments at the Garda lake, the embedded system swung rather fast attached to the floating support, due to the continuous waves and close to surface operation(see Figure 5). In such experiments no groundtruth is usually available, therefore a parameter invariant to camera motion is required to assess the precision of the proposed method. The object lies on the lake floor and the camera depth remains approximately constant. Thus, the distance between the camera center and the cylinder axis in equation (2) approximately meets this pre-requisite. Table III illustrates the average distance and the standard deviation of the axis computed in a sequence of 302 frames. The standard deviation of $17\ cm$ is due to both the estimation error of the algorithm and to the slight variation of distances caused by waves.

Num. Frames	Avg. Distance [mm]	Std.Dev. Distance [mm]
302	1441	169

TABLE III

MONO-CAMERA ESTIMATED DISTANCE.

A second set of experiments has aimed at assessing the object detection and pose estimation performance on the point cloud acquired in the stereo camera configuration. Unfortunately, the point cloud obtained from the underwater dataset is rather sparse and noisy. As mentioned above, in water the embedded system was attached to a floating support, and the camera baseline swang due to waves. Since the webcams are not synchronized by a hardware trigger, the computed disparity image turned out to be noisy and inaccurate. Thus, an alternative dataset of images has been acquired in air to obtain an evaluation of the full stereo-processing pipeline. In this alternative setting, the target cylindrical pipes lie in a dry river bed among sand and stones, and the embedded

Fig. 7.   Example of image from the alternative dataset.
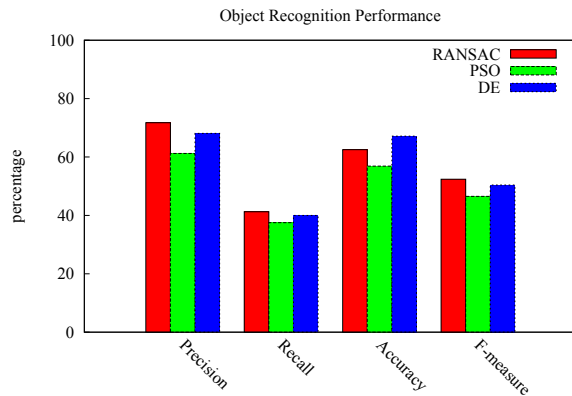
Fig. 8.   Object recognition results on the point cloud.

acquisition box is manually moved (Fig. 7).

Figure 8 summarizes the object recognition results for RANSAC, PSO, and DE recognition algorithms. The three algorithms obtain comparatively similar recognition results, but, as could be expected, RANSAC is at least one order of magnitude faster than the alternative algorithms. Figure 4 shows the recognition of a cylinder from 3D point cloud data.

V. CONCLUSIONS

This paper has presented an algorithm for underwater object detection and recognition, consisting of several steps and its experimental evaluation in real underwater environment. Suitable preprocessing and image enhancement algorithms have proven effective in improving underwater images, thereby enabling detection of regions of interest as well as detection and localization of known objects in sequential image streams gathered from a single camera. Three techniques for the detection of the ROI containing the target object have been compared. The 3D point clouds obtained from stereo processing of multiple underwater camera streams have not allowed reliable object detection and localization due to the very noisy dataset. The stereo processing pipeline has been eventually evaluated on a dataset obtained in outdoor, in-air conditions. The bio-inspired approaches of PSO and DE, as well as the RANSAC algorithm obtain the object pose estimation from the 3D point cloud and for further classify objects with a precision above 60% in all cases.

REFERENCES

[1] C. Ancuti, C.O. Ancuti, T. Haber, and P. Bekaert. Enhancing underwater images and videos by fusion. In *IEEE Conference on Computer Vision and Pattern Recognition (CVPR)*, pages 81–88, 2012.
[2] V. Brandou, A-G Allais, M. Perrier, E. Malis, P. Rives, J. Sarrazin, and P-M Sarradin. 3D reconstruction of natural underwater scenes using the stereovision system iris. In *OCEANS 2007 - Europe*, pages 1–6, 2007.
[3] R. Campos, R. Garcia, and T. Nicosevici. Surface reconstruction methods for the recovery of 3D models from underwater interest areas. In *OCEANS, 2011 IEEE - Spain*, pages 1–10, 2011.
[4] R.O. Duda, P. E Hart, and D.G. Stork. *Pattern classification*. John Wiley & Sons, 2012.
[5] R. Eustice, H. Singh, J. Leonard, M. Walter, and R. Ballard. Visually navigating the rms titanic with slam information filters. In *Proceedings of Robotics: Science and Systems*, Cambridge, USA, June 2005.
[6] R. Garcia and N. Gracias. Detection of interest points in turbid underwater images. In *IEEE OCEANS*, pages 1–9, 2011.
[7] Alan Gordon. Use of laser scanning system on mobile underwater platforms. In *Autonomous Underwater Vehicle Technology, 1992. AUV'92., Proceedings of the 1992 Symposium on*, pages 202–205. IEEE, 1992.
[8] P. Jonsson, I. Sillitoe, B. Dushaw, J. Nystuen, and J. Heltne. Observing using sound and light: a short review of underwater acoustic and video-based methods. *Ocean Science Discussions*, 6(1):819–870, 2009.
[9] Donghoon Kim, Donghwa Lee, Hyun Myung, and Hyun-Tak Choi. Object detection and tracking for autonomous underwater robots using weighted template matching. In *OCEANS, 2012 - Yeosu*, pages 1–5, 2012.
[10] M. Narimani, S. Nazem, and M. Loueipour. Robotics vision-based system for an underwater pipeline and cable tracker. In *OCEANS 2009 - EUROPE*, pages 1–6, 2009.
[11] Tudor Nicosevici, Nuno Gracias, Shahriar Negahdaripour, and Rafael Garcia. Efficient three-dimensional scene modeling and mosaicing. *Journal of Field Robotics*, 26(10), 2009.
[12] F. Oleari, F. Kallasi, D. Lodi Rizzini, J. Aleotti, and S. Caselli. Performance evaluation of a low-cost stereo vision system for underwater object detection. *World Congress of the International Federation of Automatic Control*, 2014.
[13] S. M. Pizer, E. P. Amburn, J. D. Austin, R. Cromartie, A. Geselowitz, T. Greer, B. T. H. Romeny, and J. B. Zimmerman. Adaptive histogram equalization and its variations. *Computer Vision, Graphics, Image Processing*, 39(3):355–368, September 1987.
[14] J.P. Queiroz-Neto, R. Carceroni, W. Barros, and M. Campos. Underwater stereo. In *Computer Graphics and Image Processing, 2004. Proceedings. 17th Brazilian Symposium on*, pages 170–177, 2004.
[15] S. Sural, G. Qian, and S. Pramanik. Segmentation and histogram generation using the HSV color space for image retrieval. In *International Conference on Image Processing.*, volume 2, pages II–589–II–592 vol.2, 2002.
[16] Son-Cheol Yu, Tae-Won Kim, A. Asada, S. Weatherwax, B. Collins, and Junku Yuh. Development of high-resolution acoustic camera based real-time object recognition system by using autonomous underwater vehicles. In *OCEANS 2006*, pages 1–6, 2006.

PSO-Based Automatic Object Registration for Interactive Augmented Reality

Giorgio Micconi, Jacopo Aleotti, Stefano Caselli

RIMLab - Robotics and Intelligent Machines Laboratory

Dipartimento di Ingegneria dell'Informazione, University of Parma, Italy

Email {*micconi,aleotti,caselli*}*@ce.unipr.it*

Abstract—**Advanced augmented reality (AR) applications require the ability of automatic insertion and registration of 3D models. To this purpose a bio-inspired approach for automatic generation of AR environments is proposed, based on Particle Swarm Optimization (PSO). The PSO algorithm is developed on GPU and is used for object recognition and registration from 3D range data acquired by a laser scanner. The object recognition module has been adopted in a visuo-haptic physics-based AR system for programming object manipulation tasks by demonstration. The system consists of a desktop AR application and supports 3DOF haptic interaction. The user can manipulate virtual objects superimposed upon a visual representation of the real workspace using the haptic interface. The system also supports physics-based simulation with interaction of rigid bodies. Virtual objects can be generated by CAD or created by a semi-automatic procedure, based on 3D range data. The performance of the PSO-based approach for object recognition has been assessed in multiple scenarios. Furthermore, experiments are reported to show that a precedence graph representing the logical sequence of actions of a particular task can be extracted from multiple user demonstrations in the AR environment.**

Keywords—*Augmented Reality, Particle Swarm Optimization, Programming by Demonstration.*

I. Introduction

Augmented reality (AR) is a technique that allows to add virtual information to a real context, augmenting the latter. In this way it is possible to provide more information than in the sole reality. AR has promising applications in industry, for example in remote maintenance of equipment and operator training. In these situations, it is possible to introduce virtual elements in order to simulate real counterparts, which may not be immediately available. In other contexts, simulation in AR can avoid risks associated with dangerous environments.

To reach a high level of applicability, AR must confront with problems like coherent registration of the elements in the environment and return of sensory feedback to the operator. This paper extends the work in [1] improving the user's haptic interaction within the AR environment and introducing object recognition techniques in order to automatically generate the AR scene. Furthermore, this work implements a Programming by Demonstration (PbD) technique to enable machine learning from human demonstration. The AR environment supports physics-based simulation, which provides realistic animation of the virtual scene including collision detection, friction and gravity.

The visuo-haptic AR system is implemented in a desktop setup where the user is not co-located with the real environment and a 3DOF haptic device is adopted for interaction. The haptic device provides force feedback, which is computed from collision detection, and it is coupled to a virtual proxy used for selection and manipulation of virtual objects in the AR scene. The AR environment is automatically generated using a model-based object recognition and registration algorithm. In particular, the algorithm for recognizing real objects and registering virtual 3D models is a GPU implementation of Particle Swarm Optimization (PSO), a bio-inspired optimization approach. Registration is the process of inserting a 3D model in the AR environment superimposed to the corresponding real object. The GPU implementation is developed upon CUDA architecture. PSO performs a minimization of the mean square distance between the observation of the real objects and the models in a dataset. The best matching model is selected and registered in the AR environment. 3D models can either be created using a CAD program or reconstructed from range data.

Range data are acquired from a laser scanner mounted in eye-in-hand configuration on a robot arm that is moved to observe the real workspace. Reference frames of laser scanner and AR environment are calibrated with respect to the same workspace frame.

The virtual 3D models inserted into the AR environment can either be rendered as dynamic virtual bodies, or hidden as static virtual bodies. Moreover, new dynamic virtual objects, without a real counterpart in the workspace, can be instantiated from scratch and manipulated by the user to accomplish a task.

Finally, PbD experiments have been performed exploiting the visuo-haptic AR system. The method identifies invariant precedence relations among elementary actions by examining alternative solutions to solve a task from multiple user demonstrations. A task precedence graph is then built encoding the sequential structure of the task. User demonstrations can also be performed with different initial configurations of the objects in the workspace.

The paper is organized as follows. Section II presents related works on the applications of visuo-haptic augmented reality. Section III presents the architecture of the proposed visuo-haptic AR system. Moreover, section III describes the procedure to generate 3D models of real objects, presents the method for automatic object recognition and registration and illustrates the haptic interaction paradigm. Section IV presents recognition results of PSO-based object recognition and experimental results of application of the PbD paradigm in two prototype AR environments. Finally, section V concludes the paper describing future works.

II. RELATED WORK

This analysis of related work focuses on advanced interactive AR environments and on techniques for object recognition and registration in the AR scene. An AR system with haptic interface for user interaction is presented in [1]. In the proposed application users can only push virtual objects. The system supports collaborative tasks using a ARToolKit marker and a haptic interface.

Harders et al. [2]–[4] proposed a high precision system for visuo-haptic augmented reality where the user and the environment were co-located. The system included a Phantom haptic device, it supported head mounted display and used a landmark-based method for registration. The system was successfully evaluated in both entertainment applications (table tennis game with basic physics [2]) and in medical training by interaction with a fixed deformable model [3]. The approach was extended in [4] for manipulation of deformable models using two-points interaction. The visuo-haptic system presented in this paper differs as it supports markerless object recognition and registration. Moreover, the AR system presented in this paper is an affordable solution for desktop AR, which is oriented to object manipulation for programming by demonstration with coexisting real and virtual objects.

Cosco et al. [5] presented an approach to eliminate visual obstruction in AR environments caused by the haptic devices and to achieve a consistent composition of the user's hand and virtual objects.

In [6]–[9] AR is used to create a system that allows users to program robotic tasks in an intuitive way. The system in [6], [7] is based on recognition of ARToolKit markers to register a virtual robot in the AR environment and to track user motion. The user motion is converted into a path that the robot must follow. The work also includes a collision free planning algorithm. In [8] the user guides a robot arm to complete the task. A PbD paradigm is used to learn the task. User performs demonstrations in two different setup: the first is an AR setup which provides virtual information superimposed to real images and haptic feedback; the second is a VR (Virtual Reality) setup. In [9] a complete framework for robot programming is developed. The framework consists of several modules for robotic manipulation, user interaction, object recognition and AR environment generation.

A gesture-based approach for robotic task programming in a mobile AR environment is presented in [10]. The user performs gestures with his/her hand in front of the robot. Gestures are recognized by the system and meaningful information about the task is displayed on a hand held device. Finally the system converts recognized gestures in manipulation actions of the robot.

The recognition process can be based on different methods. Lee et al. [11] proposed an object recognition and pose computation method based on template matching of RGBD data from multiple views. Object recognition and pose computation were implemented on GPU to achieve real-time performance. A different approach was proposed by Radu et al. initially in [12], [13] and subsequently extended in [14] introducing a new feature descriptor, the Fast Point Feature Histograms (FPFH). FPFH descriptors were used together with a Sample Consensus Initial Alignment (SAC-IA) algorithm. The object recognition and pose estimation approach used in this work for point cloud alignment is based on a PSO algorithm [15], [16]. The effectiveness of PSO in model-based object recognition algorithms was assessed in [17], where a CUDA implementation of the PSO algorithm was proposed and evaluated in two experiments, the first for human body pose estimation and the second about hippocampus localization in histological images.

III. VISUO-HAPTIC AUGMENTED REALITY SYSTEM

A. Setup and calibration

The system presented in this work consists of a real workspace with a supporting table on top of which objects are located and a desktop user interface for haptic interaction. Moreover, the real workspace includes a 6 DOF robot arm Comau SMART SiX and a planar laser scanner Sick LMS400. The laser scanner is mounted at the wrist of the robot manipulator in an eye-in-hand configuration. The components of the system architecture are presented in Fig. 1. The laser scanner
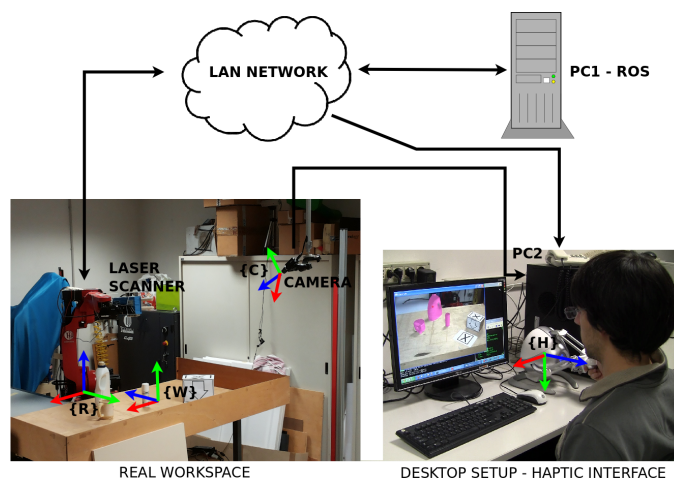
Fig. 1.   System architecture

emits 140 beams on a plane at the frequency of 190 Hz and it works at 50 nm (visible red light). 3D range data are acquired by moving the robot arm along a path, defined by a set of waypoints. The defined path allows the laser scanner to scan the workspace. The accuracy of range measurement is 1.5 cm. A first computer (PC 1 in Fig. 1, Core i7 @ 3.40 GHz, 8 GB RAM and nVIDIA GeForce 640 GT 2 GB RAM), using the ROS (Robot Operating System) framework, is dedicated to range data processing, including object recognition and registration. Moreover, the setup includes a monocular RGB camera used to acquire a video stream of the real workspace at frequency of 30 fps (images resolution is 640x480 pixels). As shown in Fig. 1, the user and the real workspace are not co-located. A second computer (PC2 in Fig. 1, Core 2 Quad @ 2.67 GHz, 4 GB RAM) is responsible of running the visuo-haptic AR application. More precisely, this second computer concurrently manages graphics rendering (OpenGL), physics-based processing, video stream acquisition and haptic rendering (1 kHz) of force feedback for user interaction. The user interface of the system includes a 3 DOF haptic device, Novint Falcon, with a resolution of 400 dpi, user range motion of 10 cm^3 and a maximum force feedback capability of about 10 N.

Physics-based animation is developed upon the Bullet Physics

Engine (http://bulletphysics.org/wordpress/), that uses a hybrid impulse and constraint-based solver with a variable time step. The table where the objects are located is modeled in the augmented reality environment as a hidden static plane.

Calibration of the individual components with respect to the same absolute frame is described in the rest of this section. There are four main reference frames (one for each component): the robot frame $\{R\}$ located on the base of the robot, the workspace frame $\{W\}$ located on the table, the camera frame $\{C\}$, oriented towards the real workspace, and the reference frame of the haptic device $\{H\}$. The laser scanner is calibrated with respect to the robot base reference frame $\{R\}$. Hence, range data are available in frame $\{R\}$ as a point cloud (set of individual points). The camera intrinsic parameters are calibrated using Zhang's method [18] by acquisition of several images of a planar chessboard pattern. The camera extrinsic parameters, i.e. the fixed transformation matrix $^W_C T$ that relates the camera reference frame to the workspace, is computed by observing the chessboard pattern laying on the table (Fig. 2). In order to calibrate the robot frame $\{R\}$ and
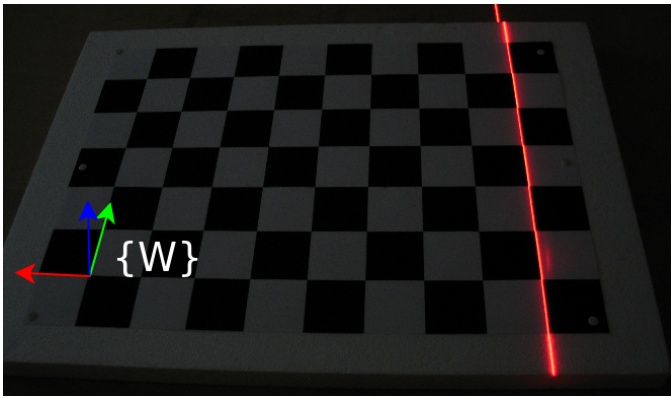
Fig. 2.   A phase of the calibration process. The Calibration chessboard, located on the workspace table, aligned to the laser line.

the camera frame $\{C\}$ with respect to the same frame, the calibration chessboard has been arranged so that the frame of the workspace $\{W\}$ is located at a known configuration in $\{R\}$. To achieve this configuration, the calibration chessboard has been arranged to be parallel to the X and Y axes of $\{R\}$, by aligning the laser line of the eye-in-hand sensor to the two axes of the chessboard. The laser has been set to project the line to a known position. This arrangement allows calibration of the robot-workspace transformation matrix $^R_W T$. Thus, all the relative transformations among frames $\{R\}$, $\{C\}$ and $\{W\}$ are known. To ensure correct registration of the AR environment the real camera and the virtual OpenGL camera must be coincident. This matching has been accomplished using the extrinsic camera parameters to set the OpenGL ModelView matrix. The intrinsic camera parameters have been used to compute in closed form the OpenGL Projection matrix for virtual camera, as shown in [1].

Finally, the relation $^W_H T$ between $\{W\}$ and the haptic frame $\{H\}$ has been defined by the composition of a scale and an axis rotation.

B. Model generation

The 3D models used as virtual objects in the AR environment can be created by a 3D CAD editor, e.g. 3D models

of mechanical parts, or can be generated by a semi-automatic procedure. This procedure has been defined to allow the generation of 3D models of real objects without preexisting CAD models. The procedure is based on the Powercrust algorithm [19] and can generate one 3D model at time. This algorithm produces a 3D triangulated mesh starting from a point cloud. The point cloud consists of the 3D range data acquired from the laser scans. Several algorithms are used to filter the noise of the point cloud. In particular, filters for removing invalid points, bounding box, removal of outliers, normal smoothing, voxel grid, plane removal, euclidean cluster extraction are applied. The last two filters are used to extract clusters (agglomerates of neighboring points) and the biggest one is consider as the real object to be reconstructed.

If the filtering process cannot fully compensate the noise affecting the point cloud, a Poisson's surface reconstruction procedure [20] is applied by the user. Poisson's surface reconstruction smooths the surface of the mesh generated by Powercrust. In some cases Poisson's surface reconstruction is not sufficient and the user must fix the model manually using a 3D CAD editor. In Fig. 3 the steps of the 3D model generation process are presented. Finally, the generated model is saved on
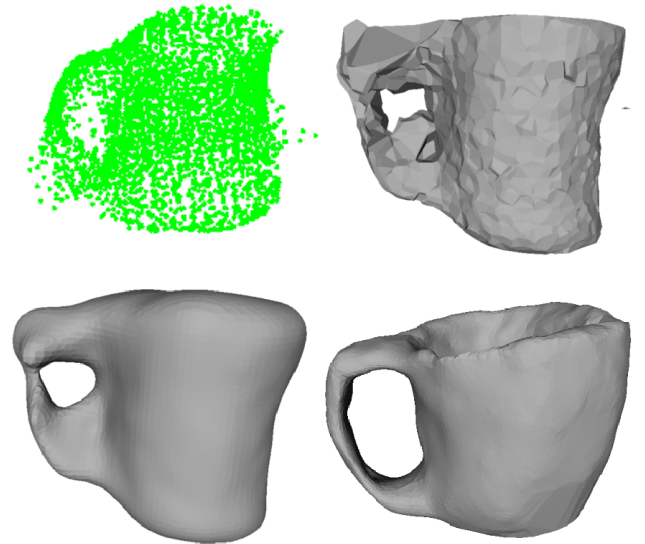
Fig. 3.   Steps of model generation phase: point cloud after the application of filters at top left corner; Powercrust reconstruction at top right corner; Poisson's surface reconstruction at bottom left corner; manual corrections applied by the user in CAD editor at bottom right corner.

two files in the dataset with different format, PCD (point cloud) for object recognition and OFF for the 3D model.

C. Object recognition and registration

To achieve realistic reconstruction of the real scene in the AR environment, correct recognition and registration of 3D models is needed. A PSO algorithm is used to recognize real objects and to register the correspondent 3D models. In this phase multiple real objects can be recognized at the same time. As described for model generation phase in III-B, the point clouds of real objects are extracted from 3D range data acquired by the laser scan. Cluster extraction uses the same filters of the model generation phase. For object recognition

and registration all the clusters bigger than a certain number of points are considered objects. No 3D reconstruction algorithm is used. The point cloud of each real object (target point cloud) that must be recognized is confronted with all the point clouds of the models in the dataset. The algorithm tries to minimize a fitness function which is the mean square distance from the target point cloud to the point cloud of the i-th model. The mean square distance is calculated as the average of the square distance from a point of the target point cloud to the nearest point of the i-th point cloud, for all points of the target point cloud. The PSO technique is used to iteratively search the transformation to be applied to the point cloud of the i-th model that minimizes the fitness function. Since the PSO technique is a heuristic method, several iterations (called generations) are required. The transformation is represented by a particle in a six-dimensional space. The algorithm instantiates several particles and the number of particles can vary widely according to the size of the problem. Each particle has a different position in the six-dimensional space and is used to apply a different transformation to the point cloud. Particles also have velocity data. At each generation position and velocity of every particle are updated based on the position of the best particle (the one that minimize the fitness function). When the value of the fitness function is below a certain threshold or the number of generations has reached a limit, the PSO algorithm terminates returning the minimum fitness function value and the associated transformation. Then, the PSO algorithm is applied on the remaining point clouds of models. Finally, the point cloud that obtains the minimum value of fitness function is considered as the correct matching and the corresponding model is registered using the computed transformation. Fig. 4 shows an example of object recognition and registration in a point cloud visualizer. Since the database
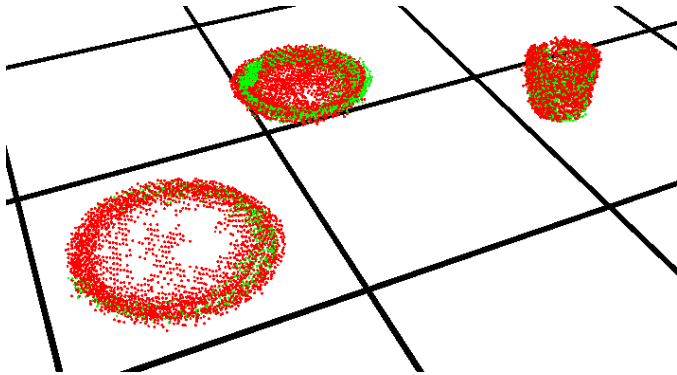

Fig. 4. Example of object recognition and registration. Target point clouds (green) and registered point clouds from the dataset (red).

of models can contain several point clouds and each point cloud consists of a large number of points (on average 6132), a GPU implementation of the PSO algorithm for nVIDIA CUDA architecture is used [17]. To achieve significant speed up two styles of parallelization are proposed: the first one is the parallelization of the update of the position of every particle; the second one is the parallelization of the fitness function calculation: for each particle (in parallel) the computation is subdivided on several parallel threads (Fig. 5).
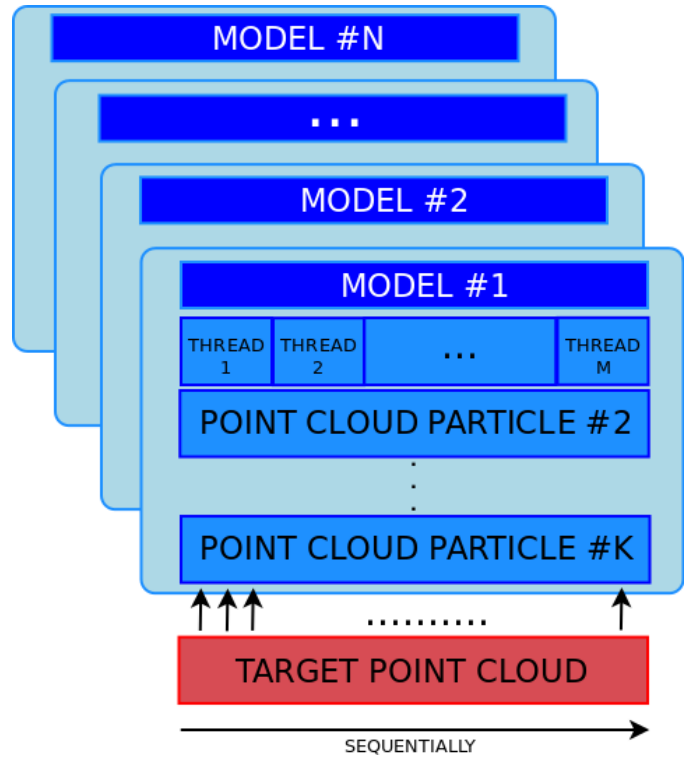
Fig. 5. Parallelization of fitness function computation on CUDA architecture: while the points of the target are confronted serially, the point clouds of i-th model are subdivided on more than one thread.

D. Haptic interaction paradigm

The AR system can contain different type of virtual bodies, that can coexist in the same environment. The registered 3D model of each recognized real object can either be rendered as a dynamic virtual body or hidden as a static virtual body. Static virtual bodies correspond to static real objects and they are hidden. The type of a virtual body is defined by manually specifying an attribute. The system also allows to instantiate dynamic virtual objects without a real counterpart in the workspace while performing a task.

Haptic interaction with the virtual objects is achieved by enabling the user to control a spherical body, called proxy, capable of physical interaction. The proxy can physically interact with both static and dynamic objects. User can select or deselect a dynamic object, attaching or detaching it from the proxy. Selection is performed by pressing a button on the haptic device when the proxy is near to a virtual object. Subsequently the user can manipulate the selected object performing translation and rotation. Finally, the user can deselect the object pressing the same button used for selection.

Since the Novint Falcon haptic interface has only 3 DOF (Degree Of Freedom), rotation can not be applied simultaneously to translation. To apply rotation the user presses a button that cause a mode-switching, from translation to rotation. This new mode maps inputs from the haptic interface to rotations of the selected object. When rotation is completed pressing another button the system switches to an intermediate mode between rotation and translation. In this mode the user moves the proxy near the 3D model. This movement is needed to return the tool point of the Falcon near the point where the user began the

TABLE I.   PARAMETERS USED BY PSO [16].

PSO parameters
$\phi_1 = 1.19$
$\phi_2 = 1.19$
$\omega = 0.5$
Ring Topology (K=1)
Population Size = 24
Generations = 90

rotational manipulation. When the proxy is near the 3D model, the system automatically switches back to translation mode.

IV.   EXPERIMENTAL EVALUATION

A. *Object recognition and registration*

The object recognition and registration phase was tested on a PC equipped with a 64-bit Intel Core i7 CPU running at 3.40GHz using CUDA v. 5.0 on an nVidia GeForce GTX680 graphics card with 1536 cores working at 1.20 GHz and compute capability 3.0. The PSO algorithm requires to set six parameters. The values of the parameters used in this work, presented in Tab. I, were tested in [21]. Moreover, in [21] different sets of PSO parameters were tested and comparison among PSO and other algorithms for object recognition and registration were presented. The purpose of the tests is to assess the ability of PSO for object recognition and registration. The tests require recognition of a point cloud of a given object among the point clouds of the dataset and registration the 3D model. The dataset contains 10 objects: a wooden mallet, a ewer, a burner, a toy horse, a mug and five different boxes of different shapes and sizes. To assess object recognition, 50 independent tests for each object were performed for a total of 500 tests. The target was confronted with other point clouds in normal conditions and simulating the presence of noise (random translation applied on all points) and partial occlusions. The presence of noise and partial occlusions was artificially generated. The results of these tests are shown in Fig. 6. The results of recognition tests show that the PSO
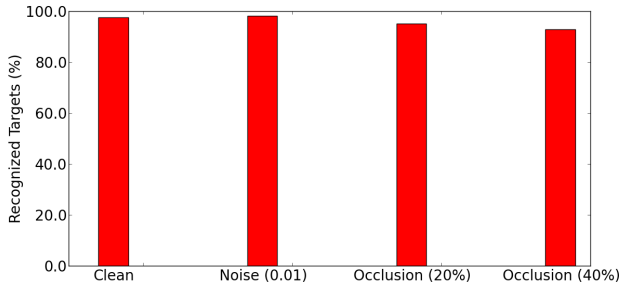
Fig. 6.   Recognition results in five different conditions: normal, noise (0.01 m), occlusion (20%), occlusion (40%).

algorithm recognizes objects in normal condition with an high rate of success (97.6%). It also recognizes objects with a similar rate in presence of noise (98.2% with 0.01m of average displacement). When objects are partially occluded (20% and 40%) the recognition rate is significantly lower but still remains at high values (95.0% and 92.8% respectively).
To test the ability of the PSO algorithm to correctly register

3D models to real objects a measurement of translation and rotation error of the registered models was performed. Error computation was based on the same data of the recognition tests. In Fig. 7 and Fig. 8 performance of registration using the PSO algorithm are presented. Fig. 7 shows the error variation in presence of increasing noise, while Fig. 8 shows the error variation in presence of increasing occlusion. While the PSO algorithm is robust to noise presence, increasing occlusion increases translation error and, in greater extent, rotation error.
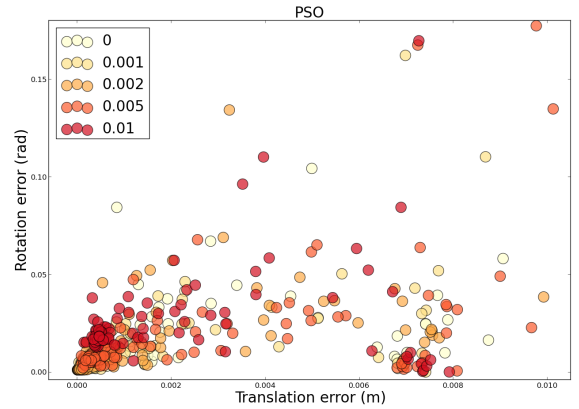
Fig. 7.   Registration error caused by noise: legend information indicate the average displacement
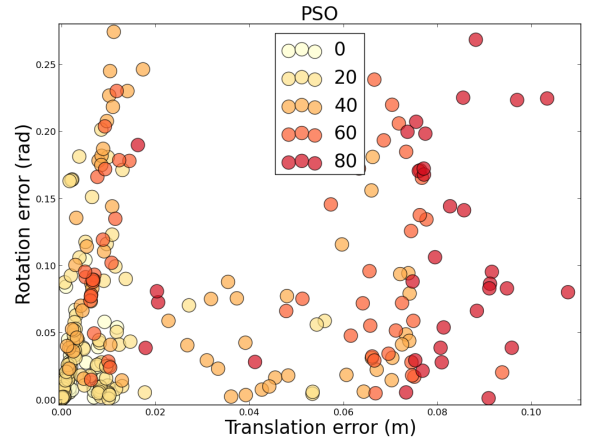
Fig. 8.   Recognition error caused by occlusion: legend information indicate occlusion percentage

B. *Programming Manipulation Tasks By Demonstration*

The user can perform manipulation actions (called elementary actions) using the haptic interface. A sequence of elementary actions, like pick and place operations of objects, is called demonstration. For this purpose, an elementary actions recognizer was implemented. The system is able to recognize elementary actions detecting the change of state of objects and the change of their relative pose. The system can recognize elementary actions like moving an object A "next to", "on top

Fig. 9. Experiment 1. Top row: first demonstration; bottom row: second demonstration. Each demonstration is a sequence of three elementary actions. Object colors are not relevant to the task.

of" or "inside" an object B.

The PbD approach enables learning manipulation tasks from multiple user demonstrations in the AR environment, generating a task precedence graph (TPG). A TPG [22] is a directed acyclic graph that defines precedence relations among the elementary actions that define a task. Precedence relations define what actions must be considered as predecessors of other actions, i.e. which actions must be performed before others to complete the task in a correct way. Precedence relations are extracted from multiple demonstrations provided by the user, updating the TPG iteratively for any new demonstration of the same task. Each demonstration must contain the same number of actions and every sequence of actions must be a permutation of the others. Hence, each demonstration must be represented by the same actions but in a different order. Since the actions are the same for every demonstration and the graph is built in an iterative way, when providing new demonstrations the cardinality of the set of precedence relations may only decrease. Indeed, new demonstrations have the effect of removing previous constraints by showing alternative solutions to complete the task.

Two experiments were performed to assess the visuo-haptic AR environment. The first experiment, shown in Figure 9, consists of 3 elementary actions: picking the jug and placing it next to the box (action A_1); picking the cup and placing it on the box (A_2); picking the cylindrical object and putting it inside the cup (A_3). The 3D model of the box is registered as a hidden static object, the cylindrical object is not real and it is instantiated by pressing a button on the keyboard. The user provides two demonstrations of the task. In the first demonstration D_1 the user performs the sequence of actions $A_1A_2A_3$, while in the second demonstration D_2 the sequence is $A_2A_3A_1$. The system learns that precedence relation (A_2, A_3) holds, i.e. the cylindrical object must be put inside the cup after the cup is placed on the box. The second experiment, shown in Figure 10, consists of a kitchen task of laying a table. The task is composed by four recognizable actions: picking the dinner plate and placing it next to the glass (A_1); picking the soup plate and placing it on top of the dinner plate (A_2); picking the knife and placing it to the right of dinner plate (A_3); picking the fork and placing it

to the left of the dinner plate (A_4). The glass 3D model is registered as a hidden static object, the fork and the knife are not real. The user provides two demonstrations of the task. In the first demonstration D_1 the user performs the sequence of actions $A_1A_2A_3A_4$, while in the second demonstration D_2 the sequence is $A_1A_4A_3A_2$. The second demonstration is performed with a different initial configuration of the object, thus requiring the environment to be re-scanned using the range sensor after the first demonstration. The system learns that precedence relations (A_1, A_2), (A_1, A_3) and (A_1, A_4) hold, i.e. the soup plate, the fork and the knife can be placed in any order but only after the dinner plate has been placed.

V. CONCLUSIONS

In this paper a PSO-based object recognition and registration technique for automatic generation of visuo-haptic AR environments has been presented. The bio-inspired approach (PSO) for object recognition has shown to successfully cope with significant amount of noise and occlusion in perception. The system supports physics-based animation and object manipulation. The AR environment has been successfully tested in a desktop setup with a 3DOF haptic device. Range data used for object recognition and registration are acquired from an eye-in-hand laser scanner mounted on a robot manipulator. The performance of the registration algorithm has been estimated quantitatively, confirming that the accuracy is adequate enough to allow the user to program sequential manipulation tasks. The system is also capable of generating 3D models of real objects without prior CAD models, based on the range data acquired from the laser scanner.

Possible extensions of this work include support for more advanced AR interaction solutions such as 6DOF haptic interfaces and head mounted displays. Future development will also focus on the execution of the learned task in the real workspace by using the robot manipulation capabilities.

REFERENCES

[1] J. Aleotti, F. Denaro, and S. Caselli, "Object manipulation in visuo-haptic augmented reality with physics-based animation," in *IEEE Intl Symposium on Robot and Human Interactive Communication*, 2010, pp. 38–43.
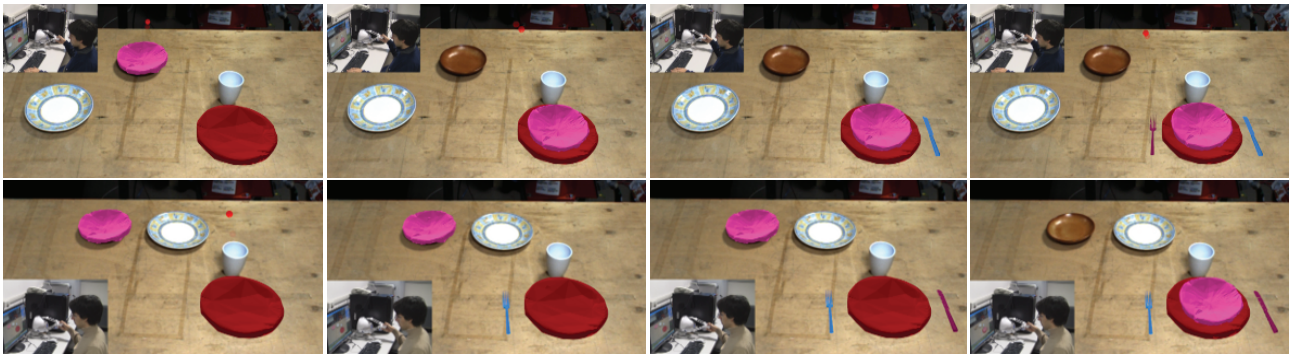
Fig. 10. Experiment 2: laying the table. Top row: first demonstration; bottom row: second demonstration. Each demonstration is a sequence of four elementary actions. Object colors are not relevant to the task.

[2] G. Bianchi, B. Knörlein, G. Székely, and M. Harders, "High Precision Augmented Reality Haptics," in *Eurohaptics*, July 2006, pp. 169–177.

[3] M. Harders, G. Bianchi, B. Knoerlein, and G. Szekely, "Calibration, Registration, and Synchronization for High Precision Augmented Reality Haptics," *IEEE Transactions on Visualization and Computer Graphics*, vol. 15, no. 1, pp. 138–149, Jan 2009.

[4] S. Jeon and M. Harders, "Extending haptic augmented reality: Modulating stiffness during two-point squeezing," in *IEEE Haptics Symposium, 2012*, March 2012, pp. 141–146.

[5] F. Cosco, C. Garre, F. Bruno, M. Muzzupappa, and M. Otaduy, "Visuo-Haptic Mixed Reality with Unobstructed Tool-Hand Integration," *Visualization and Computer Graphics, IEEE Transactions on*, vol. 19, no. 1, pp. 159–172, 2013.

[6] J. Chong, S. Ong, A. Nee, and K. Youcef-Youmi, "Robot programming using augmented reality: An interactive method for planning collision-free paths," *Robotics and Computer-Integrated Manufacturing*, vol. 25, no. 3, pp. 689–701, 2009.

[7] H. C. Fang, S. K. Ong, and A.-C. Nee, "Robot Programming Using Augmented Reality," in *International Conference on CyberWorlds, 2009*, Sept 2009, pp. 13–20.

[8] T. Hulin, V. Schmirgel, E. Yechiam, U. Zimmermann, C. Preusche, and G. Pohler, "Evaluating exemplary training accelerators for Programming-by-Demonstration," in *IEEE RO-MAN, 2010*, Sept 2010, pp. 440–445.

[9] A. Pichler and M. Ankerl, "User centered framework for intuitive robot programming," in *IEEE International Workshop on Robotic and Sensors Environments, 2010*, Oct 2010, pp. 1–6.

[10] J. Lambrecht and J. Kruger, "Spatial programming for industrial robots based on gestures and Augmented Reality," in *IEEE/RSJ International Conference on Intelligent Robots and Systems*, 2012, pp. 466–472.

[11] W. Lee, N. Park, and W. Woo, "Depth-assisted Real-time 3D Object Detection for Augmented Reality," in *International Conference on Artificial Reality and Telexistence*, 2011.

[12] R. Rusu, Z. Marton, N. Blodow, and M. Beetz, "Learning informative point classes for the acquisition of object model maps," in *10th International Conference on Control, Automation, Robotics and Vision*, 2008, pp. 643–650.

[13] R. Rusu, N. Blodow, Z. Marton, and M. Beetz, "Aligning point cloud views using persistent feature histograms," in *IEEE/RSJ International Conference on Intelligent Robots and Systems, 2008*, Sept 2008, pp. 3384–3391.

[14] R. Rusu, N. Blodow, and M. Beetz, "Fast Point Feature Histograms (FPFH) for 3D registration," in *IEEE International Conference on Robotics and Automation*, 2009, pp. 3212–3217.

[15] J. Kennedy and R. Eberhart, "Particle swarm optimization," in *IEEE International Conference on Neural Networks*, vol. 4, 1995, pp. 1942–1948.

[16] R. Poli, J. Kennedy, and T. Blackwell, "Particle swarm optimization – An Overview," in *Swarm Intell*, Aug. 2007.

[17] R. Ugolotti, Y. Nashed, P. Mesejo, v. Ivekovič, L. Mussi, and S. Cagnoni, "Particle Swarm Optimization and Differential Evolution for model-based object detection," *Applied Soft Computing*, vol. 13, no. 6, pp. 3092–3105, June 2013.

[18] Z. Zhang, "A flexible new technique for camera calibration," *IEEE Transactions on Pattern Analysis and Machine Intelligence*, vol. 22, no. 11, pp. 1330–1334, Nov 2000.

[19] N. Amenta, S. Choi, and R. Kolluri, "The Power Crust," in *Sixth ACM Symposium on Solid Modeling and Applications*, ser. SMA '01. ACM, 2001, pp. 249–266.

[20] M. Kazhdan, M. Bolitho, and H. Hoppe, "Poisson Surface Reconstruction," in *Fourth Eurographics Symposium on Geometry Processing*. Eurographics Association, 2006, pp. 61–70.

[21] R. Ugolotti, G. Micconi, J. Aleotti, and S. Cagnoni, "GPU-based Point Cloud Recognition using Evolutionary Algorithms," *EvoApplications*, April 2014.

[22] R. Zoliner, M. Pardowitz, S. Knoop, and R. Dillmann, "Towards Cognitive Robots: Building Hierarchical Task Representations of Manipulations from Human Demonstration," in *IEEE International Conference on Robotics and Automation, 2005*, April 2005, pp. 1535–1540.

Multilayer framework combining body movements and contextual descriptors for human activity understanding

Consuelo Granata, Philippe Bidaud and Axel Buendia

Abstract— The deep understanding of the human activity is an essential key for a successful Human-Robot Interaction (HRI). The translation of the sensed human behavioral signals/cues and context descriptors into an encoded human activity is still a challenge because of the complex nature of the human actions. We propose a multilayer framework for the understanding of the human activity and suitable for being implemented in a mobile robot. It is based on the ideomotor theory which argues that each human action can be seen as goal-directed movements that cause intended effects in the environment [16]. The perception layer collects data related to the kinematics and dynamics of human body and the environment/context descriptors; the classification layer combines a segment-based Support Vector Machine (SVM) method with the Video Annotation Tool from Irvine, California (VATIC) for the classification of the elementary actions; the interpretation layer allows the understanding of goal-directed activity by using a fuzzy logic-based decisional engine (developed with SpirOps AI software). In the paper, the method, the tools and the preliminary results of the framework customized for "Making coffee" task recognition are given.

I. INTRODUCTION

Social robots must be able to interact effectively with humans, to understand theirs needs, to interpret theirs orders and to predict theirs intentions. These challenging tasks can obviously benefit from considering the body language which creates a very important part of the communication. For a successful HRI, the robot must be able to translate the sensed human behavioral signals/cues and context descriptors into an encoded behavior. The question is how to map information available from uncertain and scarce data, often coming from simple sources onto natural human activities. The difficulty of this mapping process stems from the diversity and the complexity of the human activities. Even the simplest tasks can be performed with both interpersonal and intrapersonal variability. In addition, the human activity is rarely atomic: usually, a set of behaviors are performed in parallel (gestures, speech, posture etc.). Therefore the human activity is not easily codified into machine programmable constructs.

There is a vast amount of literature focusing on human action recognition. A large number of methods grounds on

C. Granata, Senior Research Engineer CNR-Sant, Centre National de Réfrence Santé à Domicile et Autonomie 33, rue Marceau 06000 Nice France, Visiting researcher Imperial College London, Department of Bioengineering, South Kensington Campus SW7 2AZ, UK. `consuelo.granata@cnr-sante.fr`

P. Bidaud, Professor Institut des Systèmes Intelligents et Robotique , UPMC-CNRS UMR 7222, 4, place Jussieu, 75005 Paris, France, ICT Scientific Deputy ONERA French AerospaceLab, Chemin de la Hunière, 91123 Palaiseau, France. `Philippe.Bidaud@upmc.fr`

A. Buendia, CEO SpirOps, 8, passage de la bonne graine 75011 Paris, France, PAST CEDRIC CNAM, 292 rue Saint Martin 75003 Paris, France. `axel.buendia@spirops.com`

the observation of body pose trajectories by using either motion capture or visual techniques in highly constrained settings. Some of these works exploit optical flow measurements from videos [7], others use motion history images to represent actions [2]. Ramanan [23] approached activity recognition by first tracking humans in the sequence, then by comparing the human body configurations to annotated motion library. Blank [1] proposed a representation of actions as space-time shapes that can be recognized by extracting space-time features from a sequence of images. In [25] the authors used dynamic time warp to analyse the stretching of trajectories in space and time. Rao and Shah [24] proposed a method to transform a trajectory into a sequence of signed dynamic instants that allows a view-invariant representation. These types of methods are effective for the classification of activities characterized by distinctive pose (e.g. performing gestures, running and jumping) but cannot be used to distinguish actions that have similar body pose trajectories.

Another approach consists on the extraction of space-time interest points in videos. Laptev [17] proposed a space-time interest point detector inspired by the idea of interest point operator presented in [11]. The approach consists on the detection of the local structures where the image has significant variation in both space and time dimensions. This method presents the limitation of producing not enough stable interest-points for the characterization of complex sequences. Another method based on interest points was proposed by Ke [15]: the interest points detected over motion vectors (optical flow) were employed as features for activity recognition with a discriminative cascade classifier. Niebles [20] proposed an unsupervised learning method for human activity recognition based on latent topic models such as probabilistic Latent Semantic Analysis (pLSA) model and Latent Dirichlet Allocation (LDA).

Due to the computational time and inaccuracy of pose detectors in video, recent systems for activity recognition grounded on feature-based approach. Dollár et al. [6] used a bag-of-words approach over visual spatio-temporal words. In [18], [19] general methodologies are proposed to capture the spatial and temporal distribution of these words. With a similar approach, Hamid et al. [10] investigated activity sequences in terms of their constituent subsequences called event *n*-grams. The authors proposed a computational frameworks that exploits this representation to discover various activity done in an environment. These methods have been proven quite effective for recognition of activities with prominent physical cues, but are not suitable to recognize fine motion like slight limbs movements. Other authors proposed

methods based on the combination of body pose and image features. For instance, Karlinsky [13] used detected body parts to find relevant visual features, Yao and Fei-Fei [27] clustered pose models that interact with objects to classify actions. Both of these methods are restricted to still images. Paker et al. [22] proposed a framework that combines the pose-based and feature-based action recognition methods. The system uses a human pose tracker that requires a one-time calibration phase to record a depth image of the scene for background subtraction. This requirement makes this method not suitable to be implemented on a mobile robot. However, the improvement of the recognition rate obtained by Paker's method suggests that combining the human body poses and the objects trajectories is an effective strategy for human activity recognition. This idea is closely related to the "predictive coding" hypothesis from the ideomotor theory [8]. The principle of "ideomotor" argues that during the execution of a particular action, a motor model (reduced order model) is automatically associated with the input of perception representing the perceptual effects of the action on the environment [12]. Our approach is based on this principle. In this context the term *action* is used to refer to *goal*-directed movements that cause intended effects in the environment [16]. Having such a model suggests to design a perception-reasoning framework to interpret the human activity taking into account both the observed person's movements (in the sense of kinematic and dynamic performances) and the effects of his actions on the environment. In this paper we present such a framework based on a multilayer reasoning system: human movements, environment and context are observed (perception layer) and used to classify the human elementary actions (classification layer); eventually the classified actions are processed to interpret and understand the general goal of the activity (interpretation layer).

For a detailed review of video-based human activity recognition we refer the reader to [14].

II. THE IDEOMOTOR APPROACH FOR HUMAN ACTIVITY RECOGNITION

The ideomotor theory suggests that the human brain continuously generates expectations on sensory input from motor activities. It considers that actions are cognitively represented in terms of their perceived effects. In this context the term *elementary action* (or more simply *action*) is used to refer to *goal*-directed movement that leads intended effects in the environment [16]. How an *action* is performed (in kinematic and dynamic points of view) is the result of pre-acquired control models and the execution of an *action* happens with unconscious awareness (unless some specific constraints are imposed). On the contrary each single *action* is programmed by humans considering the specific *goal* to achieve and the effect to produce on the *environment*. Considering such a model of human acting (Figure 1) suggests to design for the robot understanding a system that works in the opposite way: first, the analysis of the human movements and of the effects produced on the *environment* allows the understanding of the single *actions*; then, the investigation of the sequence of the
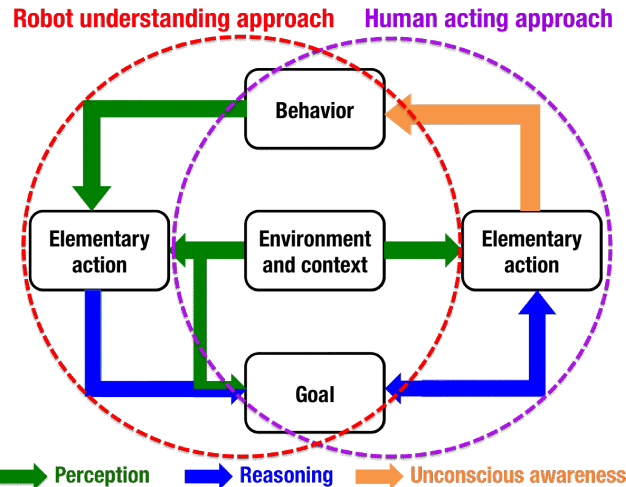
Fig. 1. Overall schema of the ideomotor theory-based approaches of human acting and robot understanding.

single *actions* can lead to the comprehension of the final *goal* of the activity. This approach suggested the hierarchical framework described in the following section.

A. Multilayer framework for encoding human activities

We propose a multilayer framework for encoding and recognizing human activities in unconstrained situations. This framework consists on: a perception layer to perceive environmental end contextual descriptors and the dynamics and kinematics of the observed human body, a classification layer to recognize the human elementary actions and an interpretation layer to understand the activities purpose. An overall view on the tools and methods implemented is given in Figure 2.

1) Perception layer: With the term *behavior* we refer to the range of humans' mannerisms while executing an action, including body movements and posture, gaze direction, facial expressions, voice and so on. In the presented system the perception of the human behavior is limited to the analysis of the body posture and motion. In most of the literature, the perception of whole body kinematics is grounded on motion capture technologies such as wearable sensors, markers and instrumented platforms. We use a marker-less system designed to capture in real-time multi-segmental human motion by using a Kinect sensor and the Microsoft Kinect SDK. The serious inaccuracy of the skeleton detection algorithm provided by the Kinect software [21], is faced and properly fixed by animating with the Kinect output a physical model of the observed human body on the dynamic simulator XDE [4]. The control implemented in the simulator filters the input data by forcing the respect of the kinematics and dynamics body constraints [9].

2) Classification layer: This layer aims to recognize the elementary actions by classifying different features such as human body posture/movements and contextual descriptors (i.e. environment and objects in the scene). We propose a method that combines the use of VATIC [26] (interactive
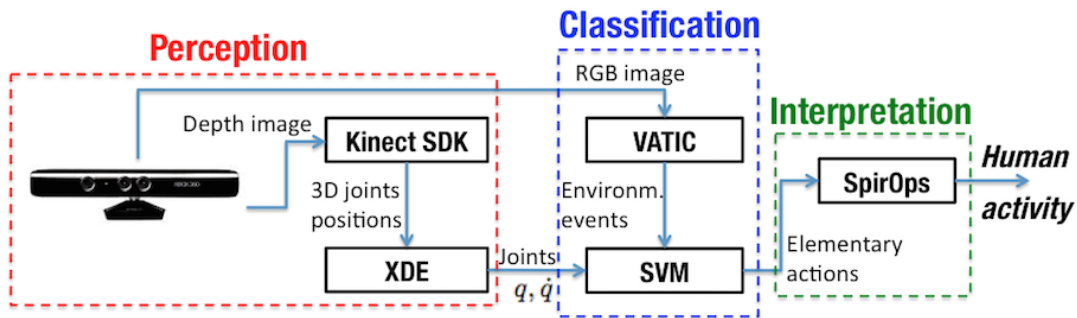
Fig. 2. General schema describing tools and methods used in the framework.

video annotation tool computer vision) and a segment-based SVM with a 2nd degree polynomial kernel classifier. The VATIC system allows a manual annotation of entities and relationships in video streams and supports some rule-based classes and subclasses (pre-annotated). It also provides the automatic tracking of target objects in the videos (Figure 3). In our knowledge, the Vatic system is the only annotation tool that provides this function. SVMs are state-of-the-art large margin classifiers which have a lot of popularity especially, but not only, within visual pattern recognition. Let $(z_1, y_1), ..., (z_n, y_n)$ (where n is the number of training samples) be a sequence pairs of labeled samples, the classical frame-based SVMs treat each labeled pair (z_i, y_i) as a training exemple (for more details on the theory behind SVM algorithm we refer the reader to [5]). This frame-based approach is not suitable in the case of events recognition, where the discriminative features consist on the evolution of the observed signals. In segment-based classification, let labeled pairs $(z_1, y_1), ..., (z_n, y_n)$, we associate to each ground truth annotation the pair $[s_i, e_i]$ where s_i indicates the start of the event and e_i the end. For each labeled event z_i observed in the interval $[s_i, e_i]$ the classifier analyzes the evolution of selected features from s_i until e_i. The SVM processes the results of the VATIC annotation in combination with the parameters computed by the virtual simulation of the body kinematics. The features considered for the classification process are the angular velocities of the body joints, the annotated objects speeds and the relative distances between the hands and the other objects.

3) Interpretation layer: This layer consists on a decision engine aimed to understand the human activity goal by considering the sequence of the classified elementary actions and the specific context (e.g. the time of the day, the room where the actions are achieved etc.). Relaying on the observation of humans achieving the "Making coffee" task we defined a probabilistic model that takes into account the nature (*compulsory* or *optional*) of the elementary actions and their order of achievement *fixed* or *variable*. For instance, "take the cup" is a compulsory elementary action, "put the sugar" is optional, "put the sugar" and then "stir" have to be executed in a fixed order, while the order of "put capsule in coffee machine" and "put water in coffee machine" can be variable. Once the model acquired, we translated it in fuzzy

TABLE I
CLASSIFIED ELEMENTARY ACTIONS.

ID	Action
1	Nothing
2	Take water
3	Move bottle
4	Manipulate bottle
5	Take cup
6	Move cup
7	Manipulate cup
8	Take coffe capsule
9	Move capsule
10	Manipulate capsule

rules, which constitute the core of the decision engine. The choice of using fuzzy logic mechanisms is motivated by the fact that we deal with a problem of decision under uncertainties (missing data, imprecise data). The compositional rules of inference, which consists in combination, intersection and projection of the fuzzy sets, are used to interpret the human activity. For the development of the decision engine we use SpirOps AI [3], a middleware dedicated to the definition of autonomous decision processes.

III. RESULTS

A. Classification

In order to train and assess the classifier, 3 persons were asked to execute randomly some elementary actions (see Table I) and than to prepare a coffee with a commercial expresso machine. We use a Kinect located in front of the person to register the video of the trials and to collect the skeleton data. In total, we registered 500 elementary actions distributed as shown in Figure 4.

To assess the performance of the classifier preventing the overfitting problem in the training phase, we use 10-fold cross validation method and we computed the number of true positive (TP), false positive (FP), true negative (TN) and false negative (FN). These 4 parameters are used to compute Precision (TP/(TP+FP), Recall (TP/(TP+FN)), Specificity (TN/(FP+TN)) and Accuracy ((TP+TN)/(TP+FP+TN+FN)) of the system for each class. The classifier showed good performances in terms of Precision ($MeanValue = 0.94$),
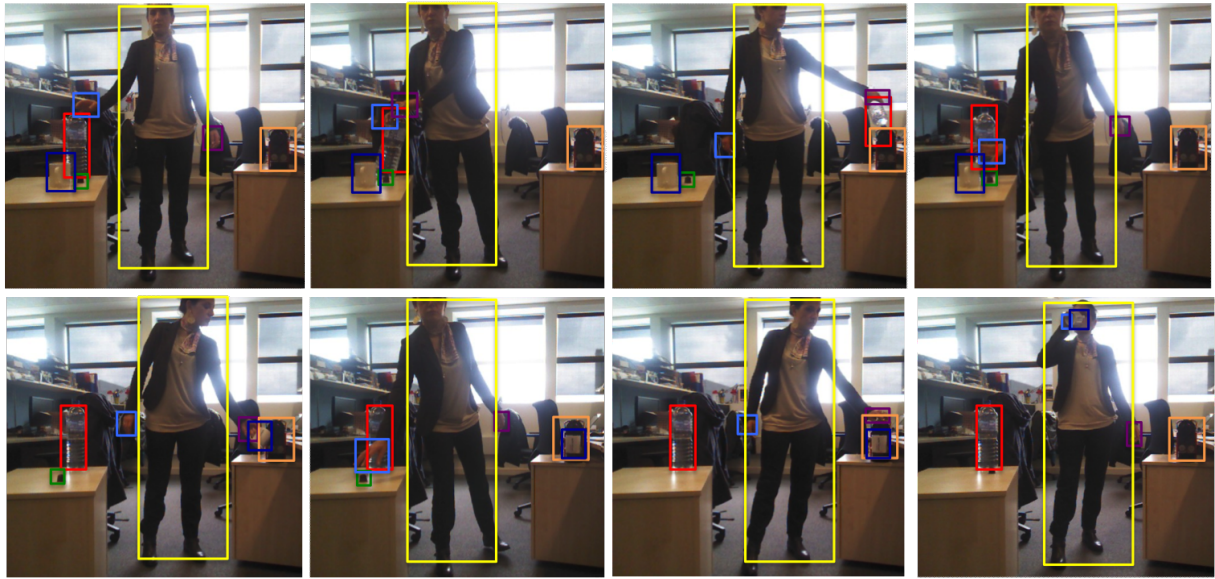
Fig. 3.   Exemple of items annotation by using Vatic.
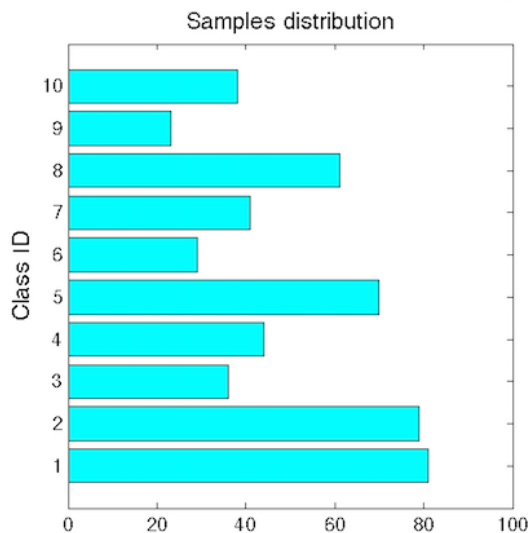
Fig. 4.   Distribution of elementary actions samples. The IDs correspond to the actions listed in Table I.

Recall ($MV = 0.91$), Accuracy ($MV = 0.98$) and Specificity ($MV = 0.98$) (see Figure 5).

B. Interpretation

A total of 35 sequences of elementary actions were extracted from the trials: 5 sequences of actions executed while preparing a coffee were used to compute the probabilistic model which was tested on 10 sequences of actions achieved to prepare coffee and 20 sequences of random actions. The average number of elementary actions per sequence was 15. After each observed elementary action the decision engine computed the probability that the current activity was the "Making coffee" task. The Figure 6 shows the number of actions that the engine required to associate to the activity

the probabilities 0.4, 0.7 and 1. 90% of the sequences was interpreted with probability $P = 1$ after a min of 7 and a max of 15 elementary actions. In Figure 7 the same results obtained for the sequences of random actions are given: the max rate associated to these sequences was $P = 0.3$. By choosing a threshold $P = 0.7$ on the interpretation rate, the system had 100% of success. These findings prove the accuracy and the precision of the decision engine but also its anticipatory capability: for all the trials the system was able to predict the final goal of the activity before having observed all the elementary actions executed by the person.

IV. CONCLUSION

We proposed the general working principles of a multi-layer framework for the understanding of human activities in unconstrained situations and inspired by the ideomotor theory of human motor control. The proposed framework combines environmental end context descriptors with the dynamics and kinematics of the observed human body (perception layer) in order to recognize the human elementary actions (classification layer) and eventually understand the goal of the activities (interpretation layer). In this paper we detailed in particular the method used for the classification and the perception layers. A segment-based SVM with a 2nd degree polynomial kernel classifier that takes into account the kinematic of the human body and some environment descriptors is used for the classification of elementary actions. The annotation is realized by using the VATIC tool. The latter is very practical to use for the learning step, but it has to be replaced by automatic detector. The classifier showed good performances in terms of Precision ($MeanValue = 0.94$), Recall ($MV = 0.91$), Accuracy ($MV = 0.98$) and Specificity ($MV = 0.98$). The interpretation layer consists on a decision engine which exploits fuzzy mechanism based on a probabilistic model extracted by the direct observation. We
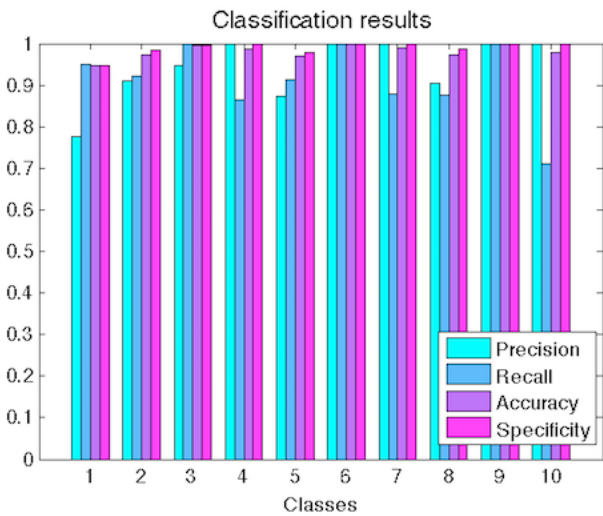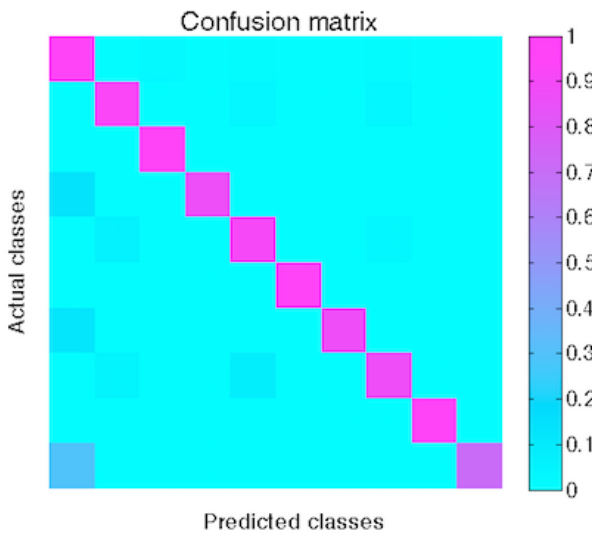
Fig. 5. Confusion matrix (top) and classification results for each class (bottom).
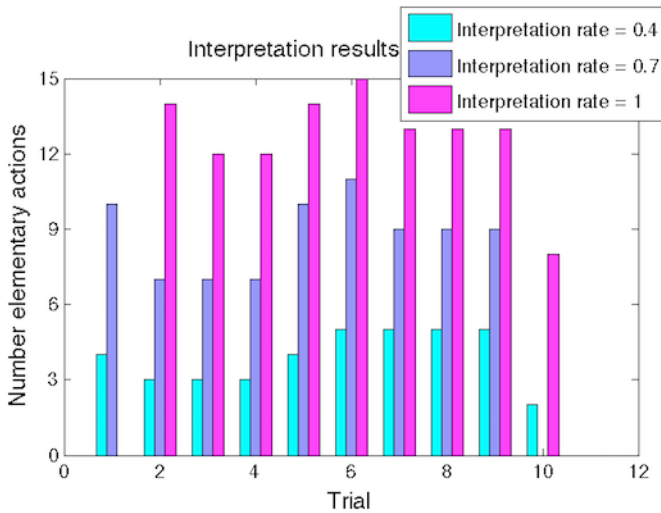
Fig. 6. Interpretation rates with respect to the number of observed elementary actions for "Making coffee" sequences.
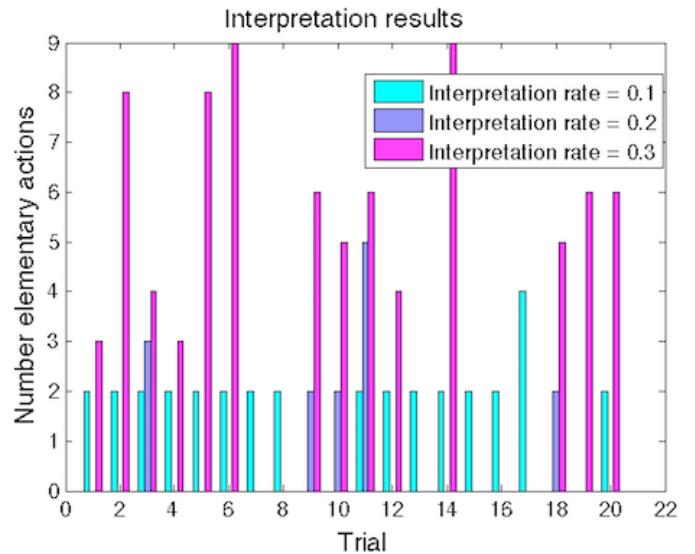
Fig. 7. Interpretation rates with respect to the number of observed elementary actions for random actions sequences.

showed the effectiveness of the decision engine in distinguish the "Making coffee" activities from the sequences of random actions (in same environment and context). Additionally, the interpretation layer proved its anticipatory capability: for all the trials the system was able to interpret correctly the activity before having observed all the elementary actions executed by the person.

REFERENCES

[1] Moshe Blank, Lena Gorelick, Eli Shechtman, Michal Irani, and Ronen Basri. Actions as space-time shapes. In *Computer Vision, 2005. ICCV 2005. Tenth IEEE International Conference on*, volume 2, pages 1395–1402. IEEE, 2005.
[2] Aaron F. Bobick and James W. Davis. The recognition of human movement using temporal templates. *Pattern Analysis and Machine Intelligence, IEEE Transactions on*, 23(3):257–267, 2001.
[3] Alex Buendia. Spirops ai, a behavior production tool. urlhttp://www.spirops.com/SpirOpsAI.php.
[4] CEA. Interactive simulation laboratory, 2012. urlhttp://www.kalisteo.fr/lsi/en/aucune/a-propos-de-xde.
[5] Nello Cristianini and John Shawe-Taylor. *An introduction to support vector machines and other kernel-based learning methods.* Cambridge university press, 2000.
[6] Piotr Dollár, Vincent Rabaud, Garrison Cottrell, and Serge Belongie. Behavior recognition via sparse spatio-temporal features. In *Visual Surveillance and Performance Evaluation of Tracking and Surveillance, 2005. 2nd Joint IEEE International Workshop on*, pages 65–72. IEEE, 2005.
[7] Alexei A Efros, Alexander C Berg, Greg Mori, and Jitendra Malik. Recognizing action at a distance. In *Computer Vision, 2003. Proceedings. Ninth IEEE International Conference on*, pages 726–733. IEEE, 2003.
[8] Birgit Elsner and Bernhard Hommel. Effect anticipation and action control. *Journal of experimental psychology: human perception and performance*, 27(1):229, 2001.
[9] Consuelo Granata, Philippe Bidaud, Ragou Ady, and Joseph Salini. Human activity analysis: a personal robot integrating a framework for robust person detection and tracking and physical based motion analysis. *PALADYN Journal of Behavioral Robotics*, 7, 2013.
[10] Raffay Hamid, Siddhartha Maddi, Amos Johnson, Aaron Bobick, Irfan Essa, and Charles Isbell. A novel sequence representation for unsupervised analysis of human activities. *Artificial Intelligence*, 173(14):1221–1244, 2009.

[11] Chris Harris and Mike Stephens. A combined corner and edge detector. In *Alvey vision conference*, volume 15, page 50. Manchester, UK, 1988.

[12] Marc Jeannerod. *The cognitive neuroscience of action.* Blackwell Publishing, 1997.

[13] Leonid Karlinsky, Michael Dinerstein, and Shimon Ullman. Using body-anchored priors for identifying actions in single images. In *NIPS*, pages 1072–1080, 2010.

[14] Shian-Ru Ke, Hoang Le Uyen Thuc, Yong-Jin Lee, Jenq-Neng Hwang, Jang-Hee Yoo, and Kyoung-Ho Choi. A review on video-based human activity recognition. *Computers*, 2(2):88–131, 2013.

[15] Yan Ke, Rahul Sukthankar, and Martial Hebert. Efficient visual event detection using volumetric features. In *Computer Vision, 2005. ICCV 2005. Tenth IEEE International Conference on*, volume 1, pages 166–173. IEEE, 2005.

[16] Iring Koch, Peter Keller, and Wolfgang Prinz. The ideomotor approach to action control: Implications for skilled performance. *International Journal of Sport and Exercise Psychology*, 2(4):362–375, 2004.

[17] Ivan Laptev. On space-time interest points. *International Journal of Computer Vision*, 64(2-3):107–123, 2005.

[18] Ivan Laptev, Marcin Marszalek, Cordelia Schmid, and Benjamin Rozenfeld. Learning realistic human actions from movies. In *Computer Vision and Pattern Recognition, 2008. CVPR 2008. IEEE Conference on*, pages 1–8. IEEE, 2008.

[19] Juan Carlos Niebles, Chih-Wei Chen, and Li Fei-Fei. Modeling temporal structure of decomposable motion segments for activity classification. In *Computer Vision–ECCV 2010*, pages 392–405. Springer, 2010.

[20] Juan Carlos Niebles, Hongcheng Wang, and Li Fei-Fei. Unsupervised learning of human action categories using spatial-temporal words. *International journal of computer vision*, 79(3):299–318, 2008.

[21] S Obdrzalek, Gregorij Kurillo, Ferda Ofli, Ruzena Bajcsy, Edmund Seto, Holly Jimison, and Michael Pavel. Accuracy and robustness of kinect pose estimation in the context of coaching of elderly population. In *Engineering in Medicine and Biology Society (EMBC), 2012 Annual International Conference of the IEEE*, pages 1188–1193. IEEE, 2012.

[22] Benjamin Packer, Kate Saenko, and Daphne Koller. A combined pose, object, and feature model for action understanding. In *CVPR*, pages 1378–1385, 2012.

[23] Deva Ramanan and David A Forsyth. *Automatic annotation of everyday movements*. Computer Science Division, University of California, 2003.

[24] Cen Rao, Alper Yilmaz, and Mubarak Shah. View-invariant representation and recognition of actions. *International Journal of Computer Vision*, 50(2):203–226, 2002.

[25] Alireza Vahdatpour, Navid Amini, and Majid Sarrafzadeh. Toward unsupervised activity discovery using multi-dimensional motif detection in time series. In *IJCAI*, volume 9, pages 1261–1266, 2009.

[26] Carl Vondrick, Donald Patterson, and Deva Ramanan. Efficiently scaling up crowdsourced video annotation. *International Journal of Computer Vision*, 101(1):184–204, 2013.

[27] Bangpeng Yao and Li Fei-Fei. Modeling mutual context of object and human pose in human-object interaction activities. In *Computer Vision and Pattern Recognition (CVPR), 2010 IEEE Conference on*, pages 17–24. IEEE, 2010.

Entrainment to natural modes of oscillation in limbless locomotion, with adaptive frequency oscillators

Alessio Alessi, Dino Accoto, Eugenio Guglielmelli

Biomedical Robotics and Biomicrosystems Laboratory
Università Campus Bio-Medico di Roma

Via A. del Portillo 21, 00128, Roma, Italy
a.alessi@unicampus.it

Abstract — **In limbless locomotion thrust arises from the interaction between the environment and the undulating body of the animal. Robots inspired by snakes and fishes aim at artificially reproducing similar locomotion principles. Passive compliant elements can improve the performance of these systems in terms of efficiency, self-stabilization and complexity of control algorithms. Specifically, efficient motion patterns can be generated if robot undulation approximates one of the natural mode of oscillation of the robot mechanical structure. In this paper, a novel control architecture, designed to reach this goal, is proposed. Inspired by biological systems, the adopted architecture consists of a chain of coupled *Central Pattern Generators* (CPGs), each of which is an *Adaptive Frequency Oscillator* (AFO). The CPGs output the joints reference torques of an idealized multi-link structure with compliant joints, in order to achieve a prescribed mode of oscillation. Torques are dynamically learned using joints velocity feedback. The paper describes the CPG model and the control architecture, providing insights about their capability to actually entrain to the structure natural modes of oscillation. The effectiveness of the proposed approach is demonstrated through numerical simulations.**

Keywords—adaptive frequency oscillators, CPG, learning

I. INTRODUCTION

Taking inspiration from the principles of locomotion exploited by some animal species, it is possible to design robots that can operate in unstructured and harsh environments. Animals with slender bodies, such as snakes and fishes, exploit limbless locomotion, with characteristic body undulation [1]. In snakes this body undulation appears as a *traveling wave* with an almost uniform amplitude [2]. Eels, lampreys, and some invertebrate amphibians show similar motion patterns when swimming, although wave amplitude increases from head to tail [3]. In carangiform fish, like carps, mackerel, and trout, the amplitude of the body wave grows more rapidly toward the tail [4] and body undulation is coordinated with fins flapping motion [5]. Several solutions have been proposed in order to artificially replicate such locomotion principle in robots inspired by snakes and fishes. Some of these resort to a proper mechanical design, in the form of either multi-link rigid structures [6] or continuous flexible bodies [7]. In some cases specific actuators have been developed [8]. In order to mimic the typical gait of a species, classic feedback control strategies [9], [10], alongside a mathematical modeling of the selected animal undulatory patterns [11], are widely used.

However, reproducing motion pattern that simply mimic realistic gaits is not the main design issue, and behavioral and energetic autonomy are still a crucial aspect in the development of these systems. Behavioral autonomy can be improved by resorting to adaptive control schemes, for example based on fuzzy controllers [12], inspired to the neuronal control of biological systems [13], or endowing the robots with complex sensorial systems [14]. The energy autonomy issue can be addressed reformulating it as an optimal control problem [15], or embodying energy saving solutions in the robot. Such solutions may include the use of passive elastic elements [7] or magnetic transmissions [16]. Controllers based on optimization approaches typically lack flexibility, due to the limited knowledge of system dynamics when interacting with the surrounding environment. Moreover, their implementation requires a high computational effort, becoming ineffective in several real applications. In robots with compliant elements (either passive or active), a possible strategy to improve both behavioral and energetic autonomy could be to resort to adaptive controllers that are able to take advantage of the system intrinsic dynamics.

Indeed, locomotion in fishes and snakes is the result of three factors: 1) the ability to *locally* control visco-elastic properties of each single body segment; 2) neuronal circuits that autonomously control and regulate muscles rhythmic activity, called *Central Pattern Generators* (CPGs); 3) the continuous interaction with the surrounding environment, consisting typically in a fluid. Experiments conducted on the body segment of a leech, whose nerves were stimulated by current pulses [17], showed that when the body segment is moving in air the oscillatory movements arising from the stimulation gave rise to a *standing wave*. When interaction occurred with the watery environment, the resulting undulation was more similar to the classical traveling wave. The transition between standing and traveling wave was also observed in salamanders and other forms of amphibians with slender bodies [18]. This would

suggest that CPGs, using local feedback from muscles stretches, are able to modulate muscles rhythmic contractions in order to drive the system, comprising the animal body and the surrounding fluid, to its natural modes of oscillations. In [19], it shown as it is possible to design controllers able to generate body undulations in simple models of snake- and eel-like robots, using the same principles. In particular, it is proved that, according to the *mechanical rectifier theory* [20], a CPG control architecture that is able to entrain the system to its natural modes of oscillation (intended in a generalized way), is able to generate body undulation, which are very similar to the ones exploited by real animals. The CPGs controllers proposed in [19] are based on *positive rate feedback* and *Reciprocal-Inhibitory-Oscillators* (RIO) [21] models of neuronal oscillators. In order to entrain the system to its natural modes, the RIO-controllers must be properly designed and some knowledge about the dynamic properties of the system (especially friction coefficients) is required, limiting the possibility of effective implementation of these methods in real robots.

In [22] *Adaptive Frequency Oscillators* (AFOs) are used to design controllers that are able to self-tune to the natural frequencies of a legged robot with compliant mechanical structure. In general, AFOs are non-linear perturbed oscillators that, differently from other type of oscillators, are able to adapt their intrinsic frequency and phase to every kind of periodic perturbation, by means of a learning mechanism, embedded in their dynamics, known as *dynamic Hebbian learning* [23]. So, if the perturbation is a periodic signal, an AFO is able to learn the signal frequency and phase. In [22] it is shown that when an AFO is used in a closed loop feedback control, with a *Single Input Single Output* (SISO) system, with a proper choice of the sensorial output used to perturb the oscillator, it is possible to bring the system at one of its resonance frequency. CPGs control architecture based on the same principles have been proposed in control strategies for learning by demonstration in legged robots [24] and biomechanical models of human walking [25], but, to the best of our knowledge, their possible application to limbless locomotion has not been explored yet.

The objective of our research is to design control architectures that are able to generate and regulate biomimetic energy-efficient motion in swimming and crawling robots endowed with compliant elements. Following the approach already proposed for legged robots, these control architectures will consist in bioinspired CPGs, based on AFOs. The main expected advantage of this approach is the possibility to generate undulatory motion patterns close to the natural modes of oscillation of the mechanical structure of the robot, while interacting with the surrounding environment. In this way, the energy loss required for the actuation is dynamically minimized, without resorting to more complex optimization algorithms and without an accurate knowledge of the system and the environment dynamics, given the ability of AFOs to dynamically adapt to sensorial feedback and to learn the characteristic frequencies of the controlled system.

This paper is a first step towards the design of such a control architecture. In Section II, starting from the simple case of a 1 dof robot, it is proved the real capability of AFOs to entrain to

the natural frequency of the system. These results are then extended to a more general class of N-dof mechanical systems, in Section III. Specifically, it is shown how a CPGs control architecture based on AFOs can also be used to entrain a N-dof system to a prescribed mode of oscillation. To simplify the analysis, interaction forces with the external environment are neglected, and the robot mechanical structure is reduced to a N-dof planar multi-link system, with lumped compliant and damping elements. The resulting control architecture could be interpreted as a pool of coupled CPGs, able to capture some essential elements at the basis of the body undulation generation in slender body animals. In Section IV, a first validation, by means of numerical simulations, is also presented, while Section V is left for discussions and conclusions.
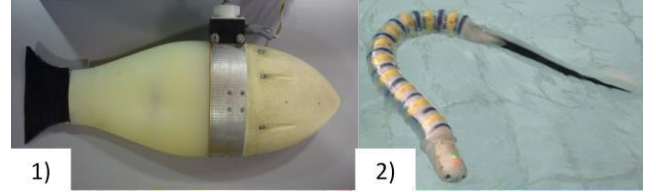
Fig. 1 – Examples of soft robots inspired to limbless-locomotion principles: 1) FILOSE EU-project carangiform robotic fish [7]; 2) LAMPETRA EU-project eel-like robot [16]

II. ADAPTIVE FREQUENCY OSCILLATORS

A. Adaptive frequency oscillator

Adaptive frequency *Hopf oscillators* can be used to simply model the adaptive dynamics of a CPG circuit [26]. Let's consider the dynamic system described, in Cartesian space, by:

$$\dot{u} = (\rho - u^2 - v^2)u - \omega v + \epsilon p_u(F) \qquad (1)$$
$$\dot{v} = (\rho - u^2 - v^2)v + \omega u + \epsilon p_v(F)$$

$$\dot{\omega} = -\mu F \frac{v}{\sqrt{u^2 + v^2}} \qquad (2)$$

$$\dot{\alpha} = \eta F u \qquad (3)$$

And

$$p_u(F) = F \frac{v^2}{\sqrt{u^2 + v^2}}$$
$$\qquad (4)$$
$$p_u(F) = -F \frac{vu}{\sqrt{u^2 + v^2}}$$
$$F = y - \alpha u \qquad (5)$$

Here ρ, ϵ, μ and η are positive real value constants and the system initial conditions are $u(0) = \sqrt{\rho}, v(0) = 0$. This dynamic system is an AFO, where (1) represents the dynamics of a perturbed Hopf oscillator, while (2) and (3) describe the frequency and amplitude learning mechanism, better known as *dynamic Hebbian learning* [23]. The state variable u is usually taken as the output of the system. The input p represents the external perturbation and can be interpreted as the AFO

feedback learning error, as described in (5). The way the perturbation affects the system dynamics is described by the *input transformations* (4). In polar coordinates the AFO equations become:

$$\dot{r} = (\rho - r^2)r \qquad (6)$$

$$\dot{\phi} = \omega - \epsilon F \sin\phi \qquad (7)$$

$$\dot{\omega} = -\lambda F \sin\phi \qquad (8)$$

$$\dot{\alpha} = \eta F r \cos\phi \qquad (9)$$

$$F = y - \alpha r \cos\phi \qquad (10)$$

where $u = r\cos\phi$. When $F = 0$, a stable limit cycle occurs. In general, if y in (5) is a periodic signal, the AFO limit cycle has the same period of y. When the limit cycle is established, the oscillator exhibits sinusoidal oscillations, described by:

$$u(t) = \sqrt{\rho}\cos(\bar{\omega}t - \varphi_0)$$

being $\bar{\omega}$ the frequency of y, φ_0 a constant related to the time needed by the AFO to reach the stable limit cycle.

If u is interpreted as the membrane potential of a neuron (Fig. 2) and y as the sensorial feedback from body segment, the AFO is able to capture the essential features of a CPG circuit, that is able to autonomously generate rhythmic inputs and to dynamically adapt to external inputs. In the next section we show how this property allows the AFO to entrain to natural resonance when coupled with a simple 1 dof system.

B. 1 dof systems

Let's consider the simple case of a 1 dof actuated rotational mass-spring-damper system (Fig. 3), whose dynamics is described by:

$$J_0\ddot{\theta} + D_0\dot{\theta} + K_0\theta = \tau \qquad (11)$$

In (11) θ and τ respectively are the joint angular displacement and actuation torque, while J_0 is the inertia, D_0 is the damping coefficient and K_0 is the stiffness of the system. As it is well known, an underdamped system, excited by a driving torque

$$\tau(t) = A\cos\omega_o t$$

oscillates at its natural frequency, the sum of kinetic and potential energy is constant and the damping effect is entirely compensated by the driven torque. Therefore, angular velocity and torque are in phase. Looking at the required power, this is an optimal condition.

Typically, the parameters in (11) are only partially known and (11) could be valid only for small amplitude oscillations, if nonlinearities and un-modeled force due to the interaction with the environment (i.e. friction in crawling robots, drag and added inertia in swimming robots) can be neglected. A controller based on the adaptive CPG presented in the previous section can overcome the problem of limited knowledge of the system dynamics.

Let's assume that the AFO (1)- (5) is coupled with (11) in a closed loop configuration (Fig. 4). For simplicity we set $y = \dot{\theta}$, and $\tau = u$. If (11) is undamped then the AFO converges to
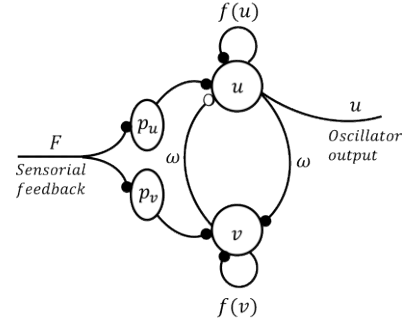
Fig. 2 – Model of a CPG based on adaptive frequency Hopf oscillator with input transformations

a limit cycle, whose frequency is exactly the system natural frequency ω_0, and this occurs for every initial condition $\left(\theta(0), \dot{\theta}(0)\right)$ and $\omega(0) \neq 0$. Indeed, when the limit cycle is established:

$$u(t) = \sqrt{\rho}\cos(\bar{\omega}t - \varphi_0)$$

The corresponding angular velocity is:

$$\dot{\theta}(t) = \sqrt{\rho}\left|\hat{H}(j\bar{\omega})\right|\cos(\bar{\omega}t + \sphericalangle\hat{H}(j\bar{\omega}) - \varphi_0)$$

where $\hat{H}(j\omega)$ is given by:

$$\hat{H}(j\omega) = \frac{j\omega}{(K_0 - J_0\omega^2) + jD_0\omega} \qquad (12)$$

The entrainment condition $F = 0$ is satisfied if and only if $\dot{\theta}(t) = \alpha u(t)$, i.e. when

$$\sqrt{\rho}\left|\hat{H}(j\bar{\omega})\right|\cos(\bar{\omega}t + \sphericalangle\hat{H}(j\bar{\omega}) - \varphi_0) \\ = \bar{\alpha}\sqrt{\rho}\cos(\bar{\omega}t - \varphi_0) \qquad (13)$$

where $\bar{\alpha}$ is the value of the amplitude at steady state. From (13) it can be found that, when the limit cycle is established, it must be:

$$\sin\left(\sphericalangle\hat{H}(j\bar{\omega})\right) = 0$$

$$\bar{\alpha} = \pm\left|\hat{H}(j\bar{\omega})\right|$$

Noticing that

$$\sphericalangle\hat{H}(j\omega) = \frac{\pi}{2} - \tan^{-1}\frac{D_0\omega}{K_0 - J_0\omega^2}$$

and therefore $-\pi < \sphericalangle\hat{H}(j\omega) < \pi$, it is possible to conclude that at the frequency $\bar{\omega}$ it is $\sphericalangle\hat{H}(j\bar{\omega}) = 0$ and $\bar{\alpha} = \left|\hat{H}(j\bar{\omega})\right|$. Since
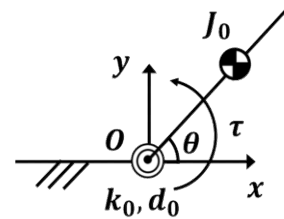
Fig. 3 – Simple 1 d.o.f. oscillating mass-spring-damper system

ω_0 is exactly the frequency at which these two conditions are satisfied, it follows that $\bar{\omega} = \omega_0$.

Furthermore, this limit cycle is stable and this means that each trajectory will be attracted asymptotically to it. It is worth notice that the parameter $\rho > 0$ can be used to control the oscillation amplitude.
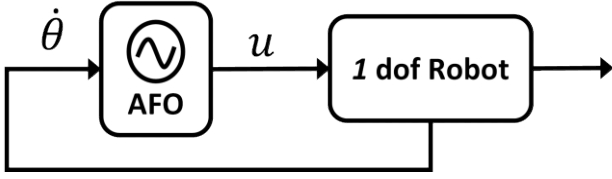
Fig. 4 – 1 dof Robot coupled with an AFO

Another interesting aspect of this controller is that, once entrainment is realized, and the oscillator has learned the system natural frequency, it can possibly act in open-loop, by disabling feedback from the system or the learning dynamics.

III. ENTRAINMENT TO NATURAL MODES OF OSCILLATION

A. Natural modes of oscillation in multi d.o.f. systems

To simplify the analysis, the mechanical structure of the robot is reduced to an open-chained multi-link system, serially connected by a finite number of rotational joints and with at least one link fixed, as shown in Fig. 5.
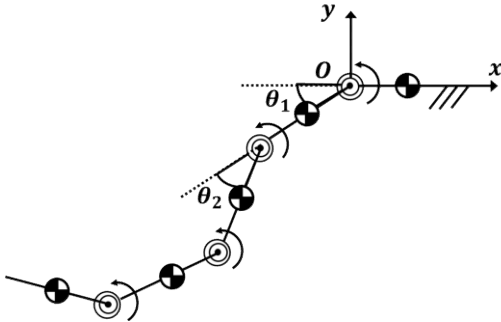
Fig. 5 – N d.o.f. multi-link system with compliant joints

We also assume that no localized external force is applied to the system and only viscous friction acts on links and joints. In these conditions, the system could be described as robotic arm with compliant joints, whose dynamic model is:

$$J_\theta \ddot{\theta} + C_\theta [\dot{\theta}\dot{\theta}] + D_{\theta,\dot{\theta}} \dot{\theta} + K_\theta \theta = \tau \qquad (14)$$

where, for a robot with N joints, $\boldsymbol{\theta} \in \mathbb{R}^N$ represents the vector of the robot joints angular displacements (joints generalized coordinates) that describes the structure configuration; $\boldsymbol{\tau} \in \mathbb{R}^N$ is the vector of joints actuators torque, and

- $J_\theta \in \mathbb{R}^{N \times N}$ is the robot inertia matrix
- $C_\theta \in \mathbb{R}^{N \times N}$ is the robot Coriolis matrix
- $K_\theta \in \mathbb{R}^{N \times N}$ is the equivalent joints stiffness matrix
- $D_{\theta,\dot{\theta}} \in \mathbb{R}^{N \times N}$ is the matrix of damping effects due to viscous friction

In general, all the dynamic matrices in (14) will depend on the mechanical structure configuration $\boldsymbol{\theta}$ and eventually on the joints angular velocities $\dot{\boldsymbol{\theta}}$. Although, inspired by the fact that efficient locomotion in elongated body animals typically occurs in the limit of small amplitude undulation, as suggested in [20], nonlinearities can be neglected, and the resulting linearized system takes the form

$$J_0 \ddot{\theta} + D_0 \dot{\theta} + K_0 \theta = \tau \qquad (15)$$

Moreover, it is reasonable to assume that K_0 and D_0 are symmetric positive definite matrices, such that:

$$K_0 = diag(k_1, k_2, \dots, k_N) \qquad (16)$$

$$D_0 = \gamma K_0 \qquad (17)$$

with $\gamma > 0$. These assumptions could be motivated by the mechanical structure of biological systems, where typically visco-elastic properties of body tissues are modeled as diagonal matrices [27]. The condition expressed by (19), known as *Rayleigh damping* model, is a further simplification, widely used in structural mechanics.

The notion of *natural modes of oscillation* in multi-dof systems is an extension of the concept of natural frequency used for single dof. While typically natural modes for discrete articulated structures are defined in terms of link orientation angles, here a different, but equivalent definition in terms of joints angles is used. Specifically, we define that a pair $(\omega_n, \boldsymbol{\vartheta}_n)$ is a *natural (or normal) mode of oscillation* of system (15) if

$$(K_0 - \omega_n^2 J_0)\boldsymbol{\vartheta}_n = \mathbf{0} \text{ and } \boldsymbol{\vartheta}_n^T \boldsymbol{\vartheta}_n = 1 \qquad (18)$$

Then, ω_n is called a *natural frequency* of the system and $\boldsymbol{\vartheta}_n$ is the corresponding *mode shape*. In general the N dof system (15) has N natural modes of oscillation and, due to the symmetry of K_0 and J_0, the associated modes shape constitute an orthonormal basis for the joint space coordinates vectors, that is

$$\boldsymbol{\vartheta}_n^T \boldsymbol{\vartheta}_m = \begin{cases} 1 \ for \ n = m \\ 0 \ for \ n \neq m \end{cases} \qquad (19)$$

B. Adaptive CPGs control architecture

We now assume to know one of the mode shape $\boldsymbol{\vartheta}_n$ of system (15). In practical applications, this would mean that the shape of the animal body undulation that the robot aims at reproducing, is known. Moreover, let's assume that the system is sufficiently underdamped to exhibit oscillations when properly driven. The objective is to design a control architecture that, similarly to what CPGs spinal circuits are supposed to do, is able to induce an undulation, that approximates the natural modes of oscillation $(\omega_n, \boldsymbol{\vartheta}_n)$ of the robot articulated structure. Taking inspiration from biological CPGs, the designed architecture should have:

- 1 CPG for each joint;
- the CPGs forming a chain of coupled oscillators; the coupling between CPGs should keep the oscillator phase-locked;
- each CPG receiving input form local sensorial feedback (i.e. joint angular displacement).

According to these considerations, the scheme used for the CPGs control architecture is the one shown in Fig. 6. Furthermore, each CPG oscillator is an AFOs, similar to the one used for the simple 1 dof mass-spring-damper system previously discussed.
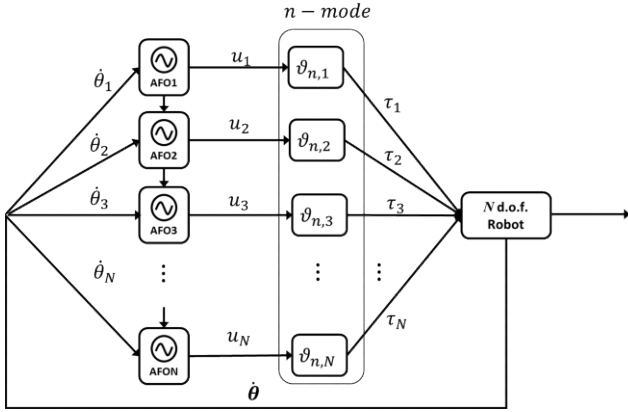

Fig. 6 – CPGs control architecture for N-d.o.f. systems

This results in a chain of coupled AFOs, where the dynamics of the $i-th$ oscillator, for simplicity of notation expressed in polar coordinates, is described by:

$$\dot{r}_i = (\rho - r_i^2)r_i \qquad (20)$$

$$\dot{\phi}_1 = \omega_1 - \epsilon F_1 \sin \phi_1$$

$$\dot{\phi}_i = \omega_i - \epsilon F_i \sin \phi_i - \beta r_i \sin(\phi_{i-1} - \phi_i - \varphi_i) \qquad (21)$$

$$i > 1$$

$$\dot{\varphi}_i = 1 - \cos(\phi_{i-1} - \phi_i - \varphi_i), i > 1 \qquad (22)$$

$$\dot{\omega}_i = -\lambda F_i \sin \phi_i \qquad (23)$$

$$\dot{\alpha}_i = \eta F_i r_i \cos \phi_i \qquad (24)$$

$$F_i = y_i - \alpha_i r_i \cos \phi_i \qquad (25)$$

The term

$$\beta r_i \sin(\phi_{i-1} - \phi_i - \varphi_i)$$

with $\beta > 0$, in (21), represents the coupling between oscillators, while (23) allows also the phase-lag between oscillators φ_i to dynamically adapt. This coupling scheme, known as unidirectional *Kuramoto coupling* [28], is typically used to describe the inter-link coordination required to reproduce undulatory motion in snake-like and fish-like robots, by means of CPGs chains [18].

According to the bio-inspired model hypothesis, each oscillator receives feedback from and control a joint of the robot. Specifically, as before, the sensorial input to the $i-th$ joint oscillator, y_i is the joint angular velocity $\dot{\theta}_i$, while the joint control torque is now given by:

$$\tau_i = u_i \vartheta_{n,i} \qquad (26)$$

being $\vartheta_{n,i}$ the $i-th$ component of the mode shape $\boldsymbol{\vartheta_n}$. This choice is justified by the fact that, in order to excite the mode $(\omega_n, \boldsymbol{\vartheta_n})$, the robot joints should be actuated by torques of the form

$$\boldsymbol{\tau}(t) = A\boldsymbol{\vartheta_n} \cos \omega_n t$$

where A is a parameter used to control joints amplitude. Indeed, it is

$$\sigma_m = \boldsymbol{\vartheta_m^T}\tau = \begin{cases} A \cos \omega_n t, & n = m \\ 0, & n \neq m \end{cases}$$

meaning that only the mode $(\omega_n, \boldsymbol{\vartheta_n})$ is excited. As for the case of a single AFO, the parameter ρ actually control torques amplitudes. It is worth noticing that this control architecture is indeed an extension of the simple case of adaptive CPG control used for 1 dof system, to which the control architecture reduces when $N = 1$.

C. Entrainment proof

Now we prove that the CPGs control architecture, introduced in the previous section, actually achieves the entrainment to the selected natural mode of oscillation. As for the case of a single AFO, the entrainment condition is realized when $F_i = 0$ for each oscillator. Then, each oscillator exhibits a stable limit cycle at a learned frequency $\bar{\omega}_i$. The Kuramoto coupling and the phase lag dynamics (22) have the effect to constraint all the oscillator to oscillate at the same frequency. Indeed, when entrainment is achieved and $\dot{\varphi}_i = 0$, it is:

$$\phi_i = \phi_{i-1} - \bar{\varphi}_i$$

$$\dot{\phi}_1 = \bar{\omega}_1 \text{ and } \dot{\phi}_i = \bar{\omega}_i, \qquad i > 1$$

where $\bar{\varphi}_i$ is the oscillator phase lag at steady state. Thus, all the oscillators are forced to oscillate at the same frequency of the only one of them that is not forced, that is oscillator 1. Then, by posing $\bar{\omega} = \bar{\omega}_1 = \bar{\omega}_i$, when entrainment is achieved, for the $i-th$ oscillator, it is:

$$\tau_i(t) = \sqrt{\rho}\vartheta_{n,i} \cos(\bar{\omega}t - \bar{\varphi}_i) = \vartheta_{n,i}u_i(t) \qquad (27)$$

$$\dot{\theta}_i(t) = \bar{\alpha}_i\sqrt{\rho} \cos(\bar{\omega}t - \bar{\varphi}_i) = \bar{\alpha}_i u_i(t) \qquad (28)$$

The two conditions expressed by (27) and (28) simply state that, at entrainment, each joint torque is in phase with the corresponding joint velocity and, for the class of mechanical systems that have been considered so far, this is a necessary and sufficient condition for the entrainment to mode $(\omega_n, \boldsymbol{\vartheta_n})$. In fact, if the system was oscillating at this mode, it would certainly be $\boldsymbol{D_0}\dot{\boldsymbol{\theta}} = \boldsymbol{\tau}$ and from (16) and (17), $\gamma k_i \dot{\theta}_i = \tau_i$ so joint velocity and torque must necessarily be in phase. Conversely, according to (28), and recalling that $u_i = r_i \cos \phi_i$ and $v_i = r_i \sin \phi_i$ in Cartesian coordinates, it is

$$\theta_i(t) = \frac{1}{\bar{\omega}}\bar{\alpha}_i v_i(t) \text{ and } \ddot{\theta}_i(t) = -\bar{\omega}\bar{\alpha}_i v_i(t)$$

or, using matrix notation:

$$\boldsymbol{\theta}(t) = \frac{1}{\omega}\boldsymbol{A}\boldsymbol{v}(t), \quad \dot{\boldsymbol{\theta}}(t) = \boldsymbol{A}\boldsymbol{u}(t), \qquad (29)$$

$$\ddot{\boldsymbol{\theta}}(t) = -\bar{\omega}\boldsymbol{A}\boldsymbol{v}(t)$$

and

$$\boldsymbol{\tau}(t) = \boldsymbol{R}\boldsymbol{u}(t) \qquad (30)$$

where

$$\boldsymbol{A} = diag(\alpha_1, \alpha_2, \dots, \alpha_N)$$

$$\boldsymbol{R} = diag(\vartheta_{n,1}, \vartheta_{n,2}, \dots, \vartheta_{n,N})$$

Substituting (29) and (30) in (15), and for the orthogonality between $\boldsymbol{u}$ and $\boldsymbol{v}$, it is found that:

$$(\boldsymbol{K_0} - \bar{\omega}^2\boldsymbol{J_0})\boldsymbol{A} = \boldsymbol{0} \qquad (31)$$

$$\boldsymbol{D_0}\boldsymbol{A} = \boldsymbol{R} \qquad (32)$$

We observe that, according to (16) and (17) in this case $\boldsymbol{D_0}$ and $\boldsymbol{A}$ are diagonal matrices, so that it is always $\boldsymbol{D_0}\boldsymbol{A} = \boldsymbol{A}\boldsymbol{D_0} = \boldsymbol{R}$. Then, it is possible to combine (31) and (32) to get

$$\begin{aligned}(\boldsymbol{K_0} - \bar{\omega}^2\boldsymbol{J_0})\boldsymbol{A}\boldsymbol{D_0}\boldsymbol{e} &= (\boldsymbol{K_0} - \bar{\omega}^2\boldsymbol{J_0})\boldsymbol{D_0}\boldsymbol{A}\boldsymbol{e} \\ &= (\boldsymbol{K_0} - \bar{\omega}^2\boldsymbol{J_0})\boldsymbol{R}\boldsymbol{e} \\ &= (\boldsymbol{K_0} - \bar{\omega}^2\boldsymbol{J_0})\boldsymbol{\vartheta_n} = \boldsymbol{0}\end{aligned} \qquad (33)$$

being $\boldsymbol{\vartheta_n} = \boldsymbol{R}\boldsymbol{e}$, with $\boldsymbol{e} = [1, 1, \dots, 1]^T \in \mathbb{R}^N$. From the definition of natural modes of oscillation (18), (33) is satisfied if and only if $\bar{\omega} = \omega_n$, thus proving that when entrainment is achieved the frequency that each oscillators reaches is no other than the natural frequency corresponding to the prescribed mode shape $\boldsymbol{\vartheta_n}$. As can simply proved from (29), this also means that at steady state all the oscillators must be in phase, that is $\bar{\varphi}_i = 0$.

IV. NUMERICAL VALIDATION

A. Uniform system

In this section we show an application of the CPG control architecture previously presented. The system considered consists of a series of cylinder bodies serially connected by rotational flexible joints. In order to capture some essential features of the characteristic dynamics of body undulation in flexible slender body animals, it is assumed that the cylinders have uniform properties and that robot links and joints have the same dynamic properties. This means that all the robot links and joints have the same mass, m_0, length, l_0, joint stiffness k_0, joint damping d_0. The first joint of the robot is assumed to be fixed (Fig. 5), so the robot dynamic model is described by (14) and (15), where the dynamic model matrices are given by:

$$\boldsymbol{J_q} = m_0 l_0^2 \left[\frac{1}{3}\boldsymbol{I_N} + \boldsymbol{N_q^T}\boldsymbol{N_q} + \boldsymbol{L_q^T}\boldsymbol{L_q} \right]$$

$$\boldsymbol{C_q} = m_0 l_0^2 \left[\boldsymbol{N_q^T}\boldsymbol{L_q} + \boldsymbol{L_q^T}\boldsymbol{N_q} \right]$$

being $\boldsymbol{N_q}$ and $\boldsymbol{L_q}$, respectively the x and y links coordinates Jacobians, normalized with respect to the links length and

$$\boldsymbol{K_q} = \boldsymbol{K_0} = k_0 \boldsymbol{I_N}$$

$$\boldsymbol{D_q} = \boldsymbol{D_0} = d_0\boldsymbol{I_N}$$

where $\boldsymbol{I_N} \in \mathbb{R}^N$ is the identity matrix. Then, for the linearized model, the inertia matrix reduces to

$$\boldsymbol{J_0} = m_0 l_0^2 \left[\frac{1}{3}\boldsymbol{I_N} + \boldsymbol{L_0^T}\boldsymbol{L_0} \right] = m_0 l_0^2 \boldsymbol{B_0}$$

An important consequence of this is that, analogously to the case of a vibrating uniform free end beam, the modes shape of the system does not depend on the robot dynamic properties. Indeed, it is easy to prove that if $(\omega_n, \boldsymbol{\vartheta_n})$ is a mode of oscillation, than it is:

$$\left[\boldsymbol{I_N} - \left(\frac{\omega_n}{\omega_0} \right)^2 \boldsymbol{B_0} \right]\boldsymbol{\vartheta_n} = \boldsymbol{0} \qquad (34)$$

with

$$\omega_0 = \sqrt{\frac{k_0}{m_0 l_0^2}}$$

Since the matrix $\boldsymbol{B_0}$ depends only on the robot kinematics (here assumed to be fixed), (34) proves that, the mode shapes of the system do not depend on the link masses and lengths. This means that for this simple case it is always possible to know the modes shape of the structure. In TABLE 1, the natural modes of a robot with $N = 6$ dofs are reported. The value of the corresponding natural frequencies are expressed with respect to the system characteristic frequency ω_0. A sketch of the first 3 modes shape of the robot is shown in Fig. 7.

TABLE 1 - Uniform N-dof system natural modes of oscillation

| n	ω_n/ω_0	ϑ_n					
		1	2	3	4	5	6
1	0.0420	0.7060	0.5393	0.3786	0.2323	0.1117	0.0297
2	0.2719	-0.5255	0.0361	0.4411	0.5720	0.4240	0.1447
3	0.7480	0.3787	-0.4100	-0.4388	0.1864	0.6022	0.3141
4	1.2679	0.2476	-0.5556	0.1473	0.5238	-0.3485	-0.4608
5	1.5931	0.1370	-0.4496	0.5848	-0.3212	-0.1568	0.5562
6	1.7186	-0.0434	0.1697	-0.3253	0.4545	-0.5469	0.5982
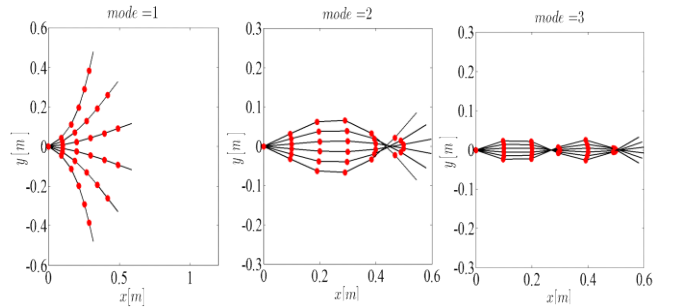
Fig. 7 – First 3 modes shape of the $N = 6$ dofs uniform system

B. Results

The adaptive CPG control architecture previously presented is tested on the (nonlinear) uniform system by means of numerical simulations. Specifically, the capability of the control architecture to entrain and possibly learn one of the natural modes of the structure is tested, with special reference to the second mode Fig. 7. The values of the parameters used for the robot model are: $m_0 = 0.1\ [kg], l_0 = 0.05\ [m], k_0 = 0.013\ [Nm], d_0 = 0.016\ [Nms]$. In Fig. 8 and Fig. 8, the time evolution of the oscillators learning errors, frequencies, amplitudes and phases is reported. As it can be seen, the learning error for all the oscillators reaches a steady state, as well as frequency and amplitude. Furthermore, all the frequencies reaches the same value $\overline{\omega} \approx 1.86\ [rad/s]$ (Fig. 8-a), proving that coupling between oscillators keeps them all phase-locked, as also proved by the phases evolution (Fig. 8-c). Although, the entrained frequency is lightly different from the theoretical one, whose value is $1.97\ [rad/s]$ for the mode 2, due to the system nonlinearities. Due to the system parameters uniformity, also amplitudes reaches the same values ($\alpha \approx 63.0\ [rad/s]$) when entrainment is established (Fig. 8-b).
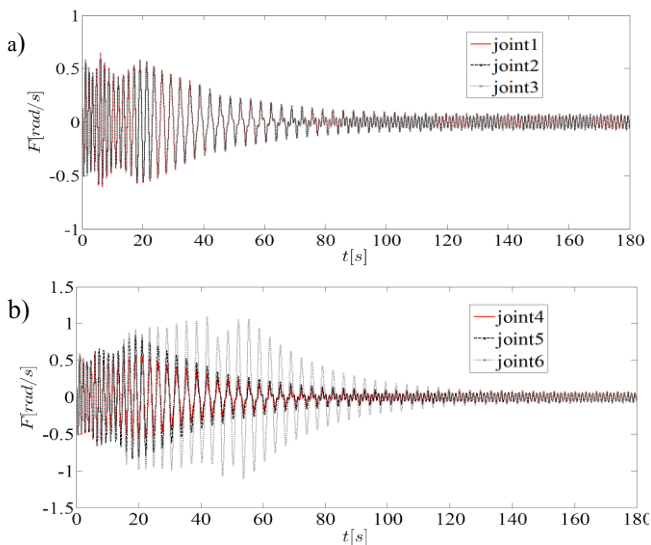
Fig. 9 – Adaptive CPGs oscillators dynamics during the simulation: learning error for joints a) 1,2, 3, b) 4,5,6. Oscillators parameters: $\epsilon = 1.0, \mu = 0.8, \eta = 380, \beta = 1.0, \omega_i(0) = 6.0, \rho = 0.015\ [Nm]$

The joints angular displacements and torques are reported in Fig. 10. Indeed, even if entrainment is theoretically exact when the system is linear, these simulations prove that the proposed control architecture is still able to let the robot to oscillate at a frequency very close to the one corresponding to the selected natural mode.

V. CONCLUSION

One of the major issue with robots inspired to the principles of limbless locomotion is autonomy, in terms both of the capability to adapt to unstructured environments and of minimizing energy consumption. A possible strategy to overcome this limitation consists in exploiting the intrinsic dynamic of the system while interacting with the environment.
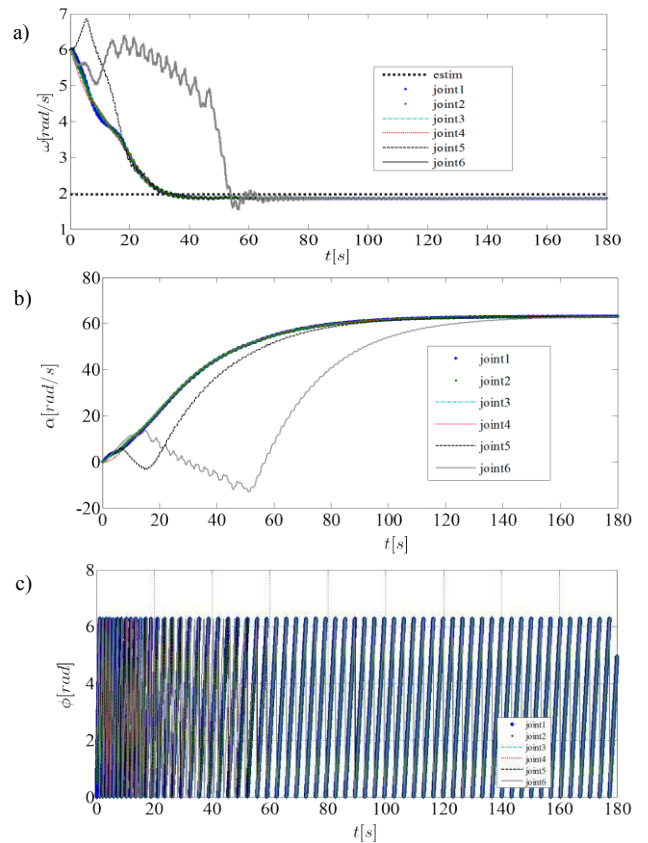
Fig. 8 – Adaptive CPGs oscillators parameters dynamics: a) frequency; b) amplitude; c) phases

Specifically, if the robot is endowed with passive compliant elements, it is possible to reproduce the typical body undulation of elongated body animals in an efficient way, by driving its mechanical structure towards one of its natural modes of oscillation, as actually real biological systems do. In this paper a novel CPGs control architecture, based on adaptive frequency oscillators, capable to entrain to a prescribed natural mode of oscillations for a class of mechanical systems used to model slender body dynamics, is presented. In these systems compliant elements and dampers are assumed to be concentrated at each joint. The effective capability of the CPGs control to drive the linearized mechanical system to one of its natural mode of oscillation, is derived starting from the simple case of a 1 dof system. Then the approach is extended to a more general class of N dof systems. A numerical validation on a N-dof robot with uniform properties (cylinder links with the same masses and link lenghts) shows the effective capability of the CPGs architecture to induce the system to oscillates at the selected natural modes.

This paper represents a first step towards the design of more complex control architectures, able to produce biomimetic and energy efficient motion patterns in swimming and crawling robots. Future works will deal with:

- the extension of the proposed architecture to more complex and realistic models, that take into account the effects on

body orientation, as well as the interactions with the surrounding environment;

- an experimental validation of the proposed architecture on snake-like and fish-like robots.
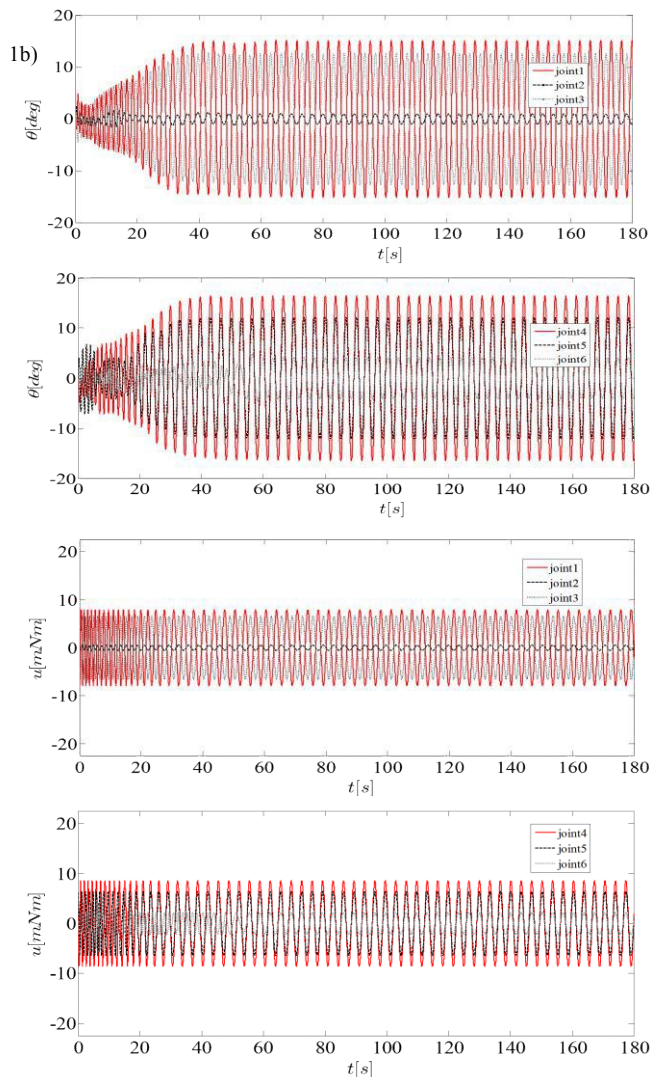
Fig. 10 – Uniform robot structure joints angular displacements, 1a) and 1b) , and torques, 2a) and 2b).

REFERENCES

[1] J. Gray, "The mechanism of locomotion in snakes," *J. Exp. Biol.*, vol. 23, no. 2, pp. 101–120, 1946.

[2] Z. V Guo and L. Mahadevan, "Limbless undulatory propulsion on land," *PNAS*, vol. 105, p. 3179-3184, 2008.

[3] I. Borazjani and F. Sotiropoulos, "On the role of form and kinematics on the hydrodynamics of self-propelled body/caudal fin swimming," *J. Exp. Biol.*, vol. 213, pp. 89–107, 2010.

[4] M. S. . Triantafyllou, S. . Triantafyllou, and D. K. P. Yue, "Hydrodynamics of Fishlike Swimming," *Annu. Rev. Fluid Mech.*, vol. 32, pp. 33–53, 2000.

[5] M. Sfakiotakis, D. M. Lane, and J. B. C. Davies, "Review of Fish Swimming Modes for Aquatic Locomotion," *IEEE J. Ocean. Eng.*, vol. 24, pp. 237–252, 1999.

[6] A. Crespi and A. J. Ijspeert, "Salamandra robotica: a biologically inspired amphibious robot that swims and walks," 2008.

[7] H. Daou, T. Salumae, and A. Ristolainen, "A bio-mimetic design of a fish-like robot with compliant tail," *... Bio-Inspired Robot. ...*, pp. 15–17, 2011.

[8] Y. Takada, R. Araki, Y. Nakanishi, M. Nonogaki, K. Ebita, and T. Wakisaka, "Development of Small Fish Robots Powered by Small and Ultra-Light Passive-Type Polymer Electrolyte Fuel Cells," *J. Robot. Mechatronics*, vol. 22, pp. 150–157, 2010.

[9] Y. Ryuh, "Generation of optimal swimming algorithm using reference velocity for robotic fish 'ichthus V3,'" in *2011 IEEE International Conference on Robotics and Biomimetics (ROBIO)*, 2011.

[10] C. Zhou, C. W. Chong, Y. Zhong, and K. H. Low, "Robust gait control for steady swimming of a carangiform fish robot," *2009 IEEE/ASME Int. Conf. Adv. Intell. Mechatronics*, pp. 100–105, Jul. 2009.

[11] J. Liu and H. Hu, "A Methodology of Modelling Fish-like Swim Patterns for Robotic Fish," in *Proceedings of the 2007 IEEE International Conference on Mechatronics and Automation*, 2007.

[12] J. Liu and H. Hu, "Biological Inspiration: From Carangiform Fish to Multi-Joint Robotic Fish," *J. Bionic Eng.*, vol. 7, pp. 35–48, 2010.

[13] M. Wang, J. Yu, and M. Tan, "Modeling Neural Control of Robotic Fish with Pectoral Fins Using a CPG-based Network," in *Joint 48th IEEE Conference on Decision and Control and 28th Chinese Control Conference*, 2009.

[14] A. Alessi, A. Sudano, D. Accoto, and E. Guglielmelli, "Development of an Autonomous Robotic Fish," in *Proceedings of the 4th IEEE RAS & EMBS International Conference on Biomedical Robotics and Biomechatronics*, 2012.

[15] M. Saito, M. Fukaya, and T. Iwasaki, "Serpentine Locomotion with Robotic Snakes," *IEEE Control Syst. Mag.*, no. February 2002, pp. 64–81, 2002.

[16] C. Stefanini, S. Orofino, S. Manfredi, S. Mintchev, S. Marrazza, T. Assaf, L. Capantini, E. Sinibaldi, S. Grillner, P. Wallén, and P. Dario, "A compliant bioinspired swimming robot with neuro-inspired control and autonomous behavior," in *IEEE International Conference on Robotics and Automation*, 2012, pp. 5094–5098.

[17] J. Chen, W. O. Friesen, and T. Iwasaki, "Mechanisms underlying rhythmic locomotion: body‐fluid interaction in undulatory swimming," *J. Exp. Biol.*, vol. 214, pp. 561–574, 2011.

[18] A. J. Ijspeert, A. Crespi, D. Ryczko, and J.-M. Cabelguen, "From Swimming to Walking with a Salamander Robot Driven by a Spinal Cord Model," *Science (80-.).*, vol. 315, pp. 1416–1419, 2007.

[19] L. Zhu, Z. Chen, and T. Iwasaki, "Oscillation, orientation, and locomotion of underactuated multilink mechanical systems," *Control Syst. Technol. IEEE ...*, vol. 21, no. 5, pp. 1537–1548, Sep. 2013.

[20] J. Blair and T. Iwasaki, "Optimal Gaits for Mechanical Rectifier Systems," *IEEE Trans. Automat. Contr.*, vol. 56, no. 1, pp. 59–71, Jan. 2011.

[21] T. Iwasaki and M. Zheng, "Sensory feedback mechanism underlying entrainment of central pattern generator to mechanical resonance.," *Biol. Cybern.*, vol. 94, no. 4, pp. 245–61, Apr. 2006.

[22] J. Buchli and A. J. Ijspeert, "Self-organized adaptive legged locomotion in a compliant quadruped robot," *Auton. Robots*, vol. 25, no. 4, pp. 331–347, Jul. 2008.

[23] L. Righetti, J. Buchli, and A. J. Ijspeert, "Dynamic Hebbian learning in adaptive frequency oscillators," *Physica*, vol. 216, pp. 269–281, 2006.

[24] L. Righetti and A. J. Ijspeert, "Programmable Central Pattern Generators: an application to biped locomotion control," in *Proceedings of the 2006 IEEE International Conference on Robotics and Automation*, 2006.

[25] R. Ronsse, J. Kieboom, and A. Ijspeert, "Automatic resonance tuning and feedforward learning of biped walking using adaptive oscillators," *Proceeding ...*, no. July, pp. 4–7, 2011.

[26] T. Wang, Y. Hu, and J. Liang, "Learning to Swim: A Dynamical Systems Approach to Mimicking Fish Swimming with CPG," *Robotica*, 2011.

[27] Y. Futakata and T. Iwasaki, "Entrainment to natural oscillations via uncoupled central pattern generators," *Autom. Control. IEEE Trans.*, vol. 56, no. 5, pp. 1075–1089, 2011.

[28] J. A. Acebrón, R. Spigler, D. Matematica, R. Tre, and L. S. L. Murialdo, "The Kuramoto model : A simple paradigm for synchronization phenomena," *Rev. Mod. Phys.*, vol. 77, no. January, 2005.

Supporting Presbycusic Drivers in Detection and Localization of Emergency Vehicles: Alarm Sound Signal Processing Algorithms

Marco Paoloni and Andrea Zanela

Robotics Lab

ENEA

Rome, Italy

marco.paoloni@enea.it, andrea.zanela@enea.it

Abstract—**The fatality rate for car drivers is more than five times higher for the 75 years and older than for the average for all ages. Presbycusis is a gradual hearing loss in both ears that commonly occurs as people age, it represent the third impairment for the elderly after arthritis and hypertension. One of the symptoms is the altered perception of the distance and the direction of a sound source especially for indoor and noisy environments. In this paper we present two algorithms, one for the early detection of alarm signal and the other for the localization of the emitting device, to be used in a car-embedded autonomous system aimed to support presbycusic and other car drivers to get a faster response in presence of an emergency vehicle in their surroundings.**

Keywords—presbycusis, car-embedded autonomous system; alarm signal detection; alarm source localization; steered response power, stochastic region contraction

I. INTRODUCTION

Age Sensitive ICT Systems for Intelligible City For All (I'CityForAll) is an ongoing project [1] partially funded by the European Ambient Assisted Living Joint Programme. The project aims at enhancing the sense of security and self-confidence of presbycusic people whose hearing degradation increases with age.

Presbycusis represent the third impairment for the elderly after arthritis and hypertension; it is a gradual hearing loss in both ears that commonly occurs as people age, it is progressive, bilateral and symmetrical and the loss is most marked at higher frequencies. Sounds appear less clear and sharp so that a severe difficulty in conversations understanding occurs and also the perception of distance and the direction of arrival of a sound source is altered.

The goal of I'CityForAll project is to design audio-aged-sensitive ICT systems enhancing self-confidence, mobility, safety, to improve social and mental well being.

The project targeted population corresponds to people older than 50 years in mobility situations and affected by presbycusis that induces a loss of sense of safety and self-confidence.

The ICT solutions consist of intelligent loudspeakers for better intelligibility of vocal messages in public confined spaces and systems embedded in vehicles for better localization of urban sound alarms like ambulances, police cars, fire trucks, etc..

The latter scenario is of particular relevance because older drivers have a relatively high fatality rate. Taking the distances travelled into account, the fatality rate for car drivers is more than five times higher for the 75 years and older than for the average for all ages [2]. Elderly are involved in 40% of fatal injuries (105000 deaths/year), and 1500 accidents/day require medical assistance according to the European Network for Safety. In a driving situation, a correct perception of the audio ambiance surrounding the car is necessary for a safe driving: it allows the driver to react in due time to a given event and even more, to anticipate on different possible scenarios, especially when are involved emergency vehicles because of their speed and behavior [3][4].

In this paper we present a set of algorithms to identify the presence of an alarm signal and to determine its direction of arrival. A first prototype solution foresees to place a microphone array on top of a car and to process these sensors data via the proposed algorithms, to extract meaningful information and displaying to the driver. Such a system will support presbycusic and other car drivers in detecting the presence of alarms in their surroundings, such as the sirens of an emergency vehicle, also helping the drivers to determine the position of the alarm. This on-board system will be "transparent" and embedded in mass products for people with presbycusic hearing without impacting normal hearing people, in a "Design for All" approach.

II. ALARM DETECTION

A. Alarm signal regulation

The alarm signals dealt within the project are constituted by alternations of two tone emissions of different frequencies and durations. For example, the Italian regulation for the alarm signals emitted by the Police vehicles [5] requires that a whole

acoustic cycle must be formed by four tone emissions of the same duration: the odd at 466 Hz, the even at 622 Hz; for the alarm signals emitted by the National Fire Corps vehicles and by the ambulances (in the rest of the paper referred together as Rescue vehicles) the regulation [6] requires that a whole acoustic cycle must be formed by eight tone emissions: the first at 392 Hz lasting 1/3 of the cycle duration, the second at 660 Hz lasting 1/18 of the cycle duration, the third at 392 Hz also lasting 1/18 of the cycle duration, the fourth at 660 Hz lasting 1/18 of the cycle duration and the last four alternating as the first ones. The frequency alternation patterns for the two alarm signals are resumed in Fig. 1.

For both of the two signals the tones must alternate without any appreciable interruption or overlap and the whole cycle duration must be 3 s; this time must also include a possible silence interval between a complete cycle of emissions and the successive one (but the duration of this silence interval must be less than 0.2 s).

When a cycle is started it must be performed entirely. The maximum tolerance for the frequencies values is required to be 5% and the same tolerance is required for the cited cycle time fractions; for the whole acoustic cycle is required a tolerance of ±0.5 s.
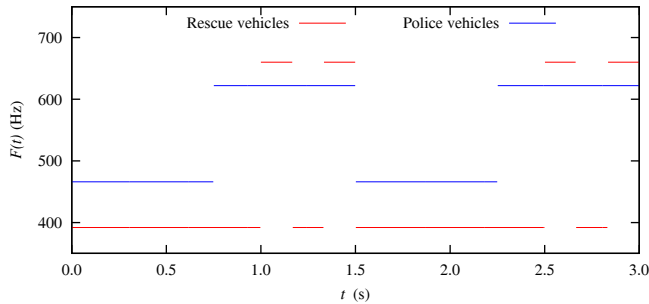

Fig. 1.   Frequency alternation patterns for the Italian alarm signals.

B. Detection algorithm

The proposed algorithm for the alarm signals detection is composed by two blocks, the first dedicated to the tone detection that provides a logical "true" value when a tone with a frequency close to those regulated is present in the microphones signals and a second that measures the timing of the logical true signals to confirm their conformity to the alarm signals regulation. At the current stage of the project development, the greater effort of the ENEA activities is devoted to the first block, while the second will be developed later.

In the proposed detection algorithm the signals from microphones array after the A/D conversion are processed to estimate the power carried in a narrow band centered on the tones regulated frequencies or in other terms the amplitude of the first harmonic of the tone; the employed technique in the process is the AM synchronous quadrature demodulation [7].

AM synchronous demodulation is a technique commonly used in many AM radio receivers (these receivers are also known as direct-conversion, homodyne, synchrodyne, or zero-IF receiver); it uses beats between the signal and a wave

generated by a local oscillator at a frequency very close to the carrier frequency; quadrature demodulation uses two waves (phased by 90°) to implement the envelope detection of AM signals and is usually employed in conjunction with DSP to process more complex modulation methods.

The adopted process is sketched in Fig. 2.
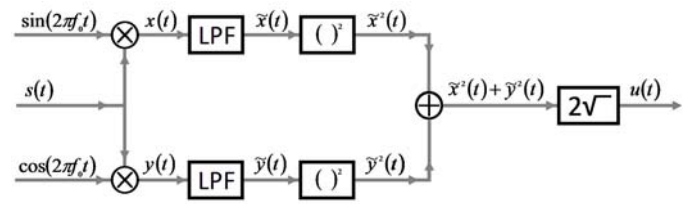
Fig. 2.   AM synchronous quadrature demodulation process representation.

As it can be seen, the incoming signal $s(t)$ is mixed with two sinusoidal waves with frequency f_0 (the tuning frequency) and then are submitted to two identical low-pass filter with cut frequency f_c; in presence of a tone with frequency f in the incoming signal the outputs of the filters are virtually null if $|f - f_0| > f_c$ or two (quadrature) sinusoids with frequency $|f - f_0|$ if $|f - f_0| \leq f_c$; from these two sinusoids the amplitude of the first harmonic of the incoming tone is then reconstructed by simple mathematical operations, giving as output the signal $u(t)$.

The algorithm uses four demodulation blocks: two for the two tones detection of the Police signals and two for the Rescue ones. After the demodulation the signals obtained are compared with a threshold of suitable value to obtain the logical value asserting the presence of one of the four tones.

C. Detection test

The proposed algorithm has been tested with simulated and real signals. Simulated signals were tones generated by the simulation program using the alternation in time of two tones according to the Italian regulation for Police and Rescue emergency vehicles. As waveforms for the tone generation were employed sinusoidal, square and saw-tooth waveforms, the latter two appropriately clipped in frequency to simulate the presence of the anti-aliasing low pass filter typical of every digital recording device. Simulated signals with Doppler effect were obtained simulating rectilinear uniform motions for the emergency vehicles and the car equipped with the microphones.

Typical results obtained for the simulated stationary emissions are represented in Fig. 3 where are reported the output signals $u(t)$ for the two Rescue demodulation channels (expressed in arbitrary units) and in Fig. 4 where are reported the same signals for the two Police demodulation channels.

The result obtained for the signals with Doppler effect are represented in Fig. 5 where are reported the signals $u(t)$ for the two Rescue demodulation channels for a Police vehicle surpassing at 60 km/h the car with microphones while it is moving at 30 km/h; the Police vehicle starts 100 m behind the

car and passes at a lateral distance of 5 m from it. In the same figure are also reported the frequency of the emitted signals and the frequency of the received ones (differing for the Doppler effect).
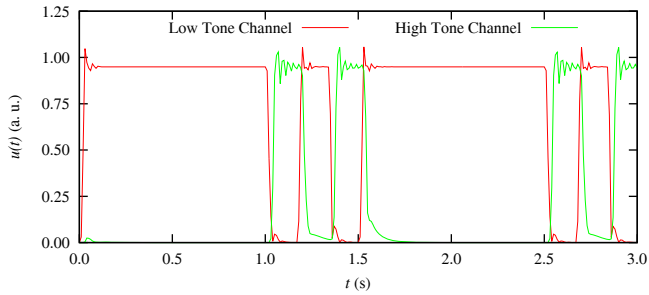
Fig. 3. Output signals of the two Rescue demodulation channels for a simulated stationary emission.
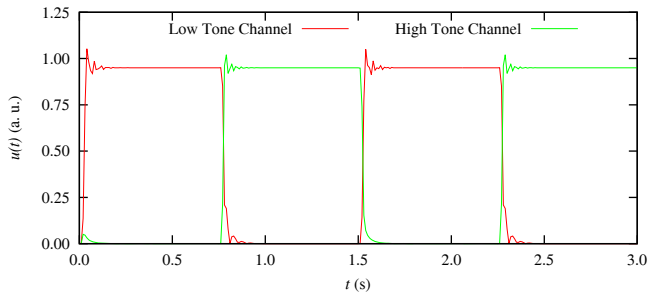
Fig. 4. Output signals of the two Police demodulation channels for a simulated stationary emission.
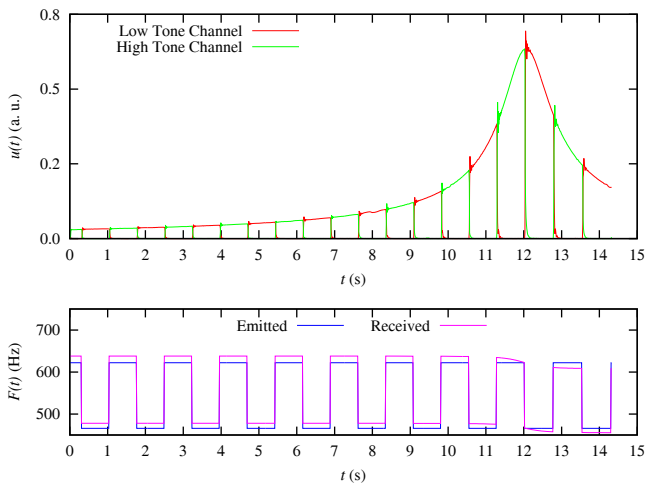
Fig. 5. Output signals of the two Police demodulation channels for a simulated emission by a moving vehicle with the representation of the frequency of the emitted and received tones.

As it can be seen, the amplitudes of the output signals of the two demodulators increase while the Police vehicle is approaching the car and decrease as the Police vehicle moves away after having passed the car; in the same way the frequencies of the received tones are greater than the ones of the emitted tones in the approaching phase and smaller in the other phase.

The proposed algorithm was then applied to real signals recorded by the Centro Ricerche FIAT, one of the project partners; these signals were recorded in their silent room with the stationary emitting device posed at 1 m from microphones and at their «Centro Sicurezza» test track using the same device mounted on a vehicle moving at 30 km/h.

Typical results obtained for these signals are reported in Fig. 6 and in Fig. 7 for the Rescue case and in Fig. 8 and in Fig. 9 for the Police case.
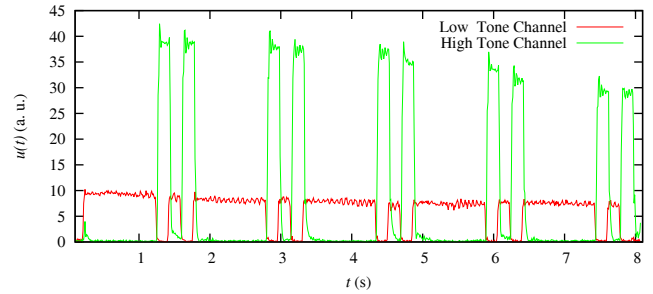
Fig. 6. Output signals of the two Rescue demodulation channels for the stationary emission of a real alarm signal.
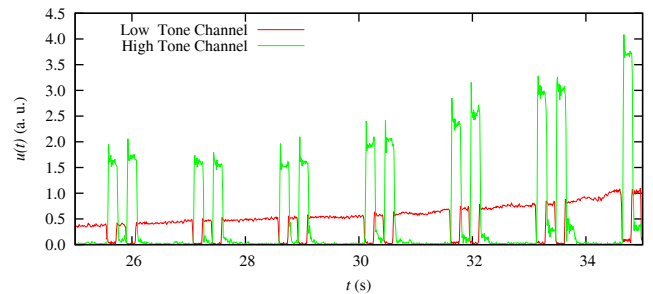
Fig. 7. Output signals of the two Rescue demodulation channels for the emission of a real alarm signal by a vehicle moving at 30 km/h.
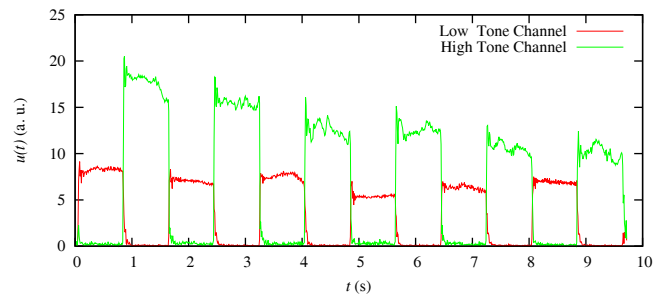
Fig. 8. Output signals of the two Police demodulation channels for the stationary emission of a real alarm signal.
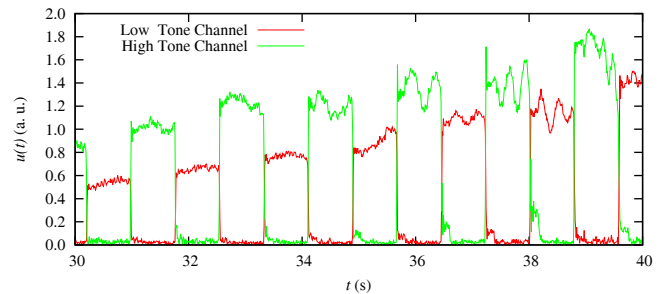
Fig. 9. Output signals of the two Police demodulation channels for the emission of a real alarm signal by a vehicle moving at 30 km/h.

As can be seen in these figures the amplitude of the demodulators output signals for the low tones is smaller than the high ones in both the two cases; this is caused by the fact that real low and high tones have very different spectral characteristics and so the respective fundamental harmonics have very different amplitude.

III. ALARM LOCALIZATION

A. Localization algorithm

A microphone array has the capability of focusing on signals generated from a specific location or direction. Such capability is referred to as a beam-former. A steered beam-former based algorithm hypothesizes a spatial, point-source location in a predefined region and computes a beam-forming functional at that location, the one yielding the maximum values of the functional is the estimated source locations [8][9].

The output of it is known as the steered response. When the point of focus matches the true source location, the steered response power (SRP) will peak. This method has been shown to be more robust under high noise and reverberation than the approaches that are based on intersecting or least-squares fitting the time-differences-of-arrival (TDOA) of the signal over the array. Also avoids the process of making early, and often incorrect, decisions of selecting "good" TDOA's as done in other methods.

In a M-microphones array system, a beam-former can be created by delaying the microphone signals $s_m(t)$ (with $m = 1,\ldots,M$) by appropriate steering delays to make them aligned in time, and then summing all these time-aligned signals together. Naming $\tau_m(\mathbf{r})$ the time delay from the focusing point (located at $\mathbf{r}$) to the microphone m and $\tau_0(\mathbf{r})$ the minimum of all these time delays, the steering delay for the microphone m will be $\delta_m(\mathbf{r}) = \tau_m(\mathbf{r}) - \tau_0(\mathbf{r})$.

When the phase transform (PHAT) pre-filtering is applied before computing the cross-correlations, to pre-whiten the signals, we obtain the SRP-PHAT algorithm. The SRP-PHAT for each point $\mathbf{r}$ in the space is defined as follows:

$$P(\mathbf{r}) \equiv \sum_{k=1}^{M}\sum_{m=1}^{M}\int_{-\infty}^{\infty} \frac{S_k(\omega)S_m^*(\omega)}{\left|S_k(\omega)S_m^*(\omega)\right|} \exp\left(j\omega[\delta_m(\mathbf{r})-\delta_k(\mathbf{r})]\right)d\omega ,$$

where $S_m(\omega)$ is the Fourier Transform of the signal $s_m(t)$.

As previously described, to find the source locations, we steer the beam-former over all possible points in a focal volume containing the source. The points that give the maximum weighted output power of the beam-former will be the source locations. For a single source, the location estimate $\mathbf{r}_s$ is the argument that maximize $P(\mathbf{r})$.

The robust performance of the beam-forming approach and its bias-free property [10][11] comes at the price of high computational cost, because the SRP surface to be searched has many local maxima. In order to cut the computational cost and thus making the SRP-PHAT single-source locator more

practical in real-time, a stochastic region contraction (SRC) approach [12] has been implemented in our work.

The basic idea of the SRC algorithm is, given an initial rectangular search volume containing the desired global optimum and perhaps many local maxima or minima, gradually, in an iterative process, contract the original volume until a sufficiently small sub volume is reached in which the global optimum is trapped. The contraction operation is based on a stochastic exploration of the SRP-PHAT functional. It can be shown that the missing probability can be made negligible throwing sufficient random points.

B. Localization test

To test the proposed algorithm, it has been simulated a setup where a microphone array was positioned in the center of a reference frame and a single alarm source with spherical emission could be placed in stationary known positions. The microphone array was composed by eight omni-directional microphones with a 20 cm radius circular geometry. Alarm source and microphones laid in the same plane.

The emergency signals employed in the simulation adopted as alternating tones clipped square waves with an amplitude normalized so that at the minimum distance microphone-source of a simulation set, the signal could cover the full range of a 16 bit analog to digital conversion. For all the other distances the amplitude was normalized to the former according to a propagation law proportional to the inverse distance between source and microphones. In this way none of the signals in the same simulation set was in a saturation condition, but the signals coming from larger distances were more attenuated.

In the first scenario was simulated a lateral pass-by, as depicted in Fig. 10.
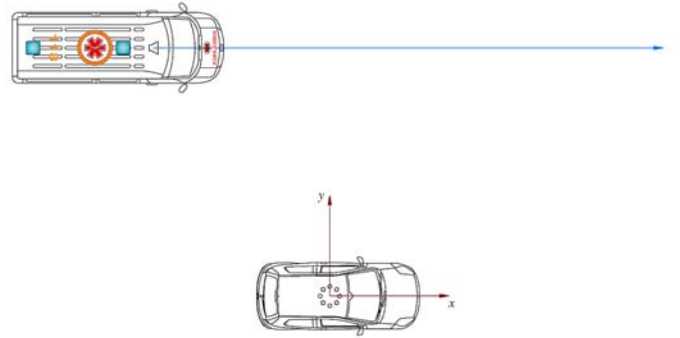
Fig. 10. Scenario 1 (Lateral Pass-By).

The simulation was performed placing the source on a set of positions starting from (-270; 2; 0) to (180; 2; 0) with steps of 10 m. For every position were processed in MATLAB framework four signals segments of length equal to 65536 samples (at a sampling frequency equal to 44110 Hz) from four microphones, the ones collocated on the coordinate axes.

The obtained results are resumed in Fig. 11 where are reported the errors on the estimate of the signals Direction of Arrival (DoA) for different x-axis source positions. As it can be seen the errors are about 1°.
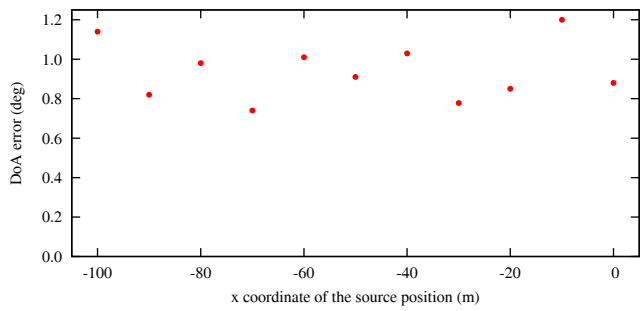
Fig. 11. Results for a simulated lateral pass-by.

In the second scenario was simulated a circular pass-by, as depicted in Fig. 12.
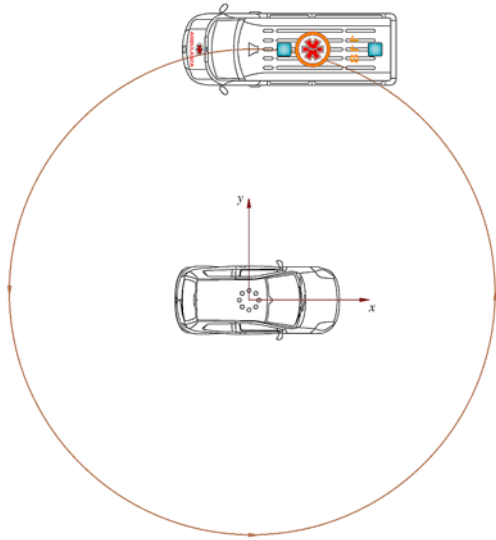
Fig. 12. Scenario 2 (Circular Pass-by)

For this scenario were performed two tests, the first with a radius of 20 m and the second with a radius of 30 m, placing the source every 20°. The obtained results are resumed in Fig. 13 where it can be seen that even in this case the errors on the estimate are about 1°.
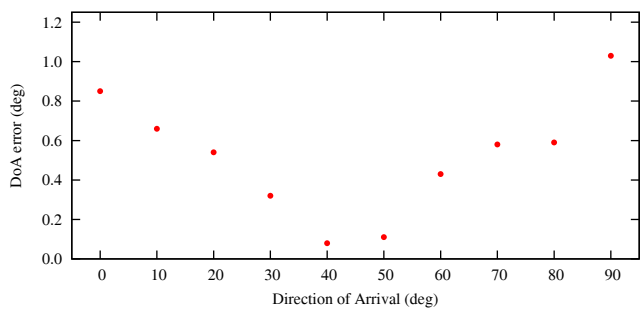
Fig. 13. Results for a simulated 20 m radius circular pass-by.

The same scenario was also considered for a real environment, thanks to the data collected by Centro Ricerche Fiat using a circular 8-microphone array realized by the laboratories of Ecole Polytechnique Fédérale de Lausanne.

Four circular passages around the car equipped with the microphone array were performed, the first and second on a circumference of about 30 m radius, the third and fourth on a circumference of about 20 m radius; during all the four passages the emergency vehicle speed was 20 km/h.

For tests in real environment, continuous data streams must be process and, unfortunately, a scenario ground truth was not given. The obtained results can be seen in Fig. 14, where are reported the estimated Direction of Arrival during the data stream.
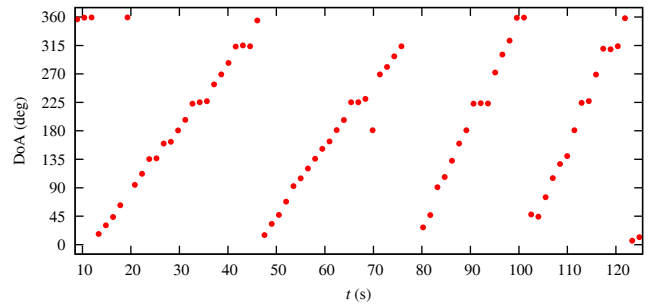
Fig. 14. Results for circular pass-by in a real scenario.

Real signals acquisitions also include a third scenario, the frontal pass-by, depicted in Fig. 15; for this scenario an emergency vehicle has been moved at 30 km/h, from the position (10; -65; 0) to the position (10; 65; 0).
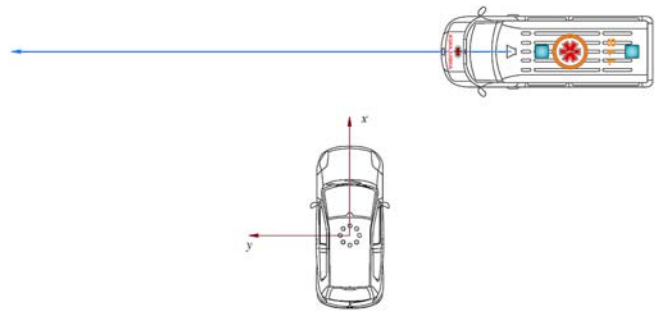
Fig. 15. Scenario 3 (Frontal Pass-By).

The obtained results processing the continuous data stream for this test can be seen in Fig. 16.
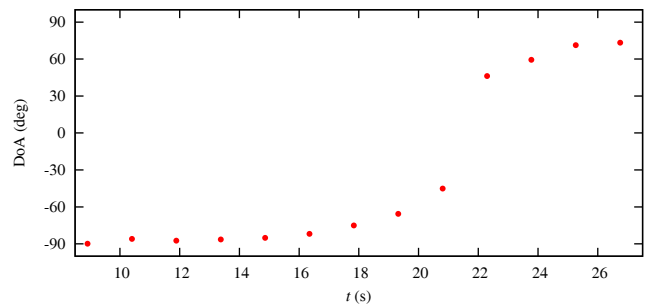
Fig. 16. Results for front pass-by in a real scenario.

The preliminary results on real signals showed in Fig. 14 and in Fig. 16 confirm that the adopted method is very effective in estimating the alarm direction of arrival.

As well known, however, this method is much less useful in estimating the source distance; thus we propose to use an

interface where the information of the approaching emergency vehicle is presented to the driver as in Fig. 17.
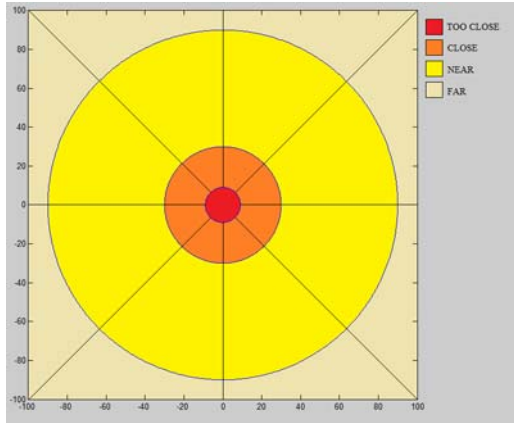
Fig. 17. A possible information rendering to the user. The car is positioned in the center.

With the car in the center of the graph we use four different zones (marked with a color code) where the approaching emergency vehicle can be localized; three zone (far/near/close) are further divided into eight sectors for the recovering of the alarm direction of arrival.

IV. CONCLUSIONS

In this paper two algorithms are presented, one for the early detection of alarm signal coming from an emergency vehicle, the other for the localization of the emitting device.

These algorithms will be implemented in a car-embedded autonomous system aimed to support presbycusic and other car drivers to get a faster response in presence of an emergency vehicle in their surroundings, enhancing the sense of safety while driving. This is of primary importance because Europe is ageing increasingly and faster, by 2020 around 25% of the Europe population will be over 65, and aged driver (75+) has a fatality rate more than five times higher than for the average for all ages.

Future activities will address the presence of the acoustic reverberations. This effect does last alarm signals more than their regular duration; when the emergency vehicle stops the first tone and switches to the second, the first tone decoder will continue to output signals for the presence of the retarded echoes. This should not be a problem if the processing of the second tone logical signal is triggered by the rising edge of the first tone rather than the falling edge.

For the source localization, as it can be seen in the results previously reported, the algorithm proposed is very effective in the recovery of sound direction of arrival, even if it is much less useful in finding the source distance, and can be a valuable aid for presbycusic drivers or other people suffering of age-related factors affecting their driving ability.

REFERENCES

[1] http://www.icityforall.eu/

[2] http://ec.europa.eu/transport/road_safety/index_en

[3] C.B. Custalow, C.S. Gravitz. Emergency medical vehicle collisions and potential for preventative intervention. Prehospital Emergency Care 2004, 8, pp 175–184.

[4] M.G. Lenné, T.J. Triggs, C.M. Mulvihill, M.A. Regan and B.F. Corben. Detection of Emergency Vehicles: Driver Responses to Advanced Warning in a Driving Simulator. Human Factors: The Journal of the Human Factors and Ergonomics Society 2008, 50, pp 135-144.

[5] Decreto Ministeriale 20 Marzo 1979, Supplemento ordinario alla Gazzetta Ufficiale N. 206 del 28 Luglio 1979

[6] Decreto Ministeriale 11 Ottobre 1980, Gazzetta Ufficiale N. 310 del 12 Novembre 1980

[7] P. Horowitz and W. Hill, The art of electronic. Cambridge, NY: Cambridge University Press, 1989.

[8] J. Dmochowski, J. Benesty, and S. Affes. A generalized steered response power method for computationally viable source localization. IEEE Trans. Audio, Speech, Lang. Process., 15(8), pp 2510–2526, November 2007.

[9] C. Zhang, D. Florencio, D. Ba, and Z. Zhang. Maximum likelihood sound source localization and beamforming for directional microphone arrays in distributed meetings. IEEE Trans. Multimedia, 10(3), pp 538–548, March 2008.

[10] J. H. DiBiase. A High-Accuracy, Low-Latency Technique for Talker Localization in Reverberant Environments Using Microphone Arrays. PhD thesis, Brown University, Providence, RI, May 2000.

[11] S. T. Birchfield. A unifying framework for acoustic localization. In Proc. of European Signal Processing Conference (EUSIPCO 2004), pp 1127–1130, Vienna, Austria, September 2004.

[12] H. Do, H.F. Silverman, and Y. Yu. A Real-Time SRP-PHAT Source Location Implementation using Stochastic Region Contraction on a Large-Aperture Microphone Array, in Proc. ICASSP 2007 pp 121-124.

Motion Principles for Designing Biologically Inspired Robots

Bolotnik N.N., Chernousko F.L., Gradetsky V.G., Knyazkov M.M.
Robotics and mechatronics laboratory
Institute for Problems in Mechanics of the Russian Academy of Sciences
Moscow, Russian Federation
e-mail: gradet@ipmnet.ru

*Abstract – **This paper discusses using biologically inspired locomotion principles in mobile robots designed for the motion in various environments and conditions.***

For the motion in sandy and stony terrains, undulatory snake-like locomotion mode could be appropriate. The underground motion can be implemented by using a push-pull mode that imitates muscle contraction of worms.

For the motion along vertical surfaces and in small diameter tubes of an arbitrary inclination, the locomotion principles inherent in a gecko lizard can be used, because these kinds of robots need a reliable means for keeping attached to the surface of motion.

For the motion in the water environment, fish-like oscillatory locomotion can be used.

Various kinds of mobile robots that are based on biologically inspired locomotion principles are described and discussed in the paper.

*Key words – **biologically inspired robots, locomotion principles, snake-like locomotion, push-pull mode, gecko-like biomimetic devices.***

I. INTRODUCTION

Locomotion principles for biologically inspired mobile robots are studied in numerous laboratories and research centers of technologically advanced countries. The area of applications of biologically inspired mobile robots permanently increases and covers a number of environments, including underground and underwater media, as well as outer space and microgravity conditions.

By now, a great number of nature-inspired mobile robots have been designed and built, including walking robots with two or more legs, robots for the motion along horizontal, inclined, and vertical surfaces, artificial snakes, insects, fish, and flies. The research in this area is performed at laboratories and research centers of Europe, USA, Asia, Australia [1].

European consortium CLAWAR proposed a modular design for different types of mobile robots, including biologically inspired robots, on the basis of "plug-and-play" method. One of the most advanced country in the fields of robotics is Japan. Since the 1970s, it has been ahead of the other countries.

In this paper we share an experience in designing biologically inspired robots by using various motion principles such as snake-like locomotion, push-pull mode that imitates muscle construction of worms, locomotion principles inherent in gecko lizard, legged locomotion for wall-climbing robots, and fish-like oscillatory locomotion. The results presented in the paper were obtained at the Institute for Problems in Mechanics of the Russian Academy of Sciences [2-4].

II. PUSH-PULL ELECTROMECHANICAL ROBOTS

A miniature push-pull in-tube robot with an electro-magnetic drive is shown in Fig 1. The robot uses a push-pull motion mode that imitates the motion of worms. The main components of the robot are its body and the rod. The rod is connected to the body by a spring that pushes out the rod from the body. The body and the rod have contact devices that provide anisotropic friction of the robot's components against the tube surface. The contact devices exert lower resistance to the forward motion than to the backward motion. The operating characteristics of the robot are presented in Table 1.

Fig. 1 Miniature in-tube robot.
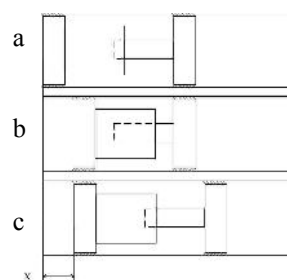
Fig. 2. Phases of the robot motion.

TABLE. 1 OPERATING CHARACTERISTICS OF THE IN-TUBE ROBOT.

Characteristic	Numerical value
Rod mass	5.8 g
Body mass	17.6 g
Stiffness of the spring	360 Н/м
Friction force resisting the forward motion	0.536 Н
Friction force resisting the backward motion	4.234 Н
Body length	50 мм
Body diameter	13.2 мм
Internal diameter of the tube	14 мм
Rod stroke	3 мм
Retracting force of the electromagnet	0.8 Н

The motion occurs due to periodic successive changes of retracting and extending phases of the motion of the rod relative to the body. The retraction of the rod is produced by an electromagnet. During this phase, the spring is compressed; the body moves toward the rod, while the rod virtually does not move because of high friction resisting the backward motion. The extension of the rod is produced by a releasing spring. At this phase, the electromagnet is switched off, the rod moves outward the body, while the body virtually does not move. As a result, the robot moves forward by a step X, which is equal to the rod stroke. The phases of the robot motion are shown in Fig. 2.

Figure 3 shows the average velocity of the robot's motion as a function of the excitation frequency $1/T$ and the on-off time ratio q of the excitation pulse. This function has a maximum at certain values of $1/T$ and q.

Fig.4. Two-module in-tube robot
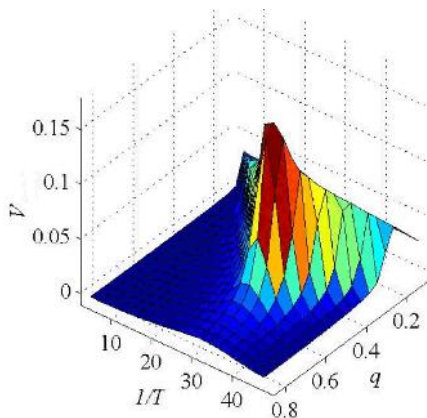
Fig. 3. The average velocity of the robot versus the excitation frequency and the pulse duration.

Another kind of an in-tube robot is shown in Fig. 4. The robot consists of two modules. The first module does not have a drive but contains a controllable contact device. The contact device consists of petals uniformly distributed around the body of the module at one of its ends. The petals can rotate synchronously about the axes that are perpendicular to the axis of the module. The rotation of the petals changes the degree and the sense of anisotropy of friction between the contact device and the tube surface. Such a design of the contact device allows the robot to change the direction of its motion. The actuator of the contact device consists of an electric motor and a screw transmission

The second module resembles the robot shown in Fig. 2, with that difference that the contact device of the body provides an isotropic friction against the tube surface, and the rod instead of a contact device has a coupling device by means of which the rod is flexibly connected to the first module. For aligning along the tube axis, this module has resilient strips stuck to the outer surface of the module.

An underground robot artificial worm [2] and its principle of motion are shown in Fig. 5.
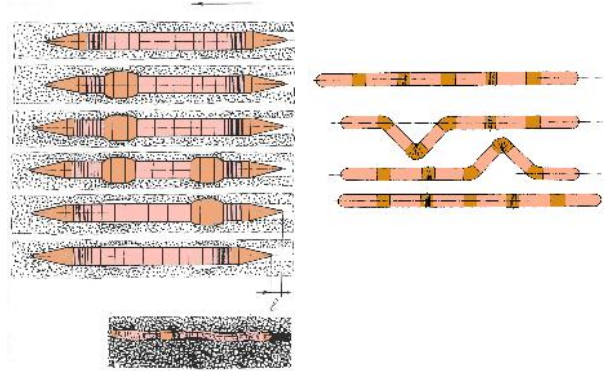
Fig. 5 Underground worm root.

III. ROBOTS USING BIOLOGICAL ADHESIVES.

Many insects and lizards have an ability to move along ceilings and walls. The most capable among the lizards are the geckos. They can easily run on walls of any type, on trees and even on glass. A gecko can move both on horizontal and vertical surfaces and even hang from a ceiling, holding itself with just one finger.

The knowledge of the mechanism of gecko coupling with the surface can help in the design of new types of devices for coupling minirobots with the surface. The study of the mechanism of coupling with a surface used by a gecko is of great interest. Having rather large body mass (several tens of grams), it possesses one of the best abilities of attaching to the surface. A gecko does not have glands on its soles which could secrete some sticky liquid. Besides, with equal ease it moves both on dry and wet surfaces. In view of these observations, a hypothesis was stated that adhesion of the gecko soles to the surface is mainly due to Van der Waals forces.

Use of multi-walled nanotubes (multiwalled carbon nanotubes MWCNT) as hairs in the microstructure of a dry adhesive material was suggested. Nanotubes are rather compliant to transverse bending, and after the load is removed they restore their former shape. The length of such hairs is about 5-10 microns, the diameter is about 20-30 nm, and the density of distribution on the substrate is $10^{10} - 10^{11}$ hairs / cm^2. The adhesion force for such a material reaches 11.7 N/cm^2 when interacting with the glass surface. Comparison of adhesion forces for some natural and synthetic micro / nanostructured materials is presented in Table 2.

References	Material	Young's modulus	Detachment force (H/cm^2)	Preloading force (H/cm^2)	The ratio of pull-off force and preload	Effective Young's modulus (кРа)
Autumn et al *Nature* 2000	β-keratin (gecko)	2 HPa	10	<0.01	8-16	100
Ge et al *PNAS* 2007	carbon nanotubes on adhesive tape	1000 HPa	5	25-50	<0.1	~200
Zhao et al *J. Vac. Sci. Tech.* 2006	carbon nanotubes on silicon	1000 HPa	11.7	>500	<0.01	~200
Kim and Sitti *Applied Physics Letters* 2006	Polyurethane	3 MPa	18	12	1.5	~300
Gorb et al *JRS Interface, 2006*	PVS	3 MPa	0.06	2	2.9	~300
Sitti and Fearing *IEEE ICRA 2003*	Polydimetilsilicon (PDMS)	0.5 MPa	0.003	0.025	0.1	~100
Geim *Nature Materials 2003*	Poliamid	3 HPa	0.03	50	0.06	3000 (without bending hairs)
Kustandi et al *Adv. Funct. Mat.* 2007	Parylene	2.8 HPa	0.007	1	0.7	–
Shan et al *IEEE Nano/Micro 2006*	PDMS	2.5 MPa	2	–	–	~240

For polymeric hairs, the major problem is frequently the adhesion of the hairs to each other and their fracture under bending loading, which reduces the adhesion (Fig. 6). For multiwalled nanotubes, the major problem is the reliability of the attachment of the robot to the surface by means of the nanotubes (after several attachment/detachment cycles part of the nanotubes is left on the surface).

Fig. 6. Robot with sliding seal.

Fig. 7. Inspection robot

IV. WALL-CLIMBING WALKING ROBOTS FOR INSPECTION.

One of important application area of wall-climbing robots is the inspection of objects and the environment by means of on-board sensory system (Fig. 7). Examples of hazardous environments are areas on which explosives are distributed, oil platforms, cargo container ships, nuclear power plants, oil transportation pipes, etc. There are mobile robots intended for hazardous condition prevention. These robots have successful applications in extreme conditions. Experience shows that it is necessary to equip mobile robots with a number of sensors to perform the desired task and a control system with elements of artificial intelligence to make some simple decisions automatically. Since the operational requirements for wall-climbing robots have been extended, we revised the functional characteristics of the robot for technological operations. One of the major tasks was to extend the functional capabilities of the control system to enable it to provide high performance of technological operations. This aim implied the following stages:

- construction of multifunctional control system on the basis of the modular design concept;

- real time processing of the data received from the sensor / measurement system;

- remote control and making independent decisions by an intelligent control system;
- automatic adaptation of the motion of the robot to changing environmental conditions;
- increasing reliability of hardware and software blocks and special modules.

V. OPTIMAL MOTION OF MULTI-LINK MOBILE ROBOTS IN A FLUID

The planar motion of a mechanical system that consists of the main body and two identical links OA and $O'A'$ attached to it by revolute joints O and O' (Fig. 8) is considered.
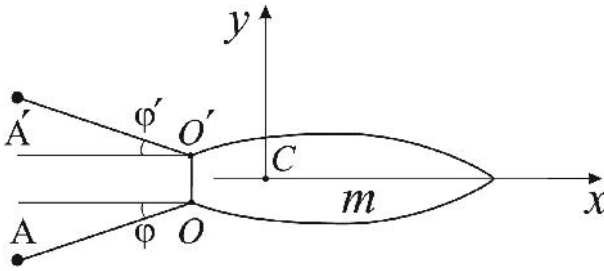

Fig. 8. A robot with two links attached to the main body.

The shape of the main body is assumed to be symmetric with respect to the plane that passes through the longitudinal axis of the body and is perpendicular to the plane of motion. The axes of the joints are arranged on the main body symmetrically relative to its symmetry plane. The links perform periodic angular oscillations with respect to the main body in such a way that the configuration of the system always remains symmetric with respect to the x-axis. If at an initial time instant the main body moves translationally along the x-axis, then it will move translationally along this axis later. This mode of motion imitates swimming of some aquatic animals, e.g., frogs. The motion of the main body generated by periodic vibrations of the links is studied. It is assumed that (i) the force applied to a moving body is directed against the velocity of the body relative to the medium and the magnitude of this force is a quadratic function of the absolute value of this velocity (quadratic friction law), (ii) the resistance forces acting on the links are applied at the points A and A', and (iii) during the period T, the angle φ first increases from 0 to φ_0 and then decreases from φ_0 to 0.

A mathematical model for the system under consideration is derived. It is shown that if the angle φ increases and decreases at constant rate, then for the main body to move progressively with periodically changing velocity and positive average speed, it is necessary and sufficient that the rate of motion of the links away from the main body axis be less than the rate of motion of the links toward this axis.

The optimal laws for the motion of the links that maximize the average speed of the main body are found. To this end, an optimal control problem is solved. The rate of rotation of the links relative to the main body is used as the control variable, which is allowed to change within a prescribed interval. The maximum angle φ_0 of deviation of the links from the axis of the main body is fixed. The optimal mode of oscillations of the links is close to their motion with piecewise constant angular velocity. The piecewise constant law for the angular velocity of the links can be regarded as a near-optimal control. The difference between the optimal and near-optimal control laws in terms of the average speed of the main body is less than 2%.

Similar optimal control problems are solved also for the motion in media characterized by more general nonlinear resistance laws than the quadratic friction.

Apart from the system with two links shown in Fig. 8, a system with one link attached to the main body is studied. In this system, the axis of rotation of the link is perpendicular to the x-axis, and to compensate the rotation of the main body for the period, the link rotates alternately to both sides of the x-axis. This system imitates swimming of fishes. For more detail, see [5, 6].

The simple models described above take into account only the drag force that is directed against the velocity of motion of a body through the medium. More complicated models that take into account the lift forces applied to the links are also considered. It is shown that the presence of the lift forces always leads to an increase in the body speed.

VI. OPTIMAL CONTROL OF A ROBOT WITH A MOVABLE INTERNAL BODY

A two-body locomotion system shown in Fig. 9 is considered.
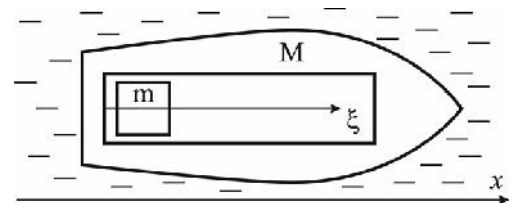
Fig. 9. A mobile robot with a movable internal body.

The system consists of the main body M that interacts with the medium and an auxiliary body m that can move relative to the main body, interacts with it but does not interact with the medium. This auxiliary body will be referred to as the internal body, although it is not necessary that this is located inside the main body. The internal body interacts with the main body by means of the force produced by the drive. The driving force applied to the internal body causes the reaction force applied to the main body. The reaction force changes the velocity of the main body relative to the medium, which leads to a change

in the force of resistance of the external medium. Therefore, by controlling the motion of the internal body, one can change the external force acting on the main body, thus controlling the motion of the entire system. This principle of motion is utilized for certain types of mini-sized locomotion robots. The main body of such robots can be made hermetic and smooth, without any protruding parts, which enables these robots to be used for nondestructive inspection of mini-sized engineering objects (e.g., thin-walled pipelines of small diameter), as well as in medicine.

We consider a simple model of the system with the internal body moving relative to the main body translationally along a straight line. The main body is assumed to move relative to the medium along the same line. For this model, it is required to find a periodic motion of the internal body relative to the main body that generates the motion of the main body relative to the medium with periodically changing velocity and provides a maximum for the displacement of the main body for the period. The period of the relative motion of the internal body is assumed to be prescribed and equal to the period of change of the velocity of the main body. The acceleration of the internal body relative to the main body or the force of interaction of these bodies is used as the control variable. Qualitative characteristics of the optimal motion, such as the number of switchings of the control function during the period, the absence or presence of a singular control mode, in which the control variable takes on an intermediate value between the minimum and maximum allowed values, the conditions for entering and leaving the singular mode, are investigated. It is proved that the singular mode necessarily occurs in the optimal motion, if the resistance law is an odd function of velocity and is either convex or concave for the velocity constant in sign. Such resistance laws are widely used for modeling the resistance of viscous media to the motion of rigid bodies. For this class of resistance laws (that include quadratic friction), the algorithms for calculating the optimal control are reduced to solving systems of finite equations for the control parameters. Illustrative examples are given. For more detail, see [6, 7].

REFERENCES

[1] "Nature-Inspired Mobile Robotics" Editors K.J. Waldron, M.O. Tokhi, C.S. Virk, Proceedings of the 16th International Conference on Climbing and Walking Robots and the Support Technologies for Mobile Machines, Australia, 2013, World Scientific Publishing, Co. Pte. Ltd, pp. 861.
[2] V.Gradetsky, M.Knyazkov, L.Fomin, V.Chashchukhin "Miniature robot mechanics", M.: Nauka, 2010, -271 p.
[3] Patent № 2175945, 20.11.01 "In pipe worm-robot".
[4] Patent № 2231463, 27.06.04 "Robot like a snake".
[5] Chernousko F.L. Optimal control of the motion of a multilink system in a resistive medium. Journal of Applied Mathematics and Mechanics, 2012, vol. 76, no. 3, pp. 255-267.
[6] Chernousko F.L., Bolotnik N.N., Figurina T.Yu. Optimal control of vibrationally excited locomotion systems. Regular and Chaotic Dynamics, 2013, vol. 18, nos. 1-2, pp. 85-99.
[7] Bolotnik N.N., Figurina T.Yu., Chernousko F.L. Optimal control of the rectilinear motion of a two-body system in a resistive medium. Journal of Applied Mathematics and Mechanics, 2012, vol. 76, no. 1, pp. 1-14.

Nikolay N. Bolotnik was born in Moscow, USSR, in 1950. He received his Ph.D degree in 1978 from the Institute for Problems in Mechanics of the Russian Academy of Sciences and his Doctor-of-Science degree in 1993 from Moscow State University. His research interests and achievements include theoretical and engineering mechanics, optimal control, shock isolation, and robotics. He is the author of 5 books and more than 80 articles.

Since 1973 he has worked at the Institute for Problems in Mechanics of the Russian Academy of Sciences. Currently, he occupies the position of the head of Robotics and Mechatronics Laboratory at this Institute. He is a corresponding member of the Russian Academy of Sciences.

Felix L. Chernousko was born in Leningrad, USSR, in 1938. He received his Ph.D. degree from Moscow Institute of Physics and Technology in 1964 and his Doctor-of Science degree in 1969 from the same Institute. His research interests and achievements cover a wide area of mechanics and applied mathematics, including theoretical and engineering mechanics, spacecraft dynamics, optimal control, control of uncertain systems, differential games, numerical and asymptotic methods for variational and control problems, and robotics. He is the author of 11 books and about 400 articles.

He works at the Institute for Problems in Mechanics of the Russian Academy of Sciences. Currently, he occupies the position of Director of this Institute. He is a full member of the Russian Academy of Sciences and a member of a number of foreign academies.

Valery G. Gradetsky was born in Moscow, USSR, in 1933. He received his MS degree in mechanical engineering from Bauman Moscow State Technical University in 1958, Ph.D. degree from the Institute of Control Sciences of the Russian Academy of Sciences in 1964, and Doctor-of-Science degree from Moscow State University of Technology in 1984. He is Professor of Robotics received from Institute for Problems in Mechanics in 1986.

From 1958 to 1975 he was Researcher at the Institute of Control Sciences of the Russian Academy of Sciences, from 1975 to 1981 he was Head of Laboratory and Head of Department at the Institute of Introscopy, from 1981 up to present time he has worked as Head and Leading Researcher of Robotics and Mechatronics Laboratory at the Institute for Problems in Mechanics of the Russian Academy of Sciences.

His research interests include mechanics, control, sensory systems of manipulation, mobile and wall climbing robots, exoskeletons, and pneumatic drive systems.

Professor Gradetsky has a number of awards, including State Prize of the Russian Federation for the development of theory and control methods for mechanical systems. He is Honored Worker of Science of the Russian Federation. He has 7 published books and 260 published scientific papers and patents.

Maxim M. Knyazkov was born in Moscow, USSR, in 1978. He received his MS degree in mechanical engineering from Moscow State University of Environmental Engineering in 2001 and his Ph.D. degree from the Moscow State University of Technology in 2007.

Since 2001 he has worked as Researcher of Robotics and Mechatronics Laboratory at the Institute for Problems in Mechanics of the Russian Academy of Sciences. His research interests include mechanics, control, mobile and wall climbing robots, exoskeletons, and pneumatic drive systems.

He has one published book and 48 published scientific papers and patents.

Structural Dynamics and Propulsion Modelling of a Pulsed-Jet Underwater Soft Robot

Federico Renda, Francesco Giorgio Serchi, Frederic Boyer, and Cecilia Laschi, *Senior Member, IEEE*

Abstract—This paper addresses the study of cephalopod-inspired pulsed-jet propulsion in the frame of underwater biomimetic robot design and modeling. This work takes the cue from an innovative underwater vehicle designed by the authors which propels itself in water by performing a routine of ingestion and expulsion of ambient water. This routine is enabled by a cable-transmitted actuation which drives the actual collapse and inflation of an elastic mantle, in close analogy to what cephalopods do when swimming. This propulsion routine is accounted for here with a coupled approach comprising of a model of the structural dynamics of the cephalopod-inspired, elastic mantle and a model of the pulsed-jet thrust production. The mantle is modelled by means of geometrically exact, axisymmetric, nonlinear shell theory which provides an accurate estimation of the forces involved in driving the deformation of this bladder-like structure. This, in turn, enables to derive the extent by which the bladder-like structure either shrinks and inflates, thus respectively driving the expulsion or ingestion of water. By coupling these results with those from a standard thrust model, the behaviour of the vehicle propelling itself in water is derived. The model is employed to test various mantles shapes and actuation routines eventually bringing evidence of the aptness of this model to study the dynamics of both man-made cephalopod-inspired robots and live specimen.

Index Terms—Dynamics, Continuum Robots, Soft Robots, Biologically-Inspired Robots

I. INTRODUCTION

TO self propel forward, cephalopod as squids and octopus have invented an original solution based on the cyclic contraction of a soft cavity named mantle. During each cycle, the mantle dilates while water runs into it and then brutally contracts in order to expel water and to generate by reaction the forward thrust [1]. The contraction of the mantle is ensured by a network of circular muscles symmetrically positioned all around the body [2]. Remarkably, these animals have developed strategies exploiting the softness of their body in order to re-capture energy from ambient flow that might otherwise be lost as this is the case of rigid rockets which also propel by jet reaction [3]. Recently these animals have represented an important source of inspiration for the development of new underwater thruster composed of soft material, capable of working in cramped environment with fast acceleration and great manoeuvrability. To reach this goal some crucial points have to be addressed, new design solutions have to be thought that take into account the use of soft materials

Federico Renda, Francesco Giorgio Serchi and Cecilia Laschi are with The BioRobotics Institute, Scuola Superiore Sant'Anna, Pisa, Italy. Frederic Boyer is with the Institut de Recherche en Communication et Cybernetique de Nantes, Ecole des Mines de Nantes, Nantes, France. f.renda@sssup.it

and new models and control strategies [4] [5] have to be developed for such soft structures. In particular a pulsed jet instead of a steady state propulsion have to be considered. A first example of pulsed jet soft robot is presented in [6] where a cable driven underwater thruster has been described, inspired by the octopus mantle (fig. 1). The prototype presented in [6] and later revised in [7] is capable of propelling itself in water by performing a thrust production routine analogous to that of cephalopods. These vehicles are composed of an elastic, hollow shell, somewhat similar to a bladder which undergoes periodic phases of collapse and inflation. During these stages the vehicle respectively expels fluid and successively refills the bladder, thus performing a sequence of pulsed-jets in a closely resemblant fashion to what cephalopods do when swimming. By propelling itself via the actual collapse of the collapsible bladder, the cephalopod-inspired underwater vehicles not only benefit of the advantages provided by vortex-ring aided thrust production, [8], but they also capitalize on the positive feedback that added-mass recovery has on thrust during shape change, [3].
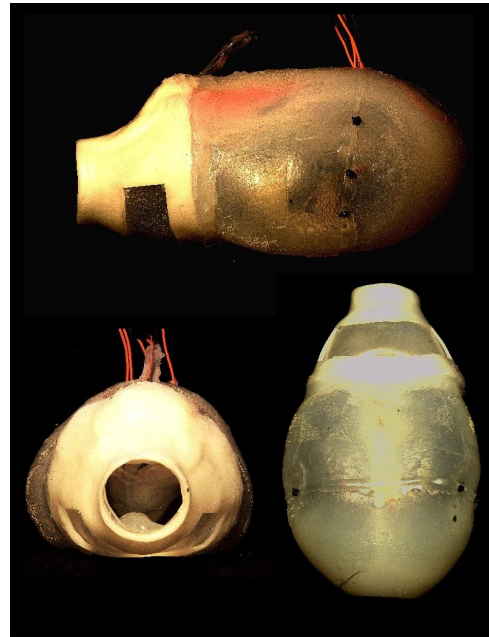

Fig. 1.   A jet-propelled soft robot inspired from cephalopods mantle [6]

In order to study the animal swimming mechanisms in detail and translate these on to the robotic artefacts, we need to state locomotion models of these jet-propelled soft animals as well as derive quantitative tools for capturing

the mechanics of the deformation of the soft tissues during propulsion. Ideally, these models would be analytical models allowing to idealize the principles of locomotion. Here we propose a numerical coupling between a model of the mantle based on the framework of the geometrically exact theory of shells in finite transformations [9], [10] and a model of the jet-propulsion based on the analogy of this mode of thrust production with that of rockets, as it was done earlier by [11].

In the geometrically exact approach the shell is considered as a Cosserat medium i.e. a continuous assembly of rigid micro-solids whose rigid overall motions are considered from the beginning without any approximations. This aspect is crucial to tackle locomotion problems where we not only need to model the internal strains occurring in the body but also the net rigid overall motions in space. While in Cosserat beams, the micro-solids are the cross sections of the beam to each of which is attached a rigid frame (3 unit vectors), in the case of shells, the micro-solids are rigid fibers transversally attached to the mid-surface of the shell to which, one can only attach a single vector named "director" [12]. Based on this Cosserat model, several internal kinematics can be adopted depending whether the shell is thin or not. In the first case, the directors remain perpendicular to the mid-surface while in the second case, they can rotate freely with respect to the mid-surface with two additional degrees of freedom which induce two further strain fields named "transverse shearing". The first kinematics correspond to the so called Kirchhoff model of shells while the second correspond to the Reissner model [13]. The model of the mantle here proposed is based on this second theory which leads to partial differential equations of minimum order. Furthermore, taking inspiration from cephalopods, the shell will be considered as axisymmetric. To derive such a model we follow the uses of nonlinear structural dynamics by first defining the shell kinematics. From these kinematics, we will build a set of strain measures and will derive the dynamic balance equations in their Cauchy form, i.e. in terms of internal stresses. Finally, this picture will be completed of the constitutive laws in section 6. All these developments will be achieved in the case of an axisymmetric shell. Afterwards the jet-propulsion model will be described and the coupling between the two will be formalized. Finally, some simulation results will be illustrated along with a few concluding remarks and future perspectives.

II. MANTLE MODEL

The mantle is a piece of tissues forming a cavity which opens into water through an orifice (see Figure 2). In the rest of the article, it is modelled by a shell of thickness $2h$ made of a soft hyperelastic isotropic material of density ρ.

Adopting the Reissner model, the configuration space of the shell can be first defined by:

$$\mathcal{C} := \{(X^1, X^2, t) \in B \times \mathbb{R} \mapsto (\varphi, \mathbf{b}) \in \mathbb{R}^3 \times S^2\} \quad (1)$$

where $B \subset \mathbb{R}^2$ defines the material domain of the mid-surface, φ represents the field of position of the points of B and $\mathbf{b}$ stands for the field of unit vectors attached to the shell fibers, i.e. the directors living in the two dimensional unit sphere S^2.

In the following, we consider axisymmetric shells. As a result, the configuration space can be reduced further. In the next section, this reduction is detailed step by step.

A. Kinematics of Axisymmetric Shells

Mathematically, an axisymmetric surface or "surface of revolution", is obtained by rotating a planar curve or "profile" around a fixed axis named "symmetry axis". This rotation changes the "profile curve" into any of the meridian curves that constitute the shell. The ambient Euclidean space is endowed with a fixed base of orthogonal unit vectors $(\mathbf{e}_1, \mathbf{e}_2, \mathbf{e}_3)$, where $\mathbf{e}_3$ supports the symmetry axis. Denoting by ϕ the angle of revolution, the orthogonal basis $(\mathbf{e}_r, \mathbf{e}_\phi, \mathbf{e}_3)$ fixed to the meridian of angle ϕ is defined by:

$$g1 \in SE(3):$$

$$\phi \in [0, 2\pi[\mapsto g1(\phi) = \begin{pmatrix} R_{\mathbf{e}_3}(\phi) & 0 \\ 0 & 1 \end{pmatrix}$$

where $R_{\mathbf{e}_3}(\phi)$ is a rotation ϕ around the axis $\mathbf{e}_3$. For the sake of convenience, we introduce another reference frame $(\mathbf{e}_r, \mathbf{e}_3, -\mathbf{e}_\phi)$ adding the transformation

$$g2 \in SE(3) : g2 = \begin{pmatrix} R_{\mathbf{e}_r}(\pi/2) & 0 \\ 0 & 1 \end{pmatrix}$$

Now, denoting by X the material coordinate along the meridian curves, the profile of the shell is defined by the curve $\mathbf{r} : (X, t) \in [0, L] \times [0, \infty) \mapsto \mathbf{r}(X, t) = (r(X, t), z(X, t), 0)^T$ that lies in the plane $(\mathbf{e}_r, \mathbf{e}_3)$ and for which, $r(.)$ and $z(.)$ are two smooth functions which define the radius and the altitude of the point X on the profile (see Figure 2). Let us call $\theta(X, t)$ the angle between $\mathbf{e}_3$ and the shell fiber located at any X along the ϕ-meridian, then the so called *director orthogonal frame* $(\mathbf{a}, \mathbf{b}, -\mathbf{e}_\phi)$ with centre $\mathbf{r}$ is defined by:

$$g3 \in SE(3) : (X, t) \in [0, L] \times [0, \infty) \mapsto$$

$$g3(X, t) = \begin{pmatrix} R_{-\mathbf{e}_\phi}(\theta) & \mathbf{r} \\ 0 & 1 \end{pmatrix}$$

Finally, putting them all together, the shell configuration space is

$$g \in SE(3) : g(X, \phi, t) = g1g2g3 = \begin{pmatrix} R & \varphi \\ 0 & 1 \end{pmatrix}$$

As a result, we can now introduce the following definition of the configuration space of an axisymmetric shell:

$$\overline{\mathcal{C}} := \{(X, \phi, t) \in \overline{B} \times \mathbb{R} \mapsto g \in SE(3)\} \quad (2)$$

where, referring to the more general context of (1), $X^1 = X$ and X^2 has been replaced by ϕ ($\overline{B} \subset \mathbb{R} \times S^1$) with $X^2 = r^o(X)\phi$, and $r^o(X)$ the value of $r(X)$ in the reference configuration of the shell (before any deformation).

The tangent plane on the surface $g(X, \phi, t)$ is represented by two vector field: $\widehat{\xi^1}(X, t) = g^{-1}g_{,X} = g^{-1}g\prime = g3^{-1}g3\prime$ and $\widehat{\xi^2}(X, t) = g^{-1}g_{,r^o\phi}$. The hat represents the isomorphism
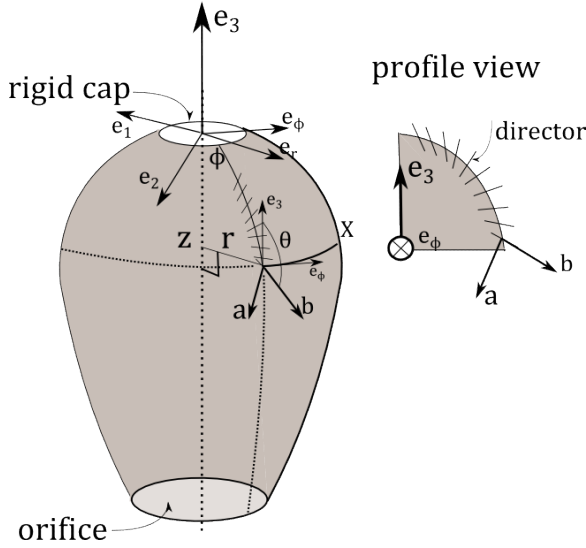
Fig. 2. Axisymmetric shell kinematics (left). Profile view, beam-like parametrization (right).

between the twist vector space $\mathbb{R}^6$ and the Lie algebra $se(3)$. Below their components are specified:

$$\widehat{\xi^1} = \begin{pmatrix} \widetilde{\mathbf{k}}^1 & \mathbf{q}^1 \\ 0 & 0 \end{pmatrix} \in se(3)$$

$$\widehat{\xi^2} = \begin{pmatrix} \widetilde{\mathbf{k}}^2 & \mathbf{q}^2 \\ 0 & 0 \end{pmatrix} \in se(3)$$

$$\xi^1 = (\mathbf{k}^{1T}, \mathbf{q}^{1T})^T = (0,0,\mu,\lambda,\eta,0)^T \in \mathbb{R}^6$$

$$\xi^2 = (\mathbf{k}^{2T}, \mathbf{q}^{2T})^T = (\frac{\sin(\theta)}{r^o}, \frac{\cos(\theta)}{r^o}, 0, 0, 0, \frac{-r}{r^o})^T \in \mathbb{R}^6$$

where the tilde is the usual isomorphism between a vector of $\mathbb{R}^3$ and the corresponding skew-symmetric matrix.

The time evolution of the configuration curve g is represented by the twist vector field $\varsigma(X,t) \in \mathbb{R}^6$ defined by $\widehat{\varsigma} = g^{-1}\delta g/\delta t = g^{-1}\dot{g} = g3^{-1}\dot{g3}$, where, thanks to the axisymmetry, only $g3$ depend on time. Let us specify the component of

$$\widehat{\varsigma} = \begin{pmatrix} \widetilde{\mathbf{w}} & \mathbf{v} \\ 0 & 0 \end{pmatrix} \in se(3)$$

$$\varsigma = (\mathbf{w}^T, \mathbf{v}^T)^T = (0,0,w,v_a,v_b,0)^T \in \mathbb{R}^6$$

Finally, from the last equivalence, the kinematic equation is

$$\dot{g3} = g3\widehat{\varsigma} \qquad (3)$$

and outlining the components:

$$\begin{aligned} \dot\theta &= w \\ \dot{r} &= \cos(\theta)v_a - \sin(\theta)v_b \\ \dot{z} &= \sin(\theta)v_a + \cos(\theta)v_b \end{aligned} \qquad (4)$$

B. Compatibility Equations

We have seen above that $g3\prime = g3\widehat{\xi^1}$. By taking the derivative of this equation with respect to time and recalling that $\dot{g3} = g3\widehat{\varsigma}$, we obtain the following compatibility equation between velocity and deformation variables: $\dot{\widehat{\xi^1}} = \widehat{\varsigma}\prime + \widehat{\xi^1}\widehat{\varsigma} - \widehat{\varsigma}\widehat{\xi^1}$. In terms of twist vectors it can be written as:

$$\dot{\xi^1} = \varsigma\prime + ad_{\xi^1}(\varsigma) \qquad (5)$$

where

$$ad_{\xi^1} = \begin{pmatrix} \widetilde{\mathbf{k}}^1 & 0 \\ \widetilde{\mathbf{q}}^1 & \widetilde{\mathbf{k}}^1 \end{pmatrix}$$

is the adjoint map, that represents the action of the Lie algebra on itself.

Outlining the components we obtain:

$$\begin{aligned} \dot\mu &= w\prime \\ \dot\lambda &= v_a\prime + \eta w - \mu v_b \\ \dot\eta &= v_b\prime - \lambda w + \mu v_a \end{aligned} \qquad (6)$$

C. Strain Measures

Before all, let us introduce two quadratic forms named: $h(X)$ and $k(X)$, that represent the first and the second fundamental forms of a Reissner shell respectively.

The first fundamental form of a surface is a quadratic form that determines how the Euclidean metric of $\mathbb{R}^3$ is induced on the surface in any of its points. In our case, it is practically defined in each point (X, ϕ) of the surface by a tensor whose components are deduced from the scalar products of all the vectors of the field of basis (said natural basis) $(\mathbf{q}^1, \mathbf{q}^2)(X, \phi)$. For our revolution surface it can be simply detailed as:

$$h = \begin{pmatrix} h_{11}(X) & 0 \\ 0 & h_{22}(X) \end{pmatrix} = \begin{pmatrix} \lambda^2 + \eta^2 & 0 \\ 0 & \frac{r^2}{r^{o2}} \end{pmatrix}$$

which depends only on X due to the axisymmetry.

While the first fundamental form defines the scalar product of any tangent vectors to the mid surface, the second fundamental form defines the curvature of the surface in any tangent direction (defined by an unit tangent vector). For a Reissner shell the components of $k(X)$ are such that $k_{\alpha\beta} = \mathbf{q}^\alpha \cdot \mathbf{b}_{,X^\beta}$.

Contrary to the traditional first and second fundamental form of a surface, this "special" forms take into account the effect of the shear between two material elements, where the two forms overlap if the director $\mathbf{b}$ points in the direction normal to the mid-surface of the shell (i.e. no shear strain).

For an axisymmetric Reissner shell, we have:

$$k = \begin{pmatrix} k_{11}(X) & 0 \\ 0 & k_{22}(X) \end{pmatrix} = \begin{pmatrix} -\mu\lambda & 0 \\ 0 & -\frac{r\sin(\theta)}{r^{o2}} \end{pmatrix}$$

Following [9], the following strain tensor field has been adopted:

$$e = \frac{1}{2}(h - h^o) = \begin{pmatrix} 1/2(\lambda^2 + \eta^2 - 1) & 0 \\ 0 & 1/2(\frac{r^2}{r^{o2}} - 1) \end{pmatrix}$$

to describe the membrane strain state in the mid-surface. As regards the shear strain state, we use the following strain vector:

$$s = \begin{pmatrix} \mathbf{q}^1 \cdot \mathbf{b} - \mathbf{q}^{1o} \cdot \mathbf{b}^o \\ \mathbf{q}^2 \cdot \mathbf{b} - \mathbf{q}^{2o} \cdot \mathbf{b}^o \end{pmatrix} = \begin{pmatrix} \eta(X) \\ 0 \end{pmatrix}$$

while the flexural strain state is parameterized by using the following tensor field:

$$d = k - k^o = \begin{pmatrix} \mu^o - \mu\lambda & 0 \\ 0 & \frac{\sin(\theta^o)}{r^o} - \frac{r\sin(\theta)}{r^{o2}} \end{pmatrix}$$

In all the above definitions, the upper index o represents a field when it is evaluated in the reference relaxed configuration. Furthermore, by taking as material coordinate X, the Euclidean curvilinear abscissa along the corresponding meridian when it is in the reference configuration, we have $h^o_{11} = 1$, while it is natural to consider that there is no transverse shearing in the reference resting con figuration, i.e. $\eta^o = 0$.

D. Dynamics

The dynamic model of the shell is given by the balance of kinetic momenta, i.e. by Newton's laws or a variational principle. In any case, this model takes the form of a set of partial differential equations (p.d.e.'s) which govern the time evolution of the system (here the shell) on its configuration space. With the definition (1) of the configuration space of a shell (not forcedly axisymmetric), these p.d.e.'s have been derived in [9] as follows:

$$\begin{aligned} 1/j(j\mathbf{n}^\alpha),_{X^\alpha} + \overline{\mathbf{n}} &= 2\rho h\ddot{\varphi} \\ 1/j(j\mathbf{m}^\alpha),_{X^\alpha} + \varphi,_\alpha \times \mathbf{n}^\alpha + \overline{\mathbf{m}} &= 2\rho h\mathbf{b} \times \ddot{\mathbf{b}} \end{aligned} \quad (7)$$

where $j = \sqrt{\det(h)} = r/r^o\sqrt{\lambda^2 + \eta^2}$, $X^1 = X$, $X^2 = r^o(X)\phi$, while the vectors $\mathbf{n}^\alpha$ and $\mathbf{m}^\alpha$ are respectively the resultant of internal stress forces and couples transmitted applied by the left part ($x < X^\alpha$) into the right part ($x \geq X^\alpha$) of the shell, across the section X^α, normalized with the surface Jacobian j, $\overline{\mathbf{n}}$ and $\overline{\mathbf{m}}$ are the external force and couple per unit of mid-surface area. For the repeated α the Einstein convention has to be used as in the rest of the paper. As expected, these equations give the time-evolution of all the pairs $(\varphi, \mathbf{b})$ over the shell as a function of the external load and the internal stress.

With respect to the local reference frame equation (7) can be written, in a geometric notation, as:

$$\frac{1}{j}\frac{\partial(j\zeta_i^\alpha)}{\partial X^\alpha} + \zeta_e = \frac{\partial}{\partial t}(\Gamma\varsigma) \quad (8)$$

Here ζ_i^α is the wrench of internal forces, ζ_e is the external wrench of distributed applied forces and Γ is the screw inertia matrix.

Due to the axisymmetry, the internal and external wrench fields take the particular form [10]:

$$\zeta_i^1(X,t) = (0, 0, M_X, N_X, H, 0)^T \in \mathbb{R}^6 \quad (9)$$

$$\zeta_i^2(X,t) = (M_\phi, 0, 0, 0, 0, -N_\phi)^T \in \mathbb{R}^6 \quad (10)$$

$$\zeta_e(X,t) = (0, 0, l, f_a, f_b, 0)^T \in \mathbb{R}^6 \quad (11)$$

and the screw inertia matrix is equal to: $\mathbb{R}^6 \otimes \mathbb{R}^6 \ni \Gamma = diag(0, 0, \rho J, 2\rho h, 2\rho h, 0)$.
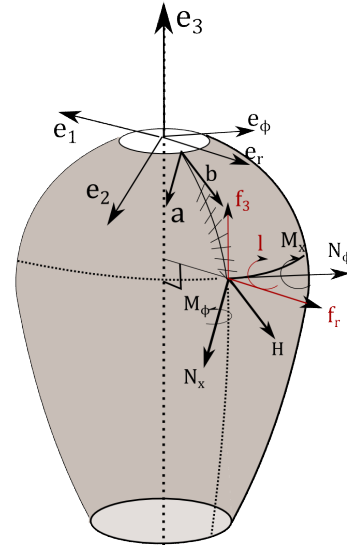
Fig. 3.   Internal (dark) and external (red) loads exerted in (X, ϕ).

Inserting this particular form of force wrenches and expanding the derivative in (8), gives the dynamic equations of an axisymmetric shell in the form:

$$\Gamma\dot{\varsigma} = 1/j(j\zeta_i^1),_{X^1} - ad^*_{\xi\alpha}(\zeta_i^\alpha) + \zeta_e + ad^*_\varsigma(\Gamma\varsigma) \quad (12)$$

where

$$ad^*_{\xi\alpha} = \begin{pmatrix} \widetilde{\mathbf{k}}^{\alpha T} & \widetilde{\mathbf{q}}^{\alpha T} \\ 0 & \widetilde{\mathbf{k}}^{\alpha T} \end{pmatrix} \qquad ad^*_\varsigma = \begin{pmatrix} \widetilde{\mathbf{w}}^T & \widetilde{\mathbf{v}}^T \\ 0 & \widetilde{\mathbf{w}}^T \end{pmatrix}$$

are the co-adjoint map.

In the equations above ρ is the body density, h is the half of the shell thickness and J is the second moment of the cross sectional line equal to $J = h^2/3$.

By outlining the components, we obtain:

$$\begin{aligned} \rho J\dot{w} &= 1/j(jM_X)\prime + \lambda H - \eta N_X - \frac{\cos(\theta)}{r^o}M_\phi + l \\ 2\rho h\dot{v}_a &= 1/j(jN_X)\prime - \mu H - \frac{\cos(\theta)}{r^o}N_\phi + f_a + 2\rho hwv_b \\ 2\rho h\dot{v}_b &= 1/j(jH)\prime + \mu N_X + \frac{\sin(\theta)}{r^o}N_\phi + f_b - 2\rho hwv_a \end{aligned} \quad (13)$$

E. Constitutive Equations

According to [9], for a hyper-elastic isotropic material, the general constitutive equations of a shell are defined in terms of the strain measures of as follows:

$$\widetilde{n}^{\beta\alpha} = \frac{2Eh}{1-\nu^2}H^{\beta\alpha\gamma\delta}e_{\gamma\delta} \quad , \quad \widetilde{m}^{\beta\alpha} = \frac{2EhJ}{1-\nu^2}H^{\beta\alpha\gamma\delta}d_{\gamma\delta}$$

$$\widetilde{q}^\alpha = 2Ghh^{o\alpha\beta}s_\beta, \quad (14)$$

where E is the Young modulus, G the shear modulus and ν is the Poisson modulus; $h^{o\alpha\beta}$ are the elements of $h^{o-1} \equiv I^{-1}$ and $H^{\beta\alpha\gamma\delta}$ define a four order (Hook-like) tensor given by:

$$H^{\beta\alpha\gamma\delta} = [\nu(h^{o\beta\alpha}h^{o\gamma\delta}) + 1/2(1-\nu)(h^{o\beta\gamma}h^{o\alpha\delta} + h^{o\beta\delta}h^{o\alpha\gamma})].$$

We extend this formulation to a visco-elastic constitutive model based on the Kelvin-Voigt model, which simply adds a

viscous contribution linearly, proportional to the rate of strain, to the elastic contribution:

$$\widetilde{n}^{\beta\alpha} = \frac{2Eh}{1-\nu^2}H^{\beta\alpha\gamma\delta}e_{\gamma\delta} + \frac{6\upsilon h}{1-\nu^2}H^{\beta\alpha\gamma\delta}\dot{e}_{\gamma\delta} \qquad (15)$$

$$\widetilde{m}^{\beta\alpha} = \frac{2EhJ}{1-\nu^2}H^{\beta\alpha\gamma\delta}d_{\gamma\delta} + \frac{6\upsilon hJ}{1-\nu^2}H^{\beta\alpha\gamma\delta}\dot{d}_{\gamma\delta}$$

$$\widetilde{q}^{\alpha} = 2Ghh^{o\alpha\beta}s_{\beta} + 2\upsilon hh^{o\alpha\beta}\dot{s}_{\beta}$$

where the Young modulus and the shear modulus has been replaced by the shear viscosity constants 3υ and υ respectively, following the some procedure developed in [15] for a beam like structure (novel analysis for the shell case are to date in progress).

The $\widetilde{n}^{\alpha\beta}$, $\widetilde{m}^{\alpha\beta}$ and $\widetilde{q}^{\alpha}$ stand respectively for the components of the *effective resultant traction, couple and shearing stresses*[1], which are related to the stresses of (7) through the relations:

$$\mathbf{n}^{\alpha} = (\widetilde{n}^{\beta\alpha} + \lambda_{\mu}^{\beta}\widetilde{m}^{\alpha\mu})\varphi_{,X^\beta} + (\widetilde{q}^{\alpha} + \lambda_{\mu}^{3}\widetilde{m}^{\alpha\mu})\mathbf{b} \qquad (16)$$

$$\mathbf{m}^{\alpha} = \mathbf{b} \times \widetilde{\mathbf{m}}^{\alpha} = \mathbf{b} \times (\widetilde{m}^{\beta\alpha}\varphi_{,X^\beta} + \widetilde{m}^{3\alpha}\mathbf{b}) \qquad (17)$$

where the functions λ_{μ}^{β} and λ_{μ}^{3} are defined by the following relation:

$$\mathbf{b}_{,X^\mu} = \lambda_{\mu}^{\beta}\varphi_{,X^\beta} + \lambda_{\mu}^{3}\mathbf{b} \qquad (18)$$

By comparing the equations (9) and (10) with the (16) and (17), after some computing, the following relations between the *effective resultant stress-couple* and our axialsymmetric resultant stress-couple are derived:

$$M_X = -\lambda\widetilde{m}^{11}, M_\phi = -\frac{r}{r^o}\widetilde{m}^{22}, \qquad (19)$$

$$N_X = \lambda\widetilde{n}^{11} - \mu\widetilde{m}^{11}, \ N_\phi = \frac{r}{r^o}\widetilde{n}^{22} - \frac{\sin(\theta)}{r^o}\widetilde{m}^{22}, \qquad (20)$$

$$H = \widetilde{q}^1 + \eta\widetilde{n}^{11}.$$

With these relations and the constitutive equations (15), the constitutive equations for our internal stresses (i.e. $N_X(X)$, $N_\phi(X)$, $H(X)$, $M_X(X)$ and $M_\phi(X)$) are given by:

$$N_X = \frac{2Eh}{1-\nu^2}\left[\lambda\left(e_{11} + \nu e_{22}\right) - J\mu\left(d_{11} + \nu d_{22}\right)\right]$$
$$+ \frac{6\upsilon h}{1-\nu^2}\left[\lambda\left(\dot{e}_{11} + \nu\dot{e}_{22}\right) - J\mu\left(\dot{d}_{11} + \nu\dot{d}_{22}\right)\right]$$

$$N_\phi = \frac{2Eh}{1-\nu^2}\left[\frac{r}{r^o}\left(e_{22} + \nu e_{11}\right) - J\frac{\sin(\theta)}{r^o}\left(d_{22} + \nu d_{11}\right)\right]$$
$$+ \frac{6\upsilon h}{1-\nu^2}\left[\frac{r}{r^o}\left(\dot{e}_{22} + \nu\dot{e}_{11}\right) - J\frac{\sin(\theta)}{r^o}\left(\dot{d}_{22} + \nu\dot{d}_{11}\right)\right]$$

$$H = 2h\eta\left[G + \frac{E}{1-\nu^2}\left(e_{11} + \nu e_{22}\right)\right]$$
$$+ 2h\dot{\eta}\left[\upsilon + \frac{6\upsilon}{1-\nu^2}\left(\dot{e}_{11} + \nu\dot{e}_{22}\right)\right]$$

$$M_X = -\frac{2EhJ}{1-\nu^2}\lambda\left(d_{11} + \nu d_{22}\right) - \frac{6\upsilon hJ}{1-\nu^2}\lambda\left(\dot{d}_{11} + \nu\dot{d}_{22}\right)$$

$$M_\phi = -\frac{2EhJ}{1-\nu^2}\frac{r}{r^o}\left(d_{22} + \nu d_{11}\right) - \frac{6\upsilon hJ}{1-\nu^2}\frac{r}{r^o}\left(\dot{d}_{22} + \nu\dot{d}_{11}\right)$$
$$(21)$$

---

[1]The word "effective" here stands to underline that these functions can be directly related to the constitutive equations of the three dimensional theory [9].

In order to avoid the polar singularity ($r^o = 0$) in the constitutive law, the mantle is assumed to be connected to a small rigid spherical cap axisymmetric with respect to the mantle axis which crosses the cap in the cap's pole (see Figure 2). The inertia of the cap is assumed to be negligible.

F. External Loads

The external loads taken into account are the drag and the added mass loads exerted by the fluid. Below the expression of all the external loads are shown.

$$\zeta_e(X,t) = (0,0,0,d_a,0,0)^T + (0,0,0,\mathbf{c}^T)^T. \qquad (22)$$

1) Drag Load: The drag load is proportional to the square of the velocity and directed toward the opposite direction. In particular, the drag force was taken to act tangentially to the shell, as expressed by eq. 22. The magnitude of the drag load is also determined by the geometry of the director X and by hydrodynamics phenomena expressed by empirical coefficients.

The equation (23) shows the resultant expression used in this model.

$$d_a = -\rho_w C_a(v_a + \sin(\theta)v)|v_a + \sin(\theta)v| \qquad (23)$$

where ρ_w is the water density, C_a is an empirical hydrodynamic coefficients which incorporates the geometric and hydrodynamics factors in the viscosity model and v is the swimming velocity of the mantle with respect to the fixed Galilean frame $(\mathbf{e}_1, \mathbf{e}_2, \mathbf{e}_3)$ (see section III).

2) Added Mass Load: The added mass , representing the load exerted locally by pressure, acts in the direction normal to the surface of the shell and is proportional to the acceleration. As in the case of the drag load, the amplitude is also determined by the geometry of the director X and by hydrodynamics phenomena expressed in part by correction coefficients. The problem accounted for here ideally requires a distinct formulation for the added mass as far as the external and internal domains are concerned. While an expression for the added mass terms is straight forward for the external flow case, treatment of the condition inside the shell are significantly more complicated by the closed geometry and the time-varying shape of the domain accounted for. As a first approximation this problem is disregarded and the following formulation is adopted.

The equation (24) shows the resultant added mass vector used in this model.

$$\mathbf{c} = -\frac{\partial(\rho F(\mathbf{v}+R^T\mathbf{y}))}{\partial t} =$$
$$-\rho F(\dot{\mathbf{v}} + R^T\dot{\mathbf{y}}) + \mathbf{w} \times \rho F(\mathbf{v} + R^T\mathbf{y}) \qquad (24)$$

where $F(X) \in \mathbb{R}^3 \otimes \mathbb{R}^3$ is a tensor which incorporates the geometric and hydrodynamics factors. It is equal to $F = diag(0, 2hB_b, 0)$, where $B_b \in \mathbb{R}$ is the hydrodynamic correction coefficient for the added mass model. As before vector $\mathbf{y}$ is the swimming velocity of the mantle with respect to the fixed Galilean frame $(\mathbf{e}_1, \mathbf{e}_2, \mathbf{e}_3)$ equal to $[0,0,v]^T$.
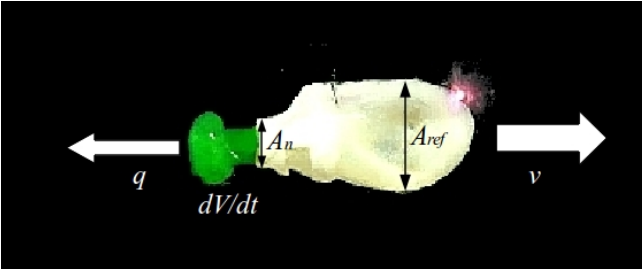
Fig. 4. Depiction of the elements accounted for in the dynamics model of the pulsed-jet propulsion.

III. JET-PROPULSION MODEL

The propulsion model is the standard one-dimensional momentum equation for a neutrally buoyant, rigid body translating in water,

$$(\rho_w V + \rho V_m)\dot{v} = -\frac{1}{2}\rho_w C_d A_{ref} v|v| - B\dot{v} + q\rho_w \dot{V} \quad (25)$$

where $V(t)$ is the mantle inner volume and V_m is the volume of elastic material composing the external shell of the mantle. $v = \dot{u}$ is the swimming velocity (where u the mantle position). The first right hand side (RHS) term represents the drag, C_d being the drag coefficient and $A_{ref}(t)$ a reference area of the mantle; the second RHS term is the added mass, with B being the axial added mass coefficient of an ellipsoid of revolution, [16], expressed by:

$$B = \frac{\alpha_0}{2 - \alpha_0} m$$

with

$$\alpha_0 = \frac{2(1-e^2)}{e^3}\left(\frac{1}{2}ln\frac{1+e}{1-e} - e\right) \qquad e = 1 - (b/a)^2$$

and

$$m = \rho_w V + \rho V_m$$

where a and b respectively represent the major and minor semi-axis of the shell.

The third term in eq. 25 is the thrust, given by the speed of the outflow q, with respect to the mantle, across the nozzle-exit area $A_n(t)$ and the variation of mass $\rho\dot{V}$ occurring within the robot due to the collapse of the elastic chamber.

The outflow speed is given by:

$$q = -\frac{C_f \dot{V}}{A_n}$$

where C_f defines a flow loss coefficient at the nozzle entrance, which varies between 0.6 and 1 [17].

The thrust term is thus rewritten,

$$q\rho_w \dot{V} = -\frac{\rho_w C_f \dot{V}|\dot{V}|}{A_n} \quad (26)$$

We have adapted this propulsion modelling to the geometry of the elastic shell-like mantle. Thus, in terms of the configuration variable $r(X, t)$, the nozzle-exit area, the reference area and the volume of the mantle are:

$$A_n(t) = \pi r(L, t)^2 \qquad A_{ref}(t) = \pi max(r(\cdot, t))^2$$

$$V_m = -\int_0^{z(L)} 4\pi r h dz = -4\pi h \int_0^L r z\prime dX$$

while the mantle inner volume and his time derivative are:

$$V(t) = -\int_0^{z(L)} \pi r^2 dz = -\pi \int_0^L r^2 z\prime dX$$

$$\dot{V}(t) = -\pi \int_0^L (2r\dot{r}z\prime + r^2\dot{z}\prime)dX$$

where ,

$$z' = \sin(\theta)\lambda + \cos(\theta)\eta \qquad \dot{r} = \cos(\theta)v_a - \sin(\theta)v_b$$

$$\dot{z}\prime = \sin(\theta)(\dot{\lambda} - w\eta) + \cos(\theta)(\dot{\eta} + w\lambda)$$

Given the orientation chosen in the kinematics (fig. 2) the orienttion of the mantle surface comes out to be negative, this lead to the minus sign before the integral above.

IV. PULSED-JET DYNAMIC MODEL

The previous formulation can be used to address the study of cephalopods locomotion. We consider that the squid is jet-propelled along the $\mathbf{e}_3$-axis while the axisymmetric external loads cannot generate a net displacement in another dimensions of the Lie group $SE(3)$. To that end, the kinematics developed in section II-A have to be slightly modified by replacing the transformation $g1(\phi, t)$ with the following

$$\overline{g1} \in SE(3):$$

$$(\phi, t) \mapsto \overline{g1}(\phi, t) = \begin{pmatrix} R_{\mathbf{e}_3}(\phi) & \mathbf{u}(t) \\ 0 & 1 \end{pmatrix}$$

where $\mathbf{u}(t)$ is the position vector of the mantle equal to $(0, 0, u(t))^T$. Consequently, the corresponding velocity twist vector field $\overline{\varsigma}(X, t)$ is

$$\widehat{\overline{\varsigma}} = \begin{pmatrix} \widetilde{\mathbf{w}} & \mathbf{v} + R^T\mathbf{y} \\ 0 & 0 \end{pmatrix} \in se(3)$$

Due to the different nature of the models to be coupled (the shell model is formulated relative to the body while the jet-propulsion model is earth-fixed) this velocity field just introduced have been used only for the kinematics equation. This implies that $\overline{\varsigma}(X, t)$ do not enter neither in the compatibility equation (5) nor in the dynamic equation (12).

Now we can state the system of second order partial differential by gathering the (modified) kinematics equations, the compatibility equations (6), the mantle dynamic equations (13) and the jet-propulsion models (25), in the state-space form $\dot{x} = f(x, x\prime, x\prime\prime, t)$ as follows:

$$\dot{\theta} = w$$
$$\dot{r} = \cos(\theta)v_a - \sin(\theta)v_b$$
$$\dot{z} = \sin(\theta)v_a + \cos(\theta)v_b + v$$
$$\dot{\mu} = w\prime$$
$$\dot{\lambda} = v_a\prime + \eta w - \mu v_b$$
$$\dot{\eta} = v_b\prime - \lambda w + \mu v_a \qquad (27)$$
$$\dot{w} = \frac{(jM_X)\prime/j + \lambda H - \eta N_X - \frac{\cos(\theta)}{r^o}M_\phi + l}{\rho J}$$
$$\dot{v}_a = \frac{(jN_X)\prime/j - \mu H - \frac{\cos(\theta)}{r^o}N_\phi + f_a}{2\rho h} + w v_b$$
$$\dot{v}_b = \frac{(jH)\prime/j + \mu N_X + \frac{\sin(\theta)}{r^o}N_\phi + f_b - 2\rho h w v_a}{2h(\rho + \rho B_b)}$$
$$\dot{v} = \frac{q\rho_w \dot{V} - \frac{1}{2}\rho_w C_d A_{ref} v|v|}{\rho_w V + \rho V_m + B}$$

where the second order partial differentiation is due to the viscosity of the constitutive equation.

In these forward dynamics, the state vector x is infinite dimensional since all its components (along with those of f) are some functions of the profile abscissa X. As a result, the above state equation has to be first space-discretised on a grid of nodes along $[0, L]$ before to be time integrated using explicit or implicit time integrators starting from the initial state $x(0)$. In this grid, all the space derivatives appearing in the f vector can be approximated by finite difference schemes, while the external and internal stress forces and couples are respectively given by (23), (24) and the constitutive law (21). The system (27) has been solved in Matlab$^{©}$ through and *ad hoc* explicit second-order finite-difference scheme. On an AMD Phenom(TM) II X4 965 processor, at 784 Mhz, 3.25 GB of RAM it took almost $27sec$ for one second of simulation.

A. Boundary Conditions

At the boundary overlooking the rigid cap, we have the following static condition:

$$\varsigma(0) = \varsigma_- = 0 \qquad (28)$$

where ς_- is fixed by the boundaries of the cap in which the mantle is clamped. At the other tip of the mantle, we have the following natural boundary conditions:

$$N_X(L) = f_{a,+}, \qquad H(L) = f_{b,+}, \qquad M_X(L) = -l_+,$$

where $f_{a,+}$, $f_{b,+}$ and l_+ denote the eventual external forces and torque along $\mathbf{a}$, $\mathbf{b}$ and $-\mathbf{e}_\phi$ respectively, applied onto the sharp boundaries of the mantle orifice.

V. SIMULATION RESULTS

In this section are shown the results of four simulations for different geometries of the mantle and different actuation routines, in order to demonstrate the functionalities of the model.

Let us remind that the squid is modelled by an axisymmetric shell internally actuated by a network of circular muscles organised in rings around the shell axis. As a result, the rhythmic muscular activity can be modelled by taking $f_a \cos(\theta) - f_b \sin(\theta) = f_r(X, t)$ as a T-periodic function with two phases. In the first phase $[0, T_c]$, or contraction phase,

TABLE I
CONE AND ELLIPSOID PARAMETERS

Parameter	Value
E	$1100\ Pa$
μ	$50\ Pa \cdot s$
ν	0
ρ	$1.08\ kg/dm^3$
L	$80\ cm$
h	$2\ mm$
R_c	$5\ cm$
R_n	$15\ cm$
a	$5\ cm$
b	$15\ cm$

TABLE II
LOAD PARAMETERS

Parameter	Value
ρ_w	$1.02\ kg/dm^3$
C_a	0.01
B_b	0
C_d	1
C_f	1
P	$3\ N/m^2$

$f_r(\cdot, t) = P$. In the second phase, or relaxation phase $(T_c, T]$, $f_r(\cdot, t) = 0$, and the mantle recover its resting shape passively thanks to the internal restoring stresses.

Below three actuation routines are presented for both a truncated cone and an ellipsoid. The parameters chosen for the simulations are reported in table I, II and III respectively for the geometry and the material properties of the cone and of the ellipsoid, the external load and the actuation routines, where R_c is the cap radius and R_n is the nuzzle radius at $t = 0$. In figure 5 the mantle velocity is shown for all these cases of study, while in figure 6 few snapshots of the ellipsoidal mantle under an actuation routine with $T_c = 1\ s$ and $T = 1.5\ s$ are presented.

The results show clearly that the ellipsoid mantle realizes better performances w.r.t. the cone one. Furthermore, an actuation routine with an high contraction phase w.r.t. the relaxation phase provides an higher trust. Although not analysed here, the present model could be used also to collect quantify data on the internal elastic power of the shell contrary to the more common kinematic models.

VI. CONCLUSION

In this paper a geometrically exact model of a shell-like underwater mantle has been developed, coupled with a rocket-

TABLE III
ACTUATION ROUTINE PARAMETERS

| Simulation	Contraction Phase	Relaxation Phase
fig. 5 (top)	$0.5\ s$	$0.5\ s$
fig. 5 (middle)	$1\ s$	$0.5\ s$
fig. 5 (down)	$0.5\ s$	$1\ s$
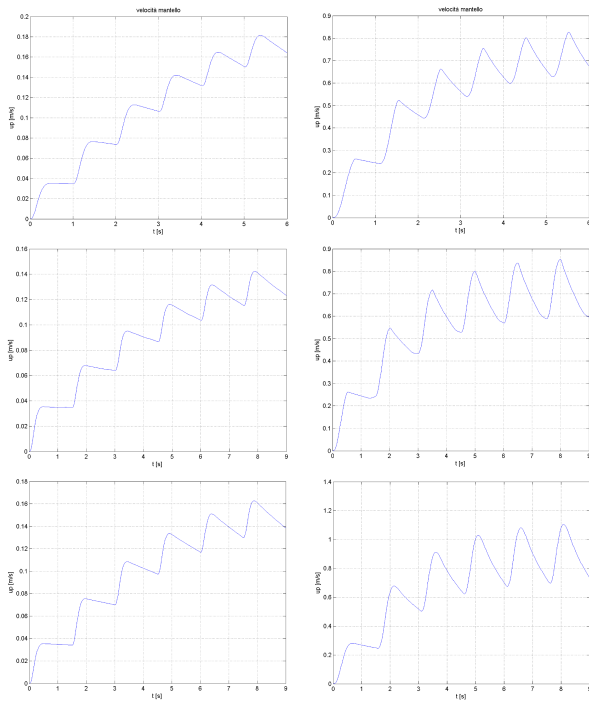
Fig. 5. Mantle velocity results for three actuation routines, in case of both cone (left) and ellipse (right) geometry. The actuation routines are characterized by the couples $T_c = 0.5\ s$, $T = 1\ s$ (top); $T_c = 0.5\ s$, $T = 1.5\ s$ (middle) and $T_c = 1\ s$, $T = 1.5\ s$ (down)

Fig. 6. Snapshots of the ellipsoidal mantle configuration under the $T_c = 1\ s$, $T = 1.5\ s$ actuation routine. From top left: $t = 0$, $t = 1$, $t = 3$, $t = 5$, $t = 7$ and $t = 9$

like jet-propulsion model. In other words, a complete fluid-structure dynamic model of the pulsed-jet swimming of an elastic mantle has been obtained, though in simplified conditions. The model could be used for the design and control of new generation of soft underwater robot as well as a simulation tools to study the cephalopod swimming.

REFERENCES

[1] J. M. Gosline and M. E. DeMont "Jet-propelled swimming in squids" *Sci. Am.* vol. 252 n 1, pp. 96-103, 1985.

[2] M. Krieg and K. Mohseni "New perspectives on collagen fibers in the squid mantle" *J Morphol.* vol. 273, n 6, pp. 586-95, Jun 2012.

[3] G. D. Weymouth and M. S. Triantafyllou "Ultra-fast escape of a deformable jet-propelled body" *Journal of Fluid Mechanics* vol. 721, pp. 367-385, 2013.

[4] M. Giorelli, F. Giorgio Serchi and C. Laschi "Forward speed control of a pulsed-jet soft-bodied underwater vehicle" *Proceedings of the MTS/IEEE OCEANS Conference*, San Diego, CA, USA, September, 21-27, 2013.

[5] F. Giorgio Serchi, A. Arienti and C. Laschi "An elastic pulsed-jet thruster for Soft Unmanned Underwater Vehicles" *IEEE International Conference on Robotics and Automation*, Karlsruhe, May 6-10, 2013.

[6] F. Giorgio Serchi, A. Arienti, C. Laschi "Biomimetic Vortex Propulsion: Toward the New Paradigm of Soft Unmanned Underwater Vehicles" *Mechatronics, IEEE/ASME Transactions on* vol.18, no.2, pp. 484-493, April 2013.

[7] F. Giorgio Serchi, A. Arienti, C. Laschi "A Soft Unmanned Underwater Vehicle with augmented thrust capability" *MTS/IEEE Proceedings Oceans*, San Diego, September 23-27, 2013.

[8] M. Krieg and K. Mohseni "Modelling circulation, impulse, and kinetic energy of starting jets with non-zero radial velocity" *Journal of Fluid Mechanics*, vol. 719, pp. 488-526, 2013.

[9] J. C. Simo and D. D. Fox "On stress resultant geometrically exact shell model. Part I: formulation and optimal parametrization" *Journal Computer Methods in Applied Mechanics and Engineering* vol. 72, n 3, pp. 267 - 304, Mar 1989.

[10] S. S. Antman *Nonlinear Problems of Elasticity*, 2nd edn (Applied Mathematical Sciences vol 107) (New York:Springer), 2005.
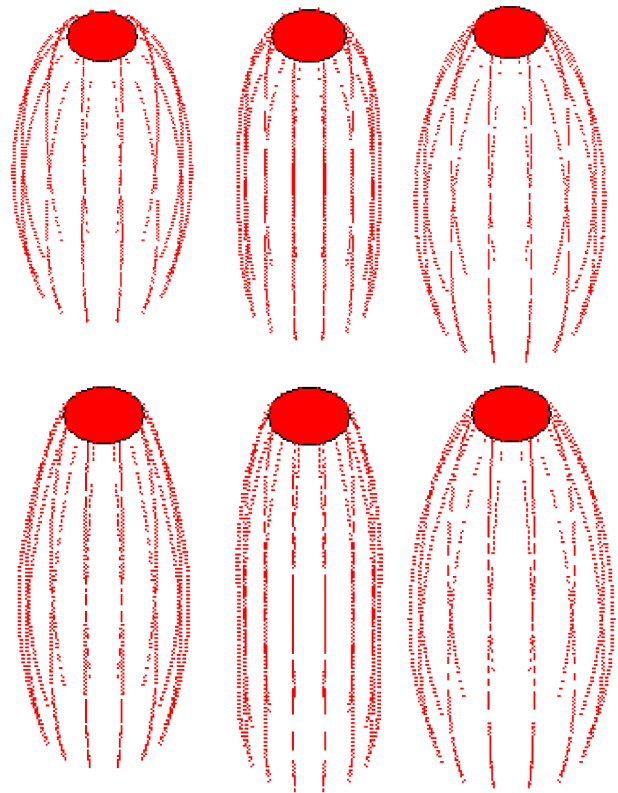
[11] E. J. Anderson and M. E. Demont "The mechanics of locomotion in squid *Loligo pelaei*: locomotory function and unsteady hydrodynamics of the jet and intramantle pressure" *Journal of Experimental Biology* vol. 203, pp. 28512863, 2000.

[12] A. E. Green, P. M. Naghdi and W. L. Wainwright "A general theory of a Cosserat surface" *Archive for Rational Mechanics and Analysis* vol. 20, n 4, pp. 287-308, 1965.

[13] E. Reissner "The effect of transverse shear deformation on the bending of elastic plates" *ASME Journal of Applied Mechanics* vol. 12, pp. 68-77, 1945.

[14] J. C. Simo and L. Vu-Quoc "On the dynamics of flexible beams under large overall motions - The plane case: Part I" *Journal of Applied Mechanics* vol. 53, no. 4, pp. 849854, 1986.

[15] J. Linn, H. Lang and A. Tuganov "Geometrically exact Cosserat rods with Kelvin-Voigt type viscous damping" *Mech. Sci.* vol 4., pp. 79-96, 2013.

[16] T. I. Fossen "Guidance and control of ocean vehicles" *Wiley*, 1999.

[17] W. Johnson, P. D. Soden, and E. R. Trueman A study in jet propulsion: an analysis of the motion of the squid, Loligo Vulgaris, Journal of Experimental Biology, vol. 56, pp. 155165, 1972.

Safe Physical Human-Robot Interaction
Based on Dynamic Analysis and Use of Residuals

Claudio Gaz   Emanuele Magrini   Fabrizio Flacco   Alessandro De Luca

EXTENDED ABSTRACT

Realization of a safe physical interaction between a robot and a human is becoming an increasingly relevant feature in both industrial and service settings [1]. Robot co-workers may collaborate with humans in some complex manufacturing operations so as to find the right balance in efficiency between automated solutions and flexible skills. Similarly, operators in medical or other professional service domains may enhance their performance by relying on a user-friendly robotic partner.

In all cases, safety of robot operation is of primary concern. This requirement is pursued through a combination of lightweight robot design, with intrinsic compliance and joint torque sensing [2], with the additional use of external sensors to monitor the workspace [3], and novel control capabilities for collision avoidance [4] and physical contact detection and reaction [5]–[7]. The robot control architecture should also reflect a hierarchy of consistent behaviors, from safety to coexistence and up to active collaboration [8].

There are a two basic control ingredients that have been used in recent research works in order to achieve a safe physical Human-Robot Interaction (pHRI). One is the availability of a reliable dynamic model of the robot. This allows designing of model-based feedforward/feedback control strategies for the accurate execution of trajectories in free space or for impedance control of the interaction with the environment. A second feature is the availability of joint torque sensing in the presence of compliant joints (or transmission/reduction elements like Harmonic Drives). This allows to switch from the more traditional position control to direct torque control. The combination of these two ingredients enables also implementing the residual-based method of [6], [7] for a reliable detection and isolation of contacts/collisions occurring at any point along the robot structure, without the use of external sensing (e.g., cameras) or touch/skin sensors.

Except for some few cases realized on industrial robots having a closed control architecture [9], the large bulk of research on safe pHRI has been conducted on the KUKA LWR (*Light Weight Robot*) manipulator [10]. Among the reasons for this choice, there is certainly the availability to the user of some dynamic information and of robot

measurements through the Fast Research Interface [11] at 1 KHz rate.

The (link) dynamics of this robot is given by

$$M(q)\ddot{q} + C(q,\dot{q})\dot{q} + g(q) = \tau_J - \tau_F + \tau_{ext}, \quad (1)$$

where $q \in \mathbb{R}^n$ is the link position vector, M is the (link) inertia matrix, C is the matrix of the Coriolis and centrifugal terms, g is the gravity vector, τ_J is the joint torque, τ_F is the (unmodeled) friction torque, and τ_{ext} is the external torque resulting from some collision or contact with the human/environment.

Knowing all the terms in the dynamic model (1), *except* for the external torque τ_{ext}, we can compute [6] the residual vector $r \in \mathbb{R}^n$ as

$$r = K_I \left(p - \int_0^t \left(\tau_J - \tau_F + C^T(q,\dot{q})\dot{q} - g(q) + r \right) ds \right), \quad (2)$$

where $p = M(q)\dot{q}$ is the generalized (link) momentum of the robot, and $K_I > 0$ is a diagonal gain matrix. The main property of the residual is that it provides, without the use of acceleration measurements or estimates nor the need to invert of the inertia matrix, a very good approximation (a first-order, stable, filtered version) of the unknown torque τ_{ext}, with $r \simeq \tau_{ext}$, for sufficiently large K_I, thus enabling automatic collision detection.

If we know a priori the contact point p_c where an external Cartesian force is applied to the robot (e.g., the end-effector), or if we can extract the geometric information of the contact location from an external sensor (using the Kinect sensor as in [12]), then it is possible to extract from the residual r also an estimate of the contact force $F_c \in \mathbb{R}^3$ as

$$\widehat{F}_c = \left(J_c^T(q) \right)^{\#} r, \quad (3)$$

namely by pseudoinversion of the transpose of the $3 \times n$ Jacobian matrix $J_c = (\partial p_c / \partial q)$ related to the contact point.

Unfortunately, the robot manufacturer does *not* provide full information on the dynamic model (1), even if some of its terms are used in fact inside the KUKA controller. What is made available on line through the FRI software interface are the measurements q (from encoders) and τ_J (from joint torque sensors), and only the *numerical* values of the inertia matrix M_{num} and of the gravity vector g_{num} evaluated at the current configuration q (probably, a Newton-Euler routine is used internally). In addition, only an approximate value r_{num} of the residual (2) is provided, which is most likely computed by neglecting the friction term τ_F.
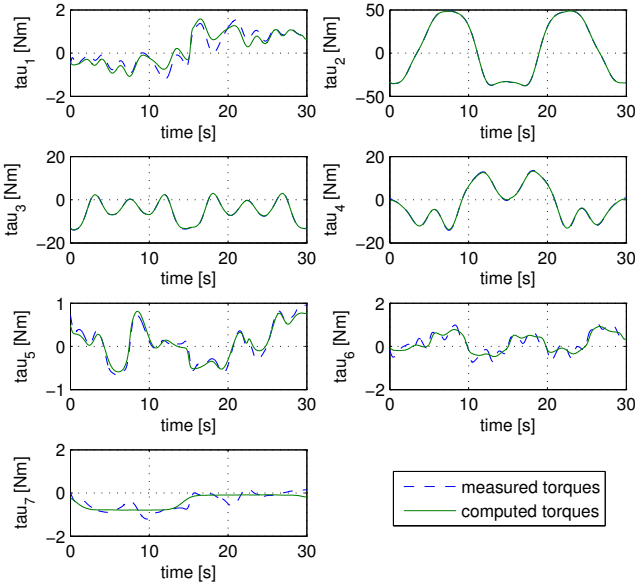
Fig. 1. Comparison between the measured joint torques $\boldsymbol{\tau}_J$, as retrieved from the KUKA LWR robot, and the joint torques $\widehat{\boldsymbol{\tau}}_J$ computed from (1) (in the absence of external torques, $\boldsymbol{\tau}_{ext} = \mathbf{0}$) when using the identified dynamic coefficients, including friction. The robot is performing a generic motion not used during the identification (validation phase).

Fig. 2. Comparison between the KUKA FRI output $\widehat{\boldsymbol{r}}_{num}$ and the residual $\widehat{\boldsymbol{r}}$ computed from (2) with the identified dynamic model coefficients. The robot performs first a rest-to-rest motion without payload for about 18 s (residuals should remain at zero). Then, a suspended payload is hung at the end effector, which is detected as an external torque $\boldsymbol{\tau}_{ext}$ (oscillations are due to the slight swinging of the payload).

To overcome this limited and inaccurate information, we have developed in [13] a novel dynamic model identification method, explicitly tailored for the hardware/software configuration of the 7R KUKA LWR manipulator. Starting from a complete derivation of the robot dynamic model in symbolic form, and using the available numerical data provided by the FRI interface in a number of random robot configurations, a linear least squares problem is solved using a minimal parameterization of the inertia matrix (30 dynamic coefficients) and of the gravity vector (12 dynamic coefficients). From the identified expressions of the elements of $\boldsymbol{M}(\boldsymbol{q})$, centripetal and Coriolis terms are then easily derived by symbolic differentiation (Christoffel symbols). Finally, a separate estimation of the static friction term $\boldsymbol{\tau}_F$ has been performed. Figure 1 shows a typical comparison between the joint torques $\boldsymbol{\tau}_J$ retrieved from the robot during a generic motion and the estimated torques $\widehat{\boldsymbol{\tau}}_J$ computed from (1), in the absence of external torques ($\boldsymbol{\tau}_{ext} = \mathbf{0}$) and using the identified dynamic coefficients. The estimation errors remain always bounded by $0.2 \div 0.3$ Nm. More results can be found in [14].

As a further validation, Figure 2 shows a comparison between the KUKA FRI output $\widehat{\boldsymbol{r}}_{num}$ and the residual $\widehat{\boldsymbol{r}}$ explicitly computed from (2) with the identified dynamic model coefficients. The differences are only due to the estimated friction term $\boldsymbol{\tau}_F$ added in our case, and remain limited again within $0.2 \div 0.3$ Nm. When there is no external torque acting on the robot, our computation of the residual provides values that are closer to zero (which is the correct ideal value in the absence of contacts, unmodeled terms, and noise on measurements).

The obtained results pave the way to the realization of advanced model-based control strategies for handling safely human-robot interaction, and in particular collaborative tasks. Physical collaboration is characterized by force exchanges between parts of the human body (typically, one or both hands, or a manually-held tool) and the robot. While most of the times it is assumed that such contacts occur only at the robot end effector, we now know that, through the use of eqs. (2) and (3), such forces may be exchanged at any point of the robot structure and can be estimated on line even without the use of tactile sensors distributed on the robot surface.
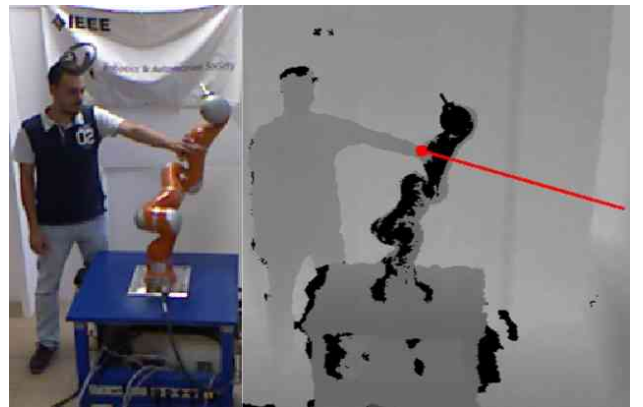
Fig. 3. Single human-robot contact at a generic location (left) and the associated depth image from the Kinect (right). Superposed in red, the detected contact point and the contact force $\widehat{\boldsymbol{F}}_c$ estimated using (3).

Figure 3 shows a typical situation of generalized physical human-robot interaction. In this case, a single contact occurs between the human left hand and the robot at a point located on the fifth link. The working environment of the robot is monitored by a Kinect depth sensor, which identifies the contact point, after some suitable filtering, in the least invasive way. The residual-based method estimates contact force vector $\widehat{\boldsymbol{F}}_c$. If the robot is in a collaborative mode (as specified by gestures or voice commands, or by the task progress status), this information is used by the controller in order to impose to the robot a collaborative behavior.

In the paper, we will review our recent works on dynamic modeling and identification for the KUKA LWR robot and on the estimation of contact forces applied by a human to the robot, presenting also experimental results on the use of this dynamic analysis and of the obtained residuals in order to distinguish between intentional contacts and undesired collisions, as well as for the design of various strategies (such as admittance control, impedance control, or explicit force control) for handling human-robot collaboration in the presence of single or multiple physical contacts.

REFERENCES

[1] A. De Santis, B. Siciliano, A. De Luca, and A. Bicchi, "An atlas of physical human-robot interaction," *Mechanism and Machine Theory*, vol. 43, no. 3, pp. 253–270, 2008.

[2] G. Hirzinger, A. Albu-Schäffer, M. Hähnle, I. Schaefer, and N. Sporer, "On a new generation of torque controlled light-weight robots," in *Proc. IEEE Int. Conf. on Robotics and Automation*, 2001, pp. 3356–3363.

[3] F. Flacco and A. De Luca, "Multiple depth/presence sensors: Integration and optimal placement for human/robot coexistence," in *Proc. IEEE Int. Conf. on Robotics and Automation*, 2010, pp. 3916–3923.

[4] F. Flacco, T. Kröger, A. De Luca, and O. Khatib, "A depth space approach to human-robot collision avoidance," in *Proc. IEEE Int. Conf. on Robotics and Automation*, 2012, pp. 338–345.

[5] A. De Luca and R. Mattone, "Sensorless robot collision detection and hybrid force/motion control," in *Proc. IEEE Int. Conf. on Robotics and Automation*, 2005, pp. 999–1004.

[6] A. De Luca, A. Albu-Schäffer, S. Haddadin, and G. Hirzinger, "Collision detection and safe reaction with the DLR-III lightweight robot arm," in *Proc. IEEE/RSJ Int. Conf. on Intelligent Robots and Systems*, 2006, pp. 1623–1630.

[7] S. Haddadin, A. Albu-Schäffer, A. De Luca, and G. Hirzinger, "Collision detection and reaction: A contribution to safe physical human-robot interaction," in *Proc. IEEE/RSJ Int. Conf. on Intelligent Robots and Systems*, 2008, pp. 3356–3363.

[8] A. De Luca and F. Flacco, "Integrated control for pHRI: Collision avoidance, detection, reaction and collaboration," in *Proc. 4th IEEE Int. Conf. on Biomedical Robotics and Biomechatronics*, 2012, pp. 288–295.

[9] M. Geravand, F. Flacco, and A. De Luca, "Human-robot physical interaction and collaboration using an industrial robot with a closed control architecture," in *Proc. IEEE Int. Conf. on Robotics and Automation*, 2013, pp. 4000–4007.

[10] R. Bischoff, J. Kurth, G. Schreiber, R. Koeppe, A. Albu-Schäffer, A. Beyer, O. Eiberger, S. Haddadin, A. Stemmer, G. Grunwald, and G. Hirzinger, "The KUKA-DLR Lightweight Robot arm a new reference platform for robotics research and manufacturing," in *Proc. 41st Int. Symp. on Robotics*, 2010, pp. 741–748.

[11] *KUKA.FastResearchInterface 1.0*, KUKA System Technology (KST), D-86165 Augsburg, Germany, 2011, version 2.

[12] E. Magrini, F. Flacco, and A. De Luca, "Estimation of contact forces using a virtual force sensor," in (submitted to) *IEEE/RSJ Int. Conf. on Intelligent Robots and Systems*, Chicago, IL, Sep. 2014.

[13] C. Gaz, F. Flacco, and A. De Luca, "Identifying the dynamic model used by the KUKA LWR: A reverse engineering approach," in *IEEE Int. Conf. on Robotics and Automation*, Hong Kong, PRC, Jun. 2014.

[14] The complete KUKA LWR dynamic model @ DIAG Robotics Lab, Sapienza Università di Roma. [Online]. Available: http://www.diag.uniroma1.it/labrob/lwrdyn

Kalman underwater acoustic 3D localisation in groups of robots

Fabio Fratichini[1,2], Stefano Chiesa[1], Sergio Taraglio[1]

[1]Robotics Lab, ENEA, Via Anguillarese 301, Rome, Italy
[2]Dept. of Informatica and Automazione, University of Roma Tre, Via Ostiense 159, Rome, Italy
fabio.fratichini@gmail.com, {stefano.chiesa, taraglio}@enea.it

Abstract— **A three dimensional localisation algorithm for a swarm of underwater vehicles is revised and further experiments are presented. The proposed approach is grounded on an extended Kalman filter (EKF) scheme used to fuse some proprioceptive data such as the vessel's speed and some exteroceptive measurement such as the time of flight (TOF) sonar distance of the companion vessels. The implementation of the algorithm has been carried out under Matlab and ROS (Robot Operating System). The results of several simulations are presented showing the robustness of the approach. The case of a supporting surface vessel is also considered.**

Keywords— *Distributed Control Systems, Mobile Robots and Intelligent Autonomous Systems, Space and Underwater Robots, Sensor Fusion.*

I. INTRODUCTION

The exploration of the oceans both for scientific and economic purposes is becoming more and more important. Out of the limitations of our biological characteristics, underwater robotics has gained an essential role in the study and exploitation of the seas. Its more promising branch is that of the autonomous underwater vehicles (AUV), i.e. those vehicles that are capable of performing the required tasks without human supervision, coping with the mission unknowns.

In the latest years the research on AUVs has broadened towards the simultaneous use of more vessels, i.e. the implementation of multi robot configurations all the way to full swarms of underwater vehicles.

Whether a single or more AUVs are considered, one of the focal points of autonomy is the reliable knowledge of the vessel pose. Unfortunately an underwater system suffers the limiting characteristics of its environment. Water, especially salted one, blocks electromagnetic waves, inhibiting the use of positioning systems such as the GPS. At the same time this implies a difficult communication among the AUVs of a swarm or with a remote operator. The available means to localise a single AUV are thus the exploitation of inertial sensors, velocity ones and/or gyroscopes combined in dead reckoning.

However, in the framework of an underwater swarm, the localisation of a single vehicle can profit from the existence of the other vessels, gathering information from the fellow AUVs. The key issue of all the swarm localisation methods is the best possible combination of proprioceptive measures (dead reckoning) and exteroceptive sensor readings, the main difference being the employed estimator. The localisation of swarms of robots has been extensively studied for packs of terrestrial surface robots. In this case there are no physical limitations and it is possible to use GPS, if outdoors, or different methods for indoor teams. In addition the communication of information among the robots is unproblematic over the radio link.

An approach is based on the subdivision of the swarm in subgroups one of which, in turn, is kept at a fixed position and acts as a set of landmarks for the moving others [1][2]. In [3], [4] and [5] it has been successfully employed belief functions combined with a Montecarlo approach and particle filtering optimization. [6] and [7] employ a Kalman filter where the proprioceptive measures are used to estimate the future state of the system and the exteroceptive ones are used to correct and update the estimate. In [8] this approach is extended by considering the most generic relative observations between two robots. More recently the work of Olfati-Saber, see e.g. [9], has addressed the problem of decentralized Kalman filtering in sensor networks through consensus algorithms for the swarm controlling strategies. [10] have investigated the consistency of EKF based cooperative localisation considering observability. The typical operative environment considered in these works is a two dimensional terrestrial one.

In [11] a three dimensional algorithm for the global positioning of a swarm of underwater robots based on a Kalman filter approach is presented. A simple kinematic model of the AUV is considered, capable of measuring its own velocity and to communicate over an ultrasonic acoustic link with the other vessels. Through the measurement of the time of flight (TOF) of the ultrasound transmission the AUVs can measure their relative distance. All the available information is then combined with an extended Kalman filter distributed among the vessels.

Here further experiments are presented in order to assess the robustness of the approach and its dependence on some algorithm parameters. Since an operative swarm of underwater robots will be deployed from some kind of surface vessel, in the following the case of a swarm supporting boat able to measure its own position via a GPS and able to furnish this data to the swarm is described and tested.

In the second section of the paper the problem is stated in a three dimensional environment and the multi robot Kalman based algorithm is revised. In the third section the AUV characteristics are presented and discussed, showing the available sensors. In the fourth section some experimental results are presented relative to different experimental situations. In the fifth section the conclusions and future work are discussed.

II. MULTI-ROBOT KALMAN LOCALIZATION

The key point for a cooperative localisation in a swarm of robots is viewing the group as a single entity that can access the information of a large number of proprioceptive and exteroceptive sensors.

In the following all the vessels are described by the same motion equations and each robot possesses proprioceptive sensors for the motion estimate. Each AUV encompasses also an ultrasound communication link, which can collect the information from the other vehicles in the swarm.

Let us consider the global dynamical state X of the whole swarm, it will be a vector composed of $Mx6$ items where M is the number of robots and 6 is the number of variables describing the single vehicle (x, y, z, roll, pitch, yaw), i.e. a vector composed of the poses $\vec{x}_i$ of all the robots.

$$\vec{X} = [\vec{x}_1, \vec{x}_2, ..., \vec{x}_M] \tag{1}$$

The vessel coordinate system is centred in the centre of the vehicle and its x axis is longitudinally directed from stern to bow, the y axis is towards starboard and the z one downward.

The kinematic model of the single robot uses a linear velocity parallel to the x axis (thrust) and the possibility to change all the three Euler angles through appropriate angular velocities.

The mathematical model describing the time evolution of the single vessel of the swarm is:

$$\vec{x}_i[k] = f\left(\vec{x}_i[k-1], \vec{u}_i[k-1], \vec{w}_i[k-1]\right) \ i = 1,...,M \tag{2}$$

where f is generally a non linear function of the state $\vec{x}_i[k-1]$, of the input $\vec{u}_i[k-1]$ and of the noise $\vec{w}_i[k-1]$ at the preceding time step k-1. The vessels can also measure all the other ones and this can be described by the:

$$z_i[k] = h\left(\vec{x}_i[k], \vec{x}_j[k], n_i[k]\right) \ i = 1,...,M, \ j \neq i \tag{3}$$

here h is the measurement function linking the state of the i-th robot with the state of the measured one (the j-th) and the measure noise $n_i[k]$.

The Kalman filtering is a well known strategy that yields an estimate of a dynamical process using a feedback control. It foresee the process state at a given time and it employs a measurement feedback to update the state through a better estimate. It is an iterative process that loops through two different phases: on one side it predicts the state of the system and the error covariance, on the other it computes the so called Kalman gain to correct both the state estimate and the error covariance on the grounds of some kind of available measure. Since the time evolution function (equation 2) may be not linear, an extended version of the filter has been here employed. The EKF basically behaves as the standard procedure but uses a local linearization of the functions. A very interesting characteristic of this filter is its iterative aspect. The results of an iteration of the filter is used as input for the successive step; in this way the filter retains memory of the history of the system.

Let us consider the whole swarm, the EKF cycles between the two phases of prediction and update.

A. Prediction

Each robot, at a given time step, estimates its state at the successive time step on the grounds of the kinematic model and the available proprioceptive measures (linear and angular velocities) and their null average Gaussian noise. Also the time evolution of the cross correlation matrix is computed

$$\hat{x}_i^-(k+1) = f(\hat{x}_i^+(k), u_i(k), w_i(k)) \tag{4}$$

$$\hat{P}_{ii}^-(k+1) = \Phi_i(k)\hat{P}_{ii}^+(k)\Phi_i^T(k) + G_i(k)W_i(k)G_i^T(k) \tag{5}$$

$$\hat{P}_{ij}^-(k+1) = \Phi_i(k)\hat{P}_{ij}^+(k)\Phi_j^T(k) \tag{6}$$

here equation (4) is the state time evolution (as in equation (2)) and equations (5) and (6) describe the time evolution of the cross correlation matrix P in the diagonal (equation (5)) and off diagonal terms (equation (6)); Φ is the system propagation matrix, G is the system noise input matrix and W is the noise input covariance. The minus sign stands for a-priori and the plus one for a-posteriori. In other words the state is predicted on the basis of the kinematic model and the input velocity and the new a-priori cross correlation matrix is computed with the system proprioceptive measures for the diagonal terms (the $6N$ system variables) and with the system propagation matrix for the off diagonal terms.

In order to perform a distributed EKF it is convenient to process the a-posteriori estimated cross correlation matrix (equation 6) through a singular value decomposition (SVD). In this way each robot can compute its own term multiplying the SVD term by its dynamical matrix, see (Rumeliotis and Bekley, 2002).

B. Update

Every time a robot measures something, an update can be performed. In order to describe the procedure here are considered the availability of the heading (compass) and depth (pressure gauge) of the measuring vessel and the TOF distance of another vessel. The non linear measuring function h is that shown in equation (3) and the noise is regarded as a null average Gaussian one. It is now possible to compute the a-posteriori state estimate (i.e. after the measurement):

$$\hat{x}_r^+(k) = \hat{x}_r^-(k) + K_r(k)(z_i(k) - h(\hat{x}_i^-, \hat{x}_j^-))$$
$$K_r(k) = \hat{P}_{ri}^-(k)H_i^T(k) + \hat{P}_{rj}^-(k)H_j^T(k)S^{-1} \tag{7}$$

where the index $r = 1,...,M$ describes the vessel, $K_r(k)$ is the so called Kalman gain with S the residual covariance, and the last term is the residual. The H terms are the Jacobians of the measuring function h w.r.t. the two state vectors x_i and x_j:

$$H_i = \begin{bmatrix} -\dfrac{\Delta x}{\sqrt{\Delta r^2}} & -\dfrac{\Delta y}{\sqrt{\Delta r^2}} & -\dfrac{\Delta z}{\sqrt{\Delta r^2}} & 0 & 0 & 0 \\ 0 & 0 & 1 & 0 & 0 & 0 \\ 0 & 0 & 0 & 0 & 0 & 1 \end{bmatrix} \quad (8)$$

$$H_j = \begin{bmatrix} \dfrac{\Delta x}{\sqrt{\Delta r^2}} & \dfrac{\Delta y}{\sqrt{\Delta r^2}} & \dfrac{\Delta z}{\sqrt{\Delta r^2}} & 0 & 0 & 0 \\ 0 & 0 & 0 & 0 & 0 & 0 \\ 0 & 0 & 0 & 0 & 0 & 0 \end{bmatrix} \quad (9)$$

and $\Delta r^2 = \Delta x^2 + \Delta y^2 + \Delta z^2$. Clearly equation (8) describes the distance measurement together with the proprioceptive absolute measure of z and yaw, while equation (9) is relative to the other vessel and the distance measure alone.

Finally the *a-posteriori* covariance matrix estimate is:

$$\hat{P}_{rs}^+ = \hat{P}_{rs}^- - (\hat{P}_{ri}^- H_i^T + \hat{P}_{rj}^- H_j^T) S^{-1} (H_i \hat{P}_{is}^- + H_j \hat{P}_{js}^-) \quad (10)$$

with the indexes $r = 1,...,M$ and $s = 1,...,M$.

Until now the described process is relative to a single robot, the localization of multiple robots considers a series of multiple relative measurements among the various vessels. Such a scenario can be approached in two different ways: in a centralised or in a distributed one. In the first a central supervisor can be considered collecting all the data from all the vehicles and performing the multi robot system state estimation. The second paradigm can be split into two further classes: uncooperative or cooperative algorithms. The first class simply tries to localise each robot as if it was alone in the world, i.e. counting on its own estimate and measures alone, without gathering additional information from the others in the swarm. The second class can exploit the information coming from the companions and performing a local algorithm for the pose estimation. Regardless of the employed approach, the Kalman scheme makes use of a series of matrices and vectors that must circulate among the underwater robots.

The basic issue is the extremely limited bandwidth that is available underwater. In the following a distributed cooperative approach has been employed. Let us now examine in more detail the used scheme.

A fully distributed algorithm has been ruled out owing to communication induced constraints. Whenever a robot measures another one it should broadcast a message with its own ID and the one of the measured robot, its state vector and the vector of measurement; for the update phase an exchange of the predictions of all the swarm should be distributed among all members. Then each robot may compute the update of its own state and covariance matrix that should be both transmitted to any other robot in the swarm.

In order to limit as much as possible the communication problem in the swarm a distributed-centralized approach has been tested. The idea is as follows. Whenever a measurement is done, the measuring robot broadcast its ID and a measurement done flag, then it gathers the predictions from all the companions, performs the EKF for the whole swarm and finally broadcasts the new matrices to the fellow robots. It is obviously a centralised algorithm but it is distributed in time, at each time step only the measuring robot is computing, and at the next time step it will probably be a different one.

The difference with the fully distributed approach is in a limitation of the communication, or, more precisely, of the communication problems. The amount of exchanged data will be the same, but since only one robot is actually broadcasting its results, there will be less communication overheads and possible multi-paths deriving from multiple robots trying to communicate all at the same time.

The amount of data naturally increases if more than a single robot performs exteroceptive measures. In the following it has been supposed that at a given time step each vessel measures the distance of all the others, i.e. it performs N-1 exteroceptive measures.

The algorithm may consider this scenario in two possible ways: on one side it may compute the EKF considering one measure at a time, and updating the state N-1 times; on the other it may consider a single measurement (a vector of N-1 components) and update the state a single time only. Naturally the second approach would certainly be less computationally intensive.

A set of dedicated experiments has shown, as expected, that the results of the EKF in terms of position accuracy does not depend on the chosen method and thus the second one has been used.

III. VEHICLE DESCRIPTION

The underwater vehicle considered has proprioceptive and exteroceptive sensors in order to measure itself and its environment. It has been assumed that each vessel is equipped with:

• a tachymeter, for the measurement of the linear velocity due to the thrust of the propeller;

• an inclinometer (or gyro), for the measurement of the pitch and roll angle;

• a pressure gauge, for the depth measurement (z absolute coordinate);

• a compass, for the heading measurement (yaw absolute coordinate);

• an ultrasound transducer, for the measure of relative distance of two vessels with time of flight (TOF).

The introduction of a compass for the absolute orientation and a pressure gauge for the depth measure are of basic importance since they improve the observability of the system. In a three dimensional environment each vessel possesses six degrees of freedom, thus the overall system can be considered as unbalanced towards non observability.

The roll angle in the EKF is not considered and supposed null. The measurement noise is assumed zero mean Gaussian.

In the experimental results section several examples of simulations with sensors of varying noise characteristics will be presented. The chosen noise values considered are compatible with low cost sensors similar to the ones planned to actually equip a low cost submarine presently under development.

IV. EXPERIMENTAL RESULTS

In the experiments, the vehicles are considered as kinematic objects, i.e. without the computation of their dynamics, and are able to exchange information instantaneously. All the simulations have been performed in Matlab.

Let us consider a set of M=10 vessels moving in parallel along a straight trajectory (speed 1 m/s, angular speed 0 rad/s). The assumed standard deviation on linear and angular speed is 0.1 m/s and 0.05 rad/s respectively. The standard deviation on the TOF distance measure is 0.05 m, on the heading is 1° and 0.07 m on the depth. All these values are consistent with low cost sensors commonly available on the market.

In Figure 1 are shown the average error (on the whole swarm of ten) and the 3σ error relative to the x, y, z coordinates and the yaw angle. For figure clarity the roll and pitch ones are not showed. The average position error after 50 meters is of about 0.35%, while the 3σ error is of about 1%. The same quantities without the EKF, considering dead reckoning alone, are 8% and 30%.

As above mentioned the underwater realm is quite a difficult one and the communications should be kept at a minimum, hence it has been experimented a situation in which the vessels do not measure continuously the distance of fellow robots but perform a measure once every 100 time steps. This is reasonable since the trajectory of an underwater vessel is usually smooth and slowly varying. Fig. 1. Average and 3σ error for x, y, z and yaw as a function of time, linear trajectories.
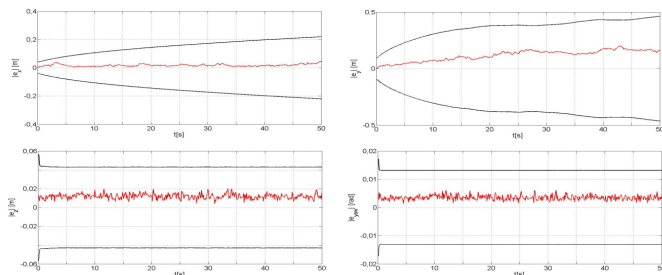

Fig 1. Average and 3σ error for x, y, z and yaw as a function of time, linear trajectories
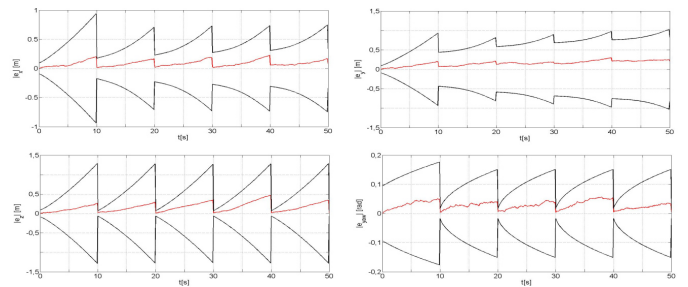

Fig. 2. Periodic measurements. The x, y and z coordinates and the yaw angle.

The results are presented in Figure 2. It is evident the saw tooth shape due to the periodical correction of the EKF. In this case after 50 m the average and 3σ errors are respectively 0.46% and 1.8%, slightly larger than the continuous case, as it could have been expected.

In an operative scenario the use of periodical corrections instead of continuous ones does affect the system performance but the gain in terms of communication limitation greatly counter balance such a choice.

In Figure 3 is shown the algorithm performance in a case where sinusoidal trajectories are considered, i.e. with a constant linear velocity but an angular one slowly varying in time as a sinusoid. The measures are periodic as in the previous experiment, the number of time steps is doubled and the average and 3σ errors are 0.28% and 1%.
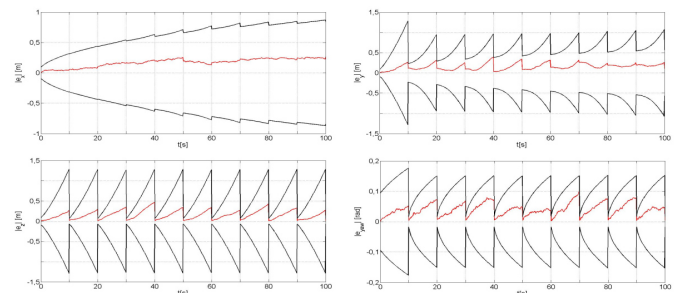
Fig. 3. Sinusoidal trajectories.

A further trial is presented in Figure 4; here the vessels are made follow a circular trajectory for 1300 m, always with periodic exteroceptive measures. In this case the two errors are respectively 0.05% and 0.2%. Only x and y are shown in the plot for better intelligibility.
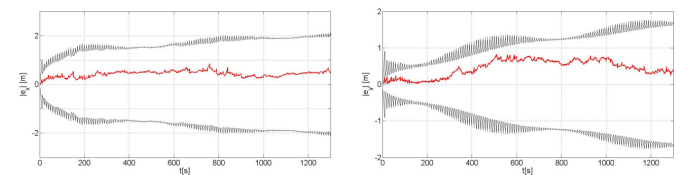
Fig. 4. Circular trajectory. Only x and y are plotted.

In Figure 5 it is shown the dependence of the average position error at the end of the simulation as a function of the number of vehicles in the swarm keeping all the other parameters fixed. It is clear that "union is strength": the more the vessels the better the estimate, until an asymptote is reached.
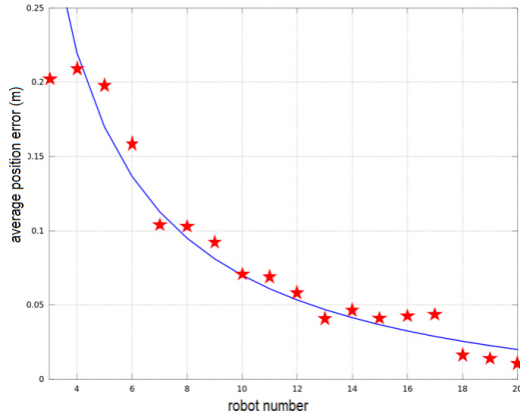
Fig. 5. Average position error as a function of the robot number.

A. Surface vessel in-the-loop

In the swarm operative conditions it may be foreseen the exploitation of a surface vessel, a boat, to deploy the underwater robots. Once that such a boat is available, it may be useful to actively use it in the swarm mission. The boat can enter the swarm as a further member of it with the added value of the possibility to directly measure its own position via a GPS sensor.

Some experiments have been thus performed considering a node of the swarm as able to measure its absolute position with the average error relative to a GPS receiver.

A swarm composed of 10 robots has been made follow a possible mission in which they start from the surface, go deeply underwater and then re-surface. The initial position of each vessel is uniformly random in a 300 by 300 meters square with an initial null error position with a standard deviation of 0.1 m, the exteroceptive measures are periodic every 100 time steps (i.e. 10 s). The measurement errors are 0.05 m on TOF distance, 0.07 m on depth, 1° for the yaw angle e 0.5° for the pitch one. The mission is 5000 s long, i.e. 2.5 Km.
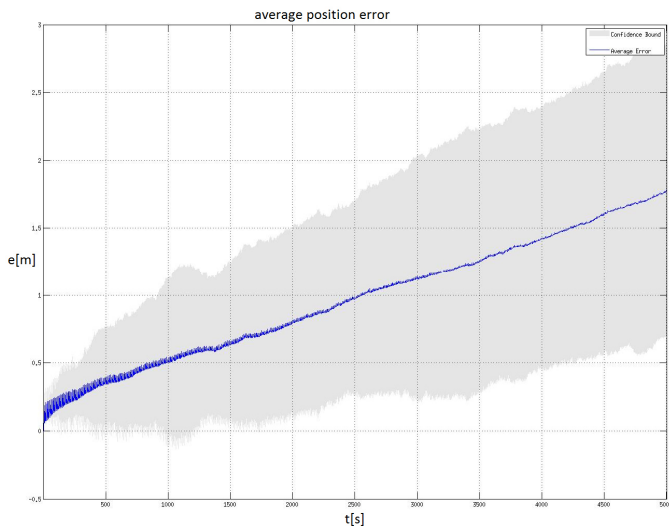

Fig. 6. Full mission average position error and error confidence (no boat).

In Figure 6 is shown a reference test where the swarm is left alone, without any surface vessel aid, in the plot the average position error as a function of time (blue) and the 3σ confidence is presented; the final position percentage error is of about 0.1%. In order to test the algorithm with the aid of a surface vessel, one of the robot has been made change its course, remaining at the surface and following a trajectory due to a linear velocity of 1 m/s and an angular one of 0.001 rad/s. In Figure 7 is shown the trajectories of the surface (green) and underwater vehicles (red). Finally in Figure 8 the average position error and error confidence for the swarm as a whole are plotted. It is evident that the presence of a reliable measure for the surface vehicle dramatically changes the algorithm performance. The average error is almost constant, the observability of the system is radically improved by the possibility to exploit the absolute position measure via GPS.
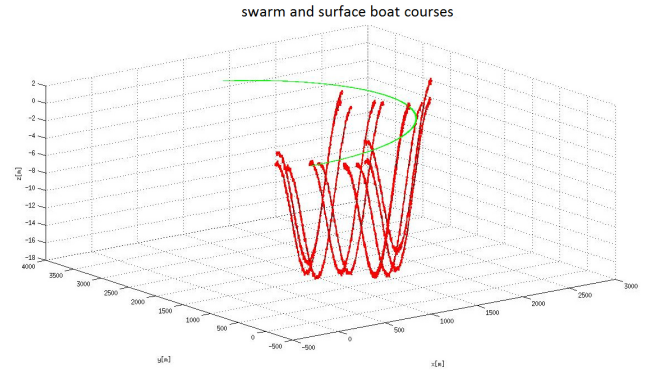
Fig. 7. Surface (green) and underwater (red) courses.
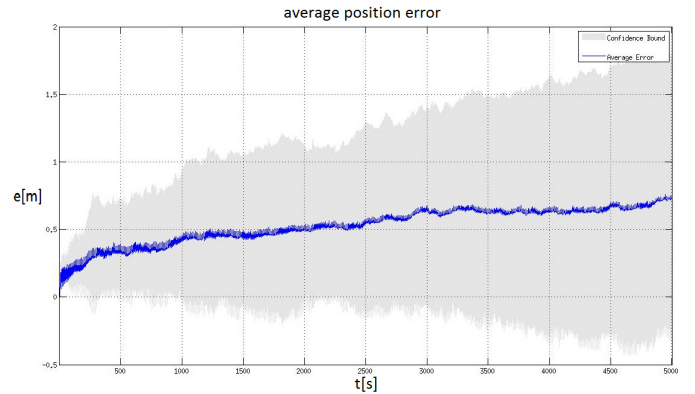
Fig. 8. Full mission average position error and error confidence with the surface boat.

B. Parameter dependence analysis

In the following the dependence of the algorithm on the initial position error and on the velocity amplitude measurement error at each time step is presented, no surface vessel is considered.

Physically, the initial position error is due to the uncertainty of the deployment of each vessel. In Figure 9 are plotted the data relative to 50 runs of the algorithm with 10 robots and a mission length of 2.5 Km.

Average final position error (mission length 2.5 Km)

Fig. 9. Average final position error as a function of the initial position standard deviation.

Naturally the final error position increases with the initial position error, but for the smaller ones (the reasonably attainable ones in operative situations) the final errors are limited. In this experiment the standard deviation on the percentage error on the velocity measure is of 0.1 m/s.

In Figure 10 is shown a similar plot where velocity measure errors are considered. At each time step the estimation of the vessel position is performed through the proprioceptive measure of the instantaneous robot velocity (dead reckoning). This measure is affected by an error whose percentage value is increased in this plot. The error on the initial position is considered null.

Average final position error (mission length 2.5 Km)
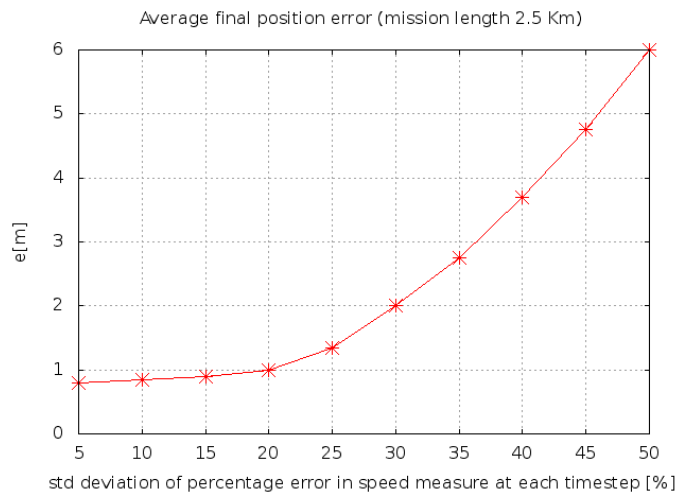
Fig. 10. Average final position error as a function of the percentage error in speed at each time step.

From the plot in Figure 10 it can be deduced that the percentage error in velocity measurement on which the dead reckoning is grounded weakly affects the final error for the typical values that can be expected in real world experiments.

V. DISCUSSION AND CONCLUSIONS

This work has presented further results of a three dimensional Kalman based localisation algorithm for a swarm of underwater vehicles.

In a three dimensional environment each vessel possesses six degrees of freedom, thus the overall system is heavily undetermined, i.e. the covariance on the system state quickly diverges. The introduction of real world measures such as the yaw angle (compass) and the z coordinate (pressure gauge) greatly improves the Kalman filter performance, enhancing the system observability.

It is here important to recall that the presented scheme greatly relies on communication among the members of the swarm. During the Kalman computation the various vehicles must distribute to the others their own estimates and covariance and all the cross correlations. This heavy communication scheme suggested the periodical exteroceptive measures in order to reduce the number of Kalman updates. Notwithstanding a reduced set of measures, the system is able to assure a good localisation.

The devised algorithm strategy is based on a mixed distributed-centralised approach. Each robot computes the Kalman filter for all of the system elements and it distributes its results to all the community, since a different robot will be the next to observe and compute the system state.

The performed robustness analysis has shown that the final average position error can be limited even in the presence of noise in the measure of each vessel speed vector and in the inaccuracy of initial position knowledge. These are the two major error sources: the initial position error is responsible for inaccuracy in relative distances among the robots and speed measure noise is responsible for render unpredictable the future positions of the vessels. The Kalman based algorithm is able to tame these two sources using the relative distance measures coming from the sonar TOF's, actively and especially correcting the speed drifting through the exploitation of the Gaussian features of the error.

In conclusion it is possible to affirm that the presented 3D Kalman based localisation system can be employed for a swarm of underwater robots, yielding accuracy in the computed positions, but with a limited swarm element number. Nevertheless further work is needed in order to reduce the so precious communication bandwidth in underwater environments allowing more numerous swarms.

REFERENCES

[1] Kurazume R., Nagata S., Hirose S., "Cooperative positioning with multiple robots," Proc. 1994 IEEE Int. Conf. Robotics and Automation, Los Alamitos, CA, vol. 2, pp. 1250–1257, 1994.

[2] Kurazume R., Nagata S., Hirose S., "Study on cooperative positioning system (basic principle and measurement experiment)," Proc. 1996 IEEE Int. Conf. Robotics and Automation, Minneapolis, MN, vol. 2, pp. 1421–1426, 1996.

[3] Rekleitis I.M., Dudek G., Milios E.E., "Multi-robot cooperative localization: a study of trade-offs between efficiency and accuracy," Proc. of International Conference on Intelligent Robot and Systems (IROS02), Lausanne, Switzerland, vol. 3, pp. 2690-2695, 2002.

[4] Fox D., Burgard W., Kruppa H., and Thrun S., "Collaborative multirobot localization," in Proc. 23rd Annual German Conf. Artificial Intelligence (KI), Bonn, Germany, pp. 255–266, 1999.

[5] Fox D., Burgard W., Kruppa H., and Thrun S., "A probabilistic approach to collaborative multi-robot localization," Autonomous Robots, 8(3), pp. 325–344, 2000.

[6] Thrun S., Fox D. and Burgard W., "Monte Carlo localization with mixture proposal distribution," Proc. AAAI Nat. Conf. Artificial Intelligence, Austin, TX, USA, pp. 859–865, 2000.

[7] Roumeliotis S.I., "Robust mobile robot localization: from single-robot uncertainties to multi robot interdependencies," Ph.D. dissertation, Elec. Eng. Dept., Univ. Southern California, Los Angeles, CA., 2000.

[8] Roumeliotis S.I. and Bekey G.A., "Distributed Multirobot Localization," IEEE Transaction On Robotics And Automation, 18,(5), pp. 781-795, 2002.

[9] Martinelli A., Pont F., Siegwart R., "Multi-Robot Localization Using Relative Observations," Proc. 2005 IEEE Int. Conf. Robotics and Automation, Barcelona, Spain, pp. 2798–2802, 2005.

[10] Olfati-Saber R., "Distributed Kalman filtering for sensor networks," Proc. Of the 46th IEEE Conf. on Decision and Control, pp 5492-5498, 2007.

[11] Huang G.P., Trawny N., Mourikis A.I., Roumeliotis S.I., "Observability-based consistent EKF estimators for multi-robot cooperative localization," Autonomous Robots, 30, (1), pp 99-122, 2011.

[12] Fratichini F., Chiesa S., Taraglio S., ., "Three Dimensional Localisation In Underwater Swarms Through A Kalman Approach," Proc. of 10th International Conference on Informatics in Control, Automation and Robotics, ICINCO 2013, Reykjavik, Iceland, pp 215-221, 2013.

Environmentally induced task partitioning in competing bio-robots

Paolo Arena, Luca Patané and Alessandra Vitanza

Dipartimento di Ingegneria Elettrica, Elettronica e Informatica, Universitá degli Studi di Catania, Italia

Abstract— Competition in living beings is always shaped by learning, which, even in simple creatures, like insects, plays a fundamental role in enhancing the basic inherited capabilities. Feeding, as well as courtship, involves environment exploration and exploitation, which mainly includes local competition: when such life-saving behavior leads to a global benefit for the colony, this can be considered as a form of global cooperation, even if the single agent is not aware of this global aspect. In this paper some key results of recent research activities based on a group of robots endowed with a simplified structure of an insect brain model are generalised to include more robots and different scenarios. The results obtained consist in the role Specialization of each robot, in a sequence learning task induced by the environment to the whole group of locally competing robots. This leads, as a side effect, to a decrease in the overall energy spent to fulfill a given task from the whole group. The description of the neural network and learning mechanisms used for robot specialization and sequence learning is reported. Some interesting simulation results are discussed and remarked to show the potentiality of the approach.

Index Terms— swarm intelligence, bio-robotics, collaborative algorithms, dynamic simulation, labor division.

I. Introduction

Coordination and collaboration among robots are the results of self-organized behaviors: social insects provide brilliant solutions for foraging, migration, mating and others [1], [2]. Transferring these characteristics to future biorobotic systems will assure high flexibility in space- and time-varying environments and high robustness to faults in the single agents [2], [3]. On the other hand, even within the same ecological niche, individuals of the same species compete for resources. This is mostly clear in simple insects like flies, which do not show apparent cooperation capabilities, but indeed compete for food and mating [4].

Indeed the boundary between cooperation and competition is rather subtle: in a sense it can be argued that simple brains mainly compete for resources. Such a competition is of course mediated by the environment: limited resources can be exhausted by other individuals even if a cycle of regeneration can be considered. The single agent behaviour and the environment co-evolve, within the single agent life cycle, to reach a global equilibrium for the colony. The environment acts so as to shape the local competitive behaviour of the single agents, to give rise to a global cooperative strategy, leading to an equilibrium state.

An open question in animal social behavior is related to the existence of a kind of social brain guiding the

Paolo Arena, Luca Patané and Alessandra Vitanza are with the Dipartimento di Ingegneria Elettrica, Elettronica e Informatica, Universitá degli Studi di Catania, Italy (email: {parena, lpatane, avitanza}@dieei.unict.it).

single behaviours through the environment. However could global order emerge from the local behavior of the agents which simply compete for survival? In this paper we try to investigate in this direction. A series of simulation results will show how a simple form of cooperation, i.e. task partitioning, can arise in a small number of competitive roving robots, endowed with the same neural controller. They succeed in adapting to different environmental induced stimuli, consisting in sequences of target activations. Here there is no need, in principle, for a kind of super organism: environment imposes the rules and the global benefit for a colony can arise from the local competition mechanisms among equally endowed individuals even in absence of a direct communication among them. Furthermore, the definition of a series of tasks is frequently met in Nature: there are different activities that have to be performed in given time windows during the daily cycle, and a division of these tasks among the individuals is requested, even if all the individuals are equally able to perform all the tasks [5].

The proposed approach starts from the results of previous works [6], [7], where the Specialization strategy was introduced and a first collaborative algorithm was formalized to fulfil an overall mission. The aim of this paper is to investigate and quantify the influence of the environmental mediation. The open problems we want to focus on regard the emergence of task partitioning induced by the environment and how the obtained solutions are robust to the robot starting positions. Unravelling the interaction among robots and the environment we identified the variables that lead to different solutions, proposing performance indexes to evaluate the final robot behaviour. The scenario considered in this work is a basically foraging task performed in a simulation environment with different number and arrangements of targets and starting position of robots. The obtained results show how a simmetric or asimmetric environment can massively modulate the different solutions. When a target is retrieved, another one becomes active following a predefined sequence, as an environment dependent rule. The single robots, while competing to foraging the maximum number of available targets, indirectly reach the global result of task partitioning specializing their behaviour and searching for specific targets decreasing the cumulative energy spent. The results show that agents evolve modelling their own basically competitive capabilities to perform globally collaborative strategies, starting from a homogeneous initial situation and exploiting the environmental mediation.
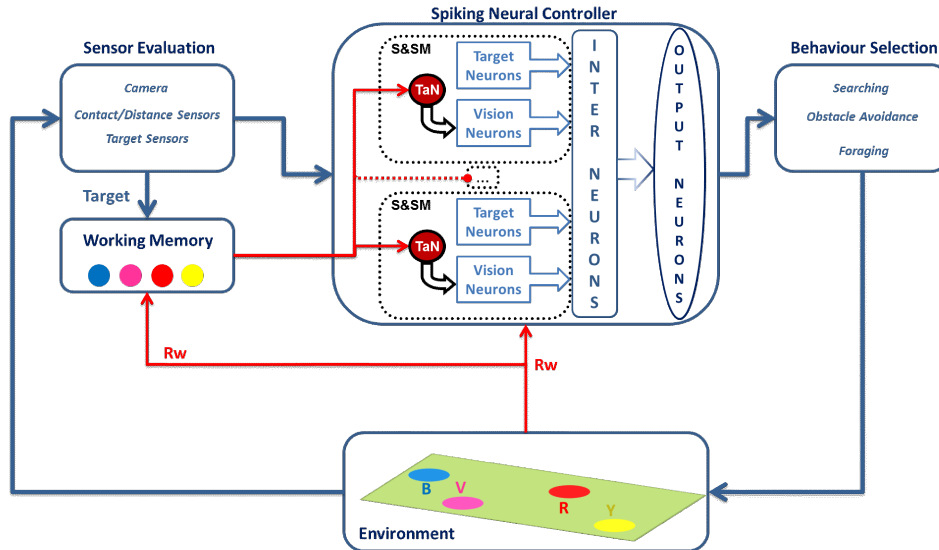
Fig. 1: Block diagram of the control architecture. In *Sensor Evaluation* block, data from the sensors are collected. The *Spiking Neural Controller* block describes the neural network model used for the foraging. The number of *Sensing and Specialization Modules (S&SM)* is related to the different targets to recognize. T_aN is the Threshold adaptation neuron, devoted to induce Specialization learning. Finally, the *Behavioural Selection* block indicates the most suitable action to be executed in the dynamic simulated Environment. The threshold adaptation is here guided by a *Working Memory*, it permits to memorize the targets retrieved during the activation sequence.

II. THE SPIKING-BASED NEURAL CONTROLLER

A brief overview of the Control Algorithm and the Neural Network (NN) controller in each robot are here reported. Further details on Specialization learning and NN model are available in [6], [7], [8], [9].

A. The Algorithm

In the experimental setup, the environment contains differently colored targets on the floor, which are cyclically activated in a mutually exclusive way. In our simulations two, three and four robots are allowed to move. Each robot starts with the same ability to identify and reach all the targets in the arena. If a target is present in the environment the robots move toward it with a fixed speed, otherwise they rotate looking for targets, performing a fixed clockwise rotation on the spot (about 45°). These rules imply that a target can be reached by a more distant but well oriented robot than by another which is nearer but badly oriented. No direct communication is introduced among the agents, but they compete for reaching the same targets once these are activated. This causes competition since a target is disabled briefly after being reached by a robot. After all targets are reached, the cycle is concluded and the reward signal (Rw) is activated for all robots. A learning phase is now performed: following the training algorithm described below, each robot increases its attractiveness to the targets reached and decreases its attractiveness to the non-reached ones. The final result emerging from this scenario is a spontaneous labor division among the robots, which become refractory to those targets they are not able to reach. The learning mechanisms concurrently act in different ways on the neural architectures in each robot: the result is the development of different skills. The presence of a global reward signal

assures diversity and specialization. The targets are circular spots on the ground worth to be reached by all the robots: this fact can hardly take place, using the avoidance robot sensors, but nevertheless this encourages competitive behaviours. The environmental setup and the other robots play a fundamental role biasing the final behavior of each single robot. The block diagram of the Control System Architecture is shown in Fig. 1, where a spiking-based neural controller selects the robot behavior depending on the information acquired by the sensory system. The retrieved targets are stored in a working memory and when the sequence of targets is completed the reward signal, generated by the environment, triggers the learning progress. This consists in a Threshold adaptation applied to the vision neurons, depending on the data stored in the memory that is then emptied to be ready for the next foraging session.

B. The Neural Model

The computational structure acting as the nonlinear controller within each robot was derived after modelling the learning mechanisms in the fruit fly *Drosophila melanogaster*: it employs a classical conditioning in spiking neural networks. Within the insect brain, Mushroom Bodies (MBs) and the Central Complex (CX) are the most studied neural assemblies for their enhanced characteristics of olfactory and visual learning and plasticity: for example, rewarding and punishing olfactory associations were peculiarly addressed into the Mushroom Bodies of the insect brain [10], [11] and efficient computational models were recently designed and implemented, which resulted useful for addressing more complex behaviors like attention, expectation and decision making [12], [13]. On the other side, visual learning and visual targeting were addressed in

the Central Complex. The complete, updated insect brain computational architecture was recently presented in [14]. Here the neural controller is a simplified version of that insect brain computational model, retaining the essential features needed for the task to be here addressed.

The structure implemented is a multi-layer neural network similar to one fan of the Fan-Shaped Boby, an area within the Central Complex devoted to visual feature discrimination and learning [15], [16]. The structure uses a class I Izhikevich neuron model [17] and is made up of tho modules: one for visual target recognition, and another for obstacle avoidance. In fact, the fruit fly CX receives information also from the mechanoreceptors distributed on the body. Moreover, output neurons in our architecture directly act on the wheels through the mediation of inter-neurons. This also resembles the CX which is connected with lower motion control neurons for controlling locomotion in both tactic and phobic behaviors elicited by the visual sense.

The peculiarity of this structure is to allow learning both in the synaptic links among the neurons, and in the threshold of each neuron. However, in the simulation presented here, synapses are already learned and fixed: a Hebbian learning method (STDP - Spike Timing Dependent Plasticity) was already applied, as shown in [8], [9], to let all the robots show tactic behavior for all the targets present in the environment. Here attention is focussed to the learning aspects related to the neuron thresholds: that elicit specialization. In particular, the module dedicated to visual and target recognition was split in as many Sensing and Specialization Modules (S&SM) as the type of targets present in the environment (see Fig. 1).

Threshold plasticity, governed by Threshold adaptation Neuron (T_aN), was applied to induce hyperpolarization or depolarization into the visual neurons within each S&SM sub-group, to make them responsive only to a specific class of targets, as shown in [6].

The modified equation of neuron model, used for T_aN, is here reported:

$$\dot{v} = 0.04v^2 + 5v + 140 - u - g_A V_{thresh} + I_i \\ \dot{u} = a(bv - u) \tag{1}$$

with the spike-resetting

$$\text{if } v \geq 0.03, \text{ then} \begin{cases} v \leftarrow c \\ u \leftarrow u + d \end{cases} \tag{2}$$

where : $a = 0.02$, $b = -0.1$, $c = -55$, $d = 6$; v, u are, respectively, the neuron membrane potential and the recovery variable. The pre-synaptic input current is composed of two terms: an adaptation parameter $g_A V_{thresh}$, that is voltage-dependent [18] and the sensorial and synaptic inputs I_i. The time unit is ms and $g_A = 1$.

Variations of V_{thresh} produce neuron facilitation or hyperpolarization and depend on events occurred before the reward-signal activation (Rw), according to the formula:

$$V_{thresh} = \begin{cases} V_{thresh} + \Delta V & Rw = 1 \\ V_{thresh} & otherwise \end{cases} \tag{3}$$

In particular, each S&SM block contains a series of *vision neurons*, each one emitting spikes only if a specific colored target is detected in the scene. This block also contains *target neurons* which spike only when a specific target is reached by the robot. Target neurons encode unconditioned stimuli coming from e.g. contact with the targets that are stored in the working memory. Threshold adaptation takes place when the Reward signal is triggered. In this case all the threshold adaptation neurons, corresponding to the targets retrieved and stored in the memory, are depolarized whereas all the others are hyperpolarized. The reward signal acts as a bias on T_aN, which adds a contribution ΔV to the threshold V_{thresh} of all the vision neurons within the block:

$$\Delta V = \begin{cases} \Delta V_D & for\ depolarization. \\ \Delta V_H & for\ hyperpolarization. \end{cases} \tag{4}$$

with $\Delta V_D = 1.8$; $\Delta V_H = -0.6$. This is a key aspect of the learning procedure which acts according to the principle of local activation and global inhibition, as explained in the following.

Although all neurons start with the same value of $g_a V_{thresh} = 20$, this value can be modified within two saturation limits: $0 \leq g_a V_{thresh} \leq 22$. Moreover, a target becomes no longer more attractive when the bias goes below a lower bound that here corresponds to $I_{ina} = g_a V_{thresh} = 14$. Below this value the vision neuron does no longer emit spikes, even if the corresponding target is within the visual field.

III. SIMULATION RESULTS AND PERFORMANCE ANALYSES

Experimental simulations are conducted using our own software/hardware framework and Dynamic Simulator (SPARKRS4CS, details in [19], [20]). The robots are a simulated version of TriBot I [21], a hybrid robot developed to investigate cognitive capabilities inspired by insects, with dimension 0.3m x 0.2m moving in an arena of 3mx2m with targets on the floor. Different targets arrangements and various activation sequences are used for simulation tests. In particular, the combination of three and four targets is used. The reward signal is activated when the last target is reached by a robot.

A number of different simulations have been performed with two, three and four robots, and results are summarized respectively in Table I and Table II. The first column shows the target arrangements in the arena, the distances among the targets and the activation sequence are reported in column 2 and 3 respectively. For each configuration an amount of at least 10 simulations were performed starting from different initial robot positions. The fourth column reports the statistical distribution robot-targets for each of the solutions reported in the last column. From the analysis of the table it derives that the emerging solutions directly depend on the target position. For example, analyzing the results with two robots, in the first activation sequence related to the first arena (Table I[1.a-e]), the initial attractiveness of each robot

Arena	Distances (m)	Activation Sequence	Percent	Solution
	BY= 1.98 BR= 2.49 BV= 0.76 YR= 1.53 YV= 2.05 RV= 2.03	[1.a] B-Y-R-V [1.b] B-V-Y-R [1.c] B-V-R-Y [1.d] B-R-V-Y [1.e] B-Y-V-R	100% 100% 100% 100% 100%	$R_{Y,R} - R_{B,V}$ $R_{Y,R} - R_{B,V}$ $R_{Y,R} - R_{B,V}$ $R_{Y,R} - R_{B,V}$ $R_{Y,R} - R_{B,V}$
	BY= 0.65 BR= 2.46 BV= 1.28 YR= 1.95 YV= 1.41 RV= 1.98	[2.a] B-Y-R-V [2.b] B-V-R-Y [2.c] B-R-Y-V	100% 67% 33% 83% 17%	$R_R - R_{B,Y,V}$ $R_R - R_{B,Y,V}$ $R_{B,Y} - R_{R,V}$ $R_R - R_{B,Y,V}$ $R_{B,Y} - R_{R,V}$
	BY= 1.26 BR= 2.46 BV= 1.28 YR= 1.22 YV= 1.29 RV= 1.98	[3.a] B-Y-R-V [3.b] B-V-Y-R [3.c] B-V-R-Y [3.d] B-R-V-Y	100% 100% 80% 20% 86% 14%	$R_{Y,R} - R_{B,V}$ $R_{Y,R} - R_{B,V}$ $R_{B,Y} - R_{R,V}$ $R_{B,V} - R_{Y,R}$ $R_{Y,R} - R_{B,V}$ $R_{B,Y} - R_{R,V}$
	BY= 1.29 BR= 2.46 BV= 1.28 YR= 1.18 YV= 1.02 RV= 1.98	[4.a] B-Y-R-V [4.b] B-Y-V-R [4.c] B-V-Y-R	100% 100% 83% 17%	$R_{Y,R} - R_{B,V}$ $R_{Y,R} - R_{B,V}$ $R_{Y,R} - R_{B,V}$ $R_R - R_{B,Y,V}$
	BY= 0.80 BR= 1.29 BV= 0.82 YR= 0.76 YV= 0.93 RV= 0.79	[5.a] B-Y-R-V	64% 36%	$R_{B,Y} - R_{R,V}$ $R_{Y,R} - R_{B,V}$
	BY=YV= 1.25	[6.a] B-Y-V	100%	$R_{B,Y} - R_{Y,V}$
	BY= BV = 1.13 YR= RV = 1.13 BR= YV= 1.60	[7.a] B-Y-R-V [7.b] B-R-Y-V	50% 50% 25% 75%	$R_{Y,R} - R_{B,V}$ $R_{B,Y} - R_{R,V}$ $R_{Y,R} - R_{B,V}$ $R_{B,Y} - R_{R,V}$
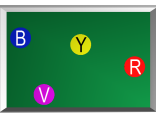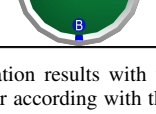
TABLE I: Synthesis of simulation results with two robots. Legend: **Arena**: the environmental setup, **Distance**: the distance between targets in meters, **Activation Sequence**: the order according with the targets are activated, **Percent**: Percentage of occurrence related to specific solution emerged (**Solution**).

for all the targets is shaped towards the two of them which are nearest one another, with the emergence of a robust solution which does not depend on the activation sequence.

For this configuration, the dynamics of the learning phase is reported in Fig.2. The bar diagram in Fig.2(e) shows in blue and green the total distance travelled by Robot1 and Robot2 respectively, at each reward cycle, whereas the red bar represents the overall distance totally travelled by all the robots normalized to the shortest path needed to complete the sequence. It is possible to observe that, at the beginning of the learning phase all the robots are attracted by all the targets, but, since they start from different initial positions, they succeed in reaching only the nearest ones (Fig.2(a)-(c)). After this phase, whenever a robot does not succeed in reaching a target, it is punished and becomes more and more refractory to this target: from this condition specialization emerges (Fig.2(d)).

A different situation arises in the second, third and fourth case (respectively Table I[2.a-c], Table I[3.a-d] and Table I[4.a-c]), where the yellow target position is shifted from the blue toward the red target. In such cases the solution is dependent, besides on the target position, also on the activation sequence.

The following two cases in Table I report two symmetric target configurations. In particular, in Table I[5.a] the slight asymmetries in the target position and the robot rotations play a fundamental role shaping the whole statistics. The case reported in Table I[6.a] shows a highly symmetric target arrangement: the yellow target remains attractive for both the robots, and it is shared in their travelled paths.

This is clearly visible in Fig.3, which shows the dwelling time for this target configuration, corresponding to the first five (Fig.3(a)(b)) and last five (Fig.3(c)(d)) reward cycles for each robot. The competition caused by the yellow target is evident. Robot2 succeeds in reaching the yellow target more frequently than the other one, since the activation sequence leads the yellow target to be active when Robot2 is oriented towards it. This does not take place for Robot1, that, in any case reaches sometimes the yellow target; more often it arrives later and is forced to avoid Robot2. Fig. 3(e)(f) reports the trend of the bias current for the two robots: the current related to the yellow vision neuron is high for the neural controllers of both robots, meaning that attractiveness for this target is never lost by them. Instead, the specialization is
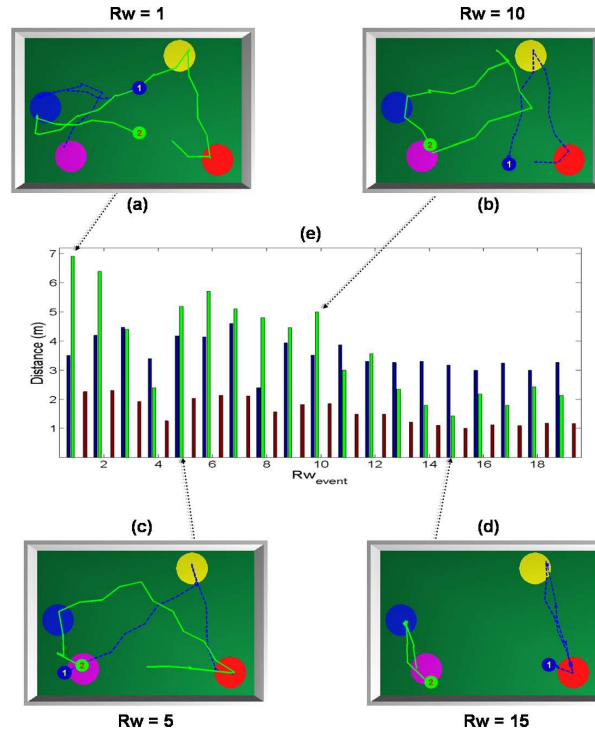
Fig. 2: Dynamics of the learning phase. The trajectories performed by Robot1 and Robot 2, at specific reward events, are showed in **(a-d)**, the starting position of each robot is also indicated. **(e)** - The bar diagram shows: the total distance travelled by Robot1 and Robot2, in each reward cycle, in blue and green respectively. Finally, the red bar represents the normalized distance travelled by both robots.

quite fast for the remaining targets: as soon as the bias current decreases below the inactivation level I_{ina} the corresponding vision neuron does no longer emit spikes even in presence of the corresponding coloured target.

Finally, in the last arrangement Table I[7.b] in most cases (75%) the solution $R_{B;Y} - R_{R;V}$ is preferred, since a robot once reached a target, spends some time to turn, leaving more possibilities to the other robot to reach the active target.

A number of simulations were also performed increasing the number of agents; in particular three and four robots were employed in different, symmetric and asymmetric target arrangements involving a sequence of four targets, as shown in Table II. Whereas the experiments involving four robots and four targets reach the most obvious solution (i.e. each robot specialises in one target), it is interesting to analyse the dynamics leading to this steady state condition. In [6] we introduced an index to quantify the dynamics of the global performance of the whole system, taking as a reference the works [22], [23]. In particular, following the formula:

$$S(t) = \frac{\#Task\ accomplished\ events}{\#Tot.\ events} \quad (5)$$

we can evaluate the evolution of the effect that learning induces in the number of times the foraging task is properly accomplished (in this case, visiting the targets following the activation sequence). In Fig. 4(a)(b) two different evolutions of the Specialization index S(t) are shown for the simulations with four robots, referring to asymmetric and symmetric arenas (respectively, the first and fifth arena in Table II). The index is evaluated using sliding windows of Rw successful
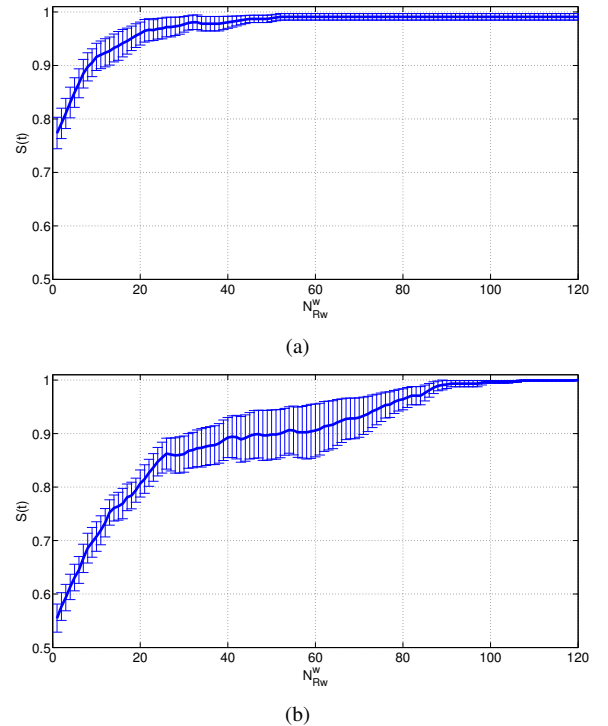

Fig. 4: Specialization index ($S(t)$) trend. The error bar shows the deviation along the mean evolution of the S(t). The mean of Specialization and the standard error of the mean (SEM) are evaluated using a sliding window of w Reward events ($w = 30Rw$) in a set of 20 experiments with four robots in the **(a)** asymmetric arena Table II[A1] and **(b)** symmetric arena Table II[A5].
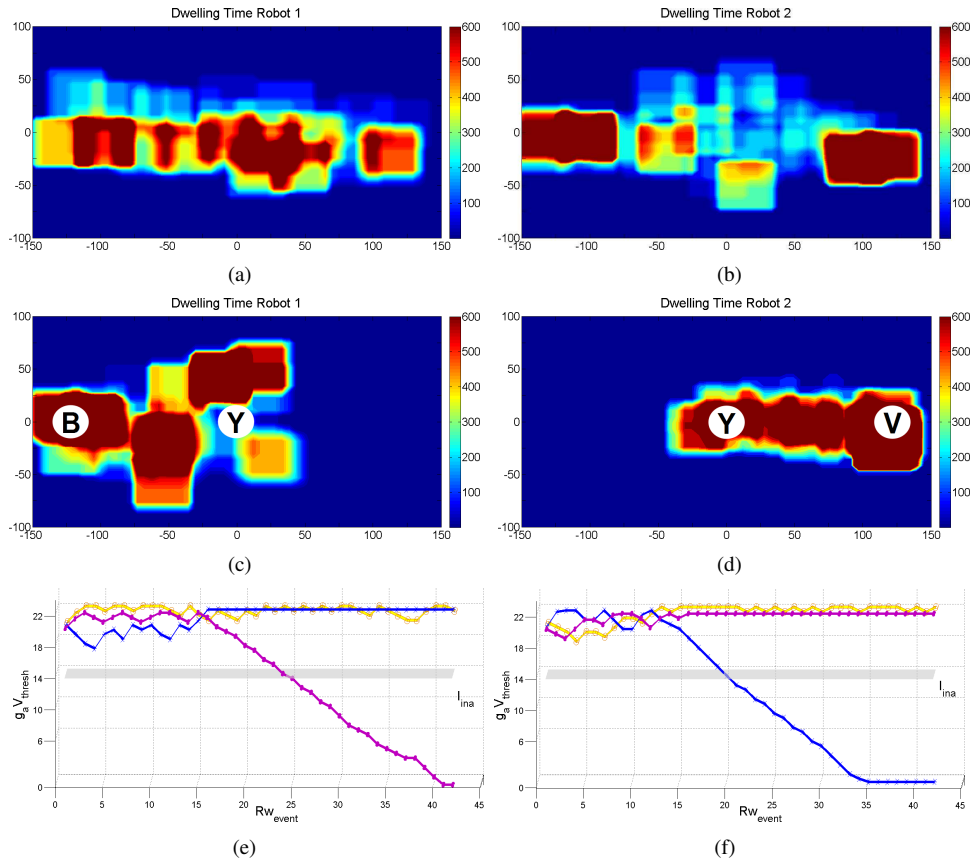
Fig. 3: **(a)-(b)** Dwelling Time of Robot1/Robot2 during the first five reward events and the last five ones in **(c)-(d)**. **(e)** Dynamic trend of the bias current related to Robot 1. This robot specializes itself in blue and yellow targets. After approximately 25 reward events, the bias current of violet target comes below the lower bound value ($I_{ina} = 14$). **(f)** Trend of the bias current related to Robot 2. On the contrary, this robot becomes attractive only to violet and yellow targets. The bias current related to yellow target remains at high values although it presents a lot of fluctuations. It is the consequence of symmetric environmental setup, which encourages competitive behaviours.

events (N_{Rw}^w). Comparing the two figures it is possible to notice how the arrangement of the targets strongly influences the dynamic of learning, in fact in Fig. 4 the asymmetric configuration forces a very fast convergence, and polarizes the index to high values (75% of success) since the beginning. In a symmetric situation the convergence trend is slower. The index shows how the initial situation is quite balanced (55% of success): all robots visit the targets before converging to a specific solution. Moreover from 20 N_{Rw}^w to 80 N_{Rw}^w it is possible to see how the symmetric arrangement affects the convergence; in fact, although the whole group converges to the same solution in all of the trials, competitive behaviours are here strongly present.

IV. REMARKS AND CONCLUSIONS

The aim of this paper is to experimentally observe the emergence of labour division among robots in completely decentralized situations: in fact each robot has no information about the task to be globally pursued (in this case the sequence of target activation) and during the learning phase it becomes more attracted to the targets it succeeds more frequently to reach, whereas it looses interest in the other ones. This behavior is frequent in insects: flies are initially attracted by all the targets in the environment and they

learn positive or negative associations as a consequence of rewarding or punishing events. This basic neural structure has been embedded into the all robots simulated in this work, to evaluate how these simple but efficient plastic networks can bias the single individual behavior and indirectly contribute to shape the collective capabilities. The presented results show that the emergence of collective behaviors, at least in these simple cases, can arise from very simple, egocentric and non-communicating single robotic architectures.

The possibility to use an adaptation mechanism, which is biased toward exploiting the capabilities of each individual to induce specialization in a group of robots is an interesting approach to permit the emergence of collective behaviours and labour division. The key remark to be underlined is that in this approach no particular capabilities are ascribed to each agent within the group. Even in this case, a suitable task division among the agents is obtained, exploiting the mediation of the environment through the action of the reward function.

The neural structure was derived after modelling the learning system in the fly and employing a classical conditioning approach in spiking neural networks. Indeed, such a structure is only a block of a more complex insect brain computa-

Arena	3 Robots		4 Robots	
	Percent	**Solution**	**Percent**	**Solution**
[A1]	100%	$R_{B,V}$ R_Y R_R	100%	R_B R_V R_Y R_R
[A2]	100%	$R_{B,Y}$ R_R R_V	100%	R_B R_V R_Y R_R
[A3]	36% 27% 18% 9% 9%	$R_{B,Y} - R_{Y,R} - R_V$ $R_{B,V} - R_{Y,R} - R_{Y,V}$ $R_{B,V} - R_Y - R_R$ $R_B - R_{Y,R} - R_V$ $R_{B,Y} - R_{Y,R} - R_{B,V}$	100%	R_B R_V R_Y R_R
[A4]	42% 42% 8% 8%	$R_{B,V} - R_Y - R_R$ $R_{B,V} - R_{Y,R} - R_{Y,V}$ $R_{B,Y} - R_R - R_V$ $R_{B,Y} - R_{B,V} - R_{Y,R}$	100%	R_B R_V R_Y R_R
[A5]	33% 17% 17% 8% 8% 8% 8%	$R_{B,Y} - R_{Y,R} - R_{B,V}$ $R_{B,V} - R_{Y,R} - R_{Y,V}$ $R_{B,Y} - R_{B,V} - R_{R,V}$ $R_{B,Y} - R_{Y,R} - R_V$ $R_{B,V} - R_{R,V} - R_{Y,R}$ $R_{B,Y} - R_{Y,V} - R_{R,V}$ $R_{B,Y} - R_{Y,R} - R_{R,V}$	100%	R_B R_V R_Y R_R
[A6]	31% 15% 15% 15% 8% 8% 8%	$R_{B,Y} - R_{Y,R} - R_{R,V}$ $R_{B,V} - R_{Y,R} - R_{R,V}$ $R_{B,Y} - R_{B,V} - R_R$ $R_{B,Y} - R_{Y,R} - R_V$ $R_{B,V} - R_Y - R_{R,V}$ $R_{B,Y} - R_{B,V} - R_{R,V}$ $R_{B,Y} - R_{B,V} - R_{Y,R}$	100%	R_B R_V R_Y R_R
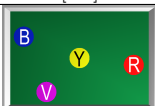
TABLE II: Synthesis of simulation results with three and four robots. The Activation Sequence is the same for all the experiments: B-Y-R-V. Legend: **Arena**: the environmental setup, **Percent**: Percentage of occurrence related to specific solution, **Solution**: the emerging solution.

tional architecture endowed with other functionalities like orientation, path integration, decision making, and also some other ones recently included, which reproduce attention and expectation [12], [13].

Starting from the simulation results here presented, the addition of the remaining blocks of the insect brain architecture within each robot is expected to give rise to the emergence of a surprising number of different collective behaviors, which will depend on the reward policy. In fact it was very recently discovered that fruit flies are indeed able to show also simple forms of imitation [24]. Even if they do not basically show evident social behaviors, nevertheless embedding their basic brain capabilities into a robotic population can lead to derive new strategies for cooperation, basically dependent on the individual capabilities rather than on the presence of a global social brain.

The simulation results demonstrate that the presence of a global reward induces diversity in a team of homogeneous robots as also derived in general approaches to swarm intelligence [25], [26] but using different tools and methodologies.

REFERENCES

[1] Y. Mohan and S. Ponnambalam, "Swarm robotics: An extensive research review." *Nature & Biologically Inspired Computing*, pp. 140–145, dec 2009.

[2] E. Bonabeau, M. Dorigo, and G. Theraulaz, *Swarm Intelligence: From Natural to Artificial Systems*. New York: Oxford Univ. Press, 1999.

[3] S. Camazine, J.-L. Deneubourg, N. R. Franks, J. Sneyd, G. Theraulaz, and E. Bonabeau, *Self-Organization in Biological Systems*. Princeton Univ. Press, 2001.

[4] L. Chittka and J. Niven, "Are Bigger Brains Better?" *Current Biology*, vol. 19, no. 21, pp. R995–R1008, Nov. 2009.

[5] J. G. Burns and A. G. Dyer, "Diversity of speed-accuracy strategies benefits social insects," *Current biology*, vol. 18, pp. R953–R954, Oct 2008. [Online]. Available: http://linkinghub.elsevier.com/retrieve/pii/S0960982208011056

[6] P. Arena, L. Patané, and A. Vitanza, "Spiking neural controllers in multi-agent competitive systems for adaptive targeted motor learning," *submitted to Special Issue on Advances in Nonlinear Dynamics and Control in Journal of the Franklin Institute*, 2014.

[7] P. Arena, L. Patané, and A. Vitanza, "Autonomous learning of collaboration among robots," in *Neural Networks (IJCNN), The 2012 International Joint Conference on*, june 2012.

[8] P. Arena, L. Fortuna, M. Frasca, and L. Patané, "Learning anticipation via spiking networks: Application to navigation control," *IEEE Transactions on Neural Networks*, vol. 20, pp. 202–216, February 2009. [Online]. Available: http://ieeexplore.ieee.org/lpdocs/epic03/wrapper.htm?arnumber=4749255

[9] P. Arena, S. de Fiore, L. Patané, M. Pollino, and C. Ventura, "STDP-based behavior learning on the TriBot robot," in *Society of Photo-Optical Instrumentation Engineers (SPIE) Conference Series*, ser. Society of Photo-Optical Instrumentation Engineers (SPIE) Conference Series, vol. 7365, may 2009, p. 736506.

[10] S. Scherer, R. F. Stocker, and B. Gerber, "Olfactory learning in individually assayed drosophila larvae." *Learning Memory*, vol. 10, no. 3, pp. 217–225, 2003. [Online]. Available: http://www.pubmedcentral.nih.gov/articlerender.fcgi?artid=202312&tool=pmcentrez&rendertype=abstract

[11] T. Nowotny, M. I. Rabinovich, R. Huerta, and H. D. I. Abarbanel, "Decoding temporal information through slow lateral excitation in the olfactory system of insects." *Journal of Computational Neuroscience*, vol. 15, no. 2, pp. 271–281, 2003.

[12] P. Arena, L. Patané, and P. S. Termini, "Learning expectation in insects: A recurrent spiking neural model for spatio-temporal representation," *Neural Networks*, Feb. 2012.

[13] ——, "Modeling attentional loop in the insect mushroom bodies," *International Joint Conference on Neural Networks (IJCNN 2012)*, July 31 – June 10-15 2012.

[14] P. Arena and L. Patané, *Spatial Temporal Patterns for Action-Oriented Perception in Roving Robots II: an insect brain computational model*. Springer, Series: Cognitive Systems Monographs, Vol. 21, 2014.

[15] P. Arena, S. De Fiore, L. Patan, P. S. Termini, and R. Strauss, "Visual learning in drosophila: application on a roving robot and comparisons," pp. 806 809–806 809–8, 2011.

[16] P. Arena, S. De Fiore, L. Patanè, P. Termini, and A. Vitanza, "Robotic experiments and comparisons," in *Spatial Temporal Patterns for Action-Oriented Perception in Roving Robots II*. Springer International Publishing, 2014, pp. 331–371.

[17] E. M. Izhikevich, "Simple model of spiking neurons," *IEEE Transactions on Neural Networks*, vol. 14, no. 6, pp. 1569–1572, Nov 2003. [Online]. Available: http://ieeexplore.ieee.org/lpdocs/epic03/wrapper.htm?arnumber=1257420

[18] J. Benda, L. Maler, and A. Longtin, "Linear Versus Nonlinear Signal Transmission in Neuron Models With Adaptation Currents or Dynamic Thresholds," *Journal of Neurophysiology*, vol. 104, no. 5, pp. 2806–2820, Nov 2010. [Online]. Available: http://jn.physiology.org/cgi/doi/10.1152/jn.00240.2010

[19] P. Arena, M. Cosentino, L. Patané, and A. Vitanza, "SPARKRS4CS: a software/hardware framework for cognitive architectures (invited paper)," in *Proceedings of the SPIE - The International Society for Optical Engineering*, vol. 8068, Prague, Czech Republic, 2011, pp. 8068A–18.

[20] P. Arena, L. Patané, P. S. Termini, A. Vitanza, and R. Strauss, "Software/hardware issues in modelling insect brain architecture," in *Intelligent Robotics and Applications*. Springer Berlin Heidelberg, 2011, pp. 46–55.

[21] P. Arena, L. Patané, M. Pollino, and C. Ventura, "Tribot: a new prototype of bio-inspired hy-brid robot," in *Proceedings of the IEEE/RSJ International Conference on Intelligent RObots and Systems*, St.Louis,Missouri,USA, 2009.

[22] L. Li, A. Martinoli, and Y. S. Abu-Mostafa, "Learning and measuring specialization in collaborative swarm systems," 2004.

[23] T. Balch, "Hierarchic social entropy: An information theoretic measure of robot group diversity," *Autonomous Robots*, vol. 8, pp. 209–237, 2000.

[24] M. B. Sokolowski, "Social interactions in "simple" model systems," *Neuron*, vol. 65, pp. 780,794, 20100325.

[25] T. Balch, "Communication, diversity and learning: Cornerstones of swarm behavior," in *Swarm Robotics*, ser. Lecture Notes in Computer Science, E. Sahin and W. Spears, Eds. Springer Berlin / Heidelberg, 2005, vol. 3342, pp. 21–30.

[26] L. Bayindir and E. Sahin, "A review of studies in swarm robotics," *Turkish Journal of Electrical Engineering*, vol. 15, no. 2, 2007.

Localisation task for underwater swarms with minimum data

Ramiro dell'Erba

Italian National Agency for New Technologies, Energy and Sustainable Economic Development Robotic Laboratory
ENEA Rome, Italy
dellerba@enea.it

Abstract— **This paper deals with the localization problem of an underwater robotic swarm in the context of the HARNESS project (Human telecontrolled Adaptive Robotic Network of SensorS) currently in progress in our laboratory. This system is based on cheap autonomous underwater vehicles (AUV) organized with swarm rules and conceived to perform tasks, ranging from environmental monitoring to terrorism attack surveillance. The aim of this work is the reconstruction of the swarm configuration using the signals they exchange between them.**

Localization and (eventually) mapping are the essence of a successful navigation in autonomous mobile platform technology and are fundamental tasks in order to achieve high levels of autonomy in robot navigation and robustness in vehicle positioning and values of the collected data.

We expose some calculations relative to possible methods that can be adopted in our system. We are dealing with the swarm configuration, therefore to get an absolute localization it is enough that one member of the swarm has an absolute localization; as example when one member comes out ad fix position by GPS.

A method to determine the shape of the swarm, based on trilateration calculation, is proposed Technically we have something of similar to a trilateration problem but we do not know the position of the beacon and this render the problem very hard.. In particular we are dealing with a very few amount of data and the speed of the robots is unknown: it will be calculated after the configuration will be determined. The calculation is based on trilateration between three robots in different steps of motion. The minimum data used in the calculation was the orientation of the robots and the distance between three robots.

Keywords-swarm; underwater; robot; localization

I. THE HARNESS PROJECT

The HARNESS project aims at the realization of an underwater multi body robotic system able to perform tasks in a fast and reliable way and with a swarm behavior. The availability of a suitable robotic swarm could be relevant in many operations: surveillance of sensitive sites, fast exploration of relatively wide interesting areas, detailed analysis of the objects (i.e. archeological goods) without removing them from their underwater sites.

II. INTRODUCTION

The aim of this work is the reconstruction of the swarm configuration using the signals they exchange between them [1], [2], [3].

This paper deals with the localization problem of an underwater robotic swarm.

The HARNESS project [1] seeks to realize an underwater multi AUV robotic system, arranged in a swarm organization where the classical flocking rules and the Communication Network protocol are merged in a novel higher level control. It is expected to improve the performance of classical AUV technology exploiting the large occupied volume and the short distances among the vessels. The speed of surface monitoring and the transmission bandpass among the vessels and towards the surface should be some of the most important results.

The use of underwater autonomous vessels or rovers has been experienced and proven to be useful in some cases, but generally expensive mainly because asks for the support of an equipped ship.

An AUV must be considered as a real cost alternative to other available technologies, such as manned submersibles, remotely operated vehicles (ROVs) and towed instruments led by ships. However, many problems are still to be solved to make AUV competitive especially for the issues relevant to power availability, information processing, navigation, and control   [4],[5].

A swarm is able to perform tasks in a more fast and robust way with respect of a single machine [6]. Moreover a swarm has the advantage of a simple way of interfacing with the human users, overcoming the problem of controlling a large number of individuals; it is expected to improve the performance of classical AUV technology exploiting the large occupied volume.

The availability of a suitable robotic swarm could be relevant in many operations: surveillance of sensitive sites, fast exploration of relatively wide areas of interest, detailed analysis of objects (i.e., archeological artifacts) without removing them from their underwater sites.

The most interesting areas to explore and protect are those in proximity to coasts and with depths ranging between 50 to 200 m. Professional and expensive divers can operate only to a maximum of 70-80 meters in recovery operations, and simple and fast explorations cannot be performed by humans beyond 100 m.
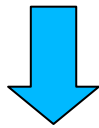

Fig. 1 – The idea of the Harness project.

On the other hand the use of rovers has proven to be useful in many cases, but generally expensive mainly because they require the support of an equipped ship.

This use of robotic technologies in ocean surveys, inspections, pipe and cable tracking, has been well established in the field of marine engineering since many years [1]. Marine robotics technology had a very quick increase in performance in recent years [2]and many autonomous underwater vehicle systems moved from the prototype stage to scientific, commercial, and military uses.

The goal of this paper is to give a presentation of the novel concepts in Harness. We will discuss advantages and drawbacks of the project concepts and explain the prototype under construction. Finally we will focus on the crucial problem of localization of the swarm with some proposal for an efficient solution suitable to some scenarios.

In a swarm the robots operate with a common objective and sharing the job workload; the lack of one member can be easily taken care of by redistributing the job among the others like bee [7], [8],[9].

The geometrical distribution of the members of this system is flexible and adaptable to the task and environmental characteristics.

In the underwater world a severe limitation to our communications technology is perhaps the main drawback: the physical medium only permits acoustical channels, since electromagnetic waves are rapidly damped. Also the acoustical technology is heavily affected by a fast decay in the signal bandpass as soon as the distance increase, also for limited ranges. This limitation can be overcome by a suitable and intelligent spatial distribution of transmission nodes (the swarm members themselves), allowing an enhanced throughput of data through logical and physical routing

To localize the configuration of the swarm we manage something of similar to a trilateration problem but we do not know the position of the beacon and this render the problem very hard. So we try to get the configuration in any case also with lack of data.

III. THE SWARM CONCEPT

The use of a large number of very low cost mini AUV [3] could limit the use of the expensive surface ships to the deployment phase, taking advantage of the parallel exploration to shorten times.

The concept of robot swarms is a study theme by the scientific community since several years. The realization of swarms of different numbers of cooperating robots has been successfully attempted, but in underwater environment it is still a challenge. Many of the difficulties coming from the unfriendly underwater environment are mainly focused on the problem of fast and reliable communication links. Swarm research has been inspired by biological behaviors, like the one of the bees [4] [5] since long time to take advantage by social activities concepts [6] labor division, task cooperation and information sharing. A single-robot approach is affected by failures that may prevent the success of the whole task. On the contrary, a multi-robot approach can benefit by the parallelism of the operation and by the redundancy given by the usage of multiple agents.

An advantage of the swarm, considered as a whole entity, lies in the possibility to parallelize very heavy computation. As example an image analysis to recognize landmark is a typical task that can be parallelized and distributed to the various machine, providing that an adequate communication network is available. In the same way it offering the advantage of a simple way of interfacing with the human end-users and overcoming the problem of the control of a large number of individuals.

In a swarm the members operate with a common objective, sharing the job workload; the lack of one member can be easily taken care of by redistributing the job among the others. This feature is especially useful if we consider, as application the discovery and the surveillance of submarine sites.

The geometrical distribution of the members of this system is flexible and adaptable to the task and environment characteristics in particular for communication. In the underwater world the physical medium makes the acoustical channels as the most convenient one, since electromagnetic waves are rapidly damped. The acoustical technology has limited performances; the band pass pass increase as increasing frequency but its damping too, limiting useful range. The swarm technology allows to avoid this drawback by a suitable and intelligent spatial distribution of transmission nodes (the swarm members themselves, modifying the physical dispersion/geometry), adapting (See Fig. 1 and Fig. 2 where there are two examples of adaptive localization of the swarm for different tasks) and allowing the exploitation of ultra-high frequencies and an enhanced data transmission through logical and physical routing. It is a multi hop network with varying geometry. One of the aims of the project is the study and implementation of different behaviors in the swarm, to generate a collective shaping as a response to environment stimuli and to modify the communication parameters in order to maximize the performance of the system.

The swarm control must balance the different requests of the operator (e.g. modify the mission task), the swarm needs and the single members management (e.g. obstacle avoidance, loss of communication link).

The result is the selection of collective behaviors that must be compatible with all the before mentioned conditions. The methods currently under evaluation to this aim include neural network techniques, fuzzy logic and genetic algorithms.

In the swarm there is no central brain, mainly because of the excess needs in band pass requested by such a brain. Instead each individual must possess an intelligent local control system capable to manage its choices according to the choices of the neighbors on the basis of the available data. Data coherence along the swarm, being affected by the position of the member and by the data propagation speed is also a research topic.

Therefore the system has to adapt itself to the environmental characteristics, with special reference to the problems arising in the communication inter-individual and between the swarm and the human. These aspects are both related to the communication channel and to the geometrical distribution of the multi robot system [8]. In the underwater world there is an evident limitation to data throughput and temporal delay caused by the physical medium.

This can be obtained by a right geometry configuration of the swarm. In case of swarm human communication an element of the swarm has to emerge, maintain the link with the other elements. Different geometry configurations of the nodes, the elements of the swarm itself, allow higher or lower data rate transmission.

The use of high frequency allows a higher band pass but it is well known as is more damped by the water. So far an intelligent configuration of the node, as indicate in the figures is desiderable varying the distances between them as function of the task.
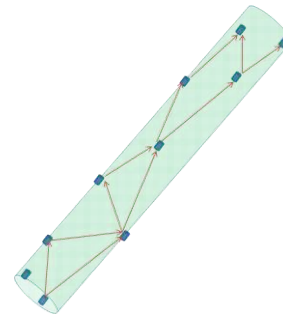
Fig. 2 – Pipe", configuration indicates when the communication is the main objective of the geometrical shape to transport data on long distances at the maximum allowed speed.
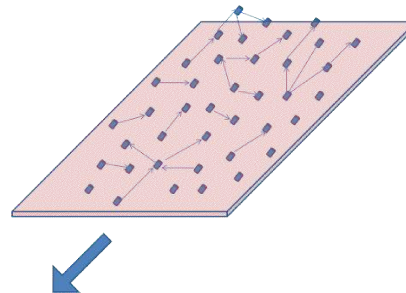

Fig. 3 –Planar distribution to carry out fast and parallel monitor operations.

IV. THE TECHNOLOGICAL CHALLENGE

The swarm control must balance the different needs of the operator on one side (e.g. the mission task) and of the single elements of the swarm on the other (e.g. obstacle avoidance, loss of communication link, etc.).

This equilibrium can change depending on the assigned tasks, the survival risk associated to the operation of each robot and the risk associated to the loss of connection with rest of the swarm. Approaches currently under study to this aim include neural network techniques, fuzzy logic and genetic algorithms.

In the swarm there is no central brain, each individual must possess an intelligent local control system capable to control its route on the basis of the available data. These data will be different depending on the position inside the swarm, the data propagation speed and, in special cases, by the role of some individuals (e.g. a scout going on surface for communication and localization by GPS).

A possible quite efficient way to achieve this result is to organize a number of cheap, small units able to change their relative cooperation modes, geometries and other functional parameters by means of relatively simple rules that every member of the "swarm" has to follow (the Reynold's boids [10] are a very famous example).

Typical objective of these rules are the maintenance of group coeherence, the capability to follow a common target, the ability to avoid foreseen or unforeseen obstacles, the ability to share and use data perceived by all the group member. All these group behaviors allow in an implicit way, usually called "emergent behavior" to fit at best with the surrounding environment. Four topics are identified as key elements of the architecture: Communication, Control, Localization, Teleoperation. Each of them will keep busy many people since long time so we shall give just a sharp look on their application in Harness project.

Communication distinguishes at least three situation

1) fast data transmission rate on relatively long distances (High Speed Transmission);

2) the need to increase the swarm internal data exchange (High Swarm Bandpass. The geometry is presumable disordered.

3) the need to maintain a disperse swarm configuration to accomplish wide area monitoring tasks (Wide Area Surveillance). In this case a Low Swarm Band Pass is probably acceptable.

It is well known as the swarm control level and the local individual control level can originate conflictual situations relevant to the optimization of global and local goals. The choice of the right strategy to manage and synchronize this multilevel adaptive system is still under investigation and will be explored in a much greater detail during the project development, but it clearly involves the definition of rules in explicit (expert system) or implicit (neural networks) form and should be capable of on-the-job learning. Three main control layers :The Communication control, the Swarm control and the Individual control. In addition a fourth layer is deputed to solve conflicts that can arise among the previous levels: The Arbiter. The most interesting is the Swarm control and its "Swarm rules". These rules are assigned but have to be changed sometimes from the operator or by learning of the swarm.

The swarm control level and the local control level can originate conflicting situations relevant to the optimization of global and local goals. The choice of the right strategy to manage and synchronize this multilevel adaptive system is still under investigation, but it clearly involves the definition of rules in explicit (expert system) or implicit (neural networks) form and should be capable of on-the-job learning.

The global control architecture will be built around three basic issues: the human supplied goals, the internal operational rules, ensuring stability and coordination of member's behavior through the communication network, the emergencies and automatic answers of the single.

The localization can be divided in three categories. Precision localization (i.e. in the arbor using fixed buoy), Rough localization (i.e. during navigation), Relative localization (Application driven). We also use three scenario: Structured environment, Free navigation, Close to objective.

Teleoperatioon is an hard task to merge with the swarm concept. Therefore we prefer to say not teleoperation but TeleCooperation. Order are passed as needs with high priority in according with the philosophy of the swarm.

V. OUR PROTOTYPE

In Fig. 3 the Venus prototype, realized in our laboratory, is showed. Its characteristics are the following:

Max depth 100m; Max speed 2 Knots; Weight about 20 Kg; Autonomy 3hrs; Dimensions 1.20cìmX0.20m diameter

Standard sensors include a stereoscopic camera, sonar, accelerometer, compass, depth meter, hydrophones side-scan sonar.
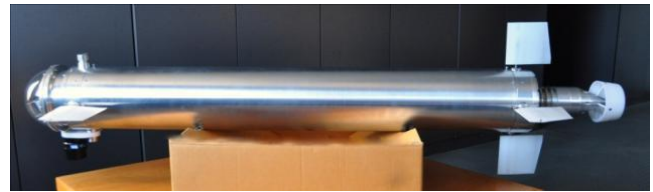
Fig. 4 – low cost Venus AUV

Fig. 5 – Robot prototype during test in pool.

We are dealing with a system thought to be a component of a swarm of about 20 objects. The distances between robots ranging between 3 and 50 m. Therefore, the maximum distance possible between two robots is about 1000 m, as a very particular alignment case; the average value of the distances is about 10 m.

An optical, high power, transmission device will be used for a number of different experimental approaches integrating the acoustical data channel and the direct vision sensing. Optical methods are very powerful but their performances are affected by many strongly variable parameters like salinity, turbidity, the presence of dissolved substances that change the color and the transparency in different optical bands and the amount of solar radiation that heavily affect the signal to noise ratio.

VI. THE LOCALIZATION PROBLEM: OUR PROPOSAL

Now we focus our attention on the relative localization problem i.e. how to determine the swarm configuration from the signals that the robots exchange between themselves. Absolute georeferenced localization will be available only when one of the member emerges to fix GPS position or some georefenced map position or landmark is available. To obtain the configuration it is enough to choose one member as axis origin and obtain the relative position of three, or better four or more, other members. Later any other member will be localize from its distance from the others using algorithms commonly used in GPS calculations; so the initial members are used as constellation of satellites. Therefore now we need to localize some members, with respect to one [11].

If we have three or (better) four vessels on the surface they can be positioned by GPS [10]. Later, using the communication system, we can obtained (i.e. from the clock time of each communications between the elements) the distance between one more vessels and the "constellation". Using the same mathematical calculation of the GPS system we can absolute localize the whole swarm. The vessels surface (That can be substituted by little boats) have the advantage that can carry a high band pass using laser communication system, owing the easy transmission vertical channel; in fact the collimation problem between vessels, in this case, can be partially avoided (Solid angle just quite selected).

If we have not the surface vessels we can calculate the Relative Localization (i.e. the configuration of the swarm) solving the distance equations and to gain a constellation by a trilateration problem; one vessel is choised as axis origin. (See figure 6).

Unfortunately we have multiple possible solutions and to select between them we need some more information. A flash, as example, to discriminate direction from which the signal is arrived. A more clever sistem is to use a whatever (but known) movement of the swarm and to repeat the calculation for the multiple solutions corresponding to the new possible configutation. We repeat the calculation and obtain a new set of solutions. Now using the preceding configuration and appliyng a coordinate trasformation (from the known movement) we obtain only one configuration matching between the old and the new. Therefore we have eliminate the degeneracy of the solution of a trilateration problem by a generic, but know, movement of the swarm .

So far the configuration problem is solved, see figure 7. Later the constellation can be varied and updated with new data, repeating the proces for other vessel. This system use every signal exchanged between the swarm elements. This work can be done in different volume of the swarm and later matched together. In othr words, to overcome signal delay problem (some vessels could be too far for the coordinate origin), other vessel can be taken as coordinate origin and later the founded configurations can be matched together.

Now we repeat in more details, but ask ourself a question. What kind of signal are exchanged between the robots? Remember that the communications are a problem in underwater environmental so we have achieve the results with the minimum data. In a previous work [3] we showed as configuration can be obtained using the following elements transmitted in a communications: 1) ID of the vessel; 2) Time; 3) speed. These data must be available not only for the member itself but also for its neighbors. From the time of fly we obtain the relative distance between the robots. At this point we face a trilateration problem but we do not know the position of the beacon so it is very difficult. From algebraic point of view it is classified as a Non Polynomial Hard problem. It has some similarities with the problem to determine the conformation of the protein starting from the molecular distances obtained by NMR experiments. But in our case we are sensitive to some symmetry conditions that make more difficult the calculation. In fact starting from the distances between the robots we obtain many possible solutions, owing to the degeneracy degree of the equations system. We have to use some information more to choose the only right one. Therefore we obtain the distances between four robots from one and the distances between them (six distances). We obtain 8 possible solution (see fig. 6). Later we repeat the measurements after a known movement (remember we have the speed of the swarm members) it has been performed. At this point we have another 8 possible solutions but only one is compatible with the displacement, using coordinate change. Note that if the movement is an uniform translation we obtain no more information and the problem cannot be solved. Lucky in the real environmental this case never appear.

Therefore we proceed in two steps
1) Building a constellation reference.
2) Classical trilaterion calculation by GPS system (non linear least squares, circle intersections etc..)

In our simulation algorithm we generate the position of the vessels. One receives a "heart beat" broadcasting signal and is chosen as the coordinate origin (green vessel). The signal contains id, time, neighbors distances and last estimated movement vector. The heart beat is a low frequency signal that each vessel transmit in broadcasting mode.

Then this vessel (each one can do) calculate the distance of the first surrounding vessels (in blue) and the distances between them whereas the others (grey) will be ignored. This can be done using whatever signal received from the vessels.

Hurt beat signal= {id, time, speed, neighbors distances}

Solving the equation system of a similar trilateration problem (Station coordinate not known!) we obtain the eight possible configuration of the four vessels; this because the problem has multiple solutions owing to the geometry symmetry, knowing only distances. They are shown in the figure. The grey ones are still unknown. Note the only one of the eight is exact but you cannot known at this time. We have multiple possible solutions and to select between them we need some more information.

Therefore you see seven vessels instead of six! Of course you must be careful because of the noise in the distance measurements, so far. an acceptance protocol data must be used. Then we repeat the whole calculation after a generic but known movement of the swarm. Eight new possible solution are now available. Knowing the movement of the swarm we apply a coordinate transformation to the first eight solution and compare with the second eight. Avoiding particular cases there is only one of the transformed solution that match one of the second eight solution. This last is the swarm configuration and is shown in the figure (red points). So far we have eliminate the degeneracy of the solution of a trilateration problem by a generic, but know, movement of the swarm . We need therefore two heart beat.

Now it is possible repeat the process for other vessels. Moreover, to overcome signal delay problem (some vessels could be too far for the coordinate origin) , other vessel can be taken as coordinate origin and later the founded configurations can be matched together. We can use these as a base constellation for the others, like GPS satellites. So far we need only the distance data from them and no more movement. Multiple combination of the method, to minimize errors, are possible. More than one constellation is possible adding new members. The coordinate of a new member can be calculated by constellation distance or by a known movement again.

Later the constellation can be varied and updated with new data, repeating the process for other vessel. This work can be done in different volume of the swarm and later matched together. In other words, to overcome signal delay problem (some vessels could be too far for the coordinate origin), other vessel can be taken as coordinate origin and later the founded configurations can be matched together. Once that a constellation is found you need only distances values to calculate the relative position like GPS system.

Therefore we have eliminate the degeneracy of the solution of a trilateration problem by a generic, but know, movement of the swarm . So far the configuration problem is solved, see figure 7.
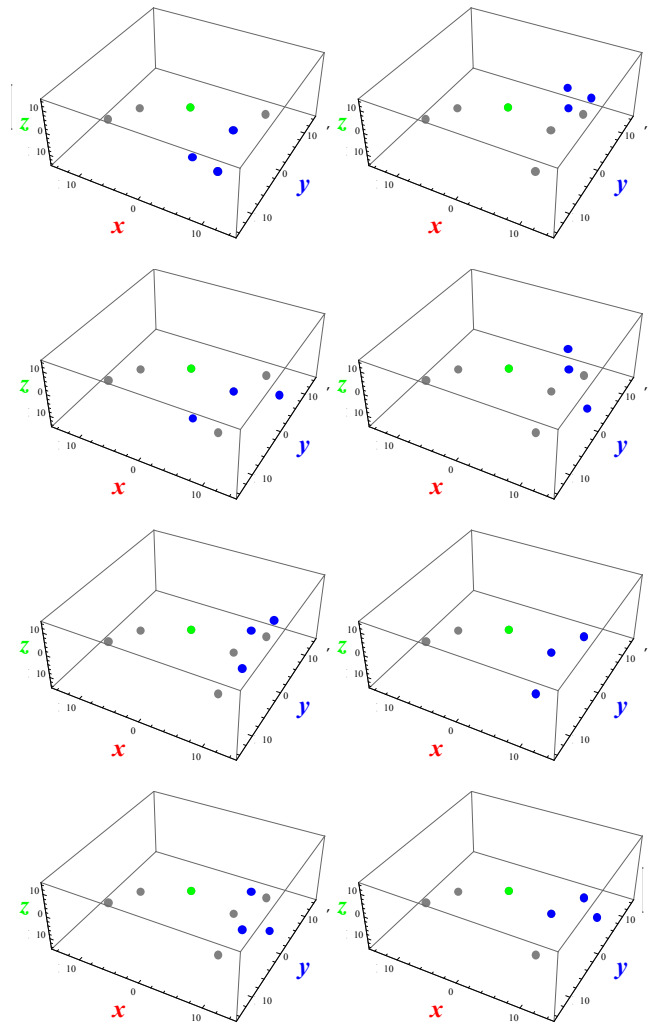

Fig. 6 – The first eight possible configuration of six vessels. Note the presence of seven points except one owing to the degeneracy of the solution. Grey vessels are unknown in their existence, green vessel is choose as axes origin and blue vessels have send a Hurt beat signal to the green one. They are candidates.
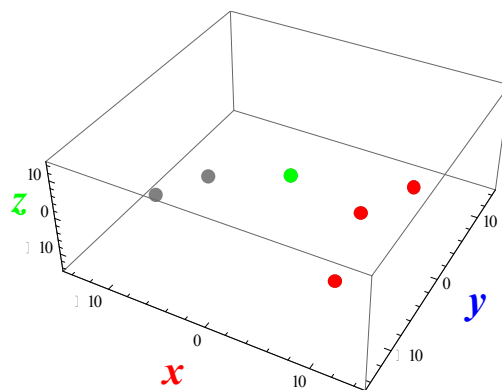

Fig. 7 – The final solution obtained after a known movement and coordinate transformation between a couple of eight solutions.

VII.   THE LOCALIZATION PROBLEM: A SIMPLER PROPOSED SOLUTION

Now we want something of more simple. Because the vessel are very cheap we do not have any information about speed, that moreover is often affected by many errors. But we have a depth meter (so the z coordinate is known, see fig 8 where the tracks of three robots are plotted) and a cheap compass that give us the orientation of the robots. Our simulation algorithm can demonstrate that this, more cheaper, information are enough to solve the degeneration of the solutions in one or more steps of movement, with some little differences with respect of the old method. So far our Hurt beat signal is = {id, time, orientation, depth, neighbors distances}.

The distances always are calculated by the time of flight of the signal, taking in account all the acceptance and errors procedure. This to consider the fading end thje many errors these measurements are affected.

It must be considered that using orientation information we are using a inequality condition on the coordinate in different time. This has a mean that can exist many compatibility conditions and one step of motion cannot be enough to solve the degeneracy of the solutions in the equation system distance. It can be that you need three or more (in simulation we found up to seven) steps of motion to resolve the degeneracy of the equations system.

The advantage of this cheaper algorithm lies in the very short amount of data that can be transmitted in each communication; moreover we can recover the speed of the robots and all the tracks followed. Note that we are using only three robots; if additional information about a fourth or other robot can be available they can be used to resolve the degeneracy quite soon.
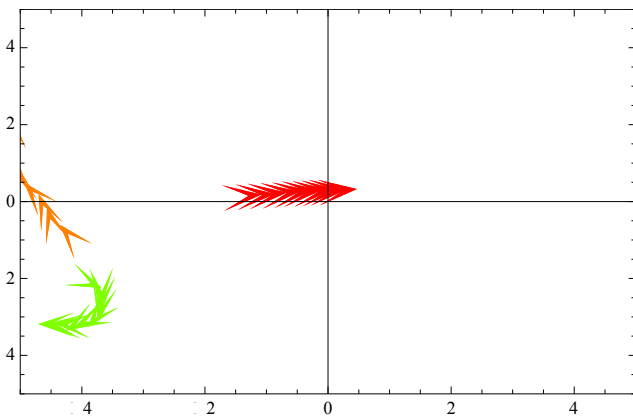
Fig. 8 – Three robots and their movements in different steps of time.

VIII.   OPEN QUESTIONS AND FUTURE WORK

Some consideration must be underlined and some points must be clarified. In particular we noted as the convergence speed of the algorithm depends on the initial configuration; so far you can need more than one step of motion to solve the swarm configuration. Simulation give as results that more similar between robots are the initial conditions (orientation and speed) more steps you need., thought if you get more than one solution they are very close each other. How many steps of movement I need before to get unique solution? It depends from the initial positions. How and in which way the initial positions influence the steps number? These are some questions we are investigating. What about if I get position and neighbors distance from a fourth robot? We obtain solutions without orientation but the system is quite different: problem to solve so we have to prune in different way. We have 16 equations to solve separately. Therefore we are working on a better mathematical treatment to determine how many steps you need and how they depend on the initial configuration. The fact that the robots do not emit the signal at the same time: it need to interpolate. The distances are uncertain and full of errors : you have to use of optimization methods. The use of GPS techniques to reduce the errors   The use of generic signal from other robots (without neighbors distances). An finally toy have to build the final configuration of the whole swarm (Put the pieces together)

IX.   CONCLUSION

In this work, we have explained that the Harness project could be useful for coastal monitoring, surveillance and many other purposes with particular attention to the localization problem. We propose a swarm of underwater cooperating robots. The advantages lie in the economy of the method, the parallelization of the task and the robustness of the system. The disadvantage lies in the major control difficulty of the swarm, owing to the presence of a new layer named as "Swarm control" which has different rules from the individual machine control. Many difficulties remain to be studied, especially in the communication between swarm elements owing to the unfriendly environment that limits the communication channel also if different methods are used together. The configuration problem (That is only one aspect of the general localization problem) of the swarm is solved using very few information exchanged between the elements of the swarm to minimize the used band pass. The work is in progress in our laboratory with some experiments into the Bracciano lake.

X. REFERENCES

[1] R. dell' Erba e C. Moriconi, «Harness: A robotic swarm for environmental surveillance», in *6th IARP Workshop on Risky Interventions and Environmental Surveillance (RISE), Warsaw, Poland*, 2012.

[2] R. dell' Erba e C. Moriconi, «HARNESS: A Robotic Swarm for Harbour Security"», presentato al International workshop Port and Regional Maritime Security Symposium, Lerici (Sp) Italy.

[3] C. Moriconi e R. dell' Erba, «The Localization Problem for Harness: A Multipurpose Robotic Swarm», in *SENSORCOMM 2012, The Sixth International Conference on Sensor Technologies and Applications*, 2012, pagg. 327–333.

[4] J. J. Leonard, A. A. Bennett, C. M. Smith, e H. Feder, «Autonomous underwater vehicle navigation», in *IEEE ICRA Workshop on Navigation of Outdoor Autonomous Vehicles*, 1998.

[5] S. Nawaz, M. Hussain, S. Watson, N. Trigoni, e P. N. Green, «An Underwater Robotic Network for Monitoring Nuclear Waste Storage Pools», *1st Int. ICST Conf. Sens. Syst. Softw. SCUBE*, pagg. 236–255, 2009.

[6] J. Yuh, «Design and Control of Autonomous Underwater Robots: A Survey», *Autonomous robot*, pagg. 7–24, 2000.

[7] J. Callmer, M. Skoglund, e F. Gustafsson, «Silent Localization of Underwater Sensors Using Magnetometers», *EURASIP J. Adv. Signal Process.*, vol. 2010, n. 709318, pagg. 1687–6172, 2010.

[8] M. Dunbabin, P. Corke, I. Vasilescu, e D. Rus, «Data muffling over underwater wireless sensor networks using an autonomous underwater vehicle», in *Proc. 2006 IEEE Intl. Conf. on Robotics and Automation (ICRA)*, 2006, pagg. 2091–2098.

[9] O. Khatib, V. Kumar, e D. Rus, *Experimental Robotics: The 10th International Symposium on Experimental Robotics*. Springer Verlag, 2008.

[10] C. W. Reynolds, «Flocks, herds and schools: A distributed behavioral model», *ACM SIGGRAPH Comput. Graph.*, vol. 21, n. 4, pagg. 25–34, 1987.

[11] E. W. Grafarend e J. Shan, «GPS solutions: closed forms, critical and special configurations of P4P», *GPS Solut.*, vol. 5, n. 3, pagg. 29–41, 2002.

Complementary redundant sensors for robot localization

Daniele Carnevale and Francesco Martinelli

Dipartimento di Ingegneria Civile e Ingegneria Informatica,

Università di Roma "Tor Vergata," via del Politecnico, I-00133, Rome, Italy

Emails: {carnevale,martinelli}@disp.uniroma2.it

Abstract— In this work we propose a technique to combine the information coming from two typologies of sensors: one typology is characterized by a low level of stochastic noise but is not univocally associated with the robot pose; the other one is univocal but has a higher noise level. This sensor configuration can be translated into a deterministic environment considering opportune nonlinearities affecting the (deterministic) sensors output. This framework may occur in robotics, for example, when the distance from a known landmark is detected by two different sensors, one based on the signal strength or time of flight of the signal, while the other one measures the phase-shift, which has a sharp but periodical dependence on the robot-landmark distance. In the stochastic case it is shown that a Kalman filter combining simultaneously the two measures does not provide satisfactory results. On the contrary, we propose an effective algorithm that exploits the periodic signal only when the innovation term of the estimation filter, that uses the non periodic signal, becomes small.

Index Terms— Redundant sensors, Kalman filtering, robot localization.

I. INTRODUCTION

It is quite common in real applications that robots rely on several sensors often providing measures related to the same physical quantity. Redundant measurements also characterize the perception system of humans and animals, mainly ensuring robustness and reliability. However, more interesting and rich consequences often characterize redundant senses in humans and animals, as, e.g., the presence of two eyes does not simply implies robustness against accidents but also allows to obtain a stereoscopic vision. However, handling this rich set of redundant information can be not trivial from a data processing point of view. More importantly, the information of some senses may be misleading in some situations and, for this reason, the brain of humans and animals usually faces the problem by inhibiting or activating senses according to the expected importance of the information they can deliver [1]. It is well known at this regard the human pathology known as *lazy eye* where the brain almost ignores the information coming from a less efficient eye.

Inspired by this biological solution of the problem, we have decided to use this kind of approach to face estimation problems, e.g., localization of mobile robots where some quantity can be measured by different typologies of sensors. The motivating application was a RFID (Radio Frequency Identification) based robot localization problem where a

reader, installed on the robot, can measure some quantities depending on the distance from a set of RFID tags located in the environment, which act as known landmarks. The use of the RFID technology for robot localization is a recent and promising line of research: RFID data used for localization vary from a binary information (i.e. the tag detection), e.g. [2]-[6], to a more complete set of information, like Received Signal Strength Indication (RSSI), e.g. [7]-[9], or phase shift of the signal, e.g. [10]-[11]. The RSSI, often available through quantized levels (e.g. of $1\ dBm$), usually presents a low sensitivity on the robot-tag distance, with a variation of a few dBm typically only for displacements of the robot in the order of $1\ m$. The phase-shift, on the contrary, is very sharp (typically one degree corresponds to displacements of the robot in the order of $1\ mm$) but presents a cycle ambiguity, since an unknown number of full wavelengths is contained in the tag-reader distance and several possible distances would produce the same phase. Both the measures are then related to the tag-reader distance, but present different and, to some extent, complementary characteristics, which should be properly combined to obtain an effective estimation of the robot state.

In a stochastic framework, the direct fusion of the information coming from these two kinds of measures in an Extended Kalman Filter may often provide scarce estimation results, as it will be illustrated in the paper. The solution approach proposed here, as mentioned, is based on the following scheme: in a first stage, only the imprecise but univocal measurement (e.g. the RSSI in our motivating example) is used in an Extended Kalman filter algorithm to estimate the state of the robot. Only when the estimate starts to become reliable (in a sense that will be specified in the paper), also the other non univocal measurement (i.e. the phase shift in the considered example) will be incorporated in the Kalman filter together with the other measure. A dynamic criterion to evaluate the time to switch between the two stages is part of the filtering approach. Notice in fact that also the possibility of resuming the first stage is contemplated by the algorithm. In the deterministic case, a similar approach is proposed by developing a switched observer that exploits both the measures.

The paper is organized as follows: in Section II the problem formulation is provided in the stochastic and in the deterministic frameworks; the proposed solutions are described in Section III for the two frameworks and numerical simulations are shown and discussed in Section IV.

II. PROBLEM FORMULATION

We consider dynamic systems described by the following set of equations:

$$\dot{x} = f(x, u, w), \tag{1a}$$

$$z_{ij} = h_{ij}[g_{ij}(x)] + d_{ij}, \quad j = 1, \ldots, q_i, \ i = 1, 2 \tag{1b}$$

where $x \in \mathbb{R}^n$ is the robot state, $u \in \mathbb{R}^p$ is a control (or in general a known) input, $w \in \mathbb{R}^{p_w}$ is an unknown disturbance acting on the dynamics of the system, z_{ij} are scalar measures depending on the state, $g_{ij}(x)$ are scalar functions of the state x (e.g. $g_{ij}(x) = \|x\|$), $h_{ij}(\cdot)$ are invertible for $i = 1$ and periodical with some period Y_j for $i = 2$ (i.e. $h_{2j}(y + kY_j) = h_{2j}(y)$ for all $y \in \mathbb{R}$ and $k \in \mathbb{Z}$), d_{ij} are unknown disturbances acting on the measures z_{ij}.

The idea of the model is that the set of measures $\mathcal{Z}_1 := \{z_{1j}\}_{j=1,\ldots,q_1}$ is such that every measure $z_{1j} \in \mathcal{Z}_1$ is a univocal transformation of some scalar function g_{1j} of the state x but is affected by a relatively strong disturbance d_{1j} and/or can be characterized by a low sensitivity on the typical robot displacements in the considered environment. On the contrary, the set of measures $\mathcal{Z}_2 := \{z_{2j}\}_{j=1,\ldots,q_2}$ is such that every measure $z_{2j} \in \mathcal{Z}_2$ is more sensitive and/or presents a better signal to noise ratio (i.e. the disturbance d_{2j} is small if not completely negligible compared to the typical excursion of the signal) but is characterized by a non univocal dependence on the scalar function g_{2j} of the state of the system.

A. STOCHASTIC SCENARIO

We assume that all the unknown disturbances reported in the main model (1a)-(1b) (i.e. w and d_{ij}, for $j = 1, \ldots, q_i$, $i = 1, 2$) are random variables. For simplicity, they will be assumed 0-mean Gaussian: $w \sim \mathcal{N}(0, \sigma_w^2)$ and $d_{ij} \sim \mathcal{N}(0, \sigma_{d_{ij}}^2)$.

In this section, the following assumptions will be taken on the general model (1a)-(1b): first of all it will be assumed that $q := q_1 \equiv q_2$, that is, the two sets of measurements $\mathcal{Z}_1$ and $\mathcal{Z}_2$ will be considered coupled, in the sense that for all $j = 1, \ldots, q$, $g_{1j}(x) = g_{2j}(x)$. Moreover, if x represents the pose of a robot, these functions will be taken as the distance of the robot from a set of landmarks, i.e. $g_{1j}(x) = g_{2j}(x) = \|x - x_j\|$, for $j = 1, \ldots, q$, where x_j are the coordinates of landmark j.

While $\sigma_{d_{2j}}$ are assumed negligible, $\sigma_{d_{1j}}$ are quite large. At this regard, for the good behavior of the estimation process, a key element is the relation between the size of $\sigma_{d_{1j}}$ with respect to the $h_{2j}(\cdot)$ period Y_j. As shown in simulation, and as intuitively can be expected, the smaller is $\sigma_{d_{1j}}$ w.r.t. Y_j for all j, the more effective will be the filtering procedure.

B. DETERMINISTIC SCENARIO

In the deterministic case all the variables are not described as random process but deterministic ones. Nevertheless it is possible to consider unknown disturbances acting on the system dynamics such as w and on the available (redundant) measurements, namely d. Also in the deterministic case it is

assumed that the magnitude of the measurement disturbances d_{1j} are considerable larger than d_{2j}. In particular, $d_{1j}(t)$ can be even discontinuous in time. Then, we are able to model sensors dead-zones letting $h_{1j}(\cdot)$ be continuous with respect to their arguments, even linear if needed, and confine the nonlinear behavior to the signals d_{1j}'s. As an example, if the j-th sensor is affected by a discontinuous dead-zone nonlinearity defined as

$$\mathrm{dz}_\sigma(s) \triangleq \begin{cases} s & \text{if } |s| \geq \sigma, \\ 0 & \text{otherwise}, \end{cases}$$

for some positive scalar σ, we could assume that $d_{1j}(t)$ is such that

$$z_{1j}(t) = h_{1j}(g_{1j}(x(t))) + d_{1j}(t) = \mathrm{dz}_\sigma(g_{1j}(x(t)))$$

holds true, with a continuous function $h_{ij}(\cdot)$. Dead-zone as well as saturation nonlinearities are often associated to low cost sensors that generally have a (time-varying) nonlinear characteristic for large readings, requiring the use of a saturation, or when high level noise makes readings close to zero too inaccurate to be acceptable and it is preferable to let the measure equal to zero via a dead-zone nonlinearity. An example that falls into this framework, in case of frequency estimation, is proposed in [12], [13]. In here, that is our starting work on multiple output allocation for state estimation and it is far to be complete, we consider a very simple system, namely a first order LTI (linear time invariant) SISO (single-input-single-output, i.e. $p = 1$ and $q_1 = q_2$ in our notation) described by

$$\dot{x} = Ax + Bu, \tag{2a}$$

$$z_1(t) = h_{11}(g_{11}(x(t))) + d_1(t) = Cx(t) + d_1(t), \tag{2b}$$

$$z_2(t) = h_{21}(g_{21}(x(t))) + d_2(t) = \mathrm{mod}(g_{21}(x(t)), Y) + d_2(t), \tag{2c}$$

where $A \in \mathbb{R}^{n \times n}$, $B \in \mathbb{R}^n$, $C \in \mathbb{R}^{1 \times n}$, $g_{21}(\cdot) : \mathbb{R}^n \to \mathbb{R}$ and the function $\mathrm{mod}(s, Y)$ evaluates the modulus after division of s where Y is the periodicity interval. It is assumed that the output disturbances satisfy the following inequalities

$$\|d_1(t)\|_\infty \leq \sigma_1, \ \|d_2(t)\|_\infty \leq \sigma_2.$$

Despite the simplicity of the considered plant a number of different considerations can be derived.

III. PROPOSED SOLUTIONS

A. STOCHASTIC SCENARIO

To simplify the discussion, the proposed solution approach will be described assuming $q = 1$ (i.e. only one measurement $z_1 := z_{11} \in \mathcal{Z}_1$ and only one measurement $z_2 := z_{21} \in \mathcal{Z}_2$). The idea of the approach is that in a first stage, only the imprecise but univocal measurement z_1 is used in an Extended Kalman filter algorithm to estimate the state x. Only when the estimate starts to become reliable (in the sense specified below), also the other non univocal measurement z_2 will be incorporated in the Kalman filter together with z_1. A dynamic criterion to evaluate the time to switch between the two stages is part of the filtering approach. Notice in fact that

also the possibility of resuming the first stage is contemplated by the algorithm. In the case of $q > 1$, a different stage can be defined for each couple of measures (z_{1j}, z_{2j}), $j = 1, \ldots, q$, and the dynamic switching rule would be performed independently on each stage.

The following algorithm summarizes the filtering approach. Clearly, the approach is presented in a discrete time context, obtained by discretizing (e.g. using an Eulero approximation with some sampling time δ_t) the continuous time model (1a)-(1b). In the discrete approximation, any discrete time quantity r_k denotes the corresponding sampled quantity $r(k\delta_t)$.

The algorithm is based on a variable, s_k, which denotes the current stage of the filter: $s_k = 1$ if the algorithm is in the first stage (and only $z_{1,k}$ is used), while $s_k = 2$ if the algorithm is in the second stage (where both the measures $z_{1,k}$ and $z_{2,k}$ are used).

The expected z_1 and z_2 measurements will be denoted by $\hat{z}_1$ and $\hat{z}_2$ respectively. If the estimated state of the robot is $\hat{x}$, $\hat{z}_1$ is simply given by $\hat{z}_1 = h_1[g_1(\hat{x})]$. More attention should be devoted to derive the expected value of the other measurement. The idea is to first set $\hat{z}_2 = h_2[g_2(\hat{x})]$. However, due to the periodicity Y of h_2, this first value of $\hat{z}_2$ is modified by a multiple of Y, where the multiple is selected in order to minimize the innovation (i.e., if z_2 is the true measurement, in order to minimize $|z_2 - \hat{z}_2|$). So, formally we have:

$$\ell^* = \arg \min_{\ell \in \{-1,0,1\}} |z_2 - (h_2[g_2(\hat{x})] + \ell \cdot Y)| \quad (3a)$$

$$\hat{z}_2 = h_2[g_2(\hat{x})] + \ell^* \cdot Y. \quad (3b)$$

To better explain the meaning of the above procedure, assume that $g_2(x) = \|x\|$ and that $Y = 360^o$, in such a way that $h_2(\|x\|) \in \{-180^o, 180^o\}$. Now, assume $z_2 = h_2(\|x\|) = 178^o$ and that $\hat{z}_2 = h_2(\|\hat{x}\|) = -179^o$. Now, this -179° should be probably read as 181°, which is very close to the true measure 178°, i.e. it is better to consider $\hat{z}_2 = -179^o + Y = -179^o + 360^o = 181^o$, with $\ell^* = 1$ in this case.

Algorithm 1: **Dynamic 2 Stage Extended Kalman Filter (D2SEKF).**

- *Initialization:* Let $\hat{x}_0$ and P_0 be respectively the initial estimate of x and its covariance matrix. Set $s_0 = 1$ and $k = 0$.
- At each time step k do the following:
  1) *Prediction:*

$$\hat{x}_{k+1}^- = \hat{x}_k + f(\hat{x}_k, u_k, 0) \cdot \delta_t \quad (4a)$$
$$P_{k+1}^- = F_k P_k F_k^T + W_k \sigma_W^2 W_k^T, \quad (4b)$$

  where F_k and W_k are respectively the Jacobian of $x + f(x, u, w)\delta_t$ w.r.t. the state x and to the noise w computed in the current estimate.
  2) *Correction:*

If $s_k = 1$, only z_1 is used:

$$K_G = P_{k+1}^- H_{1,k+1}^T (H_{1,k+1} P_{k+1}^- H_{1,k+1}^T + \sigma_{d_1}^2)^{-1} \quad (5a)$$

$$\hat{x}_{k+1} = \hat{x}_{k+1}^- + K_G (z_{1,k+1} - \hat{z}_{1,k+1}) \quad (5b)$$

$$P_{k+1} = (I - K_G H_{1,k+1}) P_{k+1}^- \quad (5c)$$

where $\hat{z}_{1,k+1} = h_1[g_1(\hat{x}_{k+1}^-)]$ is the expected measure, $H_{1,k+1}$ is the Jacobian of h_1 w.r.t. the state computed in the current estimate and I is the identity matrix.

If $s_k = 2$, both z_1 and z_2 are used:

$$K_G = P_{k+1}^- H_{k+1}^T (H_{k+1} P_{k+1}^- H_{k+1}^T + R)^{-1} \quad (6a)$$

$$\hat{x}_{k+1} = \hat{x}_{k+1}^- + K_G (z_{k+1} - \hat{z}_{k+1}) \quad (6b)$$

$$P_{k+1} = (I - K_G H_{k+1}) P_{k+1}^- \quad (6c)$$

where $z_{k+1} = [z_{1,k+1}, z_{2,k+1}]^T$ is the measurement vector, $\hat{z}_{k+1} = [\hat{z}_{1,k+1}, \hat{z}_{2,k+1}]^T$ is the vector of expected measures with $\hat{z}_{2,k+1}$ obtained as described in (3a)-(3b), H_{k+1} is the Jacobian of $[h_1, h_2]^T$ w.r.t. the state computed in the current estimate, $R = diag(\sigma_{d_1}^2, \sigma_{d_2}^2)$ and I is the identity matrix.

3) *Stage switching.* Let $k_0 = max\{0, k - k_w\}$ (where k_w is an integer, e.g. $k_w = 10$), $n_s = k + 1 - k_0$ and compute the average i_s of the innovations related to the first measurement z_1 in the last n_s steps:

$$i_s = \frac{1}{n_s} \sum_{m=k_0+1}^{k+1} [z_{1,m} - \hat{z}_{1,m}] \quad (7)$$

If $|i_s| > 3 \cdot \frac{\sigma_{d_1}}{\sqrt{n_s}}$ and $s_k = 2$,

$$s_{k+1} = 1 \quad (8a)$$

and reinitialize P taking into account the entity of the mean innovation. One possible value for P could be selected such that

$$H_{1,k+1} P_{k+1} H_{1,k+1}^T = n_s i_s^2 \quad (9a)$$

If $|i_s| < 3 \cdot \frac{\sigma_{d_1}}{\sqrt{n_s}}$ and $s_k = 1$,

$$s_{k+1} = 2 \quad (10a)$$

□

The idea of the switching step is that, if precise estimates of the state are being obtained using both the measurements (i.e. $s_k = 2$), then the mean of the innovation i_s in (7) can be seen as the mean of the independent disturbances $d_{1,m}$, $m = k_0 + 1, \ldots, k + 1$, which is a 0-mean, Gaussian random variable with standard deviation $\frac{\sigma_{d_1}}{\sqrt{n_s}}$. This is confirmed if indeed the mean in (7) is less, in modulus, than 3 times this standard deviation (it is known that a 0-mean Gaussian random variable is less in modulus than 3σ with probability 99.73%). If this mean goes outside this limit, probably something is going wrong, so the first stage is restored ($s_{k+1} = 1$) and an initial covariance matrix should be set

for the estimate of x. In fact, the current covariance P_k, based on both measures, is actually too optimistic and the algorithm would present long transitories if a correction of the covariance is not performed. Equation (9a) is based on the fact that the covariance of each element in (7) can be approximated by $H_{1,h} P_h H_{1,h}^T + \sigma_{d_1}^2$, so the variance of i_s can be approximately written as $\frac{1}{n_s}\left(H_{1,k+1} P_{k+1} H_{1,k+1}^T + \sigma_{d_1}^2\right)$. If $\sigma_{d_1}^2$ is neglected (in this case is about one order of magnitude less than the other term), then a simple choice of P_{k+1} can be as reported above. If x is scalar, and so are P and H, it is straightforward to find a solution to (9a). Otherwise, a good idea could be the one of scaling P_k in such a way that (9a) is met with $P_{k+1} = \alpha P_k$, where $\alpha > 0$ is selected large enough.

If $s_k = 1$ and the estimate starts to become good (i.e. $|i_s| < 3 \cdot \frac{\sigma_{d_1}}{\sqrt{n_s}}$), the second stage is set ($s_{k+1} = 2$).

Notice that in the algorithm the period Y is not considered: it should be observed (and this will be the subject of the simulation study in Section IV-A) that if Y is not too small w.r.t. σ_{d_1} the algorithm is effective (so $Y \geq \sigma_{d_1}$ can be considered an assumption for the correct evolution of the filtering scheme, even if an adequate estimation can be sometimes obtained also when Y is rather smaller than σ_{d_1}).

Remark 1: As shown in a numerical example in Section IV-A, better results are likely to be obtained if in stage 2 the two measurements z_1 and z_2 are not simultaneously incorporated in the EKF but they are processed separately: a first correction of the state is performed using z_1 and a successive correction is achieved with the z_2 based feedback.

B. DETERMINISTIC SCENARIO

Our approach resembles a switched linear observer that can be associated to biological systems that exploit rough measurements to obtain a coarse estimate of the interested quantity (for snakes it could be represented by odor), and then it is improved by mean of more accurate sensors (thermic and tactile perception). Then, we exploit a standard linear observer with output injection given only by z_1, namely

$$\dot{\hat{x}} = A\hat{x} + Bu + K_1(z_1 - C\hat{x}), \; x \notin \Sigma_1(t) \qquad (11)$$

with a selection of the gain matrix $K_1 \in \mathbb{R}^n$ such that $A - K_1 C$ is Hurwitz. This observer is used until $\hat{x}$ does not belong to the set $\Sigma_1(t)$, defined as follows

$$\Sigma_1(t) \triangleq \{\hat{x} \in \mathbb{R}^n : |z_1(t) - C\hat{x}| \leq \sigma_1\}. \qquad (12)$$

In fact, given to the arbitrariness of the signal $d_1(t)$, we exploit the output injection term $K_1(z_1 - C\hat{x})$ only when $d_1(t)$ can not change its sign (via z_1). Whenever x is inside the region $\Sigma_1(t)$, even the sign of the term $K_1(z_1 - C\hat{x})$ can lead to wrong estimate dynamics and then we consider the measure $z_2(t)$. Here we let $g_{21}(x) = x$, then

$$z_2(t) = \mathrm{mod}(x(t), Y) = x(t) + i^\star(t)Y,$$

for some unknown $i^\star(t) \in \mathbb{Z}$ (integer values set). Then, we propose to use a different output injection whenever $\hat{x} \in$

$\Sigma_1(t)$ that makes use[1] of $p := \lceil 2\sigma_1/Y \rceil$ admissible values for $\hat{x}$ according to the measure $z_2(t)$, i.e.

$$\hat{x}_i(t) \triangleq \hat{x}(t) + iY,$$

for all integer $i \in \mathcal{P} \triangleq [-p, p]$ and it is such that $i^\star \in \mathcal{P}$. In order to introduce the second output injection, that is used since $x(t)$ enters $\Sigma_1(t)$ at certain time t_1 and ever, we first define the time-varying set

$$\mathcal{I}(t) \triangleq \{i \in \mathbb{Z} : |z_1(t) - C\hat{x}_i(t)| \leq \sigma_1\}, \qquad (13)$$

that contains all possible integers i defining the multiple estimates $\hat{x}_i(t) \triangleq \hat{x}(t) + iY$ at time t. Furthermore, define the set $\mathcal{I}_0(t)$ as in (13) and initialized it as $\mathcal{I}_0(t_1) = \mathcal{P}$. The elements of the set $\mathcal{I}_0(t)$ are successively canceled out if there exits $t_{2i} \geq t_1$ such that $i \in \mathcal{I}_0(t_{2i})$ and $i \notin \mathcal{I}(t_{2i})$. In this way the cardinality of the set $\mathcal{I}_0(t)$, for all $t \geq t_1$, can only shrink and never grow, and the set maintains only the integers that never left the set $\mathcal{I}(t)$ and were contained in $\mathcal{I}(t_1)$. We define also a new measure $\overline{z}_2(t)$ which is defined as follows

$$\overline{z}_2 = z_2 + \zeta Y \qquad (14)$$

where ζ is such that the new measure $\overline{z}_2(t)$ is **continuous** and has the same time derivatives of $z_2(t)$ almost everywhere. To accomplish this task, ζ is obtained as an hybrid arc solution of the following (switched) hybrid system [14]

$$\dot{\zeta} = 0 \quad \text{if} \quad z_2(t^-) = z_2(t^+), \qquad (15a)$$

$$\zeta^+ = \begin{cases} \zeta + 1 & \text{if} \quad z_2(t^-) > z_2(t^+) \\ \zeta - 1 & \text{if} \quad z_2(t^-) < z_2(t^+) \end{cases} \qquad (15b)$$

where $z_2(t^\pm) := \lim_{s \to t^\pm} z_2(s)$ and $\zeta_0 = 0$. The resulting ζ is then constant if $z_2(t)$ is continuous in t, whereas ζ is incremented of one if the measure $z_2(t)$ jumps to zero, meaning that its argument is incrementing and then moving to the next periodic interval. On the contrary, it is decremented when $z_2(t)$ has a jump toward its maximum value. To render continuous also the "multiple" estimates $x_i(t)$, it is possible to analogously define

$$\overline{\hat{x}}_i = \hat{x}_i + \zeta_i Y,$$

where the initial values of $\zeta_i(0) = i$, for $i \in \mathcal{P}$, and its flow and jump dynamics are given as in (15).

At time t_1, and since on, we define the hybrid observer (switched) dynamics such as

$$\dot{\hat{x}} = A\hat{x} + Bu + K_2 \left(\overline{z}_2 - |\overline{\mathcal{I}}_0(t)|^{-1} \sum_{i \in \overline{\mathcal{I}}_0(t)} C\overline{\hat{x}}_i \right), \qquad (16)$$

where $\overline{\mathcal{I}}_0(t)$ is the set defined in (13) with $\overline{\hat{x}}_i$ in place of $\hat{x}_i$ and with cardinality denoted by $|\overline{\mathcal{I}}_0(t)|$. Note that this injection is proportional to the mean value estimation error among the estimates $\overline{\hat{x}}_i(t)$ for those $i \in \overline{\mathcal{I}}_0(t)$ that can be considered admissible with respect to the information given by the measure $z_1(t)$. Note that the injection term

---

[1] The operator $\lceil s \rceil$ yields the upper integer number closer to s.

is discontinuous at time instants the set $\mathcal{I}_0(t)$ changes. To conclude, K_2 is designed such that $A - K_2 C$ is Hurwitz.

Once the observer dynamics are (16), the output estimation error $z_1(t) - C\hat{x}(t)$ amplitude is smaller than σ_1. Note that if $\sigma_1 = 0$ and the pair (A, C) is detectable, then the estimation error system $e = x - \hat{x}$ has the origin Globally Asymptotically Stable (GAS) and, when $\sigma_1 > 0$, it is Input to State Stable (ISS) with respect to the disturbance d_1. These features allow easily to conclude that there exists a time $t_1 > 0$ such that the set $\Sigma_1(t_1)$ is attractive.

Note that we do not attempt here to identify the disturbance signal z_1, given that it could be the signal introduced to model a dead-zone nonlinearity, whose time derivative is represented by mean of differential inclusion and not by differential equation, introducing considerable difficulties. For $t > t_1$ the observer dynamics are (16) and even if (A, C) is observable or detectable the attractivity of the origin of the estimation error can be lost. Certainly, with the previous assumptions, the estimation error $e(t)$ tends to zero as t goes to infinity if $\overline{\mathcal{I}}_0(t) = \{i^\star\}$. As will be shown in the simulation results, the set $\overline{\mathcal{I}}_0(t)$ shrinks when the noise signal z_1 sufficiently changes in time and spans the amplitudes ranging from $-\sigma_1$ to σ_1. The control input u, that changes z_1 as well as $\overline{z}_2$, does not help in reducing the set $\overline{\mathcal{I}}_0(t)$ to identify which one among the estimates $\hat{\overline{x}}_i$ is the right one. These properties noticed by numerical simulations and motivated by intuitive reasoning will be formally addressed in next papers.

IV. SIMULATIVE RESULTS

A. STOCHASTIC SCENARIO

Consider a robot moving along a line and let $x(t)$ be its position at time t. To simplify things, we will assume that the robot moves on the positive half of the line (that is $x(t) > 0$ for all t). Assume that a landmark is located in $x = 0$ and that $g_1(x) = g_2(x) = x$ (i.e. the robot-landmark distance). Now, let $z_1 = x + d_1$ and $z_2 = mod(x, Y) + d_2$ for some period Y and noises d_1 and d_2. The considered dynamics is very simple: in the discrete time domain is given by

$$x_{k+1} = x_k + u_k + w_k$$

where u_k can be seen either as a noisy control input or as a noisy encoder reading of the displacement of the robot in the time interval $(k\delta_t, (k+1)\delta_t)$. The noise associated with u_k is $w_k \sim \mathcal{N}(0, \sigma_w^2)$, with $\sigma_w = 0.1$ in our setting. We consider a sinusoidal moving law, with

$$u_k = 0.1 \, \sin(0.05 \cdot k)$$

The first measure, z_1, is very rough: we assume $\sigma_{d_1} = 2$. On the contrary z_2 is very sharp, with a very small standard deviation $\sigma_{d_2} = .01$. However z_2 is periodic, with period Y, which for now is assumed equal to σ_{d_1}, i.e. $Y = 2$.

At time $k = 300$, the state makes a 5 units jump: this is not known by the filtering algorithm, and has been added to
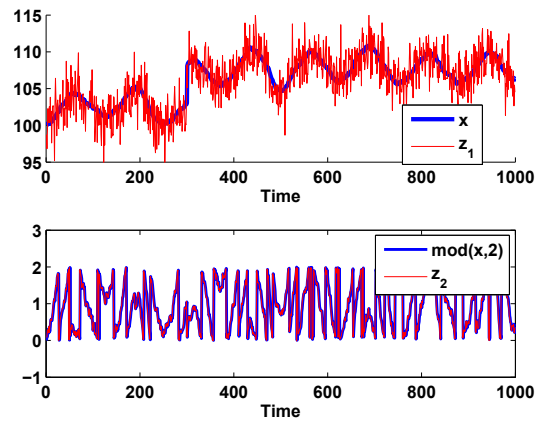
Fig. 1. The state evolution in the first example and the corresponding two measurements z_1 and z_2
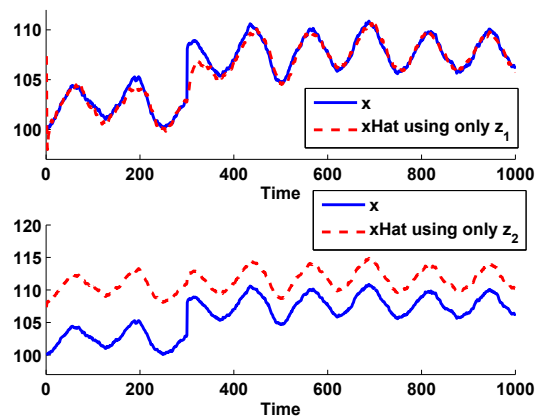

Fig. 2. The state estimation exploiting only one measurement z_1 (up) or z_2 (down)

test the approaches (kidnapped robot problem). The initial estimate is taken as

$$\hat{x}_0 = x_0 + n_0$$

where $n_0 \sim \mathcal{N}(0, \sigma_0^2)$. In the considered examples, $x_0 = 100$ and $\sigma_0 = 10$, in such a way that in the first example $\hat{x}_0 = 107.35$.

In Fig. 1 it is reported the plot of x_k together with the measurements $z_{1,k}$ and $z_{2,k}$. In particular, in the figure above, it is possible to see how the first measurement follows the state x but presents a strong noise. On the contrary z_2 would be precise (observe in the figure below how $mod(x, 2)$ almost overlaps with z_2) but it does not allow to have any information regarding the correct cycle of x.

If only z_1 is used we are actually applying a standard Kalman Filter which gives the optimal estimation of x given only z_1. However, due to the strong noise d_1, the estimate is not really precise (see Fig. 2 up) and presents in this
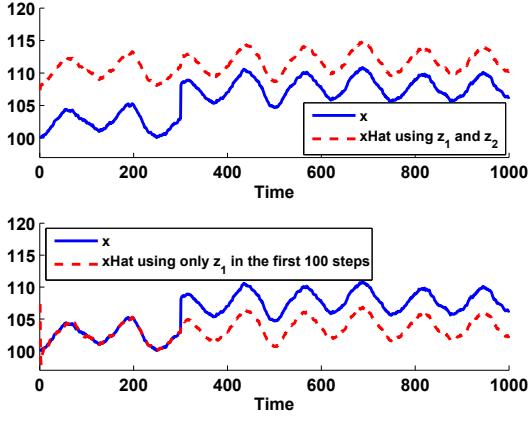
Fig. 3. The state estimation exploiting both the measurement: always (up) or only after 100 steps (down)

Fig. 5. Ratio $\rho_e := \frac{\bar{e}_{D2SEKF}}{\bar{e}_1}$ as a function of the period Y of measurement z_2


Fig. 4. The state estimation exploiting the proposed approach and comparison of errors

simulation an average estimation error $\bar{e} = 0.43$, where

$$\bar{e} = \frac{1}{T} \sum_{k=1}^{T} |x_k - \hat{x}_k| \qquad (17)$$

being T the duration of the simulation. Considering a Kalman filter which uses z_2 (but ignoring its periodicity) the estimation is almost perfect but in a wrong cycle (actually in the cycle corresponding to the initial estimate)), as seen in Fig. 2 (down).

The simultaneous use of z_1 and z_2 (Fig. 3, up) does not modify the result obtained when only z_2 is used: for the Kalman filter, which ignores the periodicity, z_2 is the more important measurement. A trick could be the one of using only z_1 at the beginning (say until step 100) and then consider also z_2: this is similar to the approach proposed in this paper except that the switching is performed in an open loop fashion with the result that after the jump in x (at step 300), the algorithm is not able to recover the correct cycle of the state (see Fig. 3, down).

The approach proposed in this paper is illustrated in Fig. 4 (up). An effective estimation is obtained, characterized by the precision of z_2 and the correct cycle of z_1. The estimation error $\bar{e}$ is now 0.06 and is about one order of magnitude less than the error of the Kalman filter exploiting only z_1. A comparison of the estimation errors $e_k = |x_k - \hat{x}_k|$ is given in Fig. 4 (down).

Considering different periods Y it is possible to see how increasing Y does not change the performance of the filter. On the contrary, reducing Y may invalidate the approach, when Y starts to become quite small w.r.t. the standard deviation σ_{d_1} of the noise d_1 characterizing z_1. In Fig. 5 it is reported the ratio $\bar{e}_{D2SEKF}/\bar{e}_1$, where $\bar{e}_{D2SEKF}$ is the average estimation error of the proposed approach considering 100 simulations like the one described above except that now Y is varying in the interval $(0.1, 4)$ and the jump in the state has been removed. Similarly $\bar{e}_1$ is the noise of the Kalman filter which only uses z_1 in the same set of simulations. When this ratio becomes larger than 1 (i.e. for $Y \leq 0.6$ from Fig. 5) it means that it is better to always neglect z_2 (at least using the approach proposed in this paper).

Consider now the case a unicycle robot moves in an environment and there is a landmark located on the ceiling (height 242 cm). Assume that the landmark is a RFID tag and that two measurements related to the position of the robot are available: the Received Signal Strength Indication (RSSI) which plays the role of z_1 and the phase shift of the RFID signal, which plays the role of z_2, since presents a 180° periodicity (see [10] and [15] for more details). The two measurements depend on the distance of the robot from the projection of the tag on the floor, as illustrated in Fig. 6. Hence, also in this case, $g_1(x) = g_2(x) = \sqrt{(x - x_t)^2 + (y - y_t)^2}$, being (x_t, y_t) the coordinates of the projection of the RFID tag on the floor. We have assumed $\sigma_{d_1} = 0.6$ dBm and $\sigma_{d_2} = 5^o$.

In Fig. 7 it is possible to see how, starting from an initial estimate such that the correction performed by the
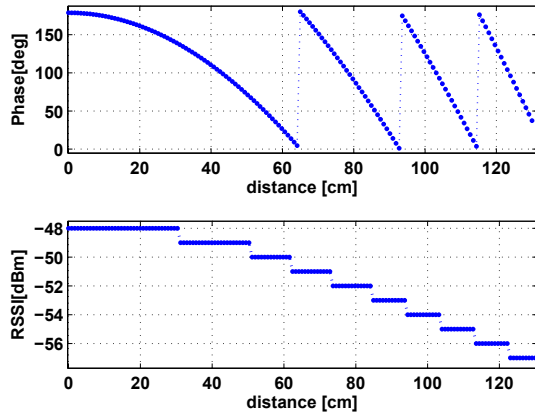
Fig. 6. The RSSI (up), which plays the role of z_1 and the phase-shift, corresponding to z_2, as a function of the robot distance from the projection of the tag on the floor

Fig. 8. Top plot: the measures $z_1(t)$ and $z_2(t)$ are shown in black and red solid lines, respectively. Approximatively at time $t_1 = 0.5$s the observer dynamics is switched from (11) to (16) and some of the estimates $\bar{\hat{x}}_i$, corresponding to the measures $\bar{\hat{z}}_{2,i} = \bar{\hat{x}}_i$, depicted in dashed colored lines, do not satisfy the constraint in $\overline{\mathcal{I}}(t)$ and are canceled out. Bottom plot: the estimated value $\hat{x}(t)$ converges to $x(t)$ although $|\overline{\mathcal{I}}_0(t)|$ does not converge to one because the disturbance $d_1(t)$ has zero mean value.

Fig. 7. Localization of a unicycle-like robot using the RSSI and/or the phase-shift associated to the signal coming from a RFID tag located on the ceiling in position $(0, 0)$

Extended Kalman based on z_2 pushes the estimate in the wrong direction (the true position of the robot is $(0, 0)$), also when using both z_1 and z_2 a bad estimation result is achieved. On the contrary, if at first the correction is performed only using z_1 and then the z_2 based correction is applied, a much more satisfactory result is obtained. The coordinates of the projection of the RFID tag on the floor are $(0, 0)$. Notice that in this simple example only one step is considered. The proposed approach actually performs usually more than one step by only using z_1 and then, when the estimate appears reliable (i.e. near the true robot position, as explained in Section III-A), also z_2 is taken into account.

B. DETERMINISTIC SCENARIO

We have considered a simple first order system with $A = 0$, $B = 1$ and $C = 1$, the control $u = \sin(2\pi t)$, the disturbance acting on the measure z_1 such as $d_1 =$

$0.5 \sin(2\pi 1.5t)$ and $Y = \sigma_1/6$. The observer matrix gains are selected as $K_1 = 4$ and $K_2 = 10$. In the simulation results shown in Fig. 8 the estimated value of $\hat{x}(t)$ asymptotically (exponentially) converges toward $x(t)$ although the set $\mathcal{I}_0(t)$ does not converge on a single element, i.e. there are multiple possible selections $\bar{\hat{x}}_i$ that do not disagree (through the inequality (13)) with the measure z_1. This is caused by the fact that a $\sigma_1 = 1$ (double) larger than the actual maximal amplitude of the disturbance d_1 is considered. Nevertheless, since the disturbance d_1 has zero mean value and this is captured by the input injection in (16), the estimation error converges toward zero.

The second simulation shows in Fig. 9 that if a tight bound on the z_1 amplitude is known, i.e. $\sigma_1 = ||z_1(t)||_\infty$, when the disturbance amplitude spans between $-\sigma_1$ and σ_1 the set of the admissible estimates $\bar{\hat{x}}_i$ shrinks toward a single element. The last numerical simulations in Fig. 10 shows that whenever the disturbance $d_1(t)$ has not zero mean value, even if the tight bound $\sigma_1 = ||d_1(t)||_\infty$ is known, a constant estimation error is induced. This is given by the intrinsically symmetric (zero mean) condition in the definition of the set $\mathcal{I}(t)$ and the fact the $d_1(t) = 0.7 \sin(2\pi 1.5t) + 0.3$ has a constant (unknown) term.

V. CONCLUSIONS

In this paper the problem of fusing the information coming from two typologies of redundant sensors with complementary characteristics has been considered. The two types of sensors provide a measure related to the same quantity but possess different and, to some extent, complementary characteristics: the first one is rough and may be large grain and/or present a low sensitivity on the dynamics of the system. The second type of sensor, on the contrary, even if precise, is supposed to present a non univocal dependence
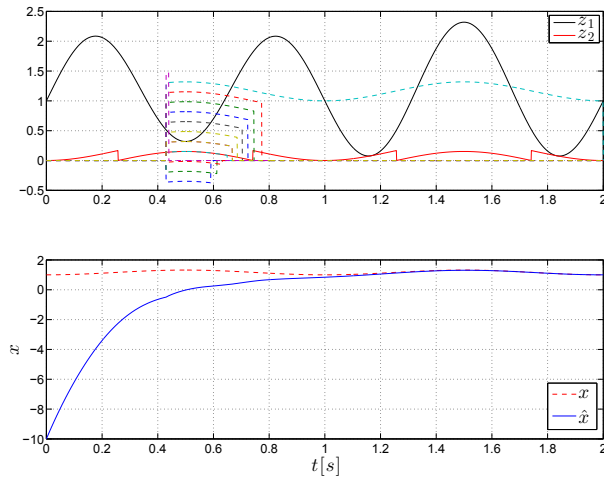
Fig. 9. Contrary to Fig. 8, σ_1 has been picked equal to the maximal amplitude of the disturbance $d_1(t)$, i.e. $\sigma_1 = ||d_1(t)||_\infty$. In this case, since the $d_1(t)$ reaches values from $-\sigma_1$ up to $-\sigma_1$, only one admissible estimate $\bar{\hat{x}}_i$ is maintained and at time 0.8s the set $\overline{\mathcal{I}}_0(t)$ has only one element.
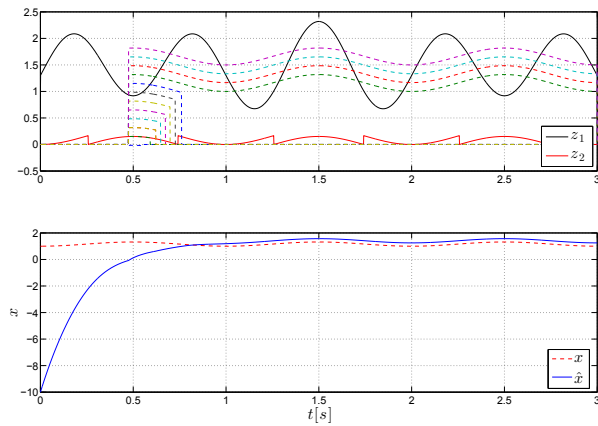

Fig. 10. In this case we considered a disturbance with no zero mean value, namely $d_1(t) = 0.7\sin(2\pi 1.5t) + 0.3$ and $\sigma_1 = 1$, yielding a constant error.

on the state of the system. This kind of situation also characterizes humans and animals where some perception organs are duplicated. In some cases, the biological solution adopted to face the problem of fusing the information is to inhibit or activate senses based on the expected importance of the information they deliver at the moment. Inspired by this approach, in the stochastic context, a two-stage Extended Kalman filtering algorithm is proposed which, in a first stage, only uses the imprecise but univocal measurement and, only when the estimate starts to become reliable, also incorporates the other non univocal measurement in the filter. The direct fusion of the two measures in a standard Kalman filter would often provide scarce results as shown in the paper. In the deterministic setting a similar approach has

been shown to yield effective results. Future developments could include an analytical investigation of the observability and the detectability properties of the considered problem.

REFERENCES

[1] Martin Brooks. Highly redundant sensing in robotics - Analogies from biology: Distributed sensing and learning. In Julius T. Tou and Jens G. Balchen, editors, *Highly Redundant Sensing in Robotic Systems*, volume 58 of *NATO ASI Series*, pages 35–42. Springer Berlin Heidelberg, 1990

[2] Tesoriero, R., J.A. Gallud, M.D. Lozano and V.M.R. Penichet, "Tracking Autonomous Entities using RFID Technology," IEEE Transactions on Consumer Electronics, Vol. 55, No. 2, pp. 650–655, May 2009

[3] Boccadoro, M., F. Martinelli and S. Pagnottelli, "Constrained and quantized Kalman filtering for an RFID robot localization problem," Autonomous Robots, Vol. 29, Numbers 3-4, pp. 235–251, 2010

[4] Choi, B.-S., J.-W. Lee, J.-J. Lee and K.-T. Park, "A hierarchical algorithm for indoor mobile robot localization using RFID sensor fusion," IEEE Trans. on Industrial Electronics, vol. 58, no. 6, pp. 2226–2235, 2011

[5] Yang, P., W. Wu, M. Moniri and C.C. Chibelushi, "Efficient Object Localization Using Sparsely Distributed Passive RFID Tags," IEEE Transactions on Industrial Electronics, Vol. 60, No. 12, pp. 5914–5924, 2013

[6] DiGiampaolo, E. and F. Martinelli, "A passive UHF-RFID system for the localization of an indoor autonomous vehicle," IEEE Trans. on Industrial Electronics, Vol. 59, n. 10, pp. 3961–3970, October 2012

[7] Bekkali, A., H. Sanson and M. Matsumoto. "RFID Indoor Positioning based on Probabilistic RFID Map and Kalman Filtering," Proc. of the 3rd IEEE Int. Conf. on Wireless and Mobile Computing, Networking and Comm., pp. 21–28, 2007

[8] Saab, S.S. and Z.S. Nakad, "A standalone RFID indoor positioning system using passive tags," IEEE Transactions on Industrial Electronics, Vol. 58, No. 5, pp. 1961–1970, 2011

[9] Park, S. and H. Lee, "Self-recognition of Vehicle Position Using UHF Passive RFID Tags," IEEE Trans. on Industrial Electronics, Vol. 60, n. 1, pp. 226–234, January 2013

[10] Di Giampaolo, E. and F. Martinelli, "Mobile robot localization using the phase of passive UHF-RFID signals," IEEE Trans. on Industrial Electronics, Vol. 61, n. 1, pp. 365–376, January 2014

[11] Sarkka, S., V.V. Viikari, M. Huusko and K. Jaakkola, "Phase-Based UHF RFID Tracking With Nonlinear Kalman Filtering and Smoothing," IEEE Sensors Journal, vol. 12, n. 5, p. 904–910, 2012

[12] D. Carnevale and A. Astolfi, " Semi-global frequencies estimation in the presence of deadzone and saturation", *IEEE Trans. Aut. Control*, *available on-line*, 2014, 10.1109/TAC.2013.2294818

[13] D. Carnevale and A. Astolfi, "Hybrid observer for global frequency estimation of saturated signals", *IEEE Trans. Aut. Control*, 2009, Vol. 54, pages 2461–2464, N. 10,doi 10.1109/TAC.2009.2029395.

[14] R. Goebel, R. Sanfelice, and A.R. Teel, "Hybrid dynamical systems. Robust stability and control for systems that combine continuous-time and discrete-time dynamics", IEEE Control Systems Magazine, Vol. 29, Issue 2, 2009, pages 28-93.

[15] Marrocco, G., E. Di Giampaolo and R. Aliberti, "Estimation of UHF RFID Reading Regions in Real Environments," Antennas and Propagation Magazine, IEEE, vol.51, no.6, pp. 44–57, Dec. 2009

The challenge of analysis, survey and conservation of historical sites for service robotics

Giuseppe Carbone[1], Franco Tedeschi[1], Michela Cigola[2]
[1]DICIME, [2]DART, Università degli studi di Cassino e del Lazio Meridionale
Cassino (FR), Italy
carbone@unicas.it

Abstract— **Nowadays, architectonic survey and conservation of historical sites is getting more and more attention from the media. Many sites such as Pompei seem to require significant efforts for properly achieving their preservation. A possible aid for addressing the above mentioned issues may come from service robotics. However, the design of a service robot includes a very wide range of possibilities and characteristics, also according to its specific application tasks. Thus, this paper pays significant attention in defining a proper operation scenario in order to fulfill tasks of architectonic survey and conservation of historical sites. The proposed scenario has been defined as based on common conditions in historical sites. In particular, for a general case, it has been considered the need of operating over delicate surfaces and in presence of obstacles. Authors propose a possible design solution of a service robot for analysis, survey and conservation of historical sites, based on the characteristics of the outlined scenario. A preliminary built prototype is also herewith described.**

Keywords— hexapod walking robots; analysis, survey, conservation of historical sites.

I. INTRODUCTION

Architecture survey and restoration of historical sites require significant efforts for successfully achieving their goals. Many problems are in fact related to the analysis, safeguard and conservation of historical architectural sites as described for example in [1]. Modern surveying process involves measuring, drawing, checking and comparing the data collected, using an accurate methodology [2]. Surveying involves a complex series of operations, not only in terms of the geometric-spatial form of the architectural work, but also in term of structural and historical data [3].

A survey carried out before restoration work must lead to an overall understanding of the good under examination, completely exhaustive in terms of dimensional, structural and construction aspects. It must reveal the state of health of a good, its conditions of decay and static conditions [4]. The problems involved in surveying for safeguard mainly highlight the need to acquire a great quantity of information to be integrated. Measuring must be carried out precisely and the graphical representation must give precise details of the characteristics of the works and all its distinctive features [5]. In order to carry out the above mentioned task, a survey for restoration should use all modern available methodologies and techniques. A new challenge in architectonical survey can be the analysis and safeguard of historical architecture through the use of mobile robots performing complex task on various kind of surface such as proposed in Fig. 1.

Hexapod legged robots can be suitable for survey operation, since they can overcome obstacles that are comparable with the size of their legs [6]. Hexapod walking robots also benefit from a low impact on the terrain and have great mobility in natural surroundings. This is especially important where it is essential to keep the terrain largely undisturbed such as survey applications of historical sites [3]. Hexapod robot can establish a static equilibrium easily while moving. Besides, it can go forward with many kinds of gaits to adapt different speeds and loads. Hexapod robots architecture can easily allow the operation a of 3D Scanning system. This innovative technology allows creating virtual 3D models of large and complex objects with remarkable levels of definition.

Despite the above referenced aspects many challenges remain before hexapod walking robots can have a more widespread use. Some of their current design open issues include high complexity and cost, low energy efficiency [7], and relatively low speed. Walking robots are usually requiring high level specific skills for managing the many needed actuators, sensors, transmissions and supporting hardware/software.
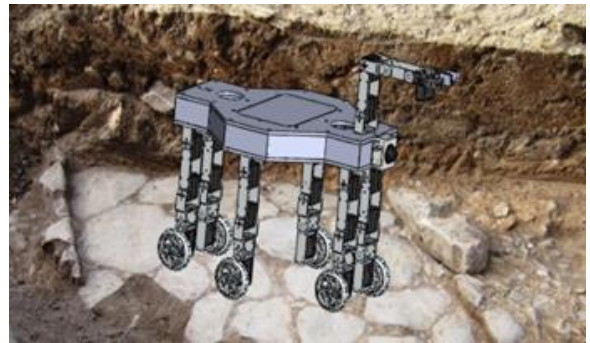
Fig. 1 A 3D simulation of hexapod robots in survey activity

II. THE ATTACHED PROBLEM

Analysis and survey activity on historical architectonic goods are generally carried out with manual operations with few assisting devices. Usually, the activity consists of related tasks,

which can be often repetitive, for acquiring data from the historic works, both in terms of dimensions and figures of details. Those repetitive tasks can be enhanced with suitable assisting robotic devices. In addition, a certain automation of current manual operation in Survey can help to get results in short time and with more accurate results. Moreover, there are several cases and situations in which those measuring activity and figure acquisition cannot be performed by human operators, like for examples in no accessible sites, but even for obtaining proper resolution of the results.

Typical survey on-field activity on Architecture can be recognized in measuring dimensions of the goods, detecting their general figures in term of shapes and volumes, acquiring images or even videos both for the general status and details, inspecting structure of the goods [8]. Most of these activities can be helped with assisting robotic devices and they can be even more successful both in term of productivity and quality of results as well as shortening the operation time. The Survey activity in most of the cases requires to close the historical goods to the public visit. The possibility to have assisting robotic devices that can operate in short time, even without requiring large frames obscuring the historical goods is a strong demand. Main tasks related with solutions using robots, can be identified as:

- high-resolution image acquisition of surfaces with the aim of a detailed graphical reconstruction and interpretation;
- identification of details and their location within the plan of the work in which they are located;
- representation and reconstruction of work images that are on curved surfaces or in hidden surfaces;
- acquisition of images with suitable static mechanisms that are not available with current photographic means both for the light sources and the camera location with respect to orthogonally of work surface;
- possibility to use additional instrumentation, even in one unique campaign/action of Survey;
- possibility to use the robot performance for additional evaluations and computations of work characteristics.

III. A DESIGN METHODOLOGY

According to [8], a general methodology for the robot application in Survey can be described as a sequence of steps such as shown in Fig. 2.

A first step is addressed to define requirements and operation characteristics that are suitable for a certain automation or improvement by using assisting robotic devices. Since the variety of irregular terrain is unlimited, it is difficult to cover all the different cases of the walking over irregular terrain. In order to study this problem the real features are simplified into standard geometric features. Fig. 3 shows the geometric features and related parameters that have been considered: crest, ditch and vertical step.

Second step regards development of survey methodologies. The design of survey activity has been carried out through simulations and experiences to define procedures for the analysis and to conceive operation strategies for the systems
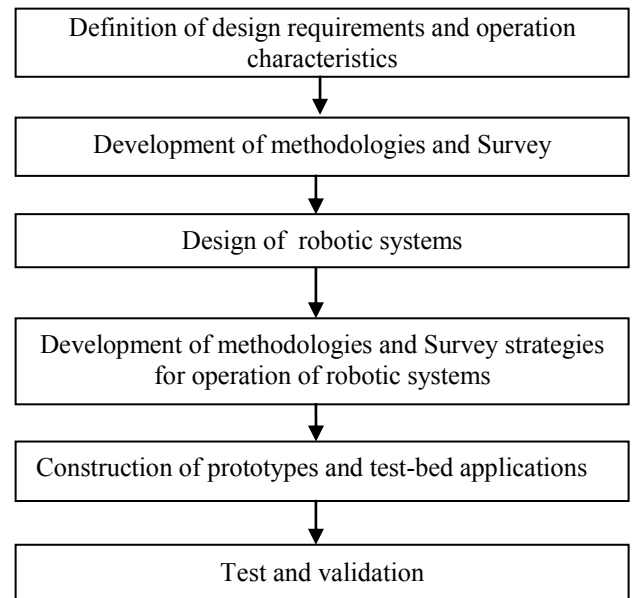

Fig.2 Basic step for robotics application in survey
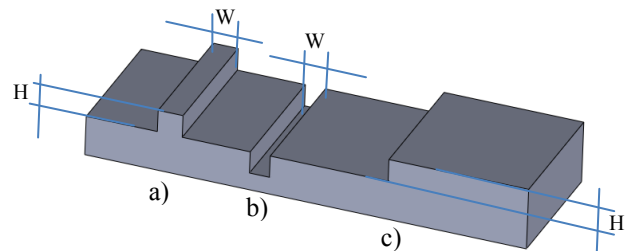
Fig. 3 Geometry of standard obstacles: a) crest b) ditch c) step

and their use in survey activity. Attention has been addressed to operation features in terms of user-oriented facilities, human-machine interfaces that can determine a successful user oriented results for survey operators.

In a third step, the design process will be focused on system architectures that can perform the required survey strategies. Design algorithms have been formulated for the design of robotic systems by approaching the problems for the structure types, dimensional synthesis, mechanical design of parts, endowment of suitable internal and external instrumentation. SolidWorks environment has been used due to its convenient features in structure analysis and in the operation study of multi-body systems in order to check the feasibility of a real prototype. Simulations are used for investigating basic robot performances in order to check the design feasibility before prototyping.

The fourth step dial with methodology for survey operations with a robotic system. Simulations have been carried out in Solidworks environments in order to validate the proposed operation strategies. In this elaboration process, significant efforts have been addressed in the activity of analysis and simulation of proposed solutions and operations. These simulations can be summarized up as follows: the robot's first

characteristic is its capacity to move within the area under examination, carrying image capturing equipment to perform the first analyses on the object. Main attention has been focused on walking gaits and basic operation such as step climbing, ditch overcame, operation on a slope. At the same time, since the surface in historical sites is extremely irregular, in addition to forward motion the robot must also ensure that the image capturing equipment remains parallel to the floor.

To start testing the suitability of the elements proposed, these operations are being verified with Solidworks simulations that provide virtual 3D models, allowing a reduction in time and costs in the planning phase. Solidworks environment allows to thoroughly evaluate and test the model from the initial stage of design, also by simulating the environment in which the robot will works.

In the fifth step design results of previous step can be applied for construction of a prototype. In the last step results can be validated with tests that can be carried out with the prototype in laboratory experiences and finally in on-fields applications of survey activity.

IV. A CASE OF STUDY

Having in mind the basic above mentioned steps, in the following we describe a case of study that has been developed at LARM and DART Laboratory aiming to design a walking robot for survey activity, analysis and conservation of historical sites.

Main characteristics for the robotic system can be outlined in a mobile platform carrying several instruments such as image capturing in terms of photos and videos, thermal inspection, laser scanner or other sensor for distance and orientation measures. Thus, this will require a certain volume and payload available on board of the robotic system. Careful motion of the robotic system is expected in order to ensure full image capturing of the surface and its environment and to avoid damage of the terrain itself or other components of the environment under exploration.

Other characteristics of the proposed robot have been selected by considering previous experiences at LARM and can be summarized as the follows:
- low-cost both in design and operation (< 1000 Euros);
- user-friendly operation, also for non-expert users;
- wireless operation in environments that cannot be reached or
  unsafe by human operators;
-operating speed on regular terrain must be > 0.1 m/s
-operating speed on uneven terrain must be > 0.05 m/s.

In this case of study we assume to survey a flat surface with max 1% slope, 1 cm unevenness and resolution of survey equal or lower than 0.5 cm. Size of the overall surface to be surveyed is assumed as 20 m^2. Obstacle of max 50 mm can be found. The above numbers have been assumed by referring to a Cosmatesque pavements at Montecassino Abbey [9].

Many efforts have been addressed to defining a proper operation scenario in order to fulfill tasks of architectonic survey and restoration of historical sites. The geometric features have been chosen as based on common conditions in historical sites. Referring to the above features, main

characteristics of the operation scenario can be outlined as follow:
  a) a crest, with maximum width W=60mm, height H=50mm;
  b) a ditch, with maximum width W=60 mm;
  c) a step, with maximum height H = 50mm.

Once considered the above mentioned conditions and constraints, it has been thought convenient to design a multilegged robot with a suitably large body and powered wheeled feet. In particular, the structure with six legs has been chosen in order to ensure contact with ground always with at last three feet so that a plane can be easily determined for the robot body. Powered wheeled feet are installed on the legs in order to have the possibility to smooth and regulate the contact force during the walking motion of the robot. This choice is useful in order to prevent damage of the pavement surface and to improve stability.

Axi-simmetrical configuration with rectangular shape has been adopted. The overall robot configuration is presented in Fig. 4). This robots can fit into a cube of 0.4m x 0.3m x 0.2m. The robot body structure can be composed of two main plates made of Delrin that are connected with screws and nuts as show in Fig. 5a). The main body can carry on-board a control card and battery. The overall robot weight is about 30N.

A modular design of one leg has been used as basic component for the novel Hexapod. Kinematic configuration is based on few components with fairly simple mechanical design, that consists of two links connected through a knee joint. This assembly solution has been designed as based on previous experiences that are reported in [10,11,12]. Each of the legs has 3 DoFs: two of them have a movement that has a range between -90° and 90° that allows the robot to overpass obstacles and to walk without moving the wheels. The third motor allows the wheels to move in a full rotation range. An exploded view of the leg is shown in Fig. 5b) to make the assembly scheme clear. Chosen actuators are digital servomotors. The leg measures 160mm in length, 45mm in width and 20mm in depth. Total weight is about 2.5 N. The diameter of omni-wheels is 60mm. They allow to steering the robots in a wheeled operation. The arm above the robot body allows to manipulate objects [13] and 3D laser scanner operation.
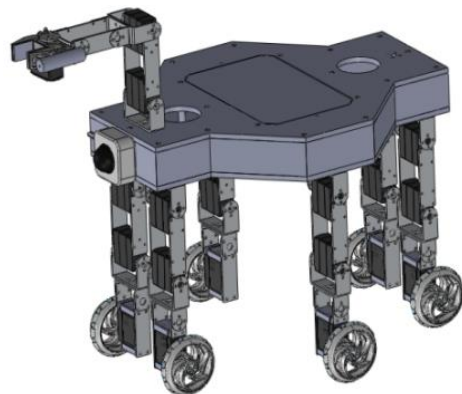


Fig. 4 A 3D CAD model of the proposed hexapod
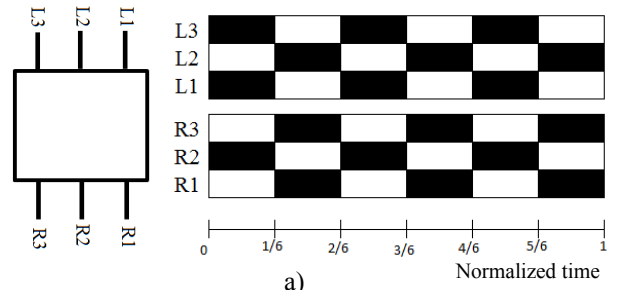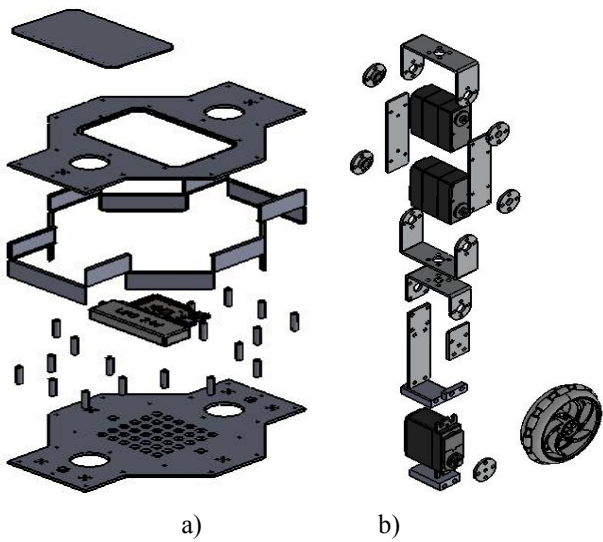
Fig. 5 a) b) exploded view of main body c) exploded view of one leg .

Fig. 6 shows a simulation detail of avoidance obstacle capability for a single leg. The proposed design allows overpassing a step of 80 mm.


80mm
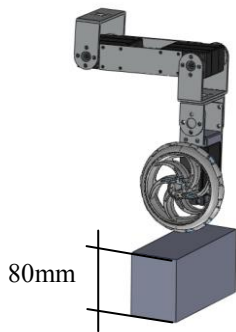
Fig. 6 Simulation detail of obstacle avoidance capability of one leg.

Walking strategies in tripod gaits has been simulated in virtual environments. Fig. 7a shows a tripod gait diagram, while fig. 7b), 7c), show a main steps frame of a simulated walking strategies.Tripod gait is a regular, periodic gait, where the front and back legs on one side lift at same time with the contralateral middle leg, forming alternating tripods. A tripod consists of the front-back legs on one side and the middle leg on the opposite side. For each tripod, the legs are lifted, lowered, and moved forwards and backwards at same time. Tripod gait is suitable for relatively high speed walking over relatively flat ground.

In order to study a step climbing strategy, here we define the first two legs close to the step as the "front legs". The second two legs are defined as the "mid legs" and the third two legs as the "back legs". As the assumptions, initially the robot is near the step. The flow for climbing a high step is as follows:

1. the robot raises the front legs aside to match the height of the step (Fig. 8a).
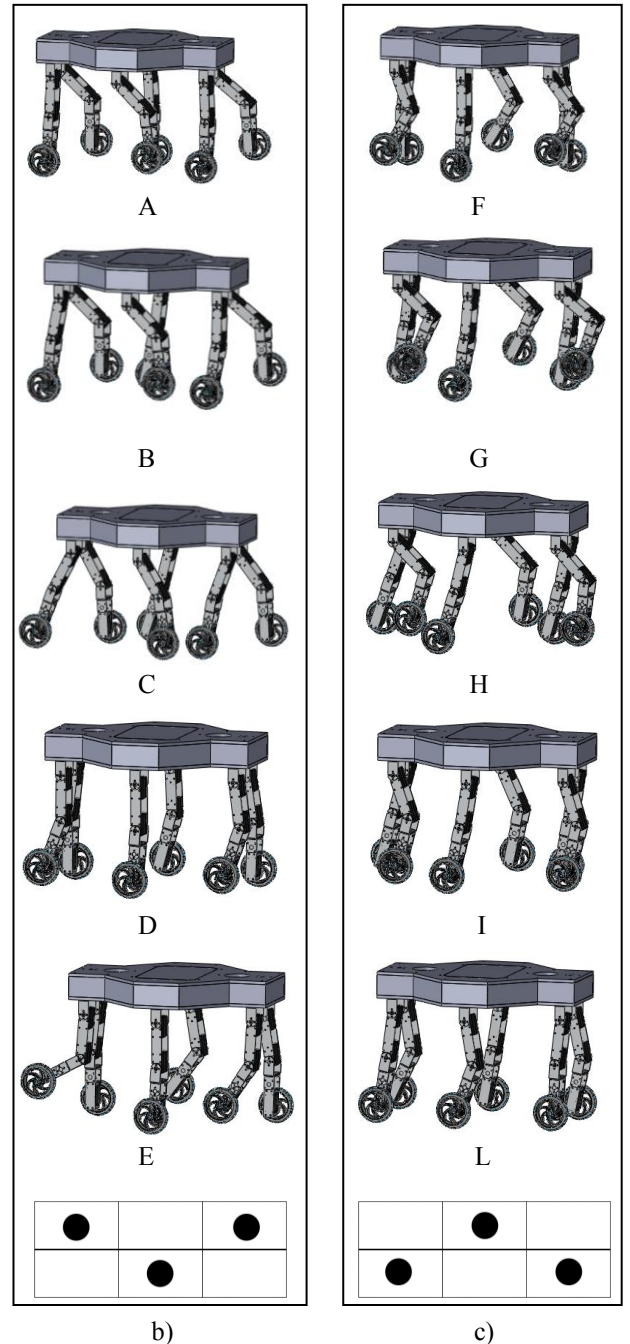
Fig. 7 a) Walking diagram b) main steps frames in a first tripod c) main steps frames in a second tripod.

2. The robot supports its body with the mid and back legs and goes forward as much as possible without hitting the step. Then the robot puts the front legs on the step (Figure 8b).
3. The robot raises the middle legs back to match the height of the step. The robot supports its body with the front and back legs and moves its body forward as much as possible. Then the robot puts the mid legs on the step (Figure 8c).
4. The robot raises the back legs back to match the height of the step. The robot puts the back legs on the step. Then the robot supports its body with all the legs and move forward (Fig. 8d).


a)

b)

c)

d)
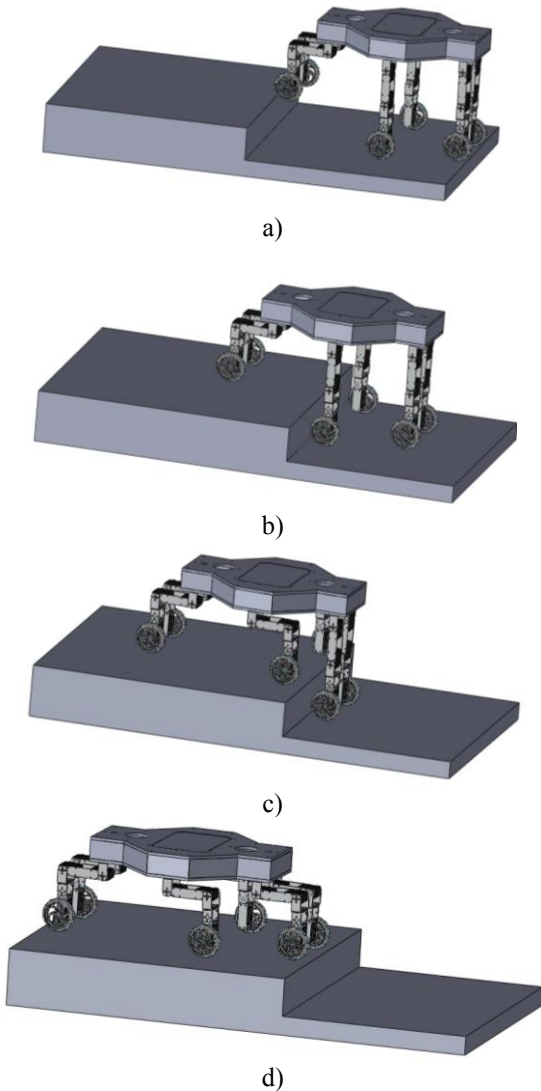
Fig. 8 Main steps in a climbing strategy a) first step b) second step c) third step d) fourth step.

In order to study a ditch overcame strategy, we first define the max operation sizes by referring to a terrain depression of which the robot leg cannot touch the bottom or cannot step across (Fig. 9). Solidworks simulation allow to find the max operation depth that is H= 80 mm and the max operation width tath is W= 85 mm.
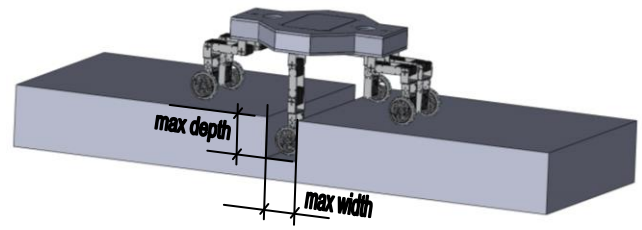

Fig. 9 A scheme of cliff and gap definition.

The flow for ditch overcame is as follows:
1. the robot raises the legs and goes forward as much as possible without hitting the ditch (Figure 10a).
2. the robot puts the front legs on the other side of the ditch (Figure 10b).Then the robot supports its body with the mid and back legs and moves forward as much as possible.
3. the robot overcame the ditch with the mid legs and moves forward as much as possible (Figure 10c).
4. the robot supports its body with the front and middle legs and it overcame the ditch with back legs (Fig. 10d).


a)

b)

c)

d)
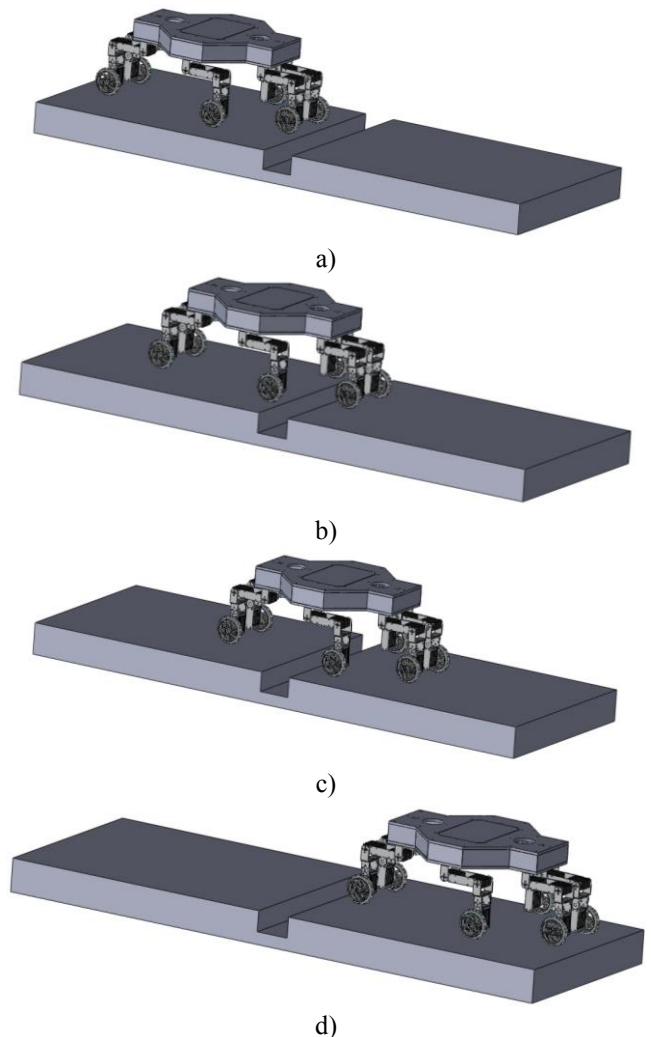
Fig. 10 Ditch overcame strategy a) first step b) second step c) third step d) fourth step.

Figure 11 shows a detail of operation on a slope. The hexapod equipped with rubber wheels is walking transversely across a gradient, of an inclined slope with inclination angle θ. The high H of Center Gravity (CG) body is kept parallel to the gradient surface and the legs are kept normal to the surface of the ground. The projection centre of the CG is shifted laterally to the downhill side by a distance H·tg θ. For walking gait, the maximum gradient which can be handled by this strategy occurs when the offset of the projection of the CG is equal to half the distance between trasversal legs W/2. That is H· tg θ = W/2 [14]. Thus feasible operation is about 20°slope.
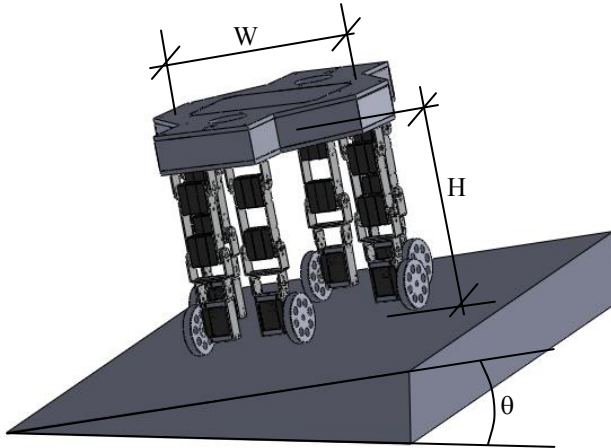

Fig. 11 Operation on a slope

The soundness of results will be proved with tests that will be carried out with the prototype during a near future. Fig. 12 shows a detail of a built prototype of one leg.
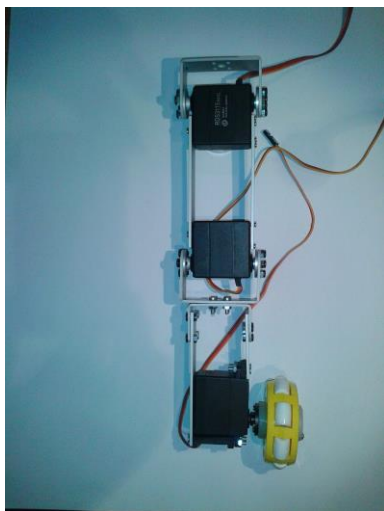
Fig. 12 A built prototype of one leg

V CONCLUSION

The goal of this work is to test the possibility of designing robotic systems that are specifically dedicated to the field of architectonic survey. A specific design methodology has been proposed by referring to main survey and restoration features and constraints. A case of study of the proposed methodology has been described. A design solution has been proposed and it is under patenting [15]. A prototype is currently under construction. A preliminary leg prototype and basic simulation experiences show the feasibility of the proposed design in the simulated scenario.

REFERENCES

[1] M. Docci and D. Maestri, Handbook of Architectural and Urban Survey, Roma-Bari, 1994.

[2] M. Docci and M. Cigola, "Drawing as memory, memory as drawing, The benedictine Abbey of Montecassino", in: Proceedings of International Congress "Drawing as place of memory", Florence, 1995, pp. 600–610.

[3] M. Cigola, "Architectural survey and robotics: New frontiers in study, preservation and restoration of historical sites", in: Proceedings of International Conference on Innovative Methods in Product Design, Padova, 2011, p. 147.

[4] M. Ceccarelli, M. Cigola, E. Ottaviano, A. Gallozzi, G. Carbone, A. Pelliccio, "A study of feasibility of using robots in architecture analisi and survey of a historical pavement", Proceedings of 11th International Workshop on Robotics in Alpe-Adria-Danube Region, pp. 113-118, Balatonfired, 2002, Budapest Polytechnic Editor, Budapest.

[5] M. Cigola, A. Pelliccio, O. Salotto, G. Carbone, E. Ottaviano, M. Ceccarelli. "Application of Robots for inspection and restoration of Historical sites". In: Proc. International Symposium on Automation and Robotics in Construction, Ferrara, paper 37, 2005.

[6] G. Carbone, M. Ceccarelli, "Legged Robotic Systems", Cutting Edge Robotics ARS Scientific Book, Wien, pp.553-576, 2005.

[7] P. Gregorio, M. Ahmadi, M. Buehler. "Design, control, and energetics of an electrically actuated legged robot". Systems, Man and Cybernetics, Part B, IEEE Transactions on, vol. 27, pp. 626–634, 1997.

[8] M. Cigola and M. Ceccarelli. "A Robot Application for Analysis, Survey and Conservation of Historical Architectures", Robotics and Automation in Construction, C. Balaguer and M. Abderrahim (Eds.), ISBN: 978-953-7619-13-8, 2008.

[9] M. Cigola, "Mosaici pavimentali cosmateschi: segni, disegni e simboli", Palladio, Vol. VI No. 11, 1993, (101-110).

[10] G. Carbone, M. Ceccarelli. "A Mechanical Design of a Low-Cost Easy-Operation Anthropomorphic Wheeled Leg for Walking Machines", International Journal Robotica Manager, vol. 9 n.2, pp. 3-8, 2004.

[11] F. Tedeschi, G. Carbone, D. Cafolla, "Design and operation of Cassino Hexapod" in proceeding of RAAD'2013, 22th International Workshop on Robotics in Alpe-Adria-Aanube Region, Portoroz, Slovenia, pp. 94-101, 2013.

[12] D.Cafolla, F. Tedeschi, G. Carbone, "Design and simulation on Cassino Hexapod II" in Proc. of the 3rd IFToMM International Symposium on Robotics and Mechatronics (ISRM 2013) Singapore, 2013, pp. 3-12.

[13] Ceccarelli, M. Fundamentals of Mechanics of Robotic Manipulation, Kluwer Academicublishers, ISBN1-4020-1810k 2004, Dordrecht, The Netherlands.2004

[14] S.M. Song, K. Waldron. Machines that walk: The adaptive suspension vehicle, MIT Press: Cambridge, 1989; pp.107-112.

[15] G. Carbone, F. Tedeschi, Sistema robotico a gambe per telerilevamento, domanda di brevetto IS 2014A1.